8-2024

Relationship Between the Physical Properties and Oil Binding Capacity of Fats

Melissa Abigail Marsh
Utah State University

RELATIONSHIP BETWEEN THE PHYSICAL PROPERTIES AND OIL BINDING CAPACITY OF FATS

by

Melissa Abigail Marsh

A dissertation submitted in partial fulfillment
of the requirements for the degree

of

DOCTOR OF PHILOSOPHY

in

Nutrition and Food Sciences

Approved:

Silvana Martini, Ph.D. Major Professor	Luis Bastarrachea, Ph.D. Committee Member
Robert E. Ward, Ph.D. Committee Member	Prateek Sharma, Ph.D. Committee Member
David Britt, Ph.D. Committee Member	D. Richard Cutler, Ph.D. Vice Provost for Graduate Studies

UTAH STATE UNIVERSITY
Logan, Utah
2024

ABSTRACT

Relationship Between the Physical Properties and Oil Binding Capacity of Fats

by

Melissa Marsh, Doctor of Philosophy

Utah State University, 2024

Major professor: Dr. Silvana Martini

Department: Nutrition, Dietetics, and Food Sciences

The ability of a fat crystal network to retain liquid oil is known as oil binding capacity (OBC). The OBC of semi-solid fats is a crucial property for nut butters, snack foods, and confectionery products as low OBC in these applications often results in deterioration of the food's quality. Therefore, this dissertation presents a comprehensive investigation into the dynamic relationship between processing conditions – cooling rate and application of high-intensity ultrasound (HIU), storage conditions, fat composition, and physical properties on the OBC of fats. In this work, three fats were examined – a stearic-rich soybean-based fat, a palmitic-rich palm-based fat, and a lauric-rich palm-kernel-based fat. In addition to evaluating the type of fatty acids present (stearic, palmitic, or lauric), the fats were also diluted with soybean oil (SBO) to examine the influence of the amount of saturated fatty acids (SFA) on OBC.

The fats were crystallized using fast (FCR) and slow cooling rates (SCR) as well as with (w HIU) or without (wo HIU) the application of HIU resulting in four processing conditions – FCR wo HIU, FCR w HIU, SCR wo HIU, SCR w HIU. Physical properties of the crystallized fats were evaluated including hardness, viscoelasticity (G′, G′′, δ), solid fat content (SFC), melting behavior (Tpeak, enthalpy), and crystal microstructure. The

aforementioned physical properties were also measured after the samples had been stored at room and refrigeration temperature – 22 °C and 5 °C; respectively. The OBC of the fats was determined via two methods – a centrifugation method and a filter paper method. Correlation analysis was performed to comprehend the relationship between the OBC and physical properties of fats.

From these studies it was found that modifying the processing conditions, composition, and storage temperatures of semi-solid fats significantly impacted the physical properties and resulting OBCs. Generally, FCRs, HIU, lower storage temperatures, and high SFAs contributed to enhancing the fat matrix's ability entrap liquid oil resulting in an increase in OBC. Correlation analysis between the physical properties and both measures of OBC for all fats studied showed SFC, G´, G´´, hardness and enthalpy were significantly positively correlated with OBC. Notably, the correlation analysis did not establish strong relationships between crystal size and OBC. Overall, the findings of these studies indicate that the development of fats with high OBC can be accomplished by formulating hard fats with high SFC and enthalpy values.

(229 pages)

PUBLIC ABSTRACT

Relationship Between the Physical Properties and Oil Binding Capacity of Fats

Melissa Marsh

Fats play a significant role in shaping the characteristics of foods, influencing texture, mouthfeel, appearance, and nutritional attributes. An important property of fats is their ability to entrap liquid oil known as oil binding capacity (OBC). Poor OBC of fats frequently leads to shortened-shelf life of foods caused by quality issues due to unwanted chemical and physical changes. In natural nut butters without additives, low OBC often results in a visual oil layer forming at the surface. In filled chocolates such as truffles, pralines, and peanut butter cups this low OBC can result in unwanted textural and visual changes.

The OBC of fats is determined by the physical and chemical characteristics. In this dissertation, the relationship between the physical properties and OBCs of fats is examined. To better understand the relationship between the physical properties and OBC of fats, a wide range of physical properties are generated by using different processing conditions, storage temperatures, and diluting the fats with liquid soybean oil (SBO). Additionally, the impact of chemical characteristics on the OBC of fats is studied by examining three types of fats – a soybean-based fat, a palm-based fat, and a palm-kernel-based fat that have different chemical compositions.

The fats studied in this project were solidified quickly or slowly as well as with or without a processing tool – high-intensity ultrasound (HIU), which has been shown to modify the structure of fats. The physical properties of the solidified fats were measured including the texture, amount of solid fat, the temperature that the fats melted at, the amount

of energy required to melt the fats, and the size of the solid particles. After the initial solidification of the samples, they were stored at room and refrigeration temperatures and the same physical properties were measured once more. The OBC of the fats was calculated using two methods. In the first method, the samples were spun in a centrifuge and the liquid oil that moved to the top was removed. In the second method, the fats were placed on top of a paper allowing the liquid oil to move onto the paper which was weighed.

The relationship between the physical properties and OBC for both methods was evaluated, and it was found that fats with high amounts of solid fat, hard textures, and higher amounts of energy required to melt the fat were related to higher OBC. Additionally, fats stored at refrigeration temperatures, that contained less liquid oil, and were crystallized quickly with HIU tended to retain more liquid oil. Overall, this work indicates that the OBC of fats can be improved by changing the physical properties.

DEDICATION

This dissertation is dedicated to my mother, Ann Lippmann, who had to discontinue her education, a privilege I have been fortunate to pursue.

ACKNOWLEDGMENTS

I would not have accomplished this without several influential people in my life.

Thank you, Dr. Silvana Martini, for believing in me and pushing me throughout the years. You have been an incredible driving force in my life and were the person who encouraged me to get involved with research and to pursue my doctorate degree. I will always be grateful for the time and energy that you have invested in me. Your unwavering support and mentorship have had a significant impact on shaping my life.

My sincerest appreciation to my committee members - Dr. Luis Bastarrachea, Dr. Robert Ward, Dr. Prateek Sharma, and Dr. David Britt. I was fortunate to learn from many of you during both my undergraduate and doctorate degrees. Thank you for helping me build my fundamental understanding of food science as well as for your guidance and support during my Ph.D.

To the fellow graduate students in the fat lab – Dr. Juhee Lee, Annalisa Jones, Audrey Lidgard, Sarah Petmecky, and Nabila Anjum I am happy to have worked with and spent time getting to know each of you.

I would like to thank all my scholarship donors. There was a time when I was not certain if I could continue my education because of the cost. Without the generosity and support of those donors I am not sure if I would have finished my undergraduate degree, not to mention my doctorate.

I am incredibly grateful to have been able to participate in extracurricular events, both product development competitions and the food science club. Thank you, Dr. Marie Walsh, for your insight and help with these endeavors. I would also like to thank my team members – Nathan Pougher, Mackenzie Taylor, Chandler Stafford, Rachel Davis, Taelie Kennedy, Audrey Lidgard, Annalisa Jones, Weston Christensen, Jared Buhler, and

Savannah Branson.

I am grateful to have the love and support of my parents – Ann Lippmann, Michael Marsh, Janna Marsh, siblings, and friends, as well as my cat – Pesto. Thank you for being there for me during the hardest times in my life. To my grandfather, Robert Lippmann, although you are not here physically, I know you were proud of me for pursuing my doctorate degree.

Thank you, Dom Koenig, for being my biggest supporter. Your constant encouragement, kindness, and love has helped me tremendously.

CONTENTS

Page

LIST OF TABLES

LIST OF FIGURES

LIST OF ABBREVIATIONS

AOCS = American Oil Chemists' Society

DSC = Differential Scanning Calorimeter

EIEPO = Interesterified Palm Oil

EIESOY = Interesterified Soybean Oil

FCR = Fast-Cooling Rate

G´ = Storage Modulus

G´´ = Loss Modulus

HIU = High-Intensity Ultrasound

NMR = Nuclear Magnetic Resonance

OBC = Oil Binding Capacity

OBC_c = Oil Binding Capacity Measured Using a Centrifuge Method

OBC_p = Oil Binding Capacity Measured Using a Filter Paper Method

PHO = Partially Hydrogenated Oils

PKO = Palm-Kernel Oil

PLM = Polarized Light Microscope

SCR = Slow-Cooling Rate

SBO = Soybean Oil

SFA = Saturated Fatty Acids

SFC = Solid Fat Content

TAG = Triacylglycerols

TPA = Texture Profile Analysis

XRD = X-Ray Diffraction

δ = phase shift angle

CHAPTER I. INTRODUCTION

Lipids play an important role in the physical properties of foods as they impact mouthfeel, texture, and melting behavior (Martini, 2013). In addition to imparting various physical properties, some lipids are essential for the diet such as unsaturated omega-6 and omega-3 fatty acids (Nelson and Cox, 2013). In general, unsaturated fatty acids have poor stability in food products resulting in phase separation and oxidation posing a problem for their inclusion in foods (Damodaran *et al*., 2007). Therefore, a technology known as partial hydrogenation was employed to saturate these fatty acids resulting in some bonds changing from a *cis* configuration to a *trans* configuration (Nelson and Cox, 2013). The process of partial hydrogenation created artificial *trans*-fatty acids which have been linked to adverse health outcomes including coronary heart disease, increased LDL cholesterol, decreased HDL cholesterol, insulin resistance, and diabetes risk (Bhandari *et al*. 2020; Iqbal 2014; c *et al*., 2006). Due to these adverse health effects, the use of partially hydrogenated oils (PHOs) in food products has been severally limited after the food and drug administration (FDA) removed their generally recognized as safe status (GRAS) in 2015. Additionally, the U.S. Department of Agriculture (USDA) suggests reduced consumption of saturated fats. However, these stable fats play an important role in the production of fats and fat-based foods due to their ideal physical properties. Food producers have been challenged to replace PHOs and fats with high content of saturated fatty acids, with healthier fats while maintaining the ideal physical properties.

Chemical composition and processing conditions impact the crystallization of fats and the resulting physical properties (Wang *et al*., 2016; Maleky *et al*., 2012; Campos *et al*., 2002; Martini *et al*., 2006; Metin and Hartel, 2005). For example, Metin and Hartel

(1996) studied induction times in milkfat (wide range of TAG species) and cocoa butter (narrow range of TAG species). Despite the fats having similar melting points, and being crystallized at the same temperature, the induction times of milkfat were significantly faster when compared with cocoa butter. Similarly, da Silva and Martini (2020a; 2020b) crystallized palm and soybean-based fats in a scraped surface heat exchanger with similar melting points and SFA; however, a higher supercooling was required to crystallize the palm-based fat than the soybean-based fat. Results from these studies highlight the role of chemical composition in dictating the crystallization behavior of fats; however, processing conditions further influence fat crystallization and resulting physical characteristics.

Typically, fats that are crystallized slowly have larger crystals and are softer than fats crystallized quickly which tend to have smaller crystals and higher hardness (Maleky *et al*., 2012; Metin and Hartel, 2005; Dibildox-Alvarado *et al*., *2004*; Campos *et al*., 2002). Fats crystallized under shear typically results in more and smaller crystals than fats crystallized statically. (Blake and Marangoni, 2014; De Graef *et al*., 2008; Herrera and Hartel, 2000). High-intensity ultrasound (HIU) has emerged as a promising tool to generate various physical properties (Martini *et al*., 2008; da Silva *et al*., 2020a; 2020b; 2020c; Giacomozzi *et al*., 2019; Lee *et al*., 2018). HIU has been used to generate harder, more elastic fats, with small crystals, and increased oil binding capacity (OBC) (Ye and Martini, 2015; Chen *et al*., 2013; Lee *et al*., 2020, Ye *et al*., 2011; da Silva *et al*., 2020a; 2020c). OBC is the ability of a fat matrix to retain liquid oil and is an important physical property in natural nut butter and confectionery products. Low OBC in natural nut butters that contain no stabilizers may result in phase separation which is observed as a visible oil layer forming on the top of the sample (Mohd Rozalli *et al.,* 2016). In confectionery products

such as peanut butter cups, truffles, and other chocolates with fat-based fillings, low OBC can lead to oil migrating from the filling to the chocolate coating. Oil migration can result in several undesirable effects including fat bloom, hardening of the filling, and softening of the chocolate coating (Smith *et al*., 2007).

OBC is dependent on the physical properties of the crystalline network and its chemical composition. For example, typically harder fats (da Silva *et al*., 2020c), with higher SFC (Acevedo *et al*., 2012) and smaller crystal sizes (Si, *et al*., 2016) are expected to have higher OBC, however it is not known which of these physical properties or combination of physical properties drives OBC as these physical properties are typically confounded. Several studies have examined the relationship between the physical properties of semi-solid fats and OBC, however due to these confounding factors there have been mixed results. For example, Acevedo *et al*., (2017) found a significant negative correlation between SFC and oil diffusivity while other studies found no relationship between SFC and OBC (da Silva *et al*., 2020a; Acevedo *et al*., 2012; Si *et al*., 2016). Further, an inverse relationship between crystal size and OBC has been observed (Acevedo *et al*., 2012). However, Acevedo *et al*., 2017; found that oil diffusivity at the molecular level was inversely related to meso-crystal dimension indicating that smaller crystals resulted in greater oil movement on the microscopic level. Additionally, Green and Rousseau (2015) found a non-linear relationship between oil migration and microstructure. The presence and orientation of fatty acids on the triacylglycerol (TAG) molecule has been shown to affect OBC. Specifically, Bouzidi and Narine (2012) observed that symmetrical TAGs exhibited lower OBC compared to asymmetrical TAGs. Furthermore, Bouzidi *et al*. (2013) investigated TAGs containing stearic and palmitic fatty acids and found that the

inclusion of stearic acid led to significantly higher OBC.

To address the variability in the observed relationships between OBC and physical properties, there is a need to investigate this problem using a multidimensional approach in which each physical property can be changed without affecting the others to reduce confounding factors (Figure 1-1).

Figure 1-1: Schematic representation of processing conditions used to change the physical properties of fats.

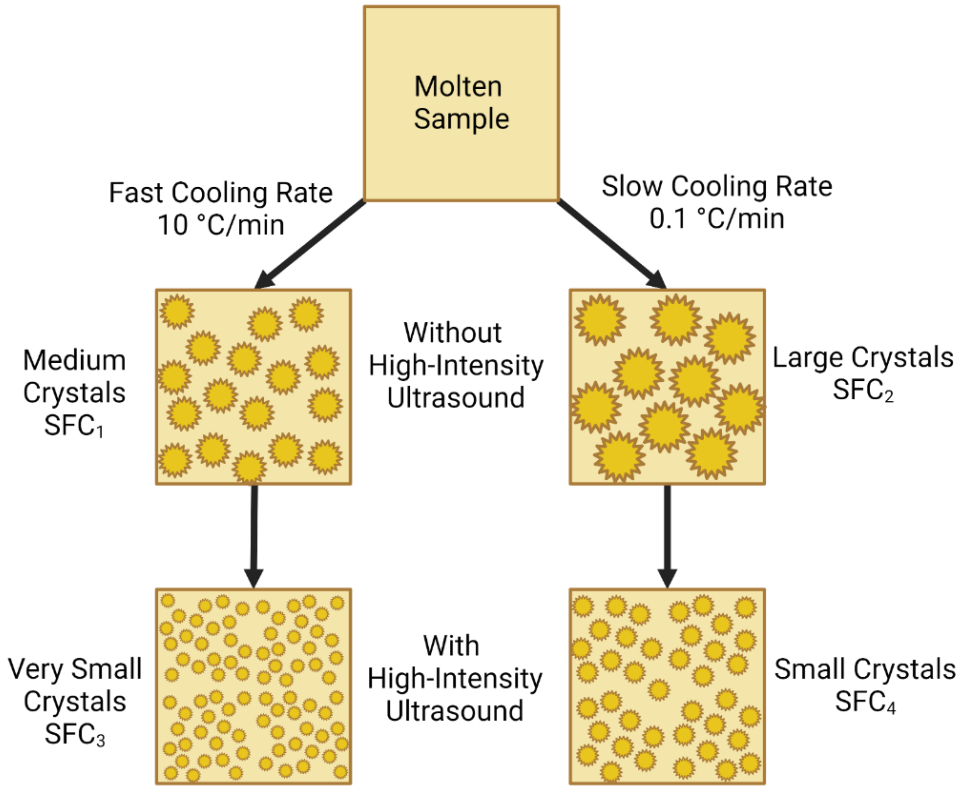

In this investigation, both a fast- (FCR) and slow-cooling rate (SCR) are used to generate samples with different crystal sizes and hardness but similar SFC. HIU was used to generate a wide range of physical properties by reducing crystal size and increasing hardness. Samples were diluted to generate different SFC, hardness, enthalpy and OBC. Due to the impact of the type of fatty acids present on the TAG molecule significantly impacting OBC, three fats are evaluated – a soybean fat with high content of stearic fatty

acids, a palm fat mainly comprised of palmitic fatty acids, and a palm-kernel fat with medium chain lauric fatty acids. These fats were chosen because they are dominant fats in the food industry and are expected to crystallize differently due to variations in their fatty acid compositions. By systematically changing the physical properties of semi-solid fats it is possible to unveil which physical properties drive OBC.

HYPOTHESIS

Oil binding capacity is affected by the physical properties of the fat and the physical properties are affected by processing conditions such as the application of HIU and the use of either a FCR or a SCR. By using different processing conditions, a wide range of physical properties and OBCs can be generated in order to better understand which factor(s) are most influential in increasing OBC.

Additionally, the level of saturation and the type of fatty acids present are also vital factors impacting physical properties and OBC. By diluting the fats with a low saturated fatty acid (SFA) containing oil - soybean oil (SBO), it is possible to understand how the level of SFA impacts OBC. In addition to SFA impacting OBC, the fatty acid composition impacts OBC. Stearic, palmitic, and lauric-rich fats display different crystallization kinetics resulting in differences in physical properties and OBC.

Figure 1-2: Schematic representation of proposed hypothesis.

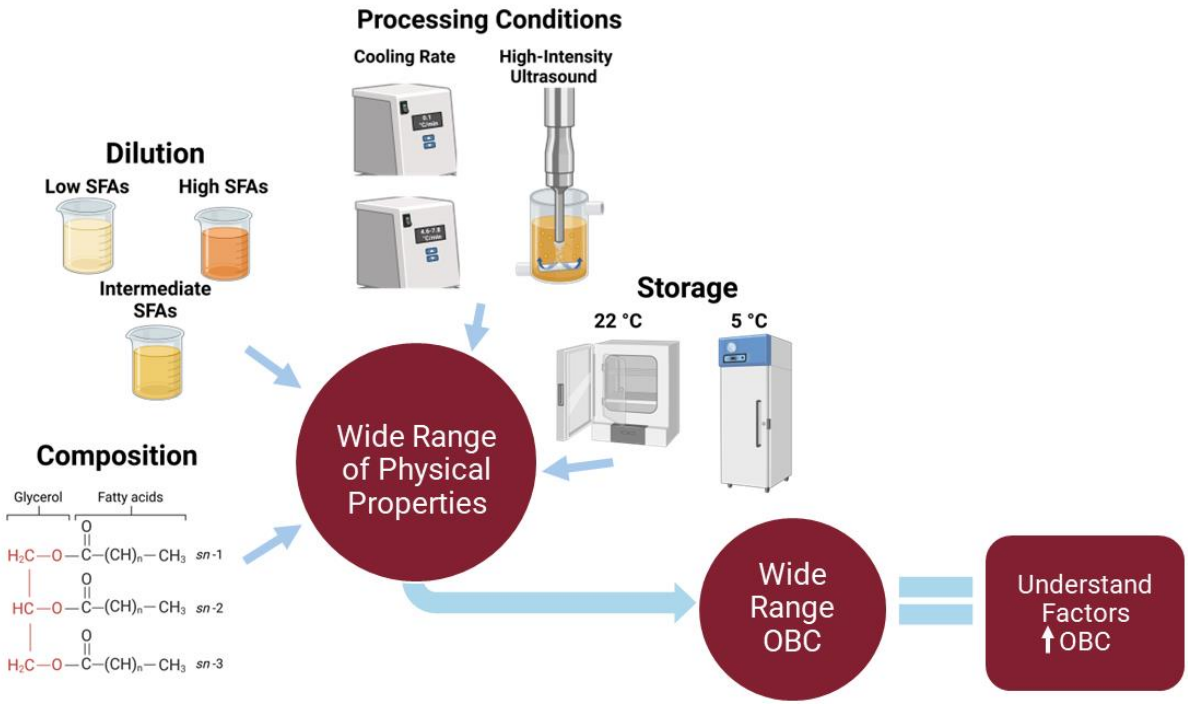

OBJECTIVES

1. Analyze the impact of processing conditions – cooling rate and HIU, SFA level, and storage on the physical properties and OBC of a stearic-based fat.
    a. Generate fats with different levels of SFA via dilution with SBO at 0%, 50%, and 80% and crystallize the diluted fats under different processing conditions – cooling rates and application of or absence of HIU.
    b. Measure the physical properties of the crystallized fats after crystallization and storage at 22 °C and 5 °C. Quantify the OBC of the fats after storage and determine the relationship between the physical properties and OBC.
2. Measure the physical properties and OBC in a palmitic-based fat crystallized using a slow and fast cooling rate and with or without the application of HIU and design a model to predict OBC.

a. Produce fats varying in SFA levels by blending with SBO at 0%, 50%, and 80% concentrations. Crystallize the blends using different cooling rates and HIU application.
b. Evaluate the physical characteristics and OBC of the fats following crystallization and storage at 22 °C and 5 °C.
c. Establish correlations between the physical properties and OBC and design a statistical model to aid in predicting OBC values based on the physical properties.

3. Assess how processing conditions and physical properties influence the OBC of a high, moderate, and low SFA lauric-rich fat, commonly used in confectionery applications.
    a. Produce high, moderate, and low SFA lauric-based fats by mixing with SBO at 25%, 50%, and 80%. Crystallize these blended fats using various processing conditions, including different cooling rates and the application or omission of HIU.
    b. Analyze the physical properties and OBC of fats after the crystallization process and storage. Identify connections between the physical properties and OBC.

REFERENCES

Acevedo NC, Block JM, Marangoni AG. Unsaturated Emulsifier-Mediated Modification of the Mechanical Strength and Oil Binding Capacity of a Model Edible Fat Crystallized under Shear. Langmuir 2012;28:16207–16217. DOI: 10.1021/la303365d

Acevedo NC, MacMillan B, Newling B, Marangoni AG. Shear effects on the diffusive movement of oil in triacylglycerol networks. RSC Adv 2017;7:1634–1642. DOI: 10.1039/C6RA24829B

Blake AI, Co ED, Marangoni AG. Structure and Physical Properties of Plant Wax Crystal Networks and Their Relationship to Oil Binding Capacity. J Am Oil Chem Soc 2014;91:885–903. DOI: 10.1007/s11746-014-2435-0

Bouzidi L, Narine SS. Relationships between molecular structure and kinetic and thermodynamic controls in lipid systems. Part II: Phase behavior and transformation paths of SSS, PSS and PPS saturated triacylglycerols--effect of chain length mismatch. Chem Phys Lipids 2012;165:77–88. DOI: 10.1016/j.chemphyslip.2011.11.005

Bouzidi L, Omonov TS, Garti N, Narine SS. Relationships between molecular structure and kinetic and thermodynamic controls in lipid systems. Part I: propensity for oil loss of saturated triacylglycerols. Food Funct 2013;4:130–143. DOI: 10.1039/C2FO30164D

Campos R, Narine SS, Marangoni AG. Effect of cooling rate on the structure and mechanical properties of milk fat and lard. Food Res Int 2002;35:971–981. DOI: 10.1016/S0963-9969(02)00159-X

Chawla P, deMan JM. Measurement of the size distribution of fat crystals using a laser particle counter. J Am Oil Chem Soc 1990;67:329–332. DOI: 10.1007/BF02539684

Chen F, Zhang H, Sun X, et al. Effects of Ultrasonic Parameters on the Crystallization Behavior of Palm Oil. J Am Oil Chem Soc 2013;90:941–949. DOI: 10.1007/s11746-013-2243-y

da Silva TLT, Martini S. Incorporation of high intensity ultrasound (HIU) to a scraped surface heat exchanger: Effect of HIU position. J Food Eng 2020a;274:109824. DOI: 10.1016/j.jfoodeng.2019.109824

da Silva TLT, Martini S. Sonocrystallization of a Palm-Based Fat with Low Level of Saturation in a Scraped Surface Heat Exchanger. J Am Oil Chem Soc 2020b;97:1253–1264. DOI: 10.1002/aocs.12409da Silva TLT, Cooper Z, Lee J, et al. Tailoring Crystalline Structure Using High-Intensity Ultrasound to Reduce Oil Migration in a Low Saturated Fat. J Am Oil Chem Soc 2020a;97:141–155. DOI: 10.1002/aocs.12321

da Silva TLT, Danthine S, Martini S. Effect of processing conditions as high-intensity

ultrasound, agitation, and cooling temperature on the physical properties of a low saturated fat. J Food Sci 2020b;85:3380–3390. DOI: 10.1111/1750-3841.15436

da Silva TLT, Marsh M, Gibon V, Martini S. Sonocrystallization as a tool to reduce oil migration by changing physical properties of a palm kernel fat. J Food Sci 2020c;85:964–971. DOI: 10.1111/1750-3841.15099

Damodaran S, Parkin KL, Fennema OR. Fennema's Food Chemistry. CRC Press

De Graef V, Goderis B, Van Puyvelde P, et al. Development of a rheological method to characterize palm oil crystallizing under shear. Eur J Lipid Sci Technol 2008;110:521–529. DOI: 10.1002/ejlt.200700315

Dibildox-Alvarado E, Rodrigues JN, Gioielli LA, et al. Effects of Crystalline Microstructure on Oil Migration in a Semisolid Fat Matrix. Crystal Growth & Design 2004;4:731–736. DOI: 10.1021/cg049933n

Giacomozzi AS, Palla CA, Carrín ME, Martini S. Physical Properties of Monoglycerides Oleogels Modified by Concentration, Cooling Rate, and High-Intensity Ultrasound. J Food Sci 2019;84:2549–2561. DOI: 10.1111/1750-3841.14762

Green NL, Rousseau D. Oil diffusivity through fat crystal networks. Soft Matter 2015;11:5523–5530. DOI: 10.1039/C5SM01355K

Herrera ML, Hartel RW. Effect of processing conditions on crystallization kinetics of a milk fat model system. J Amer Oil Chem Soc 2000;77:1177–1188. DOI: 10.1007/s11746-000-0184-4

Lee J, Claro da Silva R, Gibon V, Martini S. Sonocrystallization of Interesterified Soybean Oil: Effect of Saturation Level and Supercooling. J Food Sci 2018;83:902–910. DOI: 10.1111/1750-3841.14084

Lee J, Marsh M, Martini S. Effect of storage time on physical properties of sonocrystallized all-purpose shortening. J Food Sci 2020;85:3391–3399. DOI: 10.1111/1750-3841.15435

Maleky F, Acevedo NC, Marangoni AG. Cooling rate and dilution affect the nanostructure and microstructure differently in model fats. Euro J Lipid Sci and Tech 2012;114:748–759. https://doi.org/10.1002/ejlt.201100314

Martini S, Awad T, Marangoni A. Structure and Properties of Fat Crystal Networks

Martini S, Suzuki AH, Hartel RW. Effect of High Intensity Ultrasound on Crystallization Behavior of Anhydrous Milk Fat. J Am Oil Chem Soc 2008;85:621–628. DOI: 10.1007/s11746-008-1247-5

Martini S. Sonocrystallization of Fats. Springer, New York, NY

Metin S, Hartel RW. Crystallization of Fats and Oils. In: Bailey's Industrial Oil and Fat Products. John Wiley & Sons, Ltd, 2005.

Mohd Rozalli NH, Chin NL, Yusof YA, Mahyudin N. Quality changes of stabilizer-free natural peanut butter during storage. J Food Sci Technol 2016;53:694–702. DOI: 10.1007/s13197-015-2006-x

Nelson D, Cox M. Lipids. In: Lehninger Principles of Biochemistry. W. H. Freeman and

Company, New York, NY, pp 357–385

Si H, Cheong L-Z, Huang J, et al. Physical Properties of Soybean Oleogels and Oil Migration Evaluation in Model Praline System. J Am Oil Chem Soc 2016;93:1075–1084. DOI: 10.1007/s11746-016-2846-1

Smith KW, Cain FW, Talbot G. Effect of nut oil migration on polymorphic transformation in a model system. Food Chem 2007;102:656–663. DOI: 10.1016/j.foodchem.2006.05.045

Wang H, Shi X, Paluri S, Maleky F. Effects of processing and added ingredients on oil diffusion through cocoa butter using magnetic resonance imaging. RSC Adv 2016;6:88498–88507. https://doi.org/10.1039/C6RA11196C

Ye Y, Martini S. Application of high-intensity ultrasound to palm oil in a continuous system. J Agric Food Chem 2015;63:319–327. DOI: 10.1021/jf505041s

Ye Y, Wagh A, Martini S. Using High Intensity Ultrasound as a Tool To Change the Functional Properties of Interesterified Soybean Oil. J Agric Food Chem 2011;59:10712–10722. DOI: 10.1021/jf202495b

Figures 1-2 and 1-2 were created with BioRender.com.

CHAPTER II. LITERATURE REVIEW

Oil Binding Capacity

Oil binding capacity (OBC) is a measurement of a fat matrix's ability to retain liquid oil. When this liquid oil moves outside of the fat matrix it is known as oil migration or oil loss. The movement of oil in confectionery products, nut butters, and snack foods results in undesirable physical and chemical changes. The extent to which oil migration will occur is hypothesized to be related to several forces such as diffusion, sedimentation, and capillary action. Due to oil migration being a major factor in reducing the quality of foods, various quantification and imaging methods have been utilized to aid in understanding the degree of oil migration occurring in fat systems.

Relevance

The degree that a fat matrix retains liquid oil plays a vital role in the quality of several food products. Oil migration in confectionery products is a major concern to the industry due to the undesirable impact that oil movement has on chocolate and compound coatings. Common confectionery products that are prone to oil migration-based defects are products with fat-based fillings including truffles, nut filled products, and pralines (Lonchampt and Hartel, 2004). Due to poor OBC, oils from the filling move to the coating (either chocolate or compound) leading to softening of the coating, hardening of the filling, and fat bloom development (Smith *et al*., 2007; Delbaere *et al*., 2016; Lonchampt and Hartel, 2004). Fat bloom is caused by the recrystallization of fat resulting in an undesirable appearance due to large fat crystals on the surface diffracting light differently (Lonchampt and Hartel, 2004). Fat bloom may appear as a grayish film, a marbling effect, or as individual spots and is considered the primary defect in chocolates contributing to $70

billion in industrial annual losses (Figure 2-1; Delbaere *et al*., 2016; Briones and Aguilera, 2005; da Silva *et al*., 2017).

Figure 2-1: Various appearances of fat bloom. From left to right, grayish film, marbling effect, and individual spots.

In addition to confectionery products, oil migration in natural nut butters results in undesirable attributes – an oil layer forming at the surface and a hard layer remaining at the bottom making the nut butter difficult to spread (Feradaus *et al*., 2022). Furthermore, the oil that has risen to the top is more prone to oxidative reactions and rancidity often developing an unpleasant odor (Mohd Rozalli *et al*. 2016). To prevent oil separation in nut butters additives such as mono- and di-glycerides as well as fully hydrogenated vegetable oils are often included (Gorrepati *et al*., 2015). The addition of these stabilizers increases the OBC of the system negating many of the undesirable attributes though many consumers deliberately choose natural nut butters without additional ingredients (Carocho *et al*. 2014; Mohd Rozalli *et al*. 2016). In sandwich cookies with fat-based fillings, movement of oil from the filling to the cookie can result in softening of the cookie, negatively impacting the texture. Several strategies, including the use of oleogels, have been evaluated to increase

the oil binding capacity in these applications (da Silva *et al*., 2021; Palla *et al*., 2020). Dry snacks are also susceptible to oil migration which negatively impacts the sensory and storage properties of these foods. Oil movement can cause the formation of an oil layer on the surface of the product and residual oil inside of the package which is more vulnerable to oxidative reactions and rancidity than oil that remains inside the food matrix (Onacik-Gur and Zbikowska, 2019).

Mechanisms

Diffusion is believed to be one of the main driving forces for oil migration outside of the fat crystal network which occurs due to the triacylglycerol (TAG) concentration gradient (Maleky *et al.*, 2012). In confectionery products, the movement of TAGs between the filling and coating fats is a result of the compositional difference between the fat-based filling and the coating, typically chocolate (Cikrikci and Oztop, 2018). Therefore, diffusion of TAGs between the fats will occur until a thermodynamic equilibrium has been achieved (Figure 2-2; Maleky *et al*., 2012).

The movement of TAGs between the two surfaces can be explained by Fick's first and second laws. Fick's first law states that the movement of molecules is driven by Brownian motion and occurs from regions of higher concentration to those of lower concentration (Maleky, 2018). Mathematically, the law can be expressed as [1]:

$$J = -D\frac{d\phi}{dx} \qquad [1]$$

Where J is the diffusion flux, D is the diffusion coefficient describing the rate of diffusion, and $\frac{d\phi}{dx}$ is the change in concentration in respect to distance. Fick's second law of diffusion states that diffusion rate is proportional to the variation in the slope of the concentration

gradient. Oftentimes to describe the diffusion of oil in confectionery products, Fick's second law is rewritten as [2]:

$$\frac{m_t}{m_s} = \frac{A\sqrt{Dt}}{V} \quad [2]$$

Where $\frac{m_t}{m_s}$ is the mass of oil migrated at time t divided by the mass of oil migrated at saturation, A is the contact area, V is the sample volume, and D is the diffusion coefficient (Talbot, 2009, Wolfrum *et al.*, 1988).

Figure 2-2: Schematic representation of fat in contact with a chocolate coating displaying diffusion driven oil migration.

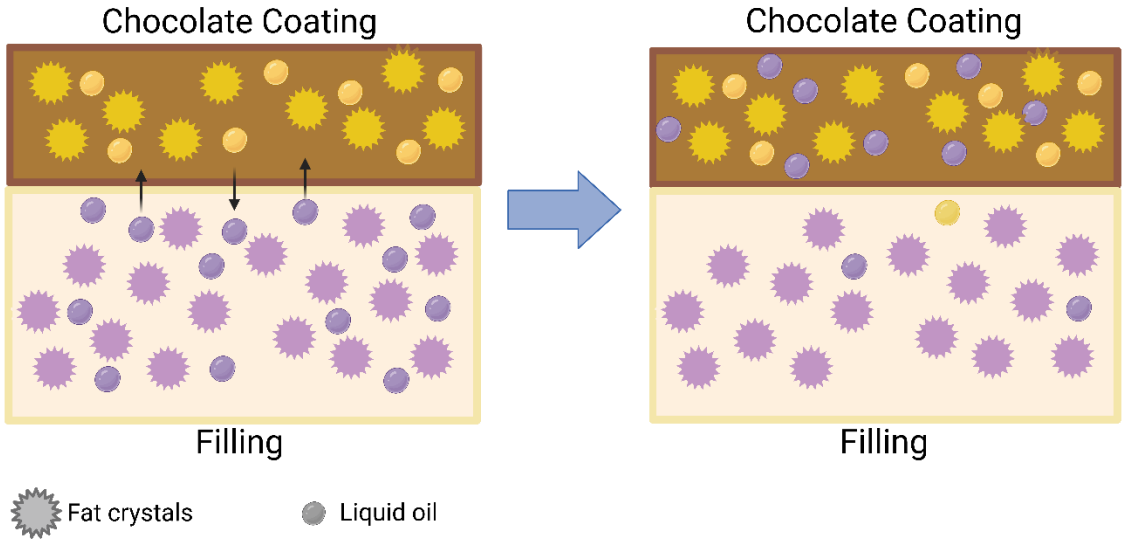

In addition to diffusion, gravitational forces can also impact oil migration and phase separation through sedimentation. Due to solid fat crystals being more densely packed than liquid oil, fat crystals tend to sink to the bottom leading to phase separation (Figure 2-3). The extent to which phase separation occurs is influenced by the fat crystal network's OBC.

Figure 2-3: Schematic representation of a fat showcasing sedimentation of fat crystals.

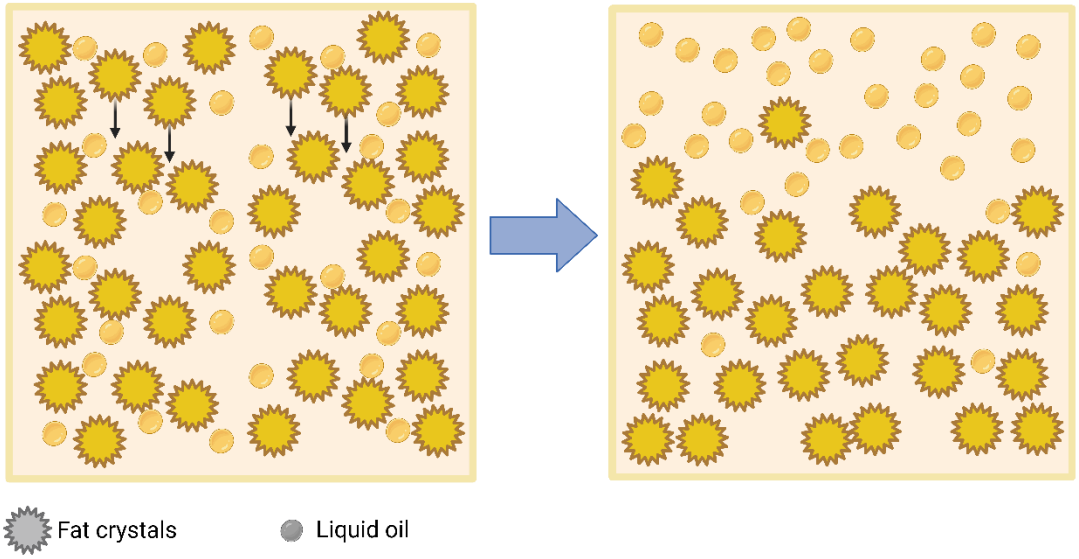

Capillary action is the ability of liquids to flow through porous materials owing to surface tension and adhesive forces and is also theorized to contribute to oil migration (Maleky, 2018). The Lucas-Washburn equation describes the kinetics of capillary rise [3]:

$$\frac{2}{r}\gamma cos\theta = \frac{8}{r^2}\mu h\frac{dh}{dt} + \rho gh \quad [3]$$

Where r is the capillary radius, γ is the surface tension, θ is the contact angle, μ is the viscosity of the fluid, h is the distance the fluid is drawn into the capillary, t is the time, ρ is the fluid's density, and g is the acceleration due to gravity (Tabolt, 2009). The capillary networks of porous foods can facilitate oil dispersion throughout the matrix (Figure 2-4). Oil migration is likely a result of the combined effects of the phenomena described above.

Figure 2-4: Schematic representation of a cookie with a fat-based filling highlighting capillary action driven oil migration.

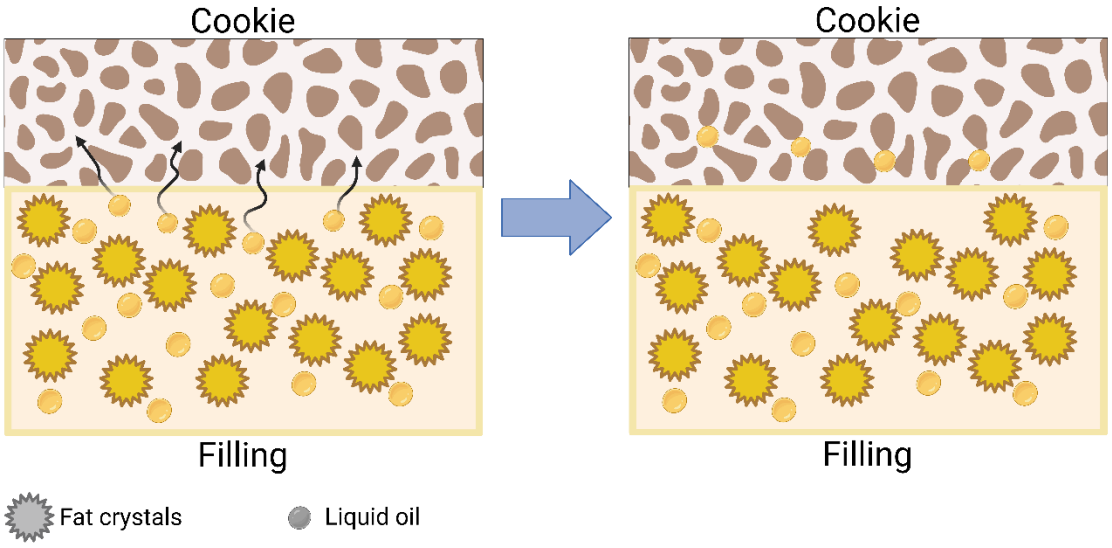

Measurement Methods

The OBC of fats can be evaluated through several methods. One method is to place the fat sample of interest in contact with chocolate or cocoa butter and measure the compositional changes of the fat after some time (Tabolt, 2009; Ali *et al*., 2001). The direct method of measuring the compositional changes considers several of the mechanisms driving OBC – diffusion and capillary action and/or gravitational forces depending on if the cocoa butter or chocolate is placed above or below the fat. Challenges with this method include ensuring that the contact area and porosity are consistent.

A widely used and easily accessible method to measure OBC is the filter paper method. In the filter paper method, the fat sample is placed onto a pre-weighed filter paper and stored. After storage, the fat sample is removed from the filter paper and the filter paper is weighed to quantify the amount of liquid oil that has stained the paper (Omonov *et al*., 2010). Additionally, some studies will measure the diameter of the oil stain to quantify OBC (da Silva *et al*., 2020a; Omonov *et al*., 2010). In the filter paper method, both capillary

and gravitational forces driving oil migration are considered (Tabolt, 2009). A disadvantage of the filter paper method is that some samples may be too soft and will stick to the filter paper.

Flatbed scanners and fluorescence recovery after photobleaching have been used to follow oil movement throughout a fat crystal network. In these experiments, a lipid soluble dye is added to the fat of interest and placed in contact with cocoa butter (Maleky and Marangoni 2011; Marty *et al*., 2005). The samples are then placed in a flatbed scanner or under a confocal microscope, imaged, and the pixel or fluorescence intensity is measured to determine the degree of oil migration. For these methods, the assumption is that oil migrates at the same rate as the added dye which is a controversial hypothesis (Tabolt, 2009; Maleky, 2018).

Another strategy used to monitor oil migration is Magnetic Resonance Imaging (MRI). MRI is a non-destructive imaging technique that utilizes magnetic fields and differences in magnetic properties between protons in liquid oil and solid fat (Maleky 2018; Maleky *et al*. 2012; Wang *et al*., 2016). Similar to other imaging techniques, the fat of interest is placed in contact with another fat – typically cocoa butter and the signal intensity is measured. Higher signal intensity suggests a higher oil content; typically, the signal intensity increases over time indicating oil migration. One advantage of MRI is that the migration process can be visualized in a single sample over the experimental time avoiding errors due to sample variation.

Lastly, centrifugation can be used to measure the OBC of fats. In the centrifugation method, a small amount of the sample is placed into a pre-weighed centrifuge tube. The tube is placed into a centrifuge and spun to expediate the movement of liquid oil out of the

fat matrix. After centrifugation, the tubes are inverted and the liquid oil is poured out, the remaining sample is then weighed to quantify the amount of oil loss (da Pieve *et al.*, 2010; da Silva *et al.*, 2020a; 2020b; 2020c; Giacomozzi *et al.*, 2019). This method helps to understand sedimentation driven oil migration; however, disadvantages include that an external force (centrifugation) is used to force the movement of liquid oil outside of the fat matrix and there can be increases in temperature potentially leading to the melting of low-melting point TAGs.

Composition of Fats

Lipids are characterized by their physical properties – they have limited solubility in water and are soluble in organic solvents (Finley and deMan, 2018). Lipids are found in various forms including phospholipids, TAGs, sphingomyelin, and free fatty acids. In fats and oils, the most common form of lipids are TAGs which are molecules that are composed of three fatty acids esterified to a glycerol backbone (Figure 2-5). The fatty acids occupy one of three positions on the glycerol molecule – *sn*-1, *sn*-2, or *sn*-3 (Berry *et al*., 2019). These fatty acids can be saturated (no double bonds) or unsaturated (one or more double bonds) (Nelson and Cox, 2013). The type and position of fatty acids on the TAG molecule greatly impacts the physical properties of lipids including texture and melting point. When a TAG is made up of long chain mono- and poly-unsaturated fatty acids, the lipid is typically soft and has a low melting point unless the double bonds are in the *trans* confirmation. On the other hand, TAGs that are made up from long chain saturated fatty acids are harder and have high melting points due to the TAG molecules packing tightly together (Nelson and Cox, 2013). The diversity of molecular species is a result of the arrangement and type of fatty acid present on the glycerol molecule.

Figure 2-5: Structure of a triacylglycerol and naming convention for the position of fatty acids.

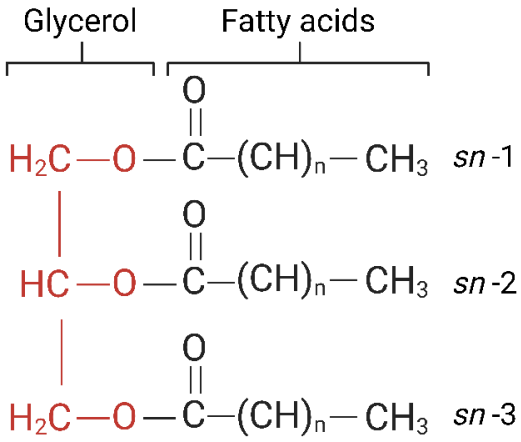

To evaluate the composition of lipids, a variety of chromatography techniques can be used including gas chromatography (GC) and high-performance liquid chromatography (HPLC). GC can be used to evaluate the fatty acid composition of fats. In GC, fatty acids are typically converted to fatty acid methyl esters (FAME; Nelson and Cox, 2013). AOCS method Ce 1k-09 is used to directly convert lipids into FAMEs by in situ acid digestions (hydrochloric acid in methanol) followed by alkali hydrolysis (sodium hydroxide in methanol) and methylation (boron trifluoride in methanol as a catalyst). The concentration of FAMEs are then measured through GC (AOCS official methods Ce lj-07). GC is a popular analysis method as it provides high resolution, has low limits of detection, has high accuracy and reproducibility and is a relatively fast measurement. HPLC is another chromatography technique used to evaluate fats as it can be used to identify mono-, di-, and triglycerides.

Fat Crystallization

Crystallization describes the process in which a crystal network is formed and is an important process during the manufacturing of fat-based foods such as margarine, butter,

shortenings, and chocolate, to name a few (Martini *et al*., 2006). There are four steps in the crystallization process of fats – supercooling, nucleation, growth, and recrystallization (Figure 2-6; Hartel, 2001). Supercooling is generated in fats when the temperature is below the melting point and is defined as the difference between the temperature of the material and its melting point [4].

$$\Delta T = T_m - T \quad [4]$$

where ΔT is the degree of supercooling, T_m is the melting point, and T is the temperature of the sample (Martini *et al*., 2006)

At this point, a thermodynamic driving force is generated because the free energy of the solid phase is lower than the liquid phase and the fat will begin to crystallize (Hartel, 2001; Martini *et al*., 2006). This driving force results in nucleation and fat crystals begin to spontaneously form. Nucleation is the transition from a metastable to a stable phase and the crystal formation is controlled by temperature and cooling rate until it reaches a critical size (Martini *et al*., 2006). How quickly these critical nuclei form from the melt is called the nucleation rate. The formation of fat crystals lowers the energy level of the system, and the crystal lattice structure begins to form.

Figure 2-6: Crystallization process of fats. (Nucleation step modified from Chem Eng Sci, Vol 56, Issue 7, 2001, Sato K, Crystallization behaviour of fats and lipids - a review, with permission from Elsevier)

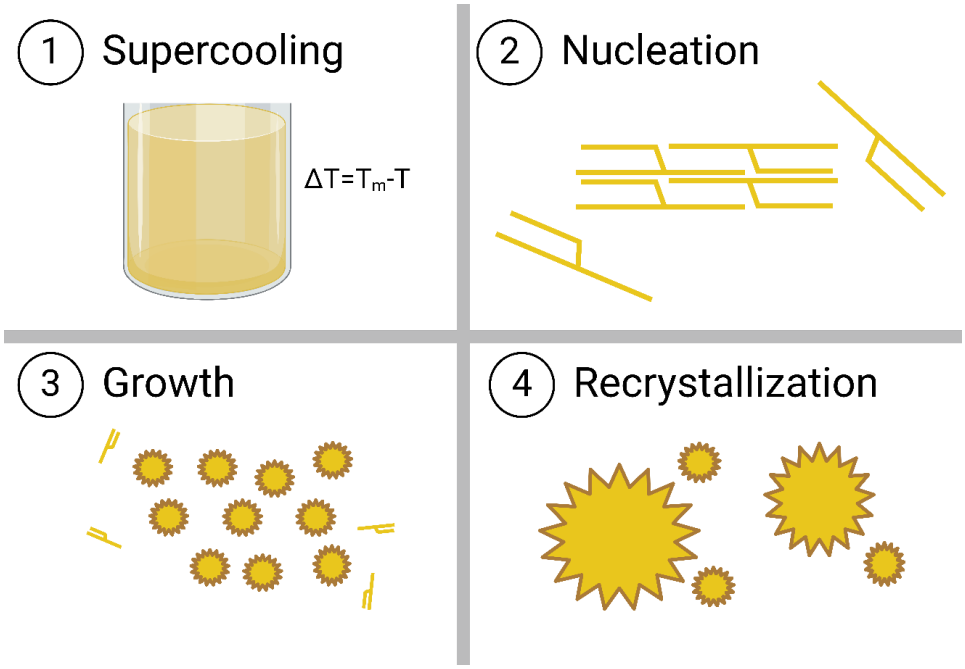

During crystal growth, the nuclei begin to grow and form larger fat crystals. Molecules move towards the stable solid-liquid interfaces of the crystals increasing the crystal's size. The growth rate of the crystal is dependent on the mobility of molecules and is restricted when the melt viscosity is too high (Martini *et al*., 2006). Crystals continue to grow until the system reaches equilibrium. However, changes continue to occur in the system during long-term storage as there are fluctuations in temperature and humidity resulting in recrystallization. Even if the temperature and humidity are constant, the system will try to achieve the lowest energy level and recrystallization will often occur.

Controlling crystallization kinetics allows manufacturers to modify fat crystal network structure and rheological properties (Martini *et al*., 2006). The controlled cooling of crystalline materials can generate various crystal sizes, polymorphic forms, and textures. Cooling fats using slow cooling rates (0.1 °C/min) tends to result in softer, less elastic fats

with large crystals. Whereas fast cooling rates (above 5 °C/min) generates harder, more elastic fats with small homogeneous crystals (Dibildox-Alvarado *et al*., 2004; Campos *et al*., 2002).

Polymorphism

Under normal atmospheric pressures and temperatures several materials, including fats, display polymorphism, the ability to crystallize in more than one form. Polymorphism is an important property of fats as it gives them their characteristic properties including texture, crystal size, and melting behavior. In fats there are three general polymorphic forms – α, β´, and β. The α polymorphic form is the least stable and therefore has the lowest melting point, whereas the β polymorphic form is the most stable and has the highest melting point and the β´ polymorphic form lays between these two. Depending on the application, different polymorphic forms are desirable. For fat spreads, the most desired polymorphic form is β´ as the crystals are relatively small and can incorporate large volumes of oil whereas β polymorphic form crystals start small but grow into needle-like agglomerates that are less able to entrap liquid oil and have a grainy texture (Gunstone, 2006). For chocolate, β crystals are desired as it results in a shiny appearance, proper mold release, and ideal mouthfeel (Afoakwa *et al*., 2007, Svanberg *et al*., 2011).

To identify the polymorphic form(s) present in materials, X-ray diffraction (XRD) measurements are needed. In XRD, a crystalline material is placed in a sample holder and an X-ray beam strikes the sample (incident beam) at a specific angle. The XRD equipment then measures the diffracted waves in the detector to determine the angle shift that the material has caused (Figure 2-7). Bragg's law [5] can then be used to calculate the d-spacing (Å) of the peaks.

Bragg's Law: $n\lambda = 2d \sin\theta$ [5]

Where n is an integer (the order of reflection), λ is the wavelength of the incident beam, *d* is the spacing between crystal planes and θ is the diffracted angle.

Figure 2-7: Example of a XRD diffractogram of a fat. Peak positions occur where the X-ray beam has been diffracted by the crystal lattice.

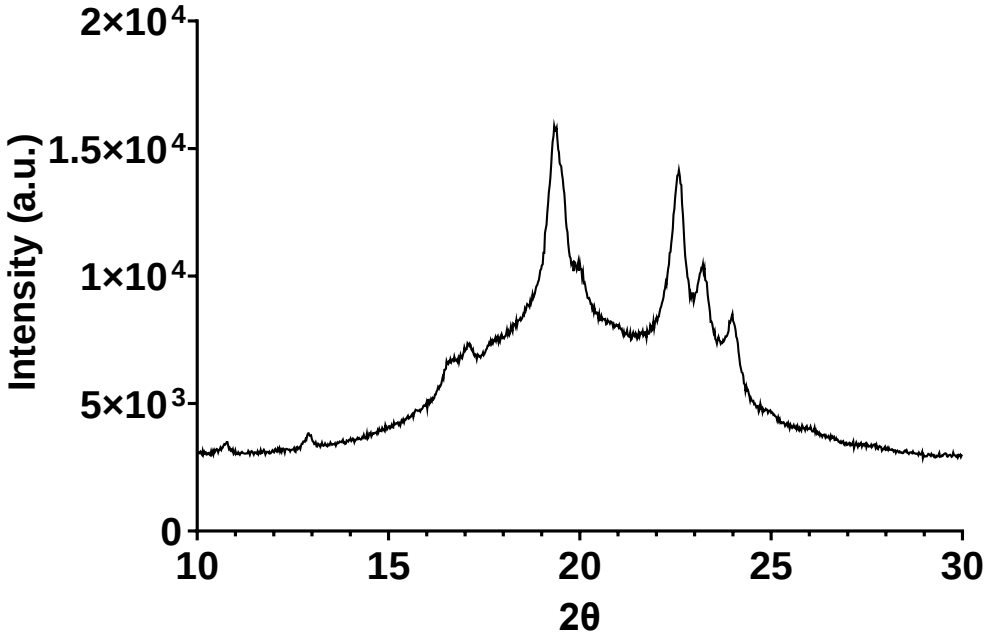

The α polymorphic form has a single peak at 4.15 Å while the β´ polymorphic form is identified by two peaks at 3.8 Å and 4.2 Å and the β polymorphic form is identified by a larger peak at 4.6 Å and a small peak at 5.2 Å (Marangoni, 2005; Sato, 2018).

Impact of TAG Composition on Crystallization Kinetics

The saturation level, position of fatty acids, and type of fatty acids present on the TAG molecule results in different physical properties and impacts the OBC of fats. Bouzidi *et al*. (2013) evaluated OBC in mixtures of pure saturated TAGs (SSS, PSP, LSL, MSM, LPL, PSS, PPS, LLS, MMS, and PPL) in canola oil (CO). Interestingly, the study noted that symmetrical TAGs had lower OBC than asymmetrical TAGs most likely due to

asymmetrical TAGs having higher nucleation and growth rates at the beginning of crystallization when compared to symmetrical TAGs. The faster nucleation for asymmetrical TAGs resulted in a greater number of nuclei forming during initial crystallization. These additional nuclei developed into small crystals that may have been able to entrap more oil when compared with symmetrical TAGs which formed fewer nuclei and larger crystals. Additionally, Bouzidi *et al*. (2013) showed significant differences in the ability of stearic and palmitic diacid TAGs (PSS and SSS) to bind liquid oil likely driven by differences in melting behavior. The SSS TAGs melted sharply at higher temperatures, approximately 62 °C and had higher enthalpy values than the PSS TAGs that melted around 52 °C.

Several studies have evaluated the crystallization kinetics of various TAGs and blends of TAGs. Bhaggan *et al*. (2018) compared the kinetic phase behavior of mixtures of tripalmitoylglycerol (PPP) and 1,3-dipalmitoyl-2-stearoyl-sn-glycerol (PSP) crystallized using either fast (10 °C/min) or slow cooling rates (1 °C/min). The study showed that as PSP increased in the blends, so did peak melting temperatures which was more evident for samples cooled slowly. In addition, cooling rate and PSP inclusion impacted the polymorphic form of the blends. In the study, faster cooling rates resulted in α crystals and slower cooling rates generating β´ crystals. When PSP was present at levels of 30% or higher in the PPP-PSP blends, the crystals formed into the β´ polymorph more easily. Bouzidi *et al.*, 2010 investigated the binary phase behavior of lauric-rich TAGs namely 1,3-dilauroyl-2-stearoyl-sn-glycerol (LSL) and 1,2-dilauroyl-3stearoyl-sn-glycerol (LLS) crystallized using fast (3 °C/min) and slow cooling rates (0.1 °C/min). Cooling rate impacted the physical properties with samples cooled quickly being harder and containing

crystals that were 25 times smaller than the samples cooled slowly. In terms of the composition of the samples, LSL-LLS blends were harder than the pure LSL and LLS fats; moreover, the crystal morphology was impacted by the LSL concentration with higher concentrations resulting in platelets growing to be longer and more defined. The study also found LSL sped up crystallization by shortening induction times with a significant impact observed for slow cooled samples with LSL concentrations of 20-40% where induction times were shortened 20-fold when compared to fast cooled samples. Interestingly, the researchers found that LSL-LLS mixtures crystallized in a more ordered phase when compared to earlier work from the same research group that measured the binary phase behavior of palmitic-rich TAGs - 1, 3-dipalmitoyl-2-stearoyl-sn-glycerol (PSP) and 1, 2-dipalmitoyl-3-stearoyl-sn-glycerol (PPS) (Boodhoo *et al*., 2009).

The diversity of TAGs also impacts crystallization kinetics. For example, cocoa butter has a narrow range of TAG species – mainly comprised of SOS, SOP, and POP; whereas milkfat has a wide range of TAG species – over 120 species (Fontecha, 2005; Naik and Kumar 2014). One might assume that fats with narrow ranges of TAG species will crystallize faster; however, this is not always the case. Metin and Hartel (1996) examined the crystallization kinetics and melting properties of anhydrous milk fat (AMF) and cocoa butter (CB). The researchers found that despite AMF and CB having similar melting points, the same crystallization temperatures, and CB having a higher SFC (CB = 61%, AMF = 18% at 25 °C; and CB = 84%, AMF = 51% at 5 °C) AMF had shorter induction times than CB (Metin and Hartel 1996; Metin and Hartel 2005). Although AMF crystallized faster, the resulting melting enthalpy after 180 min at 15 °C was 69% lower than CB, most likely due to the difference in SFC. The combination of these works

showcases the differences in crystallization and resulting physical properties between various TAGs species.

Interesterification

Interesterification (IE) is a procedure used to rearrange the fatty acid position in or among TAG molecules and is often performed to modify the functionality and nutritional aspects of fats (Berry *et al*., 2019; Berry 2009). For example, Ma *et al*. (2019) demonstrated that the IE of *Cinnamomum camphora* seed oil (CCSO) with fully hydrogenated palm oil could be effective cocoa butter substitute due to the IE blend having comparable physical properties – SFC, melting behavior, polymorphism. Similarly, Yamoneka *et al*. (2018) found that IE blends of *Irvingia gabonensis* seeds fat and *Dacryodes edulis* pulp oil could generate a fat with similar melting and polymorphic behavior as cocoa butter making it a good candidate as a cocoa butter substitute. To improve nutritional attributes, Farfán *et al.* (2015) generated fats with high concentration of linoleic acid, zero *trans*-fat, and desirable physical properties via IE of fully hydrogenated soybean and walnut oil blends (40:60).

Two types of interesterification exist – chemical interesterification (CIE) and enzymatic interesterification (EIE). CIE typically uses sodium methoxide as a catalyst and results in a random distribution of fatty acids (Gunstone, 2006; Berry *et al*., 2019). CIE has been used since the 1940s, the procedure is relatively simple and inexpensive; however, the reaction is nonspecific resulting in no control over the position of the fatty acids. (Zhang *et al*., 2020; Berry *et al*., 2019). In contrast, EIE uses lipase enzymes that can specifically arrange the fatty acids on the glycerol backbone allowing for the production of custom fats with desirable physical and nutritional characteristics and has become the predominant interesterification method in North America (Rashid *et al*., 2018; Berry *et al*., 2019; Gibon,

2011).

Interesterification is divided into three types of reactions: acidolysis, alcoholysis, and transesterification (Figure 2-8). Acidolysis is a reaction between a free fatty acid and a TAG which can be used to produce structured lipids with tailored physical and nutritional properties (Yanık *et al*., 2013). Alcoholysis is a reaction between an alcohol and a TAG often used to generate monoacylglycerols (MAGs) and diacylglycerols (DAGs) (Rousseau *et al*., 2017). Transesterification is the most common esterification reaction used in the food industry and is a reaction between two TAGs.

Figure 2-8: Interesterification reactions. (Reprinted with permission from Wiley and Sons; European Journal of Lipid Science and Technology, Vol 115, 2013, Soumanou MM, Perignon M, and Villeneuve P, Lipase-catalyzed interesterification reactions for human milk fat substitutes production: A review).

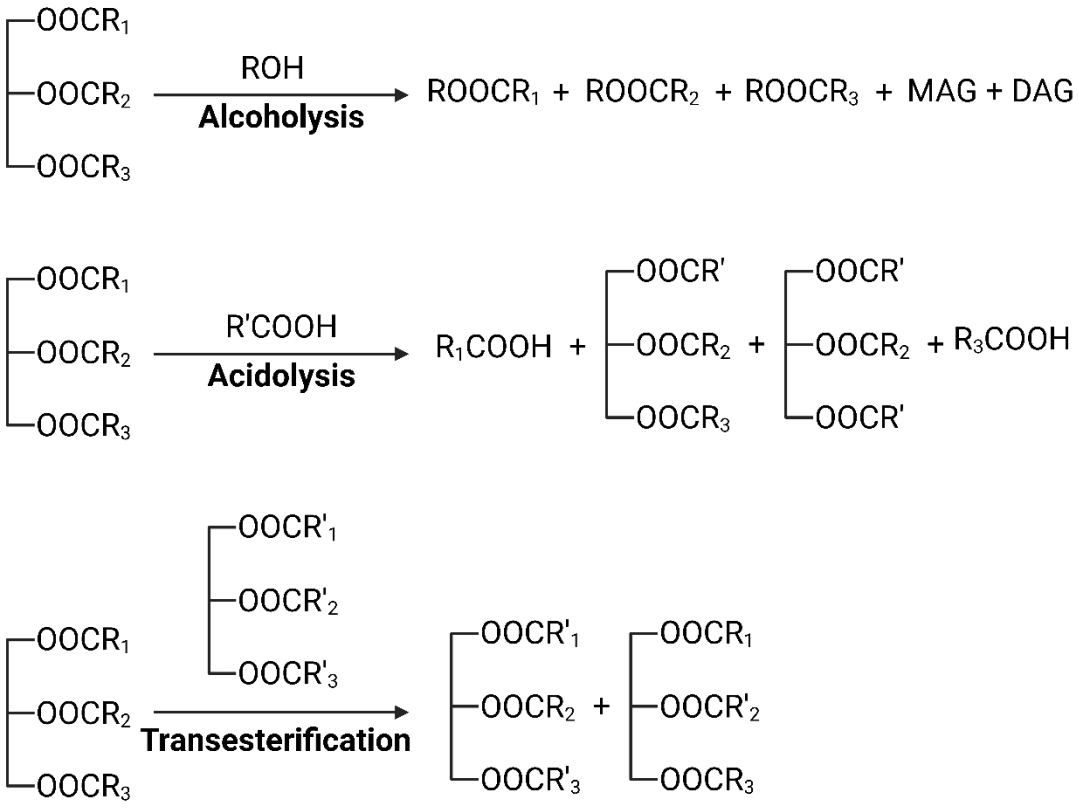

Sonocrystallization

Sonocrystallization is a technique used to control the nucleation and crystal growth of materials using ultrasound. Ultrasound refers to sinusoidal sound waves with a frequency above the upper limit of human hearing, approximately 20 kHz (Martini, 2017; Carrillo-Lopez *et al*., 2021). There are three categories of ultrasound techniques (1) diagnostic ultrasound with frequencies between 1 and 10 MHz, (2) high-frequency ultrasound with frequencies between 100 kHz and 1 MHz, and (3) high-intensity ultrasound with frequencies between 20 and 100 kHz (Martini, 2017; Tiwari and Mason, 2012). Diagnostic and high-frequency ultrasound operate at high frequencies and are non-destructive techniques (Martini, 2017). On the contrary, high-intensity ultrasound operates at low frequencies and high-power levels (10-1000 W cm^{-2}) resulting in significant physicochemical changes of materials (Martini, 2017; Tiwari and Mason, 2012).

In ultrasonic processing, acoustic cavities or bubbles are generated which generate high shear force, high pressures, and high localized temperatures (Pollet and Ashokkumar, 2019). The high shear, pressure, and temperatures result in physicochemical changes in the material. Ultrasound has been examined as a processing tool in the food industry due to it being economical, simple to use, and energy-efficient (Carrillo-Lopez *et al*., 2021). It has been used for emulsification, homogenization, extraction, defoaming, and crystallization processes (Patist and Bates, 2008). When HIU is applied to a fat sample it may increase the number of crystals through both primary and secondary nucleation. HIU promotes primary nucleation by generating bubbles that act as “seeds” that will induce crystallization. Secondary nucleation is a result of the high shear generated by HIU resulting in a dispersion of crystals which act as a starting point for additional crystal

growth (Figure 2-9; Wagh *et al*., 2016).

Figure 2-9: Representation of HIU's impact on crystal size due to shear and cavitation generated during the sonication process.

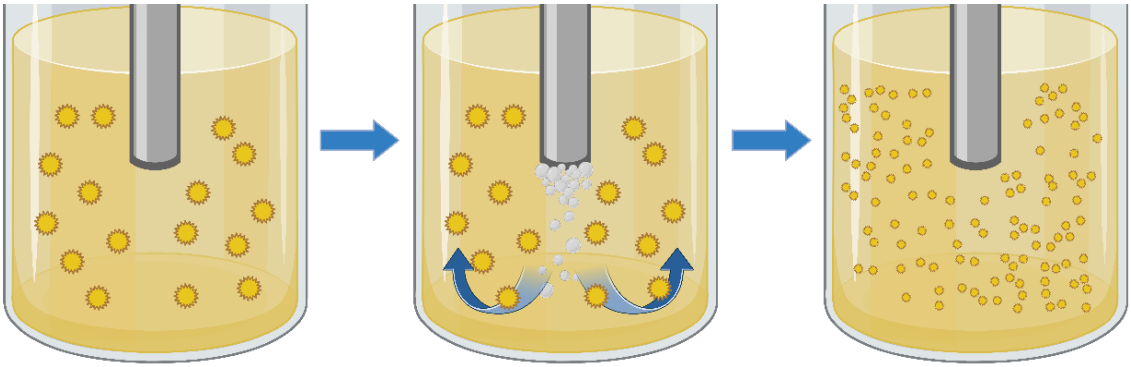

The impact of HIU on chemical composition and lipid oxidation has previously been examined. Hosseini *et al*. (2015) evaluated the effect of sonication on the quality attributes of various oils. In the study, ultrasound (20 kHz, 400 W, 300 s duration) was applied to the oil samples and the FA composition and peroxide value (PV) of the samples were measured after sonication. Hosseini *et al*. (2015) found a significant decrease in linoleic and linolenic acids content for sonicated oils. Conversely, Chemat *et al*. (2004) examined the impact of ultrasonic treatment (20 kHz, 150 W, 30-120 s duration,) on FA composition and PV in refined sunflower oil. The authors found that sonication did not significantly change the FA composition of the oil though it did generate some differences in chemical composition - hexanal and hept-2-enal in the sonicated oil. Moreover, previous work from our laboratory measured TAG and FA composition in an interesterified soybean oil before and after shorter HIU treatment (20 kHz, 110 W, 10 s duration). No significant difference in TAG or FA composition was found due to sonication (Ye, 2015).

In terms of oxidation, the studies described above by Hosseini *et al*. (2015) and Chemat *et al*. (2004) did find that sonication resulted in greater lipid oxidation as indicated by an increase in PV. Indeed, Hosseini *et al*. proposed that the difference in FA composition

for the sonicated oils was due to the lipid oxidation of linoleic and linolenic acids. However, Lee *et al*. (2022) measured the lipid oxidation of soybean oil exposed to various sonication conditions – sample size, power level, tip size, and duration. The oxidation of the samples was determined by measuring PV, oil stability index (OSI), and volatile compounds. The results of the study indicated that sonication did not induce significant lipid oxidation as measured by PV, OSI, and volatile compounds. Discrepancies between Hosseini and Lee's results could be explained by the differences in ultrasonic treatment. In Hosseini *et al*.'s work, samples are sonicated for longer durations (300 s) and higher power (500 W) when compared with Lee *et al*.'s work (5-60 s durations and 0-123.5 W power levels). These results indicate that mild sonication conditions can be used in oils without significantly disrupting the chemical composition and inducing lipid oxidation.

Physical Properties of Fats

Fats are widely used in the food industry due to their unique physical and chemical properties including solid fat content, melting behavior, texture, rheological properties, and crystal size. Each of these properties impact the functionality of fats in food applications.

Solid Fat Content

Solid fat content (SFC) is a physical property of fats that affects the textural and functional properties. SFC is a measurement of the amount of solid fat as a percentage of the total fat (Maragoni, 2005). For products such as fat spreads and chocolate, the SFC over various temperatures is vital to ensure the correct mouthfeel and end use of the product and is calculated by measuring SFC as a function of temperature to produce a SFC curve (Figure 2-10; Martini *et al*., 2006; Torbica et al., 2006). The SFC can be controlled by altering the composition (blending of soft and hard fats), or through processing such as

utilization of different cooling rates and shear (Martini *et al*., 2006).

Figure 2-10: Example of SFC as a function of temperature graph.

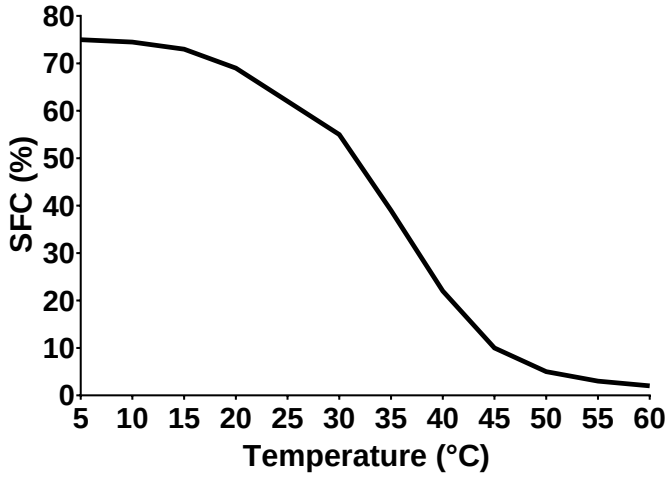

SFC is measured using pulsed nuclear magnetic resonance (p-NMR) which is a non-destructive technique and is based on the concept that proton attributes are different in a solid and liquid phase (Torbica *et al*., 2006). During the p-NMR measurement a fat sample is placed in a strong magnetic field and the nuclei of the fat's hydrogen atoms (protons) align themselves in the direction of the field (Torbica *et al*., 2006). Energy in the form of electromagnetic radiation is applied and the protons are excited to a higher energy spin state. Once the protons relax to the lower energy spin state, they release nonradioactive energy which is used to characterize the molecular state (Hartel, 2001). The efficiency and intensity of relaxation depends on the molecular mobility; therefore, solids and liquids will relax at different times (Torbica *et al*., 2006). Protons in the solid phase relax much faster than those in the liquid phase and by examining the ratio of these relaxation states it is possible to calculate the total solid fat content of a sample (Torbica *et al*., 2006).

Differential Scanning Colorimetry

In the food industry, the thermal properties of crystallization and melting in fats

and oils is imperative (Martini *et al*., 2006). Differential scanning calorimetry (DSC) is a technique that is used to study the thermal properties of materials. In DSC, the heat absorbed or produced in phase transition processes is quantified by comparing the sample to a reference over specific temperature ranges and conditions. During the measurement, an inert gas, usually nitrogen, is used to absorb or release heat. When a phase transition process occurs, a spike is displayed on the resulting thermograph which conveys the amount of heat absorbed or released by the sample.

DSC is a commonly used technique to quantify the type and amount of crystalline material present in a food (Hartel, 2001) and is often used to evaluate fats. It can be used to examine the fractions of low, medium, and high-melting point TAGs present or to determine the melting and crystallization onset temperatures, peak temperatures, and enthalpy absorbed or released during phase transitions.

Texture Analyzer

Texture analysis is commonly used to quantify the various textural properties of materials through large deformation (Martini *et al*., 2006). Although several methods may be used, the most common for food applications is texture profile analysis (TPA). TPA was designed to mimic two bites and is used to quantify various textural properties including hardness, cohesiveness, springiness, and fracturability (Rosenthal, 2010).

The test is a two-step compression or penetration process that measures the force exerted on the geometry creating a force-time graph with two peaks which is used to calculate the textural properties (Figure 2-11). Hardness is observed as the maximum load reached during the first deformation cycle (Paredes *et al*., 2022). Cohesiveness is the ratio between the area under the time/force curve for the second and first compression cycle.

Springiness measures how well a material springs back after it has been deformed and is calculated using the time of the two compressions. Not all materials will fracture but some will, in the force-time graph, fracturability is measured as the first significant peak before the graph drops off.

Figure 2-11: Example of a texture profile analysis curve. Modified with permission from Springer Nature; Food Anal Methods, Vol 15, Issue 144, 2022, Bernardo YA de A, do Rosario DKA, Monteiro MLG, et al. Texture Profile Analysis: How Parameter Settings Affect the Instrumental Texture Characteristics of Fish Fillets Stored Under Refrigeration?

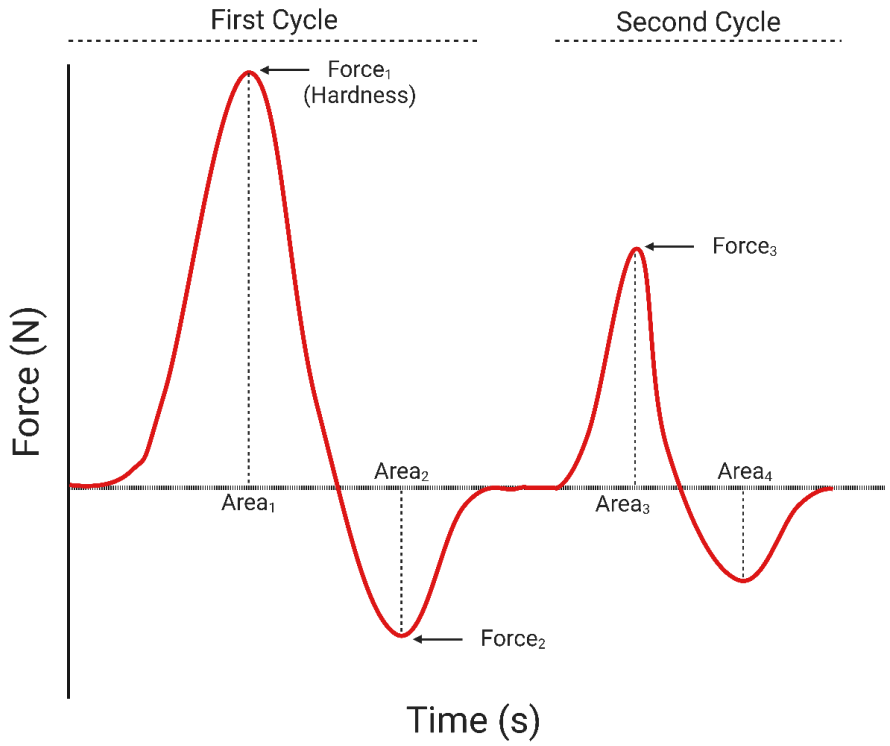

Rheological Properties

Rheology is the science of deformation of materials (Wilson, 2018). How a food deforms plays a vital role in consumer expectations and therefore many studies have examined the rheological properties of semi-solid foods. In small deformation rheology there is no structural damage to the sample, and it is performed in the linear viscoelastic region in which the stress is directly proportional to the strain (Lannes and Ignácio, 2013).

Commonly, viscoelasticity is measured using an oscillatory test in which oscillating stress input is applied to the material and the resulting oscillatory stress output is measured. From these tests it is possible to measure $G^{'}$, $G^{''}$, and phase angles (δ). $G^{'}$ or the storage modulus, is a measurement of the elastic or solid-like behavior of a material. $G^{''}$ or the loss modulus is a measurement of the viscous or liquid-like behavior of a material (Martini *et al*., 2006). From storage and loss moduli it is possible to calculate the phase angle (δ) which is related to the ratio of $G^{''}$ and $G^{'}$. A purely elastic material will have a δ of 0° while a purely viscous material will have a δ of 90°. For viscoelastic materials such as semi-solid fats, δ will lie somewhere between 0° and 90° (Tang and Marangoni, 2006).

Polarized Light Microscopy

To observe the physical structure of fats, several microscopy techniques can be utilized including polarized light microscopy (PLM). PLM is the most popular and practical microscopy technique used to study fat microstructure (Martini *et al*., 2006). PLM is useful in visualization of foods due to allowing the distinguishment of crystals from non-crystalline solids (Hartel, 2001).

During the PLM measurement, a small amount of sample is placed on a microscope slide between two polarizers. Light travels from the source through the first polarizer and is changed to a single orientation, the second polarizer is set cross to the first polarizer blocking any light. When a sample is placed between the two polarizers, it rotates light coming from the first polarizer that is not canceled out by the second polarizer (Hartel, 2001). By utilizing two polarizers and the unique properties of crystalline materials, it is possible to visualize only crystals present in a sample.

REFERENCES

AOCS Official Method. cis-, trans-, Saturated, Monounsaturated, and Polyunsaturated Fatty Acids in Extracted Fats by Capillary GL. 2017.Ce 1j-07.

AOCS Surplus Method. Fatty Acids by GC. 2009.Ce 1k-09.

Afoakwa EO, Paterson A, Fowler M. Factors influencing rheological and textural qualities in chocolate – a review. Trends in Food Science & Technology 2007;18:290–298. DOI: 10.1016/j.tifs.2007.02.002

Ali A, Selamat J, Che Man YB, Suria AM. Effect of storage temperature on texture, polymorphic structure, bloom formation and sensory attributes of filled dark chocolate. Food Chemistry 2001;72:491–497. DOI: 10.1016/S0308-8146(00)00271-5

Bernardo YA de A, do Rosario DKA, Monteiro MLG, et al. Texture Profile Analysis: How Parameter Settings Affect the Instrumental Texture Characteristics of Fish Fillets Stored Under Refrigeration? Food Anal Methods 2022;15:144–156. DOI: 10.1007/s12161-021-02095-0

Berry SE, Bruce JH, Steenson S, et al. Interesterified fats: What are they and why are they used? A briefing report from the Roundtable on Interesterified Fats in Foods. Nutrition Bulletin 2019;44:363–380. DOI: 10.1111/nbu.12397

Berry SEE. Triacylglycerol structure and interesterification of palmitic and stearic acid-rich fats: an overview and implications for cardiovascular disease. Nutr Res Rev 2009;22:3–17. DOI: 10.1017/S0954422409369267

Bhaggan K, Smith KW, Blecker C, Danthine S. Binary Mixtures of Tripalmitoylglycerol (PPP) and 1,3-Dipalmitoyl-2-stearoyl-sn-glycerol (PSP): Polymorphism and Kinetic Phase Behavior. European Journal of Lipid Science and Technology 2018;120:1700306. DOI: 10.1002/ejlt.201700306

Boodhoo MV, Bouzidi L, Narine SS. The binary phase behavior of 1, 3-dipalmitoyl-2-stearoyl-sn-glycerol and 1, 2-dipalmitoyl-3-stearoyl-sn-glycerol. Chemistry and Physics of Lipids 2009;160:11–32. DOI: 10.1016/j.chemphyslip.2009.02.008

Bouzidi L, Boodhoo MV, Kutek T, et al. The binary phase behavior of 1,3-dilauroyl-2-stearoyl-sn-glycerol and 1,2-dilauroyl-3-stearoyl-sn-glycerol. Chem Phys Lipids 2010;163:607–629. DOI: 10.1016/j.chemphyslip.2010.05.002

Bouzidi L, S. Omonov T, Garti N, S. Narine S. Relationships between molecular structure and kinetic and thermodynamic controls in lipid systems. Part I: propensity for oil loss of saturated triacylglycerols. Food & Function 2013;4:130–143. DOI: 10.1039/C2FO30164D

Briones V, Aguilera JM. Image analysis of changes in surface color of chocolate. Food Research International 2005;38:87–94. DOI: 10.1016/j.foodres.2004.09.002

Campos R, Narine SS, Marangoni AG. Effect of cooling rate on the structure and mechanical properties of milk fat and lard. Food Research International 2002;35:971–981. DOI: 10.1016/S0963-9969(02)00159-X

Carocho M, Barreiro MF, Morales P, Ferreira ICFR. Adding Molecules to Food, Pros and Cons: A Review on Synthetic and Natural Food Additives. Comprehensive Reviews in Food Science and Food Safety 2014;13:377–399. DOI: 10.1111/1541-4337.12065

Carrillo-Lopez LM, Garcia-Galicia IA, Tirado-Gallegos JM, et al. Recent advances in the application of ultrasound in dairy products: Effect on functional, physical, chemical, microbiological and sensory properties. Ultrason Sonochem 2021;73:105467. DOI: 10.1016/j.ultsonch.2021.105467

Chemat F, Grondin I, Costes P, et al. High power ultrasound effects on lipid oxidation of refined sunflower oil. Ultrason Sonochem 2004;11:281–285. DOI: 10.1016/j.ultsonch.2003.07.004

Cikrikci S, Oztop MH. Oil migration in hazelnut paste/chocolate systems using magnetic resonance imaging. Food Measure 2018;12:1460–1472. DOI: 10.1007/s11694-018-9761-0

Da Pieve S, Calligaris S, Co E, et al. Shear Nanostructuring of Monoglyceride Organogels. Food Biophysics 2010;5:211–217. DOI: 10.1007/s11483-010-9162-3

da Silva TLT, Cooper Z, Lee J, et al. Tailoring Crystalline Structure Using High-Intensity Ultrasound to Reduce Oil Migration in a Low Saturated Fat. Journal of the American Oil Chemists' Society 2020a;97:141–155. DOI: 10.1002/aocs.12321

da Silva TLT, Danthine S, Martini S. Effect of processing conditions as high-intensity ultrasound, agitation, and cooling temperature on the physical properties of a low saturated fat. J Food Sci 2020b;85:3380–3390. DOI: 10.1111/1750-3841.15436

da Silva TLT, Fernandes GD, Arellano DB. Development of reduced saturated fat cookie fillings using multicomponent oleogels. Journal of the American Oil Chemists' Society 2021;98:1069–1082 DOI: 10.1002/aocs.12527

da Silva TLT, Marsh M, Gibon V, Martini S. Sonocrystallization as a tool to reduce oil migration by changing physical properties of a palm kernel fat. J Food Sci 2020c;85:964–971. DOI: 10.1111/1750-3841.15099

Delbaere C, Van de Walle D, Depypere F, et al. Relationship between chocolate microstructure, oil migration, and fat bloom in filled chocolates. European Journal of Lipid Science & Technology 2016;118:1800–1826. DOI: 10.1002/ejlt.201600164

Dibildox-Alvarado E, Rodrigues JN, Gioielli LA, et al. Effects of Crystalline Microstructure on Oil Migration in a Semisolid Fat Matrix. Crystal Growth & Design 2004;4:731–736. DOI: 10.1021/cg049933n

Farfán M, Álvarez A, Gárate A, Bouchon P. Comparison of Chemical and Enzymatic Interesterification of Fully Hydrogenated Soybean Oil and Walnut Oil to Produce

a Fat Base with Adequate Nutritional and Physical Characteristics. Food Technol Biotechnol 2015;53:361–366. DOI: 10.17113/ftb.53.03.15.3854

Finley JW, deMan JM. Lipids. In: deMan JM, Finley JW, Hurst WJ, Lee CY (eds) Principles of Food Chemistry. Springer International Publishing, Cham, 2018, pp 39–116.

Fontecha J, Goudjil H, Ríos JJ, et al. Identity of the major triacylglycerols in ovine milk fat. Int Dairy J 2005;15:1217–1224.

Giacomozzi AS, Palla CA, Carrín ME, Martini S. Physical Properties of Monoglycerides Oleogels Modified by Concentration, Cooling Rate, and High-Intensity Ultrasound. Journal of Food Science 2019;84:2549–2561. DOI: 10.1111/1750-3841.14762

Gibon V. Enzymatic interesterification of oils. Lipid Technology 2011;23:274–277. DOI: 10.1002/lite.201100159

Gorrepati K, Balasubramanian S, Chandra P. Plant based butters. Journal of Food Science and Technology 2015;52:3965. DOI: 10.1007/s13197-014-1572-7

Gunstone F. Introduction: Modifying lipids – why and how? In: Gunstone FD (ed) Modifying Lipids for Use in Food. Woodhead Publishing, 2006, pp 1–8.

Hartel RW. Crystallization in Foods. Springer, 2001.

Hosseini S, Gharachorloo M, Tarzi BG, et al. Effects of Ultrasound Amplitude on the Physicochemical Properties of Some Edible Oils. Journal of the American Oil Chemists' Society 2015;92:1717–1724. DOI: 10.1007/s11746-015-2733-1

Lannes SC da S, Ignácio RM. Structuring Fat Foods. IntechOpen, 2013.

Lee J, Legako JF, Martini S. Degree of oxidation of sonicated soybean oil using various sonication process parameters. International Journal of Food Science & Technology 2022;57:4473–4482. DOI: 10.1111/ijfs.15781

Lonchampt P, Hartel RW. Fat bloom in chocolate and compound coatings. European Journal of Lipid Science and Technology 2004;106:241–274. DOI: 10.1002/ejlt.200400938

Ma X, Hu Z, Mao J, et al. Synthesis of cocoa butter substitutes from Cinnamomum camphora seed oil and fully hydrogenated palm oil by enzymatic interesterification. J Food Sci Technol 2019;56:835–845. DOI: 10.1007/s13197-018-3543-x

Maleky F. Oil Migration Through Fats—Quantification and Its Relationship to Structure. 2018, pp 241–266.

Maleky F, Marangoni A. Nanoscale effects on oil migration through triacylglycerol polycrystalline colloidal networks. Soft Matter 2011. DOI: 10.1039/C1SM05154G

Maleky F, McCarthy KL, McCarthy MJ, Marangoni AG. Effect of Cocoa Butter Structure on Oil Migration. Journal of Food Science 2012;77:E74–E79. DOI: 10.1111/j.1750-3841.2011.02575.x

Marangoni AG. Fat Crystal Networks. Marcel Dekker, 2005.

Martini S. Effect of Ultrasound on the Physicochemical Properties of Lipids. In: Ultrasound in Food Processing. John Wiley & Sons, Ltd, 2017, pp 464–484.

Marty S, Baker K, Dibildox-Alvarado E, et al. Monitoring and quantifying of oil migration in cocoa butter using a flatbed scanner and fluorescence light microscopy. Food Research International 2005;38:1189–1197. DOI: 10.1016/j.foodres.2005.04.008

Metin S, Hartel RW. Crystallization behavior of blends of cocoa butter and milk fat or milk fat fractions. J Therm Anal 1996;47:1527–1544. DOI: 10.1007/BF01992844.

Metin S, Hartel RW. Crystallization of Fats and Oils. In: Bailey's Industrial Oil and Fat Products. John Wiley & Sons, Ltd, 2005.

Mohamed S, Perignon M, Villeneuve P. Lipase-catalyzed interesterification reactions for human milk fat substitutes production: A review. European Journal of Lipid Science and Technology 2013;115:270–285. DOI: 10.1002/ejlt.201200084

Mohd Rozalli NH, Chin NL, Yusof YA, Mahyudin N. Quality changes of stabilizer-free natural peanut butter during storage. J Food Sci Technol 2016;53:694–702. DOI: 10.1007/s13197-015-2006-x

Naik B, Kumar DrV. Cocoa butter and its alternatives: A review. J Biores Eng Technol 2014;1:7–17.

Nelson D, Cox M. Lipids. In: Lehninger Principles of Biochemistry. W. H. Freeman and Company, New York, NY, 2013, pp 357–385.

Omonov TS, Bouzidi L, Narine SS. Quantification of oil binding capacity of structuring fats: A novel method and its application. Chemistry and Physics of Lipids 2010;163:728–740. DOI: 10.1016/j.chemphyslip.2010.07.003

Onacik-Gür S, Żbikowska A. Effect of high-oleic rapeseed oil oleogels on the quality of short-dough biscuits and fat migration. J Food Sci Technol 2020;57:1609–1618. DOI: 10.1007/s13197-019-04193-8

Palla CA, Wasinger MF, Carrín ME. Monoglyceride oleogels as fat replacers in filling creams for sandwich cookies. Journal of the Science of Food and Agriculture 2020;101:2398–2405. DOI: 10.1002/jsfa.10863

Paredes J, Cortizo-Lacalle D, Imaz AM, et al. Application of texture analysis methods for the characterization of cultured meat. Sci Rep 2022;12:3898. DOI: 10.1038/s41598-022-07785-1

Patist A, Bates D. Ultrasonic innovations in the food industry: From the laboratory to commercial production. Innovative Food Science & Emerging Technologies 2008;9:147–154. DOI: 10.1016/j.ifset.2007.07.004

Pollet BG, Ashokkumar M. Introduction to Ultrasound, Sonochemistry and Sonoelectrochemistry. In: Pollet BG, Ashokkumar M (eds) Fundamental and Applied Aspects of Ultrasonics and Sonochemistry. Springer International Publishing, Cham, 2019, pp 1–19.

Rashid NA, Kamarulzaman NA, Omar Z. Influence of enzymatic and chemical interesterification on crystallisation properties of refined, bleached and deodourised (RBD) palm oil and RBD palm kernel oil blends. Food Research International 2018;106:982–991. DOI: 10.1016/j.foodres.2018.02.001

Rosenthal A. Texture Profile Analysis – How important are the parameters? Journal of Texture Studies 2010;41:672–684. DOI: 10.1111/j.1745-4603.2010.00248.x

Rousseau D, Mirzaee Ghazani S, Marangoni A. Chemical Interesterification of Food Lipids: Chemistry, Nutrition, and Biotechnology, Fourth Edition, 2017, pp 349–380.

Sato K. Crystallization behaviour of fats and lipids — a review. Chem Eng Sci 2001;56:2255–2265. DOI: 10.1016/S0009-2509(00)00458-9.

Sato K. Crystallization of Lipids: Fundamentals and Applications in Food, Cosmetics, and Pharmaceuticals. John Wiley & Sons, 2018.

Silva TLT da, Grimaldi R, Gonçalves LAG. Temperature, time and fat composition effect on fat bloom formation in dark chocolate. Food Structure 2017;14:68–75. DOI: 10.1016/j.foostr.2017.06.006

Smith KW, Cain FW, Talbot G. Effect of nut oil migration on polymorphic transformation in a model system. Food Chemistry 2007;102:656–663. DOI: 10.1016/j.foodchem.2006.05.045

Svanberg L, Ahrné L, Lorén N, Windhab E. Effect of sugar, cocoa particles and lecithin on cocoa butter crystallisation in seeded and non-seeded chocolate model systems. Journal of Food Engineering 2011;104:70–80. DOI: 10.1016/j.jfoodeng.2010.09.023

Talbot G. Science and technology of enrobed and filled chocolate, confectionery and bakery products. Woodhead Publishing, 2009.

Tang D, Marangoni AG. Microstructure and fractal analysis of fat crystal networks. J Amer Oil Chem Soc 2006;83:377–388. DOI: 10.1007/s11746-006-1216-9

Tiwari BK, Mason TJ. Ultrasound Processing of Fluid Foods. In: Cullen PJ, Tiwari BK, Valdramidis VP (eds) Novel Thermal and Non-Thermal Technologies for Fluid Foods. Academic Press, San Diego, 2012, pp 135–165.

Torbica A, Jovanovic O, Pajin B. The advantages of solid fat content determination in cocoa butter and cocoa butter equivalents by the Karlshamns method. Eur Food Res Technol 2006;222:385–391. DOI: 10.1007/s00217-005-0118-7

Wagh A, Birkin P, Martini S. High-Intensity Ultrasound to Improve Physical and Functional Properties of Lipids. Annual Review of Food Science and Technology 2016;7:23–41. DOI: 10.1146/annurev-food-041715-033112

Wang H, Shi X, Paluri S, Maleky F. Effects of processing and added ingredients on oil diffusion through cocoa butter using magnetic resonance imaging. RSC Adv 2016;6:88498–88507. DOI: 10.1039/C6RA11196C

Wilson DI. What is rheology? Eye (Lond) 2018;32:179–183. DOI: 10.1038/eye.2017.267

Wolfrum C, Lang H, Moser H, Jordan W. Determination of Diffusion Coefficients Based on Ficks Second Law for Various Boundary Conditions. Radiochimica Acta 1988;44–45:245–250. DOI: 10.1524/ract.1988.4445.2.245

Yamoneka J, Malumba P, Lognay G, et al. Enzymatic Inter-Esterification of Binary Blends Containing Irvingia gabonensis Seed Fat to Produce Cocoa Butter Substitute. European Journal of Lipid Science and Technology 2018;120:1700423. DOI: 10.1002/ejlt.201700423

Yanık DK, Keskin H, Fadıloğlu S, Göğüş F. Acidolysis Reaction of Terebinth Fruit Oil with Palmitic and Caprylic Acids to Produce Low Caloric Spreadable Structured Lipid. Journal of the American Oil Chemists' Society 2013;90:999–1009. DOI: 10.1007/s11746-013-2250-z

Ye Y. Effect of High Intensity Ultrasound on Crystallization Behavior and Functional Properties of Lipids.

Zhang Z, Lee WJ, Wang Y. Evaluation of enzymatic interesterification in structured triacylglycerols preparation: a concise review and prospect. Critical Reviews in Food Science and Nutrition 2021;61:3145–3159. DOI: 10.1080/10408398.2020.1793725

Figures 2-2, 2-3, 2-4, 2-5, 2-6, 2-8, 2,9, and 2-11 were created with BioRender.com.

CHAPTER III. RELATIONSHIP BETWEEN OIL BINDING CAPACITY AND PHYSICAL PROPERTIES OF INTERESTERIFIED SOYBEAN OIL[1]

ABSTRACT

The objective of this study was to identify the physical properties of an interesterified soybean oil (EIESOY), containing 45% saturated fatty acids (SFA), that correlates with high oil binding capacity (OBC). In this study, three EIESOY samples were analyzed; a 100% sample, a 50% sample diluted with 50% soybean oil, and a 20% sample diluted with 80% soybean oil. All samples were crystallized using fast (7.78 °C/min) and slow (0.1 °C/min) cooling rates as well as with and without high-intensity ultrasound (HIU, 20 kHz). The 100%, 50%, and 20% samples were crystallized at 38.5 °C, 27.0 °C, and 22.0 °C; respectively. HIU was applied at the onset of crystallization and all samples were allowed to crystallize isothermally for 90 min. After 90 min, physical properties such as crystal microstructure, hardness, solid fat content (SFC), viscoelasticity, and melting behavior were evaluated. The aforementioned physical properties were also measured after storage for 48 h at 22 °C and 5 °C as well as the OBC_c and the OBC_p measurement was started and continued for 7 days. Results show that OBC_c was correlated with hardness, SFC, enthalpy, Tpeak, G, and G´´. Additionally, OBC_p was positively correlated with hardness, SFC, enthalpy, G´, and G´´. Neither measurement of OBC was correlated with crystal diameter nor the number of crystals.

[1]Reprinted (with modification) from the Journal of American Oil Chemists' Society. Abigail Marsh M and Martini S. Relationship between oil binding capacity and physical properties of interesterified soybean oil. Volume 99, February 2022, 313–330. Original copyright notice as given in the publication in which the material was originally published with permission from John Wiley and Sons.

INTRODUCTION

Oil migration is a common occurrence in fat-based foods such as truffles, peanut butter cups, and natural nut butters and is observed as a movement of liquid oil in the fat matrix. This movement can cause undesirable properties in many products including filled chocolates with fat-based centers where oil migrates from the fat filling to the chocolate coating. Some of the defects caused by oil migration include fat bloom development on the surface of the chocolate, hardening of the filling, and softening of the chocolate coating (Smith *et al.*, 2007). Oil migration is determined by the fat's oil binding capacity (OBC) which describes the ability of the fat matrix to entrap liquid oil, therefore, preventing oil migration from occurring. The OBC of fats can be influenced by processing conditions including cooling rate (Dibildox-Alvarado *et al.*, 2004), shear (Acevedo *et al.*, 2012a; 2012b), and high-intensity ultrasound (HIU) (da Silva *et al.*, 2020a; 2020b, 2020c). OBC can also be influenced by the chemical composition of the samples such as the type and concentration of triacylglycerols (TAG) (Ghosh *et al.*, 2002). The effect of processing conditions and chemical composition on OBC is ultimately determined by the physical properties of the crystalline networks obtained. Healthy fats with low levels of saturated fatty acids (SFAs) are desirable for human health. However, they lack some of the physical properties needed for certain food applications and they can be difficult to incorporate into fat-based foods as they can result in oil migration occurring due to the low OBC. Thus, it is vital to understand what physical properties of fats are most influential in increasing OBC to aid in the development of healthy fats with high OBC.

Since OBC is essential in reducing the amount of oil migrating from the fat matrix, many studies have examined the relationship between the physical properties of fats and

OBC with mixed results. One study found that larger fat crystals resulted in greater oil migration and therefore lower OBC (Dibildox-Alvarado *et al.*, 2004). However, a study by Green and Rousseau (2015) found a non-linear relationship between oil migration and microstructure. Additionally, Acevedo *et al.* (2017) found that higher solid fat content (SFC) resulted in less oil movement in soy-based fat while other studies found no relationship between oil migration and SFC (Si *et al.*, 2016; Acevedo *et al.*, 2012a).

Although many studies have examined the relationship between the physical properties of fats and OBC, these studies may have confounding factors that conceal which factor, or combination of factors are responsible for higher OBC. For example, usually, harder fats with high SFC and small crystals have higher OBC, but it is not known if the fat has a higher OBC due to only SFC, a combination of SFC and crystal size, or a combination of hardness, SFC, and crystal size. The purpose of this research was to identify which physical properties of an interesterified soybean-based fat (EIESOY) sample correlate with high OBC. To do this, a wide range of physical properties was generated through various processing conditions such as cooling rate, level of SFAs, and the use of high-intensity ultrasound (HIU).

MATERIALS AND METHODS

Materials

An EIESOY supplied by Archer Daniels Midland (ADM, Decatur, IL) was used in this research. According to the information supplied by the manufacturer, the EIESOY contained 45% SFAs, 16.0% cis-monounsaturated fatty acids, 39% cis-polyunsaturated fatty acids, and 1.5% trans fatty acids. Three concentrations of the EIESOY sample were

used to evaluate how the concentration of SFAs influenced OBC and OL. The objective of using various concentrations of EIESOY was to obtain a similar crystal size but decreased hardness and SFC. The first sample was the 100% sample which was undiluted EIESOY that had a high SFA content of 45%.

The other two concentrations were created by mixing the EIESOY with soybean oil purchased from a local grocery store (Great Value). The second concentration was a 50% sample diluted with 50% soybean oil (w/w) that had an intermediate SFA content of 29.6%. The third concentration was a 20% sample diluted with 80% soybean oil (w/w) that had a low SFA content of 20.4%. After formulating each concentration, the samples were melted and filtered to remove any contaminants.

Fatty Acid Analysis

The fatty acid composition was determined using gas chromatography (GC; Shimadzu 2010, Columbia, MD, USA) equipped with a flame ionization detector (Shimadzu, Columbia, MD, USA). The analysis involved the conversion of fatty acids to fatty acid methyl esters (FAME) through trans-esterification. Initially, samples were melted at 60 °C for 15 min. Afterwards, 40 µL of the melted sample was mixed with 6.3 mL of MeOH and 0.7 mL of 10N KOH in water in a culture tube. The mixture was then incubated in a 55 °C water bath for 90 min with auto shaking. After cooling, 0.58 mL of 24 N H_2SO_4 was added, followed by another 90 min incubation at 55 °C. Next, 2 mL of hexane was added to the tube and thoroughly mixed before centrifugation. The upper hexane layer containing the FAME was transferred to a 2 mL GC vial and injected into the GC column (Agilent Technologies, Santa Clara, CA, USA). Hydrogen was used as the carrier gas with a linear velocity of 41 cm/s. The initial oven temperature was set at 125

°C, ramped to 145 °C at a rate of 26.2 °C/min, and held for 7.9 min. The temperature was then increased at a rate of 6.5 °C/min until it reached 220 °C and maintained for 8 min. Both the injector and detector temperatures were set at 250 °C. Peak identification was achieved by comparing retention times with FAME standards (GLC 463, NuChek Prep, Elysian, MN, USA). The analysis was conducted in duplicate, and results were reported as normalized area percentages.

Melting Point

To measure the melting point of the samples, a differential scanning calorimeter was used and calibrated using a pure indium standard. The melting point was measured by filling a hermetic aluminum pan with 5-15 mg of sample and sealing it with a lid. The sample was then placed in a freezer at -20 °C for one week to develop the most stable polymorphic form. After one week, the sample was placed in a DSC oven set at -20 °C, left at this temperature for 1 min, and then heated to 100 °C using a ramp rate of 20 °C/min. The melting peak observed at the highest temperature was used to determine the melting point. This measurement was performed in duplicate.

Crystal Polymorphism

The polymorphic form of the samples was measured with an X-ray diffraction system that had a PW3050/00 (θ/2-θ) goniometer. The radiation source was Cu Kα and a P23123/00 monochromator detector system was used. The following samples were measured - 100% EIESOY FCR wo HIU 90 min and 48 h 5 °C, 100% EIESOY FCR w HIU 90 min and 48 h 5°C, 50% EIESOY FCR wo HIU at all time points, 50% EIESOY FCR w HIU 90 min and 48 h 5°C, 50% EIESOY SCR w HIU 90 min and 48 h 22 °C, 20% EIESOY FCR wo HIU 90 min and 48 h 22 °C, 20% EIESOY FCR w HIU 90 min and 48

h 22 °C, and 20% EIESOY SCR wo HIU 48 h and 22 °C. These samples were chosen based on the peak temperature and crystal microstructure. Prior to measuring, the samples were filtered under vacuum to concentrate the crystals and obtain a better resolution. An alpha polymorphic form was identified with a peak at 4.2 Å, a β' polymorphic form was identified with two peaks at 3.8 Å and 4.2 Å, a β polymorphic form was identified with two peaks at 3.8 Å and 4.6 Å (Marangoni, 2004; Sato, 2018).

Crystallization

Prior to crystallization, 100 g of sample was completely melted and placed in a 100 °C oven for 30 min to erase the crystal memory. The sample was then poured into a double-wall crystallization cell connected to an external water bath to control the temperature. A thermocouple was placed in the crystallization cell to monitor the sample's temperature during crystallization. When the sample was placed into the crystallization cell, a timer was started, and this was time zero. The sample was crystallized using 200 rpm agitation with a magnetic stirrer which was started prior to the addition of the sample. The samples were crystallized at 38.5 °C, 27.0 °C, and 22.0 °C for the 100%, 50%, and 20% samples, respectively.

HIU has previously been found to be most effective when it is applied at the onset of crystallization (Ye and Martini, 2011), under static conditions (Kadamne and Martini, 2018), and when crystallization occurs slowly (Martini *et al.*, 2008). Therefore, the crystallization temperatures were chosen to ensure the onset of crystallization occurred between 0 and 20 min after stopping agitation. In this study, HIU was applied to the samples using a 3.2 mm titanium tip, 10 s pulse duration, 20 kHz frequency, 216 μm amplitude, and 90 W power. HIU was used to change the crystal size while minimizing

changes in SFC values.

In addition to using HIU, samples were crystallized using either a fast-cooling rate (FCR) (7.78 ± 1.2°C/min) or a slow-cooling rate (SCR) (0.1 °C/min). These two cooling rates were selected to generate different physical properties in the samples and therefore, different OBC and OL. The FCR samples were added to the crystallization cell with the water bath set to the crystallization temperature and allowed to crystallize isothermally for 90 min. For the SCR samples, the temperature was controlled using a programmable water bath which was set to 60 °C and decreased 0.1 °C/min until the crystallization temperature was reached. Once the crystallization temperature was reached, the sample was allowed to crystallize isothermally for 90 min. Table 3-1 summarizes the crystallization conditions that were used.

Table 3-1 Summary of crystallization conditions for each sample. Total duration is the total time the sample was in the cell. Agitation stopped is the time that the magnetic stirrer was stopped with time zero being the time at which the sample was added to the cell. Agitation stopped is the time that the magnetic stirrer was stopped with time zero being the time at which the sample was added to the cell. HIU applied is the time that high intensity ultrasound was applied to the system.

Crystallization Conditions				
Sample	Crystallization Temp. (°C)	Total Duration (min)	Agitation stopped (min)	HIU applied (min)
100% EIESOY FCR	38.5	90	10	27
100% EIESOY SCR	38.5	305	190	190
50% EIESOY FCR	27.0	90	8	10
50% EIESOY SCR	27.0	420	210	225
20% EIESOY FCR	22.0	90	10	15
20% EIESOY SCR	22.0	470	275	295

Crystal Microstructure

Crystal morphology was examined by placing a drop of sample on a microscope slide with a slide cover and observing the crystals with a polarized light microscope using a 10X objective lens. The microscope was connected to a camera to capture images of the

samples. Three pictures were captured for each experimental run. Crystal morphology was measured after 90 min, 48 h at 22 °C, and 48 h at 5 °C. Crystal size analysis was performed on the captured images to measure the mean diameter of the crystals and the number of crystals using the software Image-Pro® Premier E 9.2.

Solid Fat Content

Solid fat content was measured using a time-domain nuclear magnetic resonance equipment. Immediately after the sample had finished crystallizing in the cell, six NMR tubes were filled with the sample and used to measure SFC. Afterward, three tubes were stored at 22 °C and three were stored at 5 °C. After the samples had been stored for 48 h the SFC of the samples was measured.

Hardness

To measure hardness, 10 mL beakers (22 mm diameter and 35 mm height) were filled with sample and a two-cycle penetration test was performed using a texture analyzer. The texture analyzer was fitted with a 6-mm diameter cylindrical probe and a 50 N load cell. The probe was lowered 15 mm into the sample at a crosshead speed of 1 mm/s, returned to the zero position above the sample, paused for 10 s, lowered 15 mm into the sample again, and return to the zero position to complete the two-cycle penetration test. Hardness values were obtained from the resulting force-time curve and represents the maximum force from the first cycle. Hardness was measured after the samples had finished crystallizing in the cell as well as after storage for 48 h at 22 °C and 5 °C. This measurement was performed in triplicate.

Viscoelasticity

The viscoelasticity of the samples was measured with a rheometer after 90 min as

well as after storage. An oscillatory test was performed using a strain sweep procedure from 0.001% to 10% at a constant frequency of 1 Hz to determine the storage modulus (G´) from the linear viscoelastic region. An 8 mm diameter parallel plate geometry and a gap of between 500 and 2000 µm was used, depending on the hardness of the sample. Prior to placing the sample on the rheometer stage, the stage was set to the crystallization or storage temperature. Approximately one-eighth of a teaspoon of the sample was used to measure elasticity immediately after crystallization. The remaining sample was then placed in molds (9 mm diameter and 1 mm height) and stored at either 5 °C or 22 °C for 48 h. After storage, the samples were unmolded and placed on the rheometer stage to measure elasticity. Some samples were too soft to be molded (50% EIESOY 22 °C, 20% EIESOY 22 °C and 5 °C). These samples were measured in the same way that the samples were measured immediately after crystallization, using approximately one-eighth of a teaspoon of the sample. This measurement was performed in triplicate.

Melting Behavior

The melting behavior of the samples was measured using a differential scanning calorimeter, calibrated using pure indium standard, and using an empty pan as a reference. A hermetic aluminum pan was filled with 5-15 mg of sample and sealed. The sample was then placed in the DSC oven set to the crystallization or storage temperature. The sample was allowed to sit at this temperature for 1 min to stabilize and then the temperature increased 5 °C/min until it reached 80 °C, using an empty pan as the reference. Melting behavior measurements were taken after 90 min, after 48 h at 22 °C, and after 48 h at 5 °C. The overall peak temperature and change in enthalpy were then calculated from the resulting melting profiles. Additionally, the peak temperature and enthalpy was calculated

for the three peaks present in the 100% and 50% samples stored at 5 °C. This measurement was performed in duplicate.

Oil Binding Capacity

In this study, oil binding capacity was evaluated using two methods – a centrifuge method (OBC_c) and a filter paper method (OBC_p) as described below.

Centrifuge Method

OBC_c was measured using a centrifuge method previously described in other studies (da Pieve *et al.*, 2010; da Silva *et al.*, 2020a; 2020b; 2020c; Giacomozzi *et al.*, 2019). Approximately 1 g of the sample was placed in a pre-weighed microcentrifuge tube, placed in a centrifuge, and spun for 15 min at 10,000 rpm. Four tubes were prepared for each treatment after storage for 48 h at 22 °C and 5 °C. In this study, two different centrifuges were used to control the temperature of the samples. The first centrifuge was placed at room temperature, and the second centrifuge was placed in a sliding door cooler at 5 °C. After the samples had finished centrifuging, they were inverted and left to drain the liquid oil for 3 min. After 3 min, the tubes were weighed again to measure the amount of oil loss that had occurred. The following equation was used to calculate the amount of oil loss and resulting OBC_c [1]:

$$OBC_c\ (\%) = (1 - \left(\frac{w_{tb}\ (g) - w_{ta}\ (g)}{w_s\ (g)}\right)) \times 100 \quad [1]$$

Where w_{tb} is the weight of the tube and the sample prior to centrifugation, w_{ta} is the weight of sample and tube after centrifugation and inversion for 3 min, and w_s is the weight of the sample.

Filter Paper Method

OBC_p of the samples was measured using a filter paper method as previously described (Dibildox-Alvarado *et al.*, 2004; Acevedo *et al.*, 2012a; Acevedo *et al.*, 2017; Altimiras *et al.*, 2007, Peyronel et al., 2016). After the samples had finished crystallizing in the cell, they were placed in circle molds (40 mm diameter, 3mm height) and stored at 22 °C and 5 °C. Four molds were prepared for each storage temperature. After 48 h, the samples were unmolded, weighed, and placed on a pre-weighed circle filter paper (Whatman #1,125mm diameter) then stored again at 22 °C and 5 °C. In addition to the samples, a pre-weighed filter paper was used as a control at each storage temperature. Every day for seven days, the samples were removed from the filter papers, the filter papers were weighed, the samples were replaced and stored again at the appropriate temperature. The OBC_p of the samples was calculated using the following equation [2]:

$$OBC_p = \left[1 - \left(\frac{w_{p(t)} - w_{p(0)}}{w_{s(0)}}\right)\right] * 100 \quad [2]$$

Where $w_{p(t)}$ is the weight of the filter paper at specific times (0-7 days), $w_{p(0)}$ is the weight of the filter paper at time zero, and $w_{s(0)}$ is the weight of the sample at time zero. The difference in the control filter paper's weight was used to correct for environmental changes.

Statistical Analysis

Crystallization experiments were performed in triplicate, and the reported data are mean values and standard errors. Two-way ANOVA tests and t-tests were used to measure significant differences (α=0.05). Correlation analysis was performed between each physical property for all sample conditions and dilutions. Spearman correlation analysis was chosen over Pearson correlation due to the nonlinear relationship between OBC and

the physical properties (Figure A-1). All analysis was performed using GraphPad Prism software version 9 for Windows.

RESULTS AND DISCUSSION

As mentioned in the Introduction, the objective of this study is to evaluate the effect of physical properties on OBC. Various physical properties were obtained by changing the content of saturated fatty acids in the sample and by using various processing conditions. The physical properties obtained under these conditions will be shown and discussed first, and the relationships with OBC will be discussed later.

Fatty Acid Composition

Fatty acid composition is summarized in Table 3-2. The 100% EIESOY sample contained 84.93% ± 0.08 C18 fatty acids namely stearic (31.30% ± 0.07), linoleic (35.31% ± 0.02), and oleic (13.60% ± 0.02) acids. The 50% EISOY sample was comprised of 86.29% ± 0.12 C18 fatty acids with the highest proportion coming from linoleic acid (44.82% ± 0.01) followed by almost equal amounts of stearic and oleic acid (17.85% ± 0.11) and (17.82% ± 0.03); respectively. The 20% EIESOY sample had the highest percentage of linoleic acid (49.22% ± 0.02) and the lowest percentage of stearic acid (9.73% ± 0.04) when compared with the other samples.

Table 3-2: Mean fatty acid composition (% w/w) and standard errors for the 100% EIESOY, 50% EIESOY, and 20% EIESOY samples.

Fatty Acid	100% EIESOY	50% EIESOY	20% EIESOY
C8:0	0.07 ± 0.01	0.02 ± 0.01	0.03 ± 0.01
C10:0	0.10 ± 0.01	0.07 ± 0.01	0.11 ± 0.01
C12:0	0.55 ± 0.01	0.01 ± 0.01	0.01 ± 0.01
C14:0	0.25 ± 0.01	0.06 ± 0.01	0.06 ± 0.01
C16:0	10.39 ± 0.01	10.36 ± 0.01	10.25 ± 0.01
C16:1n7	0.05 ± 0.01	0.06 ± 0.01	0.08 ± 0.01
C18:0	31.30 ± 0.07	17.85 ± 0.11	9.73 ± 0.04
C18:1	13.60 ± 0.02	17.82 ± 0.03	20.90 ± 0.03
C18:2n6	35.31 ± 0.02	44.82 ± 0.01	49.22 ± 0.02
C18:3n3	4.72 ± 0.01	5.80 ± 0.01	6.55 ± 0.01
C20:0	0.47 ± 0.01	0.42 ± 0.01	0.41 ± 0.01
C20:1n9	0.12 ± 0.01	0.16 ± 0.01	0.18 ± 0.01
C20:2n6	0.02 ± 0.01	0.03 ± 0.01	0.03 ± 0.01
C20:3n6	0.05 ± 0.01	0.05 ± 0.01	0.04 ± 0.01
C22:0	0.32 ± 0.01	0.31 ± 0.01	0.34 ± 0.01
C24:0	0.10 ± 0.01	0.10 ± 0.01	0.10 ± 0.01
Others	2.60 ± 0.01	2.05 ± 0.11	1.97 ± 0.03
SFA	43.54 ± 0.05	29.21 ± 0.12	21.04 ± 0.04

Melting Point

The melting point of the samples was determined using a differential scanning calorimeter and was found to be 52.8 ± 0.8 ºC for the 100% sample, 50.8 ± 1.1 ºC for the 50% sample, and 46.3 ± 1.9 ºC for the 20% sample. The difference in MP between the concentrations was expected due to the dilution of high melting TAGs from the interesterified soybean oil with low melting TAGs from the soybean oil (Table 3-2).

Crystal Microstructure

Figure 3-1, Figure A-2 show the crystal morphology after 90 min and 48 h; respectively, and Table 3-3 summarizes the mean crystal diameter and number of crystals. For the non-sonicated samples, the 100% sample formed large, ill-defined spherulites that were in the β´ polymorph as indicated by the XRD measurement with peaks at 3.8 ± 0.1 Å and 4.2 ± 0.1 Å. Both the non-sonicated 50% and 20% samples formed defined spherulite shaped crystals with some bright, small crystals due to the samples containing both β´ and β crystals indicated by peaks at 3.8 ± 0.1 Å, 4.2 ± 0.1 Å, and 4.6 ± 0.1 Å. For the sonicated samples, the 100% sample formed needle-like shaped crystals in the β´ form with peaks at 3.8 ± 0.1 Å and 4.2 ± 0.1 Å. The 50% sample formed small, organized crystals that were in the β´ form (peaks at 3.8 ± 0.1 Å and 4.2 ± 0.1 Å) after 90 min and changed to the β form (peaks at 3.8 ± 0.1 Å and 4.6 ± 0.1 Å) after storage at 5 ºC when a FCR was used. When the 50% sample was crystallized with a SCR longer, β form (peaks at 3.8 ± 0.1 Å and 4.6 ± 0.1 Å), needle-like crystals were formed. The 20% FCR sonicated sample contained both β´ and β crystals with peaks at 3.8 ± 0.1 Å, 4.2± 0.1 Å, and 4.6± 0.1 Å. The different polymorphic forms resulted in visual differences as indicated in the PLM pictures as well as differences in melting behavior as will be discussed later.

Figure 3-1: Crystal microstructure of the 100% EIESOY, 50% EIESOY, and 20% EIESOY samples after 90 min of isothermal crystallization for each dilution and processing condition. Scale bar denotes 50 μm in all pictures.

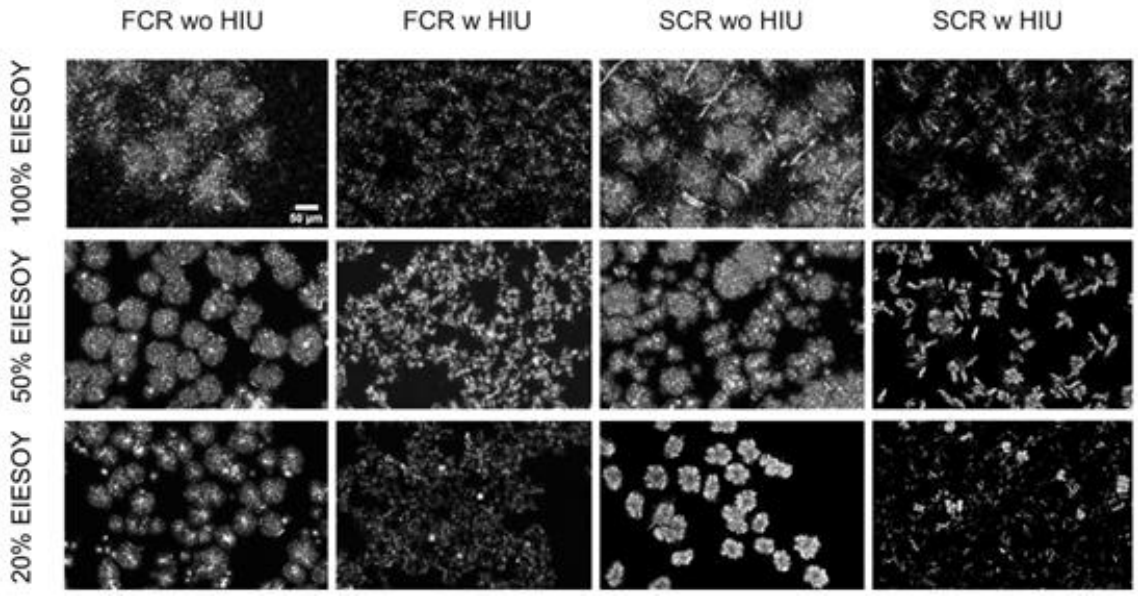

In general, there was not a significant increase in crystal diameter over time ($p > 0.05$) except for the 100% SCR non-sonicated sample having a significant increase in crystal diameter from 90 min to 48 h ($p<0.05$). In addition, the number of crystals was not significantly different between time points ($p > 0.05$) except for the 100% SCR sonicated sample at 22 °C and 5 °C, the 50% FCR sonicated sample at 22 °C, and the 20% FCR sonicated sample at 5 °C, in which the number of crystals significantly increased from 90 min to 48 h ($p < 0.05$). There were significant differences in crystal diameter by using two cooling rates. For the 100% sample, the non-sonicated SCR crystals were significantly larger than the non-sonicated FCR crystals ($p < 0.05$). However, the opposite was true for the 50% non-sonicated samples where the SCR crystals were significantly smaller than the FCR crystals ($p<0.05$). There was no significant difference in crystal diameter between the 20% FCR and SCR crystals. Typically, using a SCR results in larger crystals (Dibildox-Alvarado *et al.*, 2004) which is the case for the 100% sample but not the 50% sample. One

explanation as to why the 50% SCR crystals were smaller than the FCR could be because the FCR sample formed more uniform spherulites while the SCR sample formed ill-defined spherulites. This difference could result in the mean crystal diameter being smaller for the SCR samples due to the software calculating the diameter of the crystal fragments. Examining the number of crystals, the FCR sonicated samples had significantly more crystals than the SCR sonicated samples for every time point and concentration ($p<0.05$) with no change in crystal size.

Table 3-3: Mean crystal diameter (from microscopy) and number of crystals with standard deviations the 100% EIESOY, 50% EIESOY, and 20% EIESOY samples after 90 min isothermal crystallization in the cell and after storage at 22 °C and 5 °C for 48 h. Different letters indicate differences over all time points and conditions within each sample.

Crystal Diameter

100% EIESOY

	FCR wo HIU	FCR w HIU	SCR wo HIU	SCR w HIU
90 min	19.3 ± 3.6^{cd}	7.0 ± 0.5^{e}	36.5 ± 6.6^{b}	14.2 ± 1.7^{cde}
48 h 22 °C	23.3 ± 4.9^{c}	9.4 ± 1.5^{de}	62.7 ± 16.2^{a}	10.8 ± 0.7^{de}
48 h 5 °C	23.0 ± 5.2^{c}	8.3 ± 0.9^{e}	55.5 ± 12.4^{a}	11.2 ± 0.8^{de}

50% EIESOY

	FCR wo HIU	FCR w HIU	SCR wo HIU	SCR w HIU
90 min	36.1 ± 4.7^{ab}	11.6 ± 3.1^{de}	29.1 ± 5.3^{c}	16.3 ± 2.3^{d}
48 h 22 °C	39.1 ± 3.5^{a}	10.0 ± 1.5^{e}	30.9 ± 3.4^{bc}	14.5 ± 2.0^{de}
48h 5 °C	37.2 ± 5.9^{a}	10.4 ± 1.1^{e}	31.5 ± 3.1^{bc}	13.3 ± 1.1^{de}

20% EIESOY

	FCR wo HIU	FCR w HIU	SCR wo HIU	SCR w HIU
90 min	34.7 ± 4.3^{a}	10.7 ± 1.6^{b}	33.4 ± 9.2^{a}	12.1 ± 0.7^{b}
48 h 22 °C	36.1 ± 2.1^{a}	8.3 ± 0.6^{b}	37.1 ± 8.2^{a}	11.8 ± 1.3^{b}
48 h 5 °C	39.5 ± 3.1^{a}	7.9 ± 0.5^{b}	36.4 ± 11.5^{a}	11.5 ± 1.2^{b}

Number of Crystals

100% EIESOY

	FCR wo HIU	FCR w HIU	SCR wo HIU	SCR w HIU
90 min	196 ± 71^{d}	1712 ± 307^{a}	87 ± 24^{d}	659 ± 197^{c}
48 h 22 °C	277 ± 171^{d}	1520 ± 269^{a}	58 ± 24^{d}	984 ± 172^{b}
48 h 5 °C	199 ± 54^{d}	1622 ± 204^{a}	61 ± 21^{d}	1004 ± 252^{b}

50% EIESOY

	FCR wo HIU	FCR w HIU	SCR wo HIU	SCR w HIU
90 min	117 ± 35^{d}	894 ± 304^{b}	176 ± 64^{d}	458 ± 170^{c}
48 h 22 °C	88 ± 17^{d}	1259 ± 315^{a}	152 ± 36^{d}	472 ± 181^{c}
48 h 5 °C	106 ± 25^{d}	980 ± 325^{b}	152 ± 33^{d}	564 ± 80^{c}

20% EIESOY

	FCR wo HIU	FCR w HIU	SCR wo HIU	SCR w HIU
90 min	96 ± 22^{d}	967 ± 381^{b}	42 ± 10^{d}	507 ± 142^{c}
48 h 22 °C	84 ± 16^{d}	1222 ± 220^{ab}	35 ± 8^{d}	356 ± 128^{c}
48 h 5 °C	77 ± 13^{d}	1252 ± 263^{a}	63 ± 19^{d}	371 ± 114^{c}

Overall, a wide range of crystal sizes were obtained by using a combination of variables such as chemical composition of the fat, cooling rate, application of HIU, and storage. Allowing for a wider range of values for these physical properties.

Solid Fat Content

Figure 3-2 shows the SFC values for each concentration and time point. For the 100% sample, the non-sonicated FCR had the lowest initial SFC compared to the other conditions but had the highest SFC after storage at 22 °C ($p<0.05$). Interestingly, for the 100% samples stored at 5 °C, the SCR samples had significantly higher SFC values than the FCR samples ($p<0.05$) though this trend is not found after 90 min nor for the samples stored at 22 °C ($p>0.05$).

Figure 3-2: SFC of the 100% EIESOY, 50% EIESOY, and 20% EIESOY samples after 90 min isothermal crystallization in the cell and after storage at 22 °C and 5 °C for 48 h. Different letters indicate differences over all time points and conditions within each sample..

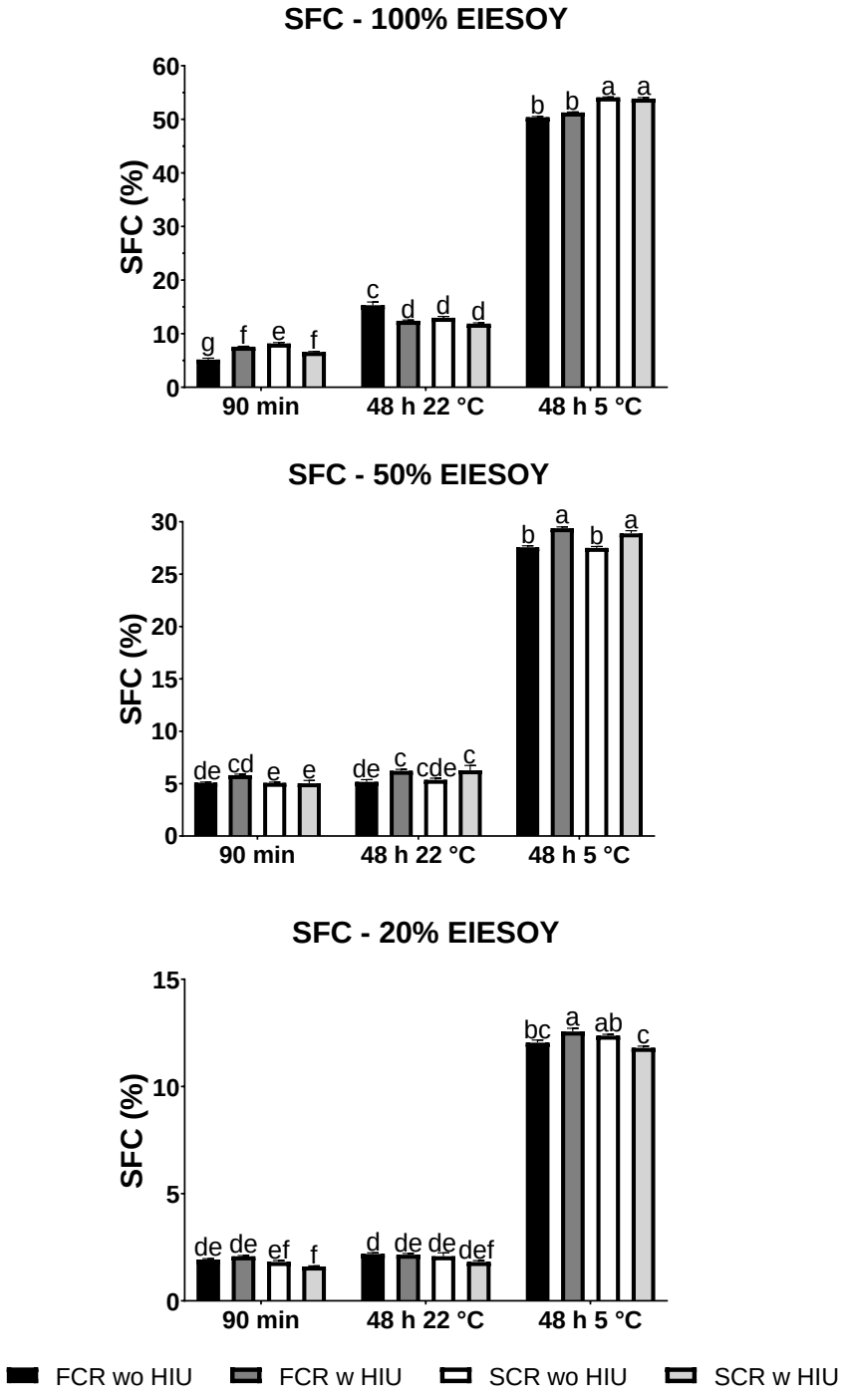

This type of experimental design controls SFC values without altering the crystal size, therefore, minimizing confounding factors. Similarly, in general, the application of HIU generated significantly smaller crystals without significant changes in SFC for a sample with a high concentration of SFAs (43.5%).

For the 50% sample, in general, the sonicated samples had higher SFC than the non-sonicated samples ($p<0.05$) except for the 50% SCR sample after 90 min of isothermal crystallization and storage at 22 °C ($p>0.05$). This suggests that generally, in a sample with intermediate SFA concentration (29.2%), the application of HIU results in significantly higher SFC immediately after crystallization as well as after storage. A previous study found similar results where the application of HIU resulted in significantly higher SFC values in interesterified soybean oil (Kadamne and Martini, 2018). Like the 100% sample, the 50% sample had no significant increase in the crystal size during storage but there were significant differences in SFC.

For the 20% samples stored at 5 °C, the SCR sonicated samples had lower SFC than the non-sonicated samples ($p<0.05$). In contrast, when the 20% sonicated samples were crystallized using a FCR, they had a higher SFC than the non-sonicated sample ($p<0.05$) at 5 °C. Generally, SFC increased as the concentration of the interesterified soybean oil increased ($p<0.05$) due to the higher concentrations having a greater amount of SFAs that would be solid when measured. Also, samples stored at 5 °C had significantly higher SFC values than samples stored at 22 °C ($p<0.05$) because of the storage temperature.

Hardness

The hardness of the samples is summarized in Figure 3-3. Hardness measurements

could not accurately be taken for some of the 50% and all the 20% samples after 90 min and storage at 22 °C because the samples were too soft. There were no significant differences between sonicated and non-sonicated samples after 90 min or storage for 48 h at 22 °C. However, at 5 °C, the sonicated samples were harder than the non-sonicated counterparts except for the 50% SCR sample. The sonicated samples may have higher hardness values because they are able to form a more uniform crystal matrix (smaller crystals, Table 3-3**)**.

Figure 3-3: Hardness of the 100% EIESOY, 50% EIESOY, and 20% EIESOY samples after 90 min isothermal crystallization in the cell and after storage at 22 °C and 5 °C for 48 h. Due to the softness of the samples hardness could not be measured and is as denoted n/a. Different letters indicate differences over all time points and conditions within each sample.

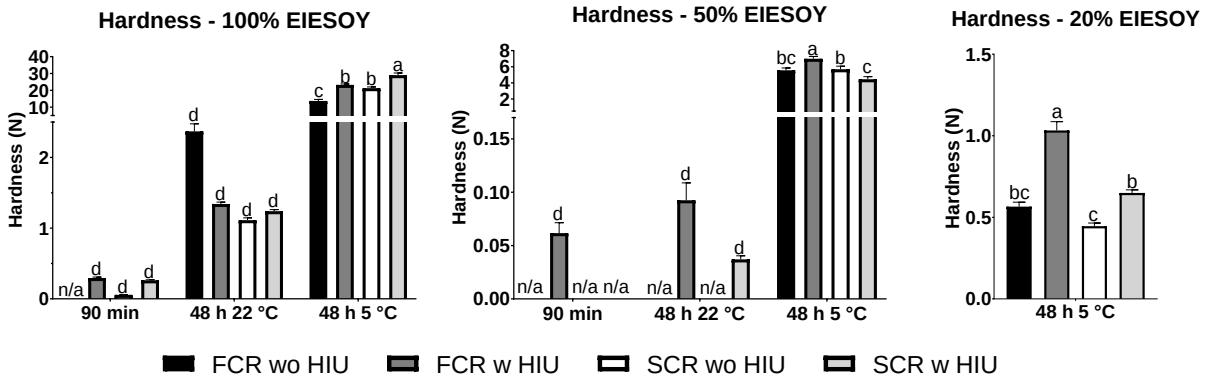

Previous research has shown that the hardness of a sample increased when smaller crystals were present (Suzuki *et al.*, 2010; Lee *et al.*, 2020; Ye *et al.*, 2011; Dibildox-Alvarado *et al.*, 2004). The sonicated samples have significantly more and smaller crystals than the non-sonicated samples (Table 3-3), thus the sonicated samples are harder even though the SFC is not significantly different between these samples (Figure 3-4). The presence of these many small crystals could have increased the hardness for samples with the same SFC due to the small crystals forming a tighter, more uniform crystal matrix compared to large crystals. Similar results were found by other authors (da Silva *et al.*,

2020a; 2020b; Suzuki *et al.*, 2010; Kerr *et al.*, 2011; Ye *et al.*, 2011; Wagh *et al.*, 2013; Ye and Martini, 2015), where the application of HIU resulted in smaller crystals, no differences in SFC, and harder materials.

The SFC of the samples could not always predict which samples would be harder as some samples had lower SFC but were harder than the non-sonicated counterparts. For example, the SCR 20% sonicated sample stored at 5 °C had significantly smaller crystals and lower SFC than the non-sonicated sample; however, it was harder suggesting that crystal size was a better predictor than SFC for the hardness of this sample. Overall, hardness is determined by a combination of SFC and crystal size.

For the samples stored at 5 °C, the 100% samples were significantly harder than the 50% sample ($p<0.05$) and the 50% samples were harder than the 20% samples ($p<0.05$). A similar trend is seen in the SFC data where, as the concentration of interesterified soybean increases, SFC and hardness increase. This is explained by the level of SFAs that the samples contained. The 20% sample contained a low level of SFAs (20.4%) which resulted in a softer texture than the 100% sample that contained a high level of SFAs (45.0%) which resulted in a harder texture. Additionally, the lower the storage temperature, the harder the samples became. In regard to cooling rate, for the 100% sample stored at 5 °C, using a SCR resulted in higher hardness values. However, the opposite was true for the sonicated 50% sample stored at 5 °C, because a SCR resulted in lower hardness values. Overall, the use of HIU increased the hardness of most samples stored at 5 °C but did not influence the samples immediately after crystallization and after storage at 22 °C.

Viscoelasticity

Elastic modulus (G´), viscous modulus (G´´) and the phase shift angle (δ) at a strain value of 0.01% for each time point and concentration are shown in Figure 3-4 and Figure 3-5. G´ was always greater than G´´ indicating the elastic nature of these samples. There were no significant differences in G´ at any time point for the 50% sample. Additionally, there was no significant difference in G´ for the 100% and 20% samples after the 90 min isothermal crystallization ($p>0.05$); however, there were significant differences after storage. For the 100% sample, the FCR non-sonicated sample had a higher G´ value than the sonicated sample after storage at 22 °C ($p<0.05$). However, when the samples were stored at 5 °C, the non-sonicated sample had a lower G´ value than the sonicated sample ($p<0.05$). For the 20% sample, the sonicated SCR sample had a higher G´ than the non-sonicated sample after storage at 22 °C.

Figure 3-4: G´ the 100% EIESOY, 50% EIESOY, and 20% EIESOY samples after 90 min isothermal crystallization in the cell and after storage at 22 °C and 5 °C for 48 h. Different letters indicate significant differences over all time points and conditions within each sample.

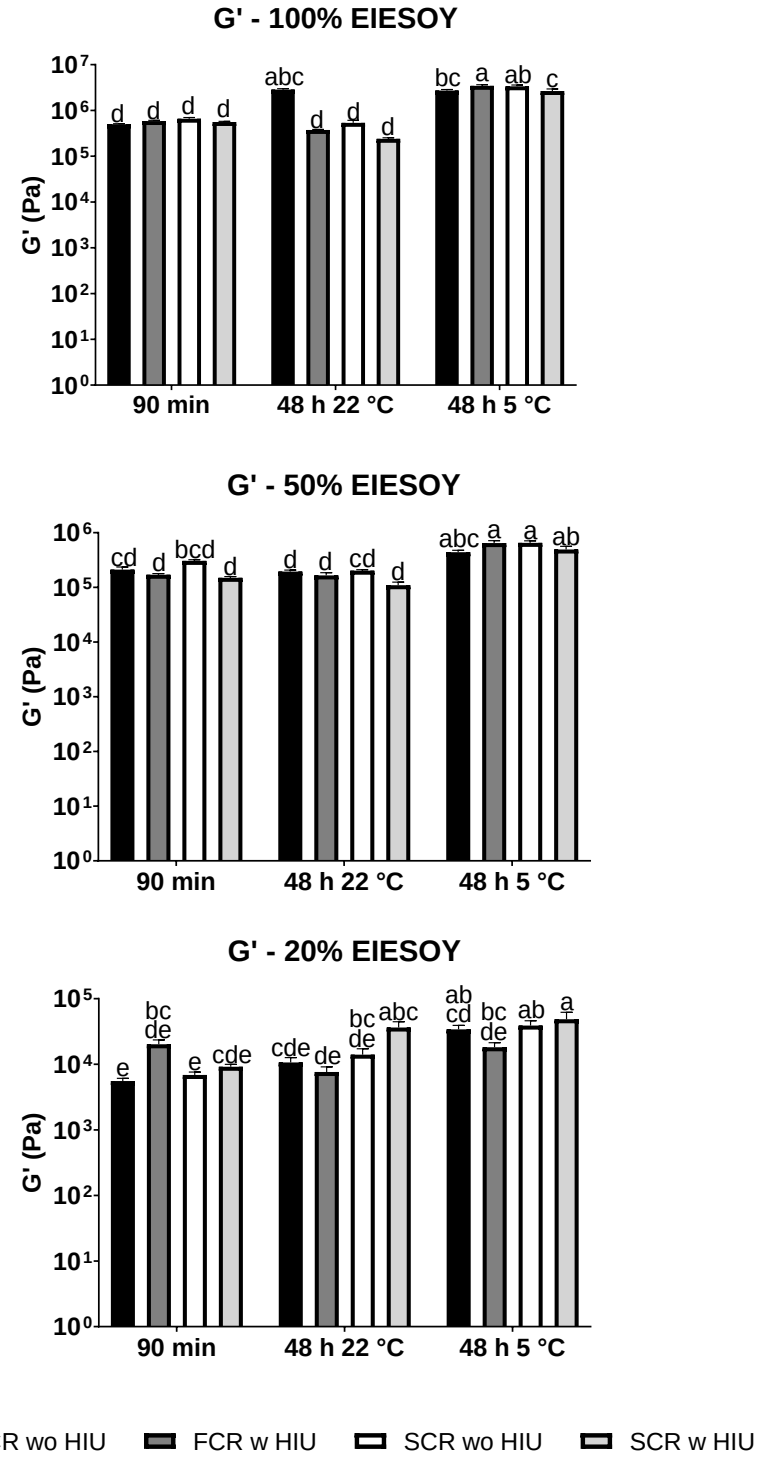

In terms of G´´, there were no significant differences for all concentrations after 90 min, the 50% and 20% samples after 48 h at 22 °C, or the 100% and 20% samples after 48 h at 5 °C ($p>0.05$). However, the non-sonicated 100% FCR sample after 48 h at 22 °C was significantly higher than the other samples at this time. Additionally, for 50% SCR sample after 48 h at 5 °C, the non-sonicated SCR sample had the highest G´´ and the non-sonicated FCR sample had the lowest G´´. In general, there were few differences in the phase shift angle (δ) between the processing conditions at each time point and δ was highest for the 20% dilution.

Interestingly, there are fewer differences between samples when examining G´ compared to hardness though they were significantly correlated ($r_s=0.489$, $p=0.010$). Both G´ and hardness are used to evaluate the crystal matrix strength so usually, these two measurements correlate. However, G´ measures the crystal matrix strength by examining interactions between the crystals while hardness measures the crystal matrix strength as its resistance to an external force. Overall, G´ and G´´ increased as the concentration of SFAs increased.

Figure 3-5: G´´ and δ of the 100% EIESOY, 50% EIESOY, and 20% EIESOY samples after 90 min isothermal crystallization in the cell and after storage at 22 °C and 5 °C for 48 h. Different letters indicate differences over all time points and conditions within each sample.

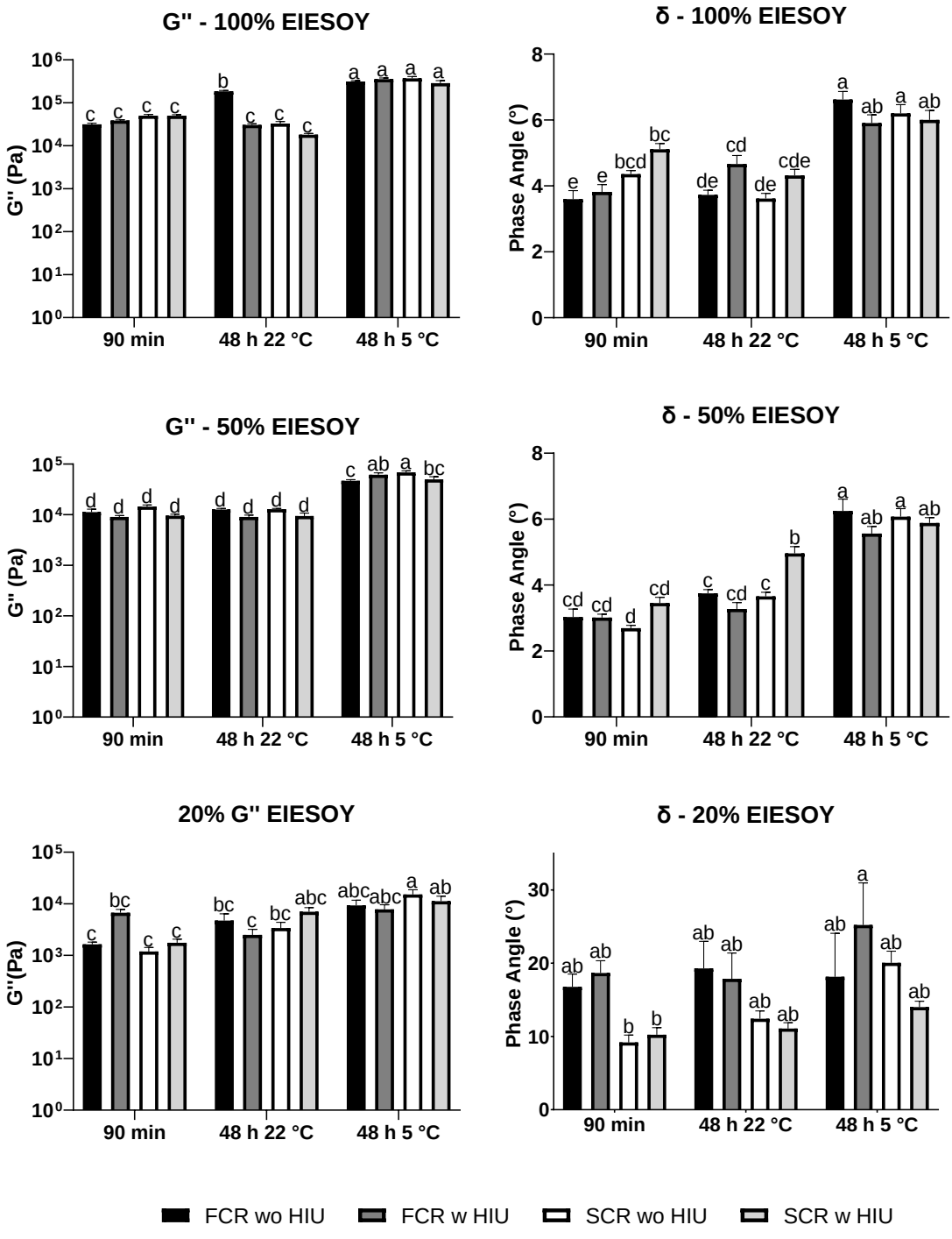

Melting Behavior

The melting profiles of the samples are shown in Figure 3-6 while the overall peak temperatures and enthalpy are summarized in Table 3-4. When looking at the melting profiles for the samples stored at 5 °C, the 100% sample had three pronounced peaks at approximately 14 °C, 25 °C, and 50 °C (see arrows in Figure 3-6). The 50% sample had three peaks at approximately 9 °C, 25 °C, and 48 °C and the 20% sample had only one peak at about 46 °C. Table 3-4 shows the melting parameters obtained when the melting curve was analyzed as a whole or the overall peak temperature and enthalpy, while Table A-1 shows the melting parameters obtained when various peaks are analyzed separately.

A shift towards low peak temperatures was observed for some sonicated samples including the third peak of the 100% FCR and SCR samples stored at 5 °C (Table A-1), the 50% FCR sample after 90 min, storage at 22 °C (Table 3-4) and the first peak after storage at 5 °C (Table A-1), the third peak of the 50% SCR sample stored at 5 °C (Table A-1), the 20% SCR sample at all time points (Table 3-4), and the 20% FCR sample stored at 22 °C (Table 3-4) ($p<0.05$). Previous studies have found similar results where the application of HIU resulted in lower Tpeak due to HIU promoting the co-crystallization of low melting point TAGs (da Silva *et al.*, 2020a, 2020c; Lee *et al.*, 2018; Lee *et al*. 2020).

Figure 3-6: Melting profile of the 100% EIESOY, 50% EIESOY, and 20% EIESOY samples after 90 min isothermal crystallization in the cell and after storage at 22 °C and 5 °C for 48 h.

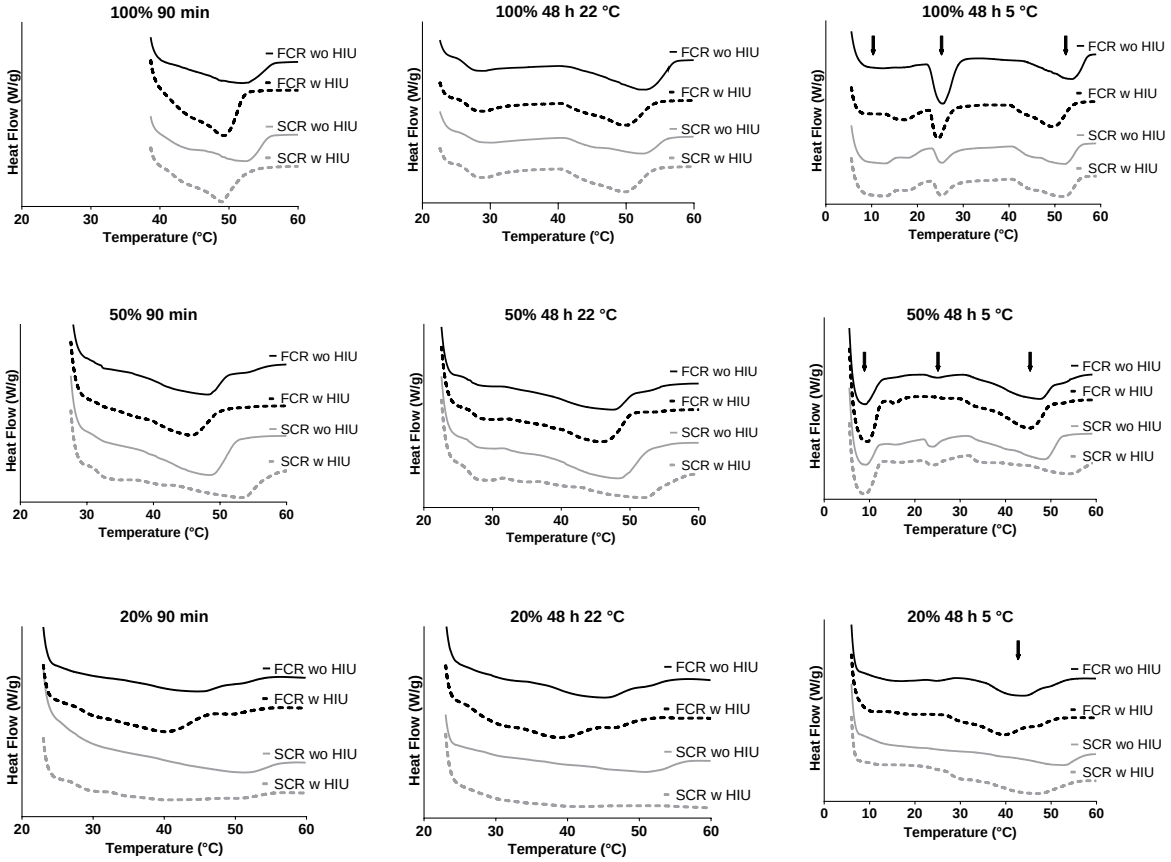

Table 3-4: Overall mean Tpeak and enthalpy of the 100% EIESOY, 50% EIESOY, and 20% EIESOY samples after 90 min isothermal crystallization in the cell and after storage at 22 °C and 5 °C for 48 h. The values represent the peaks integrated as a whole. Different letters indicate differences over all time points and conditions within each sample.

Peak Temperature (°C)

100% EIESOY

	FCR wo HIU	FCR w HIU	SCR wo HIU	SCR w HIU
90 min	52.5 ± 0.3^{a}	49.4 ± 0.2^{ab}	52.9 ± 0.1^{a}	49.5 ± 0.1^{ab}
48 h 22 °C	52.1 ± 0.8^{a}	49.9 ± 0.2^{ab}	52.6 ± 0.1^{a}	49.7 ± 0.2^{ab}
48 h 5 °C	25.8 ± 0.2^{c}	27.1 ± 5.0^{c}	29.7 ± 4.5^{c}	37.8 ± 7.2^{bc}

50% EIESOY

	FCR wo HIU	FCR w HIU	SCR wo HIU	SCR w HIU
90 min	48.2 ± 0.1^{bc}	45.0 ± 0.4^{d}	46.9 ± 0.8^{cd}	51.4 ± 0.9^{a}
48 h 22 °C	47.5 ± 0.1^{c}	44.9 ± 0.3^{d}	47.9 ± 0.2^{bc}	49.7 ± 0.7^{ab}
48 h 5 °C	8.9 ± 0.1^{e}	9.7 ± 0.1^{e}	18.1 ± 6.4^{e}	9.3 ± 0.2^{e}

20% EIESOY

	FCR wo HIU	FCR w HIU	SCR wo HIU	SCR w HIU
90 min	45.0 ± 0.3^{cd}	40.1 ± 0.2^{de}	52.0 ± 0.6^{ab}	41.9 ± 1.2^{de}
48 h 22 °C	44.4 ± 0.5^{cd}	39.2 ± 0.2^{e}	49.0 ± 1.8^{abc}	39.0 ± 2.3^{e}
48 h 5 °C	44.0 ± 0.5^{de}	39.3 ± 0.2^{e}	53.1 ± 0.4^{a}	47.3 ± 0.8^{bc}

Enthalpy (J/g)

100% EIESOY

	FCR wo HIU	FCR w HIU	SCR wo HIU	SCR w HIU
90 min	11.5 ± 0.7^{e}	13.8 ± 0.2^{de}	13.4 ± 0.3^{e}	15.1 ± 0.2^{de}
48 h 22 °C	22.6 ± 1.0^{c}	23.2 ± 0.9^{c}	19.5 ± 1.0^{cd}	21.0 ± 0.5^{c}
48 h 5 °C	46.1 ± 1.2^{a}	43.0 ± 0.6^{ab}	37.8 ± 2.6^{b}	41.7 ± 1.7^{ab}

50% EIESOY

	FCR wo HIU	FCR w HIU	SCR wo HIU	SCR w HIU
90 min	7.9 ± 0.4^{c}	7.4 ± 0.5^{c}	8.2 ± 0.7^{c}	7.2 ± 0.3^{c}
48 h 22 °C	7.8 ± 0.4^{c}	7.6 ± 0.4^{c}	8.4 ± 0.5^{c}	8.6 ± 0.3^{c}
48 h 5 °C	12.7 ± 1.1^{b}	16.8 ± 1.2^{a}	13.8 ± 1.1^{ab}	17.0 ± 1.1^{a}

20% EIESOY

	FCR wo HIU	FCR w HIU	SCR wo HIU	SCR w HIU
90 min	2.5 ± 0.1^{ab}	2.5 ± 0.3^{ab}	0.8 ± 0.1^{d}	1.3 ± 0.2^{cd}
48 h 22 °C	2.3 ± 0.2^{bc}	3.4 ± 0.4^{a}	0.9 ± 0.2^{d}	0.9 ± 0.2^{d}
48 h 5 °C	2.2 ± 0.1^{bc}	2.7 ± 0.2^{ab}	1.7 ± 0.2^{bcd}	2.3 ± 0.1^{bc}

Additionally, differences in peak temperature may be due to differences in polymorphic form. For the 100% FCR sample there were no significant differences in peak temperature for the sonicated and non-sonicated samples except for the third peak at 5 °C. This makes sense as both the sonicated and non-sonicated samples were in the β´ form. The 50% FCR sonicated sample had a lower melting point than the non-sonicated sample at 90 min and after 48 h at 22 ºC. This is due to the sonicated sample having β´ crystals at 90 min and most likely 22 °C while the non-sonicated sample had both β´ and β crystals at 90 min and at 22 °C. This mixture of β´ and β crystals resulted in the non-sonicated sample having a higher melting point than the sonicated sample. Interestingly, for the 50% FCR samples at 5 °C, the sonicated sample contained β crystals only while the non-sonicated sample contained both β´ and β. This resulted in the sonicated sample having a higher melting point for the overall 5 °C peak, as well as the first and second peaks at 5 °C due to the presence of these stable β crystals. The 50% SCR sonicated sample had a significantly higher melting point at 90 min and the third peak at 5 °C ($p<0.05$) this makes sense because the sample contained only β form crystals at the time points that were measured (90 min and 48 h at 22 °C) resulting in a higher melting point. All 20% samples measured contained both β´ and β crystals, however, there were differences in melting point between the FCR sonicated and non-sonicated sample at 22 °C. Here the non-sonicated sample had a significantly higher melting point than the sonicated sample, most likely due to the non-sonicated sample having more crystals in the stable β form. The same trend is seen for the 20% SCR samples where the non-sonicated sample had a significantly higher melting point over all time points when compared with the sonicated sample. Therefore, although both polymorphic forms are present, the non-sonicated sample most likely contains a higher

proportion of stable β crystals.

The use of a FCR also resulted in a shift to low peak temperatures for the second peak of the 100% sonicated sample at 5 °C (Table A-1) as well as the 50% sonicated samples after 90 min, storage at 22 °C (Table 3-4) and the third peak at 5 °C (Table A-1). In addition, the first peak of the 50% non-sonicated sample stored at 5 °C (Table A-1), the 20% non-sonicated sample after 90 min (Table 3-4), and the 20% sonicated and non-sonicated samples stored at 5 °C (Table 3-4) also had lower peak temperatures when a FCR was used. This is most likely due to the FCR promoting co-crystallization of low melting point TAGs due to the higher energetic drive to crystalize.

Enthalpy values were not significantly different between sonicated and non-sonicated samples except for the first peak of the 100% FCR after storage for 48 h at 5 °C (Table A-1), the first peak and overall curve of the 50% FCR stored at 5 °C for 48 h (Table 3-4), and the 20% FCR stored at 22 °C for 48 h (Table 3-4) ($p>0.05$). Additionally, the enthalpy of the samples increased as the concentration increased due to a greater amount of crystalline material being present ($p<0.05$) which is further shown by increased G´ and SFC at higher concentrations.

As previously mentioned, a wide range of melting parameters were obtained by crystallizing fats of different chemical composition under various conditions such as sonication and cooling rate. These results will allow us to establish correlations with OBC.

Oil Binding Capacity

OBC_c of the samples is shown in Figure 3-7. There were no significant differences in OBC_c for the 100% samples stored at 5 °C as the OBC_c was high for all processing conditions. However, there were significant differences in the 100% samples stored at 22

°C. In this case, a FCR resulted in lower OBC_c for the sonicated sample and higher OBC_c for the non-sonicated sample compared to a SCR ($p<0.05$). For the 50% EIESOY, the FCR sonicated sample had significantly higher OBC_c at both 22 °C and 5 °C. However, when a SCR was used, the application of HIU decreased OBC_c at 22 °C and there was no significant difference between the sonicated and non-sonicated samples at 5 °C. For the 20% samples, when a SCR was used the sonicated and non-sonicated samples were not significantly different ($p>0.05$). However, when samples were crystallized using a FCR the sonicated sample had a significantly higher OBC_c than the non-sonicated sample ($p<0.05$) at both 22 °C and 5 °C.

When examining the difference between FCR and SCR of the sonicated samples only, a SCR resulted in significantly lower OBC_c than a FCR ($p<0.05$) for the 50% and 20% samples at 22 °C and 5 °C. This aligns with Dibildox-Alvarado *et al.*'s (2004) previous findings that lower cooling rates resulted in greater oil loss. However, the opposite is true for the 100% sonicated samples stored at 22 °C because using a SCR resulted in a significantly higher OBC_c than using a FCR. This indicates the effect of cooling rate on OBC_c was dependent on the concentration of SFAs of the sample.

Figure 3-7: Mean OBC_c of the 100% EIESOY, 50% EIESOY, and 20% EIESOY samples after storage at 22 °C and 5 °C for 48 h. Different letters indicate differences over all time points and conditions within each sample.

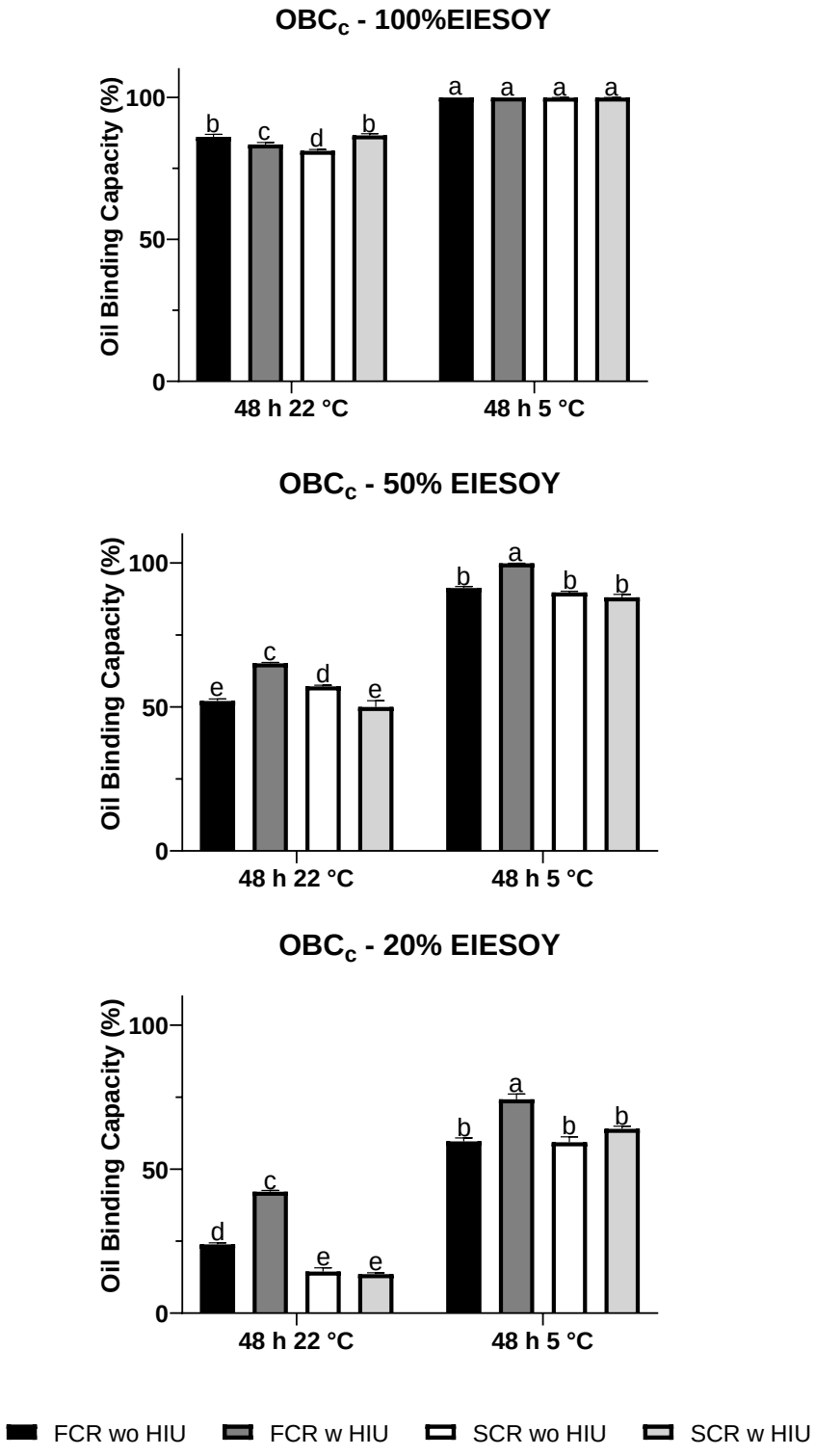

At the lowest and intermediate concentrations of SFAs, a FCR resulted in higher OBC_c, however; at the highest concentration, a FCR resulted in lower OBC_c. Previous research in our lab has shown that the application of HIU results in higher OBC_c (da Silva *et al.*, 2020a; da Silva *et al.*, 2020c). For all concentrations tested, the application of ultrasound consistently reduced the crystal size and increased the number of crystals, however, the OBC_c for the sonicated samples was not always higher which might be expected due to these samples having a small, organized crystal matrix. This suggests that crystal size and the number of crystals are not the only determining factors for OBC_c.

Additionally, OBC_c tended to increase as the concentration of SFAs increased. OBC_c was significantly higher for the samples stored at 5 °C compared to the samples stored at 22 °C probably due to a variety of factors such as the 5 °C samples being harder, more elastic, and having higher SFC than the 22 °C samples. This is also supported by the correlation analysis which shows that OBC_c was significantly correlated with hardness (r_s=0.976, p<0.001), SFC (r_s=0.948, p<0.001), overall enthalpy (r_s=0.843, p<0.001), enthalpy of the first, second, and third peaks after 48 h at 5 °C (r_s=0.738, p=0.046) overall Tpeak and the peak temperature of the first peak after 48 h at 5 °C (r_s=-0.505, p=0.012; r_s=0.833, p=0.015; respectively), G´(r_s=0.738, p<0.001), and G´´(r_s=0.905, p<0.001).

However, OBC_c was not correlated with crystal diameter (r_s=-0.137, p=0.522) nor the number of crystals (r_s=0.272, p=0.198). This is contrary to previous findings by da Silva *et al.* (2020a) who found that OBC was significantly correlated to crystal diameter in an interesterified soybean oil with low levels of saturated fats. The difference in results between da Silva *et al.* (2020a) and this study could be explained by the SFC. For this study, SFC was significantly correlated to OBC_c; however, da Silva *et al.* (2020a) found

that SFC and OBC were not significantly correlated. This indicates that SFC was more influential in increasing OBC_c than crystal size in this study. Overall, these results suggest that OBC_c can be increased by formulating harder, more elastic fats with high SFC and high enthalpy.

Figure 3-8: Mean OBC_p after seven days. The OBC of the 50% EIESOY samples stored at 22 °C and 20% EIESOY samples stored at both 22 °C and 5 °C was not measured due to the samples being too soft and sticking to the filter paper. Different letters indicate differences over all time points and conditions within each sample.

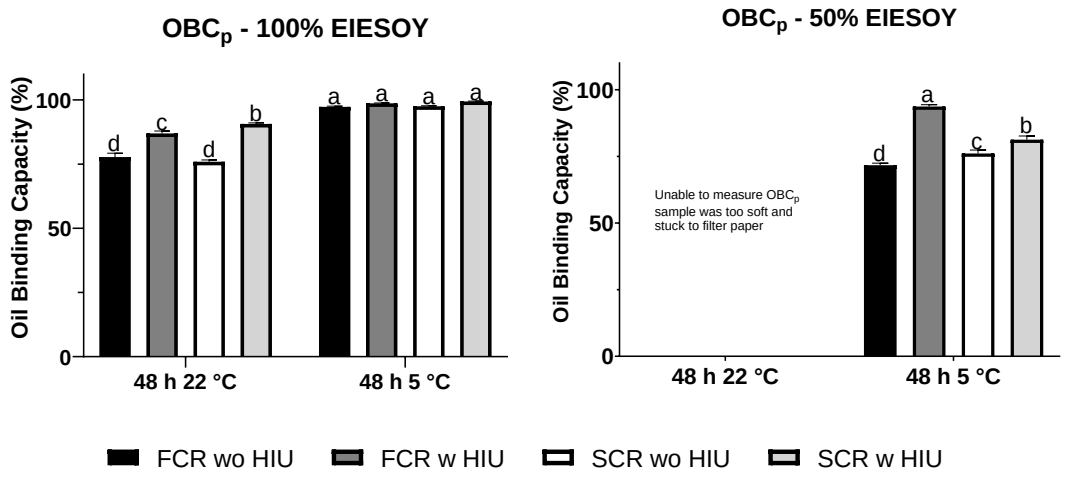

Figure 3-8 is a summary of the final OBC_p after 7 days of storage using the filter paper method. OBC_p was measured for the 100% samples stored at both temperatures as well as the 50% samples stored at 5 °C. However, OBC_p could not be measured for the 50% samples stored at 22 °C nor the 20% samples stored at either temperature due to the samples being too soft and sticking to the filter paper. The sonicated samples had significantly higher OBC than the non-sonicated samples for all conditions tested ($p<0.05$) except for the 100% samples stored at 5 °C. Additionally, for the 100% sonicated samples stored at 22 °C, using a SCR resulted in a higher OBC than using a FCR ($p<0.05$). The opposite is true for the 50% sonicated samples stored at 5 °C, where a FCR resulted in a higher OBC_p than a SCR ($p<0.05$).

Interestingly, the 100% EIESOY, FCR, non-sonicated sample stored at 22 °C for 48 h had a higher OBC_c compared to the sonicated sample and a lower OBC_p. This is counterintuitive because a sample that has higher OBC_c would be expected to also have a higher OBC_p. As mentioned previously, the OBC_c measurement was taken after 48 h of storage. At this time, the 100% FCR non-sonicated sample was harder, more elastic, and had a higher SFC than the sonicated sample so it could have been more resistant to oil loss using the centrifuge method. However, OBC_p was measured by placing disks of the sample stored for 48 h on filter paper and then measuring OBC_p over 7 days. During this additional storage time, the sonicated samples could have reached equilibrium and had a final OBC_p that was higher than the non-sonicated samples which would explain why we see this discrepancy between the two measurements. This could also be explained by the different treatments the samples undergo in the two measurements. For the OBC_c measurement, a centrifuge is used to apply force to the samples and expedite the movement of liquid oil. This applies stress to the system due to the centrifugal forces so a sample with a weaker crystalline network (G´) would lose more oil. Additionally, although measures were taken to control the temperature of the centrifuge (placing the centrifuge at room temperature or in a sliding fridge), there will be an increase in the sample's temperature due to the force that occurs when the samples are centrifuging. This increase in temperature may have resulted in the melting of some low melting point TAGs that are solid at the storage temperature (22 °C or 5 °C). As described previously, the application of HIU resulted in a peak temperature shift towards lower temperatures most likely because HIU promotes co-crystallization with low melting point TAGs. This decrease in peak melting temperature may result in more fat melting due to the increase in temperature during centrifugation and,

therefore, a higher amount of oil may have been expelled. Conversely, for the OBC_p measurement using the filter paper method, the sample undergoes gravitational and capillary forces and there is no increase in temperature of the sample during the measurement. Therefore, samples may show different OBC_c and OBC_p measurements because the samples are exposed to different conditions during these measurements. Generally, the two methods align and a sample with a high OBC_c typically has a high OBC_p which is the case for most of the conditions except for the 100% FCR sample stored at 22 °C for 48 h.

The OBC_p of the 50% sample tended to be lower than the 100% sample. This may be a result of hardness, SFC, G´, and enthalpy decreasing as the concentration of SFAs decreased because OBC_p was positively correlated with hardness (r_s=0.734, p=0.009), SFC (r_s=0.678, p=0.019), G´(r_s=0.678, p=0.019), and the whole enthalpy (r_s=0.776, p=0.004). OBC was also positively correlated with G´´(r_s=0.608, p=0.040), the peak temperature of the first peak after 48 h at 5 °C (r_s=0.857, p=0.011) and the enthalpy of the first and third peaks after 48 h at 5 °C (r_s=0.952, p=0.001 and r_s=0.881, p=0.007; respectively). OBC_p was not correlated with mean crystal diameter (r_s=-0.531, p=0.079) nor the number of crystals (r_s=0.552, p=0.067). These results suggest that OBC_p can be increased by formulating harder more elastic fats with high SFC and enthalpy.

CONCLUSIONS

Results from this study show that physical properties of an interesterified soybean fat could be changed by using various processing conditions such as HIU, cooling rate, and concentration of SFAs, generating a wide range of OBCs. HIU was able to generate significantly smaller and more crystals in all concentrations tested. Also, HIU generally

increased the hardness of the samples, shifted the peak temperature, and increased the OBC_p. Using both a FCR and a SCR resulted in different crystal microstructure and peak melting temperatures. The concentration of SFAs also impacted the physical properties because as the level of SFAs increased, hardness, SFC, G´, and OBC also increased. These changes in physical properties resulted in different OBC_c and OBC_p values.

This study showed that OBC can be increased in an interesterified soybean-based fat by formulating harder, more elastic fats, with higher SFC and enthalpy due to both measurements of OBC being positively correlated with these physical properties. Interestingly, neither crystal size nor the number of crystals was correlated with either measurement of OBC for the interesterified soybean oil; suggesting the improvement of these OBC was not dependent on the crystal microstructure in this study.

ACKNOWLEDGMENTS

This project was supported by Agriculture and Food Research Initiative (AFRI) grant no. 2020-67017-31193 from the USDA National Institute of Food and Agriculture. EIESOY samples were kindly donated by Archer Daniels Midland. This research was supported by the Utah Agricultural Experiment Station, Utah State University, and approved as journal paper number #9530. We extend our gratitude to Dr. Robert Ward for conducting the fatty acid analysis.

REFERENCES

Acevedo NC, Block JM, Marangoni AG. Critical laminar shear-temperature effects on the nano-and mesoscale structure of a model fat and its relationship to oil binding and rheological properties. Faraday discussions. 2012a;158:171-194. doi:10.1039/C2FD200008B

Acevedo NC, MacMillan B, Newling B, Marangoni AG. Shear effects on the diffusive movement of oil in triacylglycerol networks. RSC advances. 2017;7:1634-1642. doi:10.1039/C6RA24829B

Acevedo NC, Block JM, Marangoni AG. Unsaturated emulsifier-mediated modification of the mechanical strength and oil binding capacity of a model edible fat crystallized under shear. Langmuir. 2012b;28:16207-16217. doi:10.1021/la303365d

Altimiras P, Pyle L, Bouchon P. Structure-fat migration relationships during storage of cocoa butter model bars: Bloom development and possible mechanisms. J Food Engin. 2007;80;600-610. doi:10.1016/j.jfoodeng.2006.06.022

Da Pieve S, Calligaris S, Nicoli MC, Marangoni AG. Shear nanostructuring of monoglyceride organogels. Food Biophysics. 2010;5:211-217. doi:10.1007/s11483-010-9162-3

da Silva TL, Cooper Z, Lee J, Gibon V, Martini S. Tailoring crystalline structure using high-intensity ultrasound to reduce oil migration in a low saturated fat. J Am Oil Chem Soc. 2020a;97:141-155. doi:10.1002/aocs.12321

da Silva TL, Danthine S, Martini S. Effect of processing conditions as high-intensity ultrasound, agitation, and cooling temperature on the physical properties of a low saturated fat. J Food Sci. 2020b;85:3380-3390. doi:10.1111/1750-3841.15436

da Silva TL, Marsh M, Gibon V, Martini S. Sonocrystallization as a tool to reduce oil migration by changing physical properties of a palm kernel fat. J Food Sci. 2020c;85:964-971. doi:10.1111/1750-3841.15099

Dibildox-Alvarado E, Rodrigues JN, Gioielli LA, Toro-Vazquez JF, Marangoni AG. Effects of crystalline microstructure on oil migration in a semisolid fat matrix. Cryst Growth Des. 2004;4:731-736. doi:10.1021/cg049933n

Ghosh V, Ziegler GR, Anantheswaran RC. Fat, moisture, and ethanol migration through chocolates and confectionery coatings. Crit Rev Food Sc. Nutr. 2002;42:583-626. doi:10.1080/20024091054265

Giacomozzi AS, Palla CA, Carrín ME, Martini S. Physical properties of monoglycerides oleogels modified by concentration, cooling rate, and high-intensity ultrasound. J Food Sci. 2019;84:2549-2561. doi:10.1111/1750-3841.14762

Green, N. L., & Rousseau, D. Oil diffusivity through fat crystal networks. Soft Matter. 2015;27:5523-5530. doi:10.1039/c5m01355k

Kadamne JV, Martini S. Sonocrystallization of interesterified soybean oil with and without agitation. J Am Oil Chem Soc. 2018;95:571-582. doi:10.1002/aocs.12075

Kerr, R., Tombokan, X., Ghosh, S., and Martini, S. Crystallization behavior of anhydrous milk fat-sunflower oil wax blends. J Agric Food Chem. 2011;59:2689–2695 – doi: 10.1021/jf1046046

Lee J, Claro da Silva R, Gibon V, Martini S. Sonocrystallization of interesterified soybean oil: Effect of saturation level and supercooling. J Food Sci. 2018;83:902-910. doi:10.1111/1750-3841.14084

Lee J, Marsh M, Martini S. Effect of storage time on physical properties of sonocrystallized all-purpose shortening. J Food Sci. 2020;85:3391-3399. doi:10.1111/1750-3841.15435

Marangoni AG, Experimental Methodology. In Fat crystal networks. Marangoni AG, editor. New York: Marcel Dekker; 2004. p. 267-348.

Martini S, Suzuki AH, Hartel RW. Effect of high intensity ultrasound on crystallization behavior of anhydrous milk fat. J Am Oil Chem Soc. 2008;85:621-628.

Peyronel F, Campos R, Marangoni AG. Prevention of oil migration in palm mid fraction and palm olein using a stabilizer rich in behenic acid. Food Res Intern. 2016;88:52-60. doi:10.1016/j.foodres.2016.04.001

Sato, K. Polymorphism of Lipid Crystals. In Crystallization of Lipids: Fundamentals and Applications in Food, Cosmetics, and Pharmaceuticals. Sato, K editor. West Sussex: Wiley; 2018. p. 17-60.

Si H, Cheong LZ, Huang J, Wang X, Zhang H. Physical properties of soybean oleogels and oil migration evaluation in model praline system. J Am Oil Chem Soc. 2016;93:1075-1084. doi:10.1007/s11746-016-2846-1.

Smith KW, Cain FW, Talbot G. Effect of nut oil migration on polymorphic transformation in a model system. Food Chem. 2007;102:656-663. doi:10.1016/j.foodchem.2006.05.045

Suzuki AH, Lee J, Padilla SG, Martini S. Altering functional properties of fats using power ultrasound. J Food Sci. 2010;75:E208-214. doi:10.1111/j.1750-3841.2010.01572.x

Wagh, A., Walsh, M., and Martini, S. Effect of lactose monolaurate and high intensity ultrasound on crystallization behavior of anhydrous milk fat. J Am Oil Chem Soc. 2013:90:977-987 – DOI: 10.1007%2Fs11746-013-2244-x

Ye Y, Martini S. Application of high-intensity ultrasound to palm oil in a continuous system. J Agric Food Chem. 2015;63:319-327. doi:10.1021/jf505041s

Ye Y, Wagh A, Martini S. Using high intensity ultrasound as a tool to change the functional properties of interesterified soybean oil. J Agric Food Chem. 2011;59:10712-10722. doi:10.1021/jf202495b

CHAPTER IV. UNVEILING THE PHYSICAL PROPERTIES PREDICTIVE OF OIL BINDING CAPACITY IN AN INTERESTERIFIED PALM-BASED FAT[2]

ABSTRACT

This paper identifies physical properties of an interesterified palm-based fat (EIEPO) that predict oil binding capacity (OBC). A 100% EIEPO sample, 50% EIEPO sample diluted with 50% soybean oil (SBO), and a 20% EIEPO sample diluted with 80% SBO were used to test how saturation level impacts OBC. All samples were crystallized using either a fast (6.4°C/min) or slow[2] (0.1°C/min) cooling rate as well as with or without the application of high-intensity ultrasound (HIU; 20kHz) to generate a wide range of physical properties. Immediately after crystallization, the sample's physical properties, including crystal microstructure, solid fat content (SFC), viscoelasticity (G′, G″, and δ), melting behavior, hardness, and OBC (centrifuge method) were quantified. The samples were then stored for 48 h at 22 °C and 5 °C and the aforementioned physical properties were measured again, with one additional measurement for the samples stored at 5 °C - OBC using a filter paper method (OBC_p). The results indicate that OBC can be optimized in a palm-based fat by modifying the physical properties which was achieved via the processing conditions. Both measurements of OBC were significantly correlated with SFC, hardness, δ, and enthalpy. A model was developed to predict a sample's OBC_c using the following dominant variables – SFC, hardness, peak temperature, enthalpy, and the number of crystals. These results suggest that OBC can be predicted using a sample's SFC,

[2] Reprinted (with modification) from the Journal of American Oil Chemists' Society. Marsh MA, Bean B, Maleky F, Martini S. Unveiling the physical properties predictive of oil binding capacity in an interesterified palm-based fat. March 2024. Original copyright notice as given in the publication in which the material was originally published with permission from John Wiley and Sons.

hardness, peak temperature, enthalpy, and number of crystals and that SFC, hardness, and enthalpy are main drivers of OBC.

INTRODUCTION

The physical properties of semi-solid fats are influenced by the chemical composition of the fat and the crystallization processing conditions (Wang *et al*., 2016; Maleky *et al.*, 2012). For example, fats that are crystallized slowly typically have larger crystals and are softer than fats crystallized quickly (Maleky *et al.*, 2012; Dibildox-Alvarado *et al.*, 2004), and fats crystallized with shear result in more and smaller crystals than fats crystallized statically (Wang *et al*., 2016; Blake and Marangoni, 2014; De Graef *et al.*, 2008). High-intensity ultrasound (HIU) has also been examined as a novel tool to generate various physical properties (Martini *et al*., 2008; da Silva *et al.*, 2020a; da Silva *et al*., 2020b; da Silva *et al.*, 2020c; Giacomozzi *et al.*, 2019; Lee *et al.*, 2018), such as more and smaller crystals (Ye and Martini, 2015; Chen *et al.*, 2013), harder and more elastic materials (Lee *et al*., 2020, Ye *et al*., 2011), and greater oil binding capacity (da Silva *et al.*, 2020a; da Silva *et al.*, 2020c).

Oil binding capacity (OBC) is the ability of a fat's crystalline network to entrap liquid oil and is an important physical property in several products including natural nut butters and chocolates with fat-based fillings. When fats have low OBC, the liquid oil can migrate from one region of the food to another. The movement of oil promotes phase separation in natural nut butter which is observed as a liquid layer of oil on the surface. Additionally, the movement of oil due to low OBC in chocolates with fat-based filling can result in hardening of the chocolate's center, softening of the chocolate coating, and fat bloom development on the chocolate's surface (Smith *et al*., 2007). OBC is dependent on

the physical properties of the crystalline network. For example, harder fats (da Silva *et al.*, 2020c; Peyronel *et al*., 2016) with higher SFC (Acevedo *et al*., 2012) and smaller crystal sizes (Peyronel *et al.*, 2016; Si *et al*. 2016) are typically expected to have higher OBC. However, it remains unclear which specific physical property or combination of physical properties is most influential in driving OBC as hardness, SFC, and crystal size are interconnected.

Therefore, it is necessary to utilize a multidimensional method that encompasses a larger diversity of physical property combinations than is typically found in traditional samples. In this study, both a fast-cooling rate (FCR) and a slow-cooling rate (SCR) are used to generate samples with different crystal sizes and hardness but similar SFC. In addition to different cooling rates, HIU is also used to generate a wide range of physical properties by reducing crystal size and increasing hardness for some samples. Lastly, samples were diluted with soybean oil (SBO) to generate crystalline structures that will result in different SFC, enthalpy, and hardness. The same approach was previously used to study the relationship between OBC and the physical properties of an interesterified soybean-based fat (Marsh and Martini, 2022). However, it is not known if an interesterified palm-based fat (EIEPO) will have similar results due to the different composition and crystallization behavior. By systematically changing the physical properties of an EIEPO sample, it is possible to unveil which physical properties are important in predicting OBC. As well as to evaluate the differences and similarities found for the interesterified soy-based fat, determining if chemical composition (palm- vs. soy-based samples) affects OBC in a similar manner.

MATERIALS AND METHODS

Sample Information

The EIEPO sample was kindly donated by Archer-Daniels-Midland (ADM, Decatur, IL, USA). The triacylglycerol (TAG) composition of the sample was previously studied and described by da Silva *et al*. (2021). The authors measured the TAG composition via reversed-phase HPLC based on AOCS method Ce 5b-89 (AOCS, 2009) using two stainless steel Nova-Pak C18 columns (4 lm, 3.9 × 150 mm) (Waters, Belgium) and a mixture of acetone and acetonitrile (62.5:37.5) for the mobile phase. The sample contained approximately 14.3% tri-unsaturated TAGs (UUU), 40.1% di-unsaturated TAGs (SUU), 37.0% mono-unsaturated TAGs (SUS), and 9.6% tri-saturated TAGs (SSS). For this study, three concentrations of EIEPO were prepared–a 100% EIEPO sample, a 50% EIEPO sample diluted 50% w/w with SBO (Great Value, Bentonville, AR, USA), and a 20% EIEPO sample diluted 80% w/w with SBO (Great Value, Bentonville, AR, USA).

Fatty Acid Analysis

Fatty acid analysis was performed through trans-esterification to generate fatty acid methyl esters (FAME) which were run on a gas chromatogram (GC; Shimadzu 2010) equipped with a flame ionization detector (Shimadzu, Columbia, MD). To prepare the samples for analysis, they were first melted at 60 °C for 15 min and 40 µL of the melted sample was placed in a culture tube to which 6.3 mL of MeOH and 0.7 mL of 10N KOH in water were added. The tubes were then incubated in a 55 °C water bath for 90 min with auto shaking. The samples were cooled and 0.58 mL of 24 N H2SO4 was added before incubating in a 55 °C water bath for an additional 90 min. After the second incubation step, 2 mL of hexane was added to the tube and mixed prior to centrifugation. The hexane layer

on top, which contained the FAME, was pipetted into a GC vial and injected into the GC column (Agilent Technologies, Santa Clara, CA). The carrier gas was hydrogen with a linear velocity of 41 cm/sec and the detector temperature was 250 °C. The peaks were identified through a comparison of retention times with FAME standards (GLC 463, NuChek Prep, Elysian, MN). Samples were measured in duplicate and reported as normalized area percentages.

Melting Point

The melting point of the samples was determined using a differential scanning calorimeter (DSC, Q20, TA Instruments, New Castle, DE, USA) calibrated with a pure indium standard. Approximately 10-15 mg of the sample was placed into a hermetic aluminum pan and sealed with a hermetic aluminum lid. The sample was placed into the DSC oven and an empty pan was used as the reference. The initial temperature was set to 22 °C and left for 1 min. The temperature then increased to 60 °C using a ramp rate of 5 °C/min and the samples were maintained at 60 °C for 30 min to erase the crystal memory. After 30 min, the samples were cooled to -20 °C with a ramp rate of 5 °C/min and left for 90 min at this temperature to induce crystallization. Lastly, samples were heated from -20 °C to 60 °C with a ramp rate of 5 °C/min. The highest melting peak observed during this heating step was used to determine the sample's melting point. This measurement was performed in duplicate.

Crystallization Conditions

One hundred grams of each sample were weighed in a beaker and left in an oven with an internal temperature of 60 °C for 30 min prior to crystallization to erase the crystal memory. After 30 min, the sample was poured into a double-walled crystallization cell (50

mm internal diameter and 90 mm internal height) fitted with a thermocouple to monitor sample temperature. The crystallization cell was connected to an external programmable water bath (Lauda Ecoline Staredition RE310, Delran, NJ, USA) to regulate temperature. As soon as the sample was poured into the cell, a timer was started, this was time zero. Agitation was used during the crystallization process via a magnetic stirrer set to 200 rpm to evenly distribute the temperature across the sample and was stopped prior to the onset of crystallization as observed by the naked eye (Lee *et al.*, 2020; Martini *et al.*, 2008).

The samples were crystallized at 29 °C, 23 °C, and 20 °C, for the 100%, 50%, and 20% samples, respectively. These temperatures were chosen to optimize the HIU application by allowing the onset of crystallization to occur slowly. Prior to applying HIU, the agitation was stopped, and samples were allowed to continue cooling statically until the onset of crystallization occurred. Ye *et al*. (2011) and Kadamne and Martini (2018) have previously found that HIU is most effective when applied under static conditions and at the onset of crystallization, so agitation was stopped and HIU was applied 5-40 min after. HIU (Misonix S-3000, Misonix Inc., Farmingdale, NY, USA) was applied for 10 s, using a 3.2 mm titanium tip, 20 kHz frequency, 216 um amplitude, and 90 W power.

In this study, two cooling rates were used to generate a wide range of crystal sizes– a FCR of 6.4 °C/min and a SCR of 0.1 °C/min. For the FCR samples, the water bath was set to the appropriate crystallization temperature and the samples were quickly moved from the 60 °C oven to the crystallization cell. The FCR was calculated by monitoring the temperature of the samples from the moment they were added to the cell until they reached the crystallization temperature. For the SCR samples, the water bath was set to 60 °C and the temperature decreased at 0.1 °C/min until the crystallization temperature was reached.

For the SCR samples, once the crystallization temperature was reached, samples were allowed to cool isothermally for 90 min. The crystallization conditions are summarized in Table 4-1.

Table 4-1: Crystallization conditions for the 100% EIEPO, 50% EIEPO, and 20% EIEPO samples used in this study. Time zero is the time at which the sample was poured into the cell. Total duration corresponds to the total time that the sample was in the cell. Agitation stopped is the time at which the magnetic stirrer was stopped. HIU applied corresponds to the time that high-intensity ultrasound was applied to the sample.

Crystallization Conditions

Sample	Crystallization temp (°C)	Total Duration (min)	Agitation stopped (min)	HIU applied (min)
100% FCR EIEPO	29	90	10	15
100% SCR EIEPO	29	400	260	280
50% FCR EIEPO	23	90	10	15
50% SCR EIEPO	23	460	290	330
20% FCR EIEPO	20	90	15	30
20% SCR EIEPO	20	490	360	375

After 90 min of isothermal crystallization, the following physical properties were measured–crystal morphology and microstructure, SFC, hardness, rheological parameters (G', G'', δ), melting behavior, and OBC_c. The samples were then stored at 22 °C and 5 °C for 48 h. Following storage, the previously mentioned physical properties were measured again with one additional measurement–OBC using a filter paper method (OBC_p) for the samples stored at 5 °C.

Polymorphism

Polymorphism of the samples was measured using an X-ray diffractometer (XRD, D2 Phaser, Bruker, Billerica, MA, USA). After being subjected to the crystallization conditions (Section 2.4), the samples were filtered under vacuum to increase the resolution and placed on an XRD slide. The slide was placed in the XRD equipment and measured from 5 to 30 ° at a rate of 1.0 ° per min using 30 kV of voltage and a 10 mA current. The

resulting graph displayed the intensity and position (°2θ) of the peaks. Bragg's law was used to calculate the d-spacing (Å) of the peaks. A β′polymorphic form was identified by two peaks at 3.8 Å and 4.2 Å and the β polymorphic form was identified by a larger peak at 4.6 Å and a small peak at 5.2 Å (Marangoni, 2004; Sato, 2018).

Crystal Morphology and Microstructure

Crystal morphology was evaluated by placing a drop of sample on a glass microscope slide and covering it with a cover slip. The slides were examined under a polarized light microscope (PLM, Olympus BX41 microscope, Olympus, Tokyo, Japan) using a 10x objective lens. The PLM was connected to a camera (Infinity 2, Lumenera Scientific, Ottawa, ON, Canada) to capture images of the crystal microstructure. Three images were captured immediately after crystallization as well as after storage at 22 °C and 5 °C. The diameter and number of crystals were measured using the software Image-Pro Premier E 9.2 (Media Cybernetics, USA). A threshold of 5 µm diameter was used to minimize the influence of very small crystal fragments shifting the mean diameter.

Solid Fat Content

SFC of the samples was measured using time-domain nuclear magnetic resonance equipment (TD-NMR, 120 Minispec NMR analyzer, Bruker, Rheinstetten, Germany). Six NMR tubes were prepared and measured immediately after crystallization. Afterwards, 3 of the tubes were stored at 22 °C, and 3 were stored at 5 °C for 48 h. After storage, the SFC of the samples was measured.

Hardness

The hardness of the samples was determined using a penetration test on a texture-profile analyzer (TMS-Pro; Food Technology Corp., Sterling, VA, USA) fitted with a 6-mm cylindrical probe and a 50 N or 500 N load cell depending on the sample's hardness. To measure hardness, three 10 mL beakers (22mm diameter and 35mm height) were filled with sample, the probe was lowered 15 mm into the samples at a cross-head speed of 1 mm/s. Afterwards, the probe returned to its zero position above the sample, paused for 10 s, lowered 15 mm into the sample again, and returned to its zero position to complete a two-cycle penetration test. The resulting force-time curve was used to calculate the hardness of the sample determined by the maximum force of the first cycle. Hardness was measured after crystallization in the cell and storage for 48 h.

Rheological Parameters

The elastic modulus (G′), viscous modulus (G″), and phase shift angles (δ) of the samples were evaluated using a rheometer (AR-G2, TA Instruments, New Castle, DE, USA) after crystallization and storage. Two geometries were used in this study–an 8 mm parallel plate and a concentric cylinder. The parallel plate geometry was used for all 100% and 50% samples as well as all 20% samples stored at 5 °C and the 20% FCR sonicated samples at 90 min and 48 h at 22 °C. The concentric cylinder was used for the remaining 20% samples which were too soft to measure using the parallel plate geometry. For the concentric cylinder, a gap of 1000 μm and 5.28 mL of sample was used. For the parallel plate, ~1 gram of sample was placed on the rheometer stage and a gap between 2,000-5,000 μm was used depending on the hardness of the sample. All samples were measured using an oscillatory test with a strain sweep procedure from 0.001% to 10% at a constant

frequency of 1 Hz. Prior to the start of the test, the rheometer stage was set at either the crystallization or storage temperature. The G′, G″, and δ were recorded from the middle of the linear viscoelastic region corresponding to a strain of 0.01%. These measurements were performed in triplicate.

Melting Behavior

A DSC (Q20, TA Instruments, New Castle, DE, USA) calibrated with pure indium standard was used to measure the melting behavior of the samples after 90 min and 48 h of storage. To measure melting behavior, 10-15 mg of sample was placed into a hermetic aluminum pan and sealed. The pan was then placed into a DSC oven with an empty pan as a reference. The temperature of the oven was set to either the crystallization or storage temperature. Samples were left at this temperature for 1 min and then the temperature rose to 5 °C/min until it reached 60 °C. The resulting melting profiles were integrated to calculate the peak temperature and enthalpy values. These measurements were performed in duplicate.

Oil Binding Capacity

OBC was measured using two methods–a centrifuge method (OBC_c) and a filter paper method (OBC_p). OBC_c was used to understand the OBC of the samples immediately after crystallization as well as samples that were too soft to measure using the filter paper method. OBC_p was used to better understand the OBC of samples over a longer period of time and without centrifugation forces that expedite the movement of liquid oil.

Centrifuge Method

OBC_c was calculated using a centrifuge method previously described in other studies (Marsh and Martini 2022; da Pieve *et al*., 2010; da Silva *et al*., 2020b). This

measurement was performed immediately after crystallization and after storage. Four microcentrifuge tubes were weighed, filled with approximately 1 g of sample, and weighed again. The microcentrifuge tubes were then placed into a centrifuge and spun for 15 min at 10,000 rpm. To help minimize temperature changes, one centrifuge (Sorvall micro 17 centrifuge, Thermo Scientific, Germany) was placed at room temperature and a second centrifuge (accuSpin micro 17 centrifuge, Fisher Scientific, USA) was placed in a sliding door fridge set at 5 °C. After spinning, the microcentrifuge tubes were opened and inverted for 3 min to dispel the liquid oil. Afterwards, the samples were weighed, and OBC_c was calculated using the following equation [1]:

$$OBC_c = \left[1 - \left(\frac{w_b - w_a}{w_s}\right)\right] * 100 \quad [1]$$

where w_b is the sample and tube weight prior to centrifuging, w_a is the sample and tube weight after centrifuging and dispelling the liquid oil, and w_s is the sample weight.

Filter Paper Method

OBC was also measured using a filter paper method previously described in other studies (Marsh and Martini, 2022; Altimiras *et al*., 2007; Peyronel *et al*., 2016). After crystallization, circular molds (22 mm diameter x 3 mm height) were filled with sample, covered in parafilm, and stored at 5 °C for 48 h. After storage, the samples were unmolded, weighed, placed on a pre-weighed filter paper (Whatman #1, 125mm diameter), and stored for an additional 7 days. Every day the samples were removed from the filter paper and the filter paper was weighed to measure the amount of oil that the sample had expelled. During storage, a control filter paper that had no sample was kept with the samples to control for environmental changes. This measurement was performed in quadruplicate. The following equation was used to calculate the oil binding capacity of the samples [2]:

$$OBC_p = \left[1 - \left(\frac{wp_{(t)} - wp_{(0)}}{ws_{(0)}}\right)\right] * 100 \quad [2]$$

where $wp_{(t)}$ is the weight of the filter paper at specific times (day 1-7), $wp_{(0)}$ is the weight of the filter paper on day 0, and $ws_{(0)}$ is the weight of the sample on day zero.

Statistical Analysis

Crystallization experiments were performed in triplicate and the mean values and standard errors were reported. Two-way ANOVA and t-tests were used to compare sample conditions and Tukey post-hoc tests were used to determine significant differences (α=0.05). To evaluate the influence of the physical properties and OBC, both correlation analysis and statistical modeling approaches were used.

Correlation

Correlation analysis was performed to better understand how the physical properties are related to OBC. Spearman correlation was used instead of Pearson correlation due to the non-linear relationship between OBC and the physical properties (Figure B-1). The analysis was performed using the physical properties at 90 min and after 48 h overall crystallization conditions and dilutions generating Spearman r_s coefficients and p-values. These analyses were performed using statistical software (GraphPad Prism v9, San Diego, CA, USA).

Statistical Modeling

LASSO regression (Tibshirani, 1996) was used to model the relationship between OBCc and the following physical properties: SFC, hardness, G, G″, δ, peak temperature, enthalpy, crystal size, crystal number, and crystal area. Each observation used in the dataset represents one crystallization experiment either immediately after crystallization, after 48

h at 22 °C, or after 48 h at 5 °C, and the average of each physical property measured at these respective times. Hence, 108 observations were used in model development (3 dilutions*4 crystallization conditions*3 replicates*3 time and storage points). Due to some samples being too soft, the hardness value fell below the minimal detection level of 0.015 N and was imputed as 0.015 N. The LASSO penalty λ serves to reduce the inflated variance of candidate explanatory variables which are correlated with each other, and ultimately determines the number of explanatory variables retained in the model. The λ parameter was determined using the 1-SE rule, which selects the simplest model (i.e., least number of explanatory variables) whose cross-validated error is within one standard error of the minimum cross-validated error of all considered λ values. The process was repeated 50 times, each time retaining the value of λ satisfying the 1-SE rule. The λ used for the final model was taken as the median of the optimal λ values from each of the 50 trials. Because OBCc represents a percentage of retained oil, any predictions below 0 or above 100 were assigned to 0 and 100, respectively. The raw data, report, and code used to design the model can be accessed through digital commons at (https://digitalcommons.usu.edu/all_datasets/221/).

RESULTS

The purpose of this study was to understand which physical properties were most influential in increasing OBC. To evaluate this, a wide range of physical properties were generated by using different cooling rates, HIU, and dilution factors (Figure 4-1). The physical properties obtained from these conditions will be discussed first, followed by a

description of the relationship between these physical properties and OBC, and finally, a statistical model designed to predict OBC_c.

Figure 4-1: Visual observation of the 100% EIEPO, 50% EIEPO, and 20% EIEPO samples immediately after crystallization the

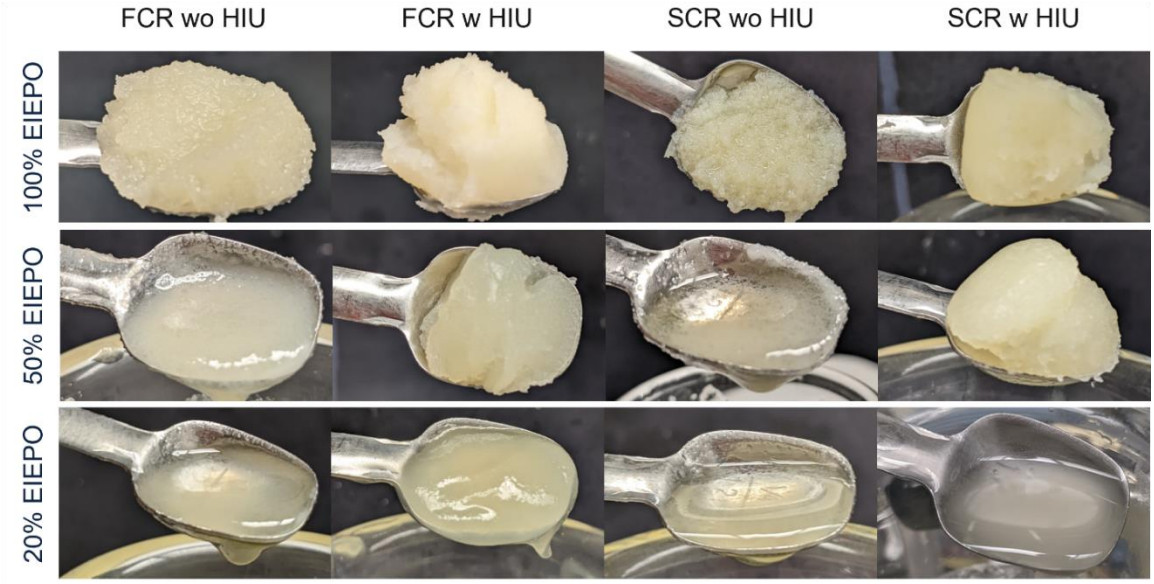

Fatty Acid Composition

Fatty acid composition is summarized in Table 4-2. The 100% (undiluted) sample was primarily composed of oleic acid (40.765% ± 0.253), palmitic acid (38.498% ± 0.334), and linoleic acid (11.988% ± 0.120). Overall diluting the samples with SBO resulted in lower amounts of oleic and palmitic acid and higher amounts of linoleic and linolenic acid.

Table 4-2: Mean fatty acid composition (% w/w) and standard errors for the 100% EIEPO, 50% EIEPO, and 20% EIEPO samples and SBO.

	Fatty Acid Composition			
Fatty Acid	100% EIEPO (% w/w)	50% EIEPO (% w/w)	20% EIEPO (% w/w)	SBO*
C8:0	0.09 ± 0.01	0.03 ± 0.01	0.03 ± 0.01	0.02 ± 0.00
C10:0	0.10 ± 0.01	0.07 ± 0.02	0.08 ± 0.01	0.02 ± 0.00
C12:0	0.66 ± 0.01	0.10 ± 0.01	0.04 ± 0.01	0.02 ± 0.00
C14:0	1.03 ± 0.01	0.47 ± 0.01	0.22 ± 0.01	0.07 ± 0.00
C16:0	38.19 ± 0.32	23.40 ± 0.23	15.41 ± 0.27	10.03 ± 0.00
C16:1n7	0.16 ± 0.01	0.13 ± 0.01	0.10 ± 0.01	0.14 ± 0.00
C18:0	4.44 ± 0.03	3.93 ± 0.03	4.49 ± 0.03	3.96 ± 0.00
C18:1	41.18 ± 0.27	33.08 ± 0.13	26.90 ± 0.09	21.09 ± 0.01
C18:2n6	11.89 ± 0.12	33.20 ± 0.30	44.58 ± 0.18	51.25 ± 0.01
C18:3n3	0.43 ± 0.01	3.58 ± 0.03	5.63 ± 0.02	6.36 ± 0.01
C20:0	0.38 ± 0.01	0.35 ± 0.01	0.39 ± 0.01	0.30 ± 0.00
C20:1n9	0.15 ± 0.01	0.18 ± 0.01	0.19 ± 0.01	0.27 ± 0.00
C20:2n6	0.00 ± 0.00	0.02 ± 0.01	0.03 ± 0.01	0.04 ± 0.00
C20:3n6	0.00 ± 0.00	0.02 ± 0.01	0.02 ± 0.01	0.02 ± 0.00
C22:0	0.08 ± 0.01	0.19 ± 0.01	0.29 ± 0.01	0.32 ± 0.01
C24:0	0.08 ± 0.01	0.09 ± 0.01	0.10 ± 0.01	0.12 ± 0.00
Others	1.13 ± 0.03	1.16 ± 0.16	1.50 ± 0.03	5.98 ± 0.03

*SBO composition was determined by Eurofins using AOCS methods Ce 2-66 mod. and Ce 1b-89

Melting Point

The melting point of the samples was 45.65 ± 0.03 °C, 41.91 ± 0.11 °C, and 29.82 ± 0.27 °C for the 100%, 50%, and 20% samples, respectively. The decrease in melting point as dilution increased is expected based on the changes in fatty acid composition shown in Table 4-2.

Polymorphism

All samples contained β' crystals (peaks at 3.86 ± 0.01 Å and 4.23 ± 0.01 Å) after 90 min isothermal crystallization except for the 20% SCR samples which contained β crystals (peaks at 4.59 ± 0.01 Å and 5.20 ± 0.01 Å). Showing that there were no changes in polymorphic form when HIU was applied to the samples. The sample's X-ray diffraction patterns are shown in Figure B-2.

Crystal Morphology and Microstructure

The morphologies of crystals obtained immediately after crystallization are shown in Figure 4-2, the morphology after 48 h is shown in Figure B-3, and the crystal diameter and number are summarized in Table 4-3.

Figure 4-2: Polarized light microscopy images immediately after crystallization for the 100% EIEPO, 50% EIEPO, and 20% EIEPO samples. Scale bar denotes 50 μm and is the same for all pictures.

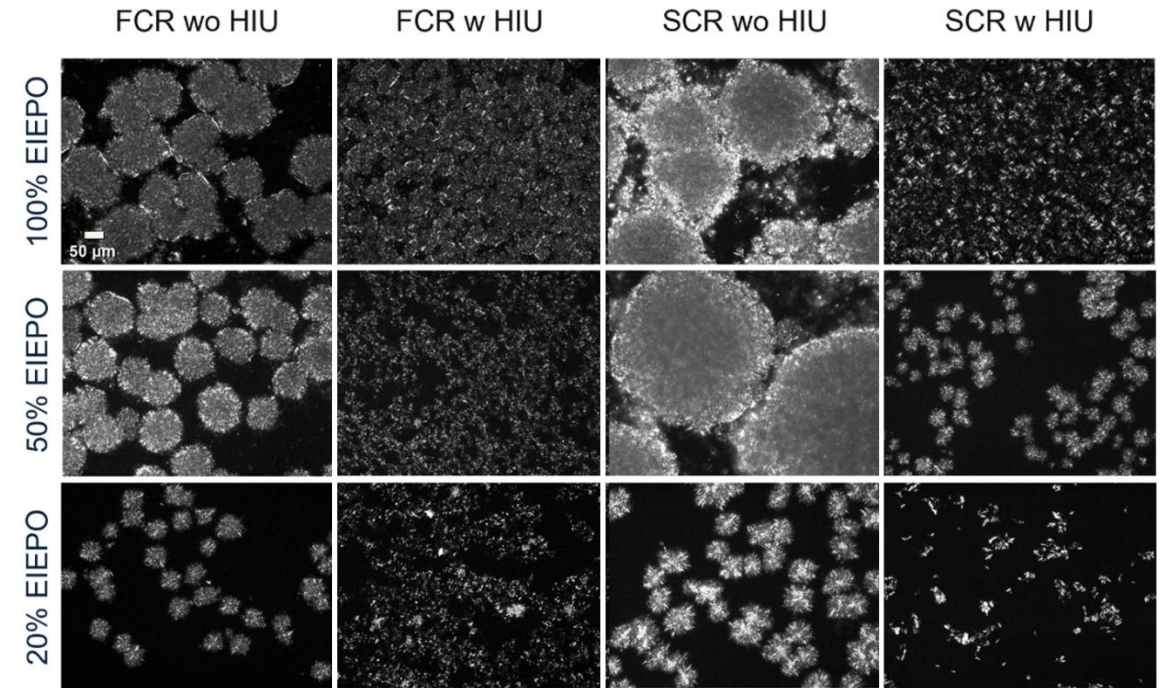

In terms of crystal diameter, there was no change in size over storage time except for the 100% FCR non-sonicated sample from 90 min to 22 °C - in which the crystal diameter decreased. This could be due to additional nucleation that occurred during storage creating smaller crystals that will then decrease the mean value reported which is supported by an observed increase in SFC after storage at 22 °C. The HIU application significantly decreased crystal diameter for all dilutions, time points, and cooling rates. For the number of crystals, sonicated samples had more crystals than non-sonicated samples except for the 50% SCR sonicated samples after 90 min and 48 h at 5 °C. Additionally, the number of crystals did not change over time for any sample conditions. As samples became more diluted, the number of crystals tended to decrease. In terms of size, the 50% dilution tended to have the largest crystals followed by the 20% dilution, and the 100% dilution tended to have the smallest crystal diameter.

Table 4-3: Mean crystal diameter (μm) and crystal number with standard errors for the 100% EIEPO, 50% EIEPO, and 20% EIEPO samples after 90 min isothermal crystallization and after storage for 48 h at 22 °C and 5 °C. Different letters indicate differences within a sample across all time points and crystallization conditions.

Crystal Diameter (μm)				
100% EIEPO				
	FCR wo HIU	FCR w HIU	SCR wo HIU	SCR w HIU
90 min	39.3 ± 4.4^{a}	8.6 ± 0.1^{d}	35.9 ± 4.9^{ab}	12.7 ± 0.6^{d}
48 h 22 °C	24.6 ± 2.3^{bc}	8.8 ± 0.2^{d}	27.5 ± 1.5^{b}	13.0 ± 0.6^{cd}
48 h 5 °C	32.6 ± 2.7^{ab}	8.2 ± 0.2^{d}	34.0 ± 3.7^{ab}	13.1 ± 1.0^{cd}
50% EIEPO				
	FCR wo HIU	FCR w HIU	SCR wo HIU	SCR w HIU
90 min	48.9 ± 3.4^{a}	8.1 ± 0.3^{c}	49.9 ± 6.3^{a}	23.6 ± 2.5^{b}
48 h 22 °C	45.9 ± 2.7^{a}	8.4 ± 0.3^{c}	49.0 ± 4.0^{a}	20.5 ± 2.0^{bc}
48 h 5 °C	45.1 ± 4.5^{a}	8.4 ± 0.2^{c}	44.5 ± 3.5^{a}	16.2 ± 2.1^{bc}
20% EIEIPO				
	FCR wo HIU	FCR w HIU	SCR wo HIU	SCR w HIU
90 min	33.0 ± 2.2^{b}	9.5 ± 0.2^{c}	43.9 ± 5.5^{a}	13.9 ± 0.6^{c}
48 h 22 °C	36.8 ± 1.5^{ab}	9.5 ± 0.2^{c}	36.6 ± 2.7^{ab}	13.6 ± 0.5^{c}
48 h 5 °C	39.8 ± 1.9^{ab}	9.1 ± 0.1^{c}	42.7 ± 3.4^{ab}	11.3 ± 0.3^{c}
Crystal Number				
100% EIEPO				
	FCR wo HIU	FCR w HIU	SCR wo HIU	SCR w HIU
90 min	122 ± 27^{c}	743 ± 196^{b}	134 ± 22^{c}	1680 ± 111^{a}
48 h 22 °C	222 ± 33^{c}	714 ± 60^{b}	163 ± 16^{c}	1446 ± 113^{a}
48 h 5 °C	178 ± 35^{c}	798 ± 53^{b}	157 ± 23^{c}	1489 ± 139^{a}
50% EIEPO				
	FCR wo HIU	FCR w HIU	SCR wo HIU	SCR w HIU
90 min	62 ± 10^{c}	445 ± 45^{ab}	58 ± 13^{c}	281 ± 56^{bc}
48 h 22 °C	70 ± 9^{c}	508 ± 59^{a}	72 ± 10^{c}	424 ± 127^{ab}
48 h 5 °C	100 ± 17^{c}	433 ± 32^{ab}	96 ± 8^{c}	275 ± 17^{bc}
20% EIEPO				
	FCR wo HIU	FCR w HIU	SCR wo HIU	SCR w HIU
90 min	79 ± 11^{d}	389 ± 41^{a}	72 ± 15^{d}	248 ± 28^{bc}
48 h 22 °C	64 ± 5^{d}	380 ± 25^{a}	74 ± 12^{d}	231 ± 32^{c}
48 h 5 °C	80 ± 7^{d}	349 ± 38^{ab}	90 ± 22^{d}	263 ± 22^{bc}

Solid Fat Content

Solid fat content (SFC) results are summarized in Figure 4-3. Overall, SFC decreased as the dilution factor increased due to the dilution of saturated fatty acids. For the 100% sample, there were no significant differences between sonicated and non-sonicated samples across all time points except for the SCR sample stored at 22 °C where the non-sonicated sample had significantly higher SFC. For the 50% sample, the FCR sonicated sample had significantly higher SFC when compared with the FCR non-sonicated sample across all time points. The same trend was observed for the SCR samples immediately after crystallization where the sonicated sample had higher SFC when compared with the non-sonicated sample; however, this trend was not maintained after storage as there was no significant difference in SFC between SCR sonicated and non-sonicated samples after 48 h. For the 20% sample, there was no difference between sonicated and non-sonicated samples except for the SCR sonicated sample stored at 5 °C which had a lower SFC than the non-sonicated counterpart. Additionally, the SFC of the samples was significantly higher ($p<0.05$) when samples were stored at 5 °C than those stored at 22 °C. After storage, the sample's SFC tended to increase while the crystal size and number remained the same. The absence of a correlation between SFC and crystal size and number ($r_s=-0.140$, $p=0.414$) and ($r_s=0.323$, $p=0.055$), respectively; could be attributed to differences in crystal density. Denser crystals could be similar in size and contain the same number of crystals but would have higher SFC due to the TAGs being tightly packed within the crystal.

Figure 4-3: Solid fat content (SFC, %) for the 100% EIEPO, 50% EIEPO, and 20% EIEPO samples after 90 min isothermal crystallization and after storage for 48 h at 22 °C and 5 °C. Different letters indicate differences within a sample across all time points and crystallization conditions.

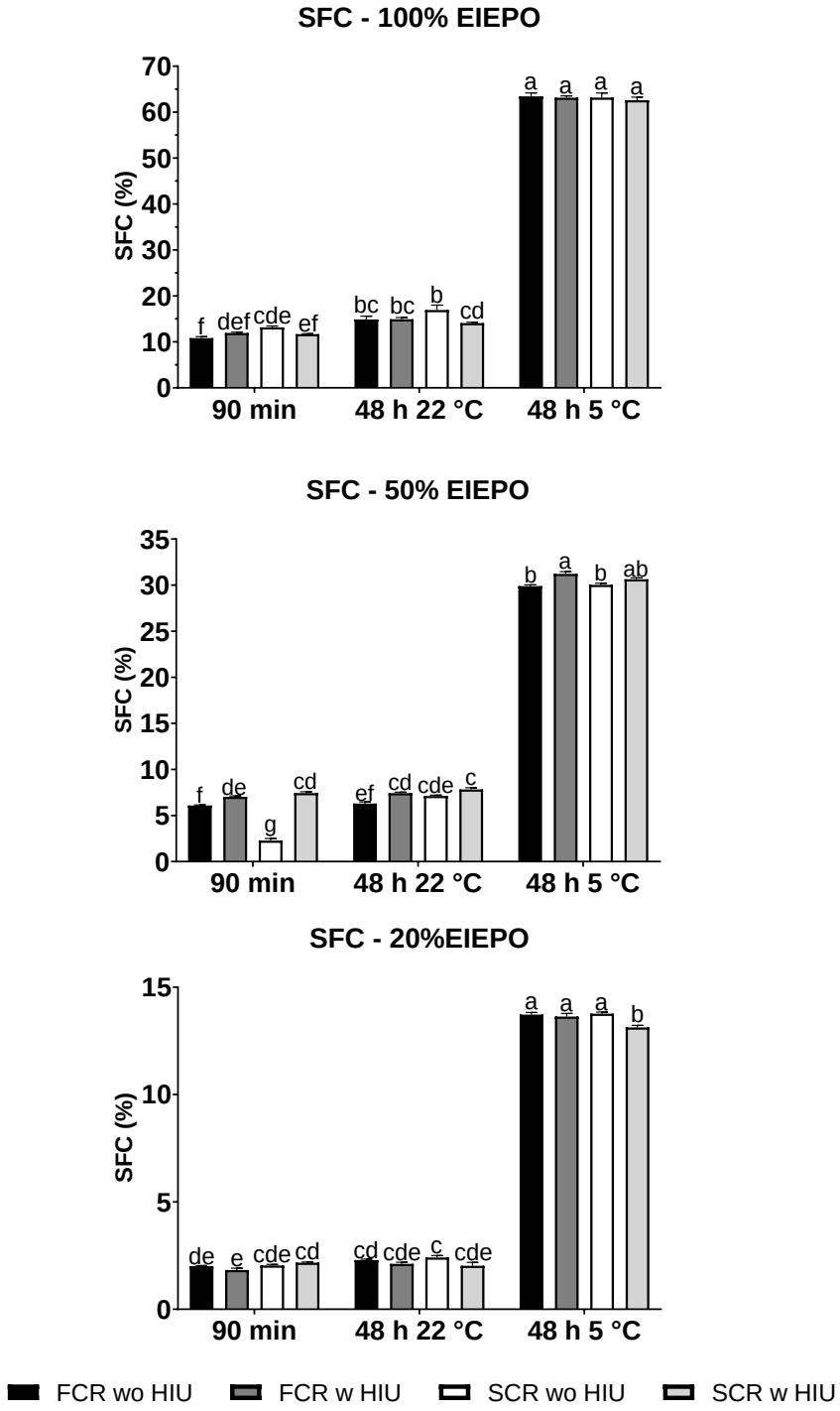

Hardness

The hardness of the samples was measured immediately after crystallization as well as after storage at 22 °C and 5 °C (Figure 4-4). There were no differences in hardness values between crystallization conditions after 90 min and 22 °C for any dilution with an overall average hardness of 0.57 ± 0.01 N. However, there were differences when samples were stored at 5 °C. In general, the hardness of the samples decreased as the dilution increased and SCR samples were softer than FCR samples for most conditions. Additionally, sonication increased the hardness of the 50% FCR and SCR samples as well as the 20% FCR samples only. Interestingly, sonicated samples crystallized using an FCR were harder than sonicated samples crystallized using an SCR ($p<0.05$). These results correspond with Giacomozzi *et al.* (2019) who found that sonicated SCR monoglyceride oleogels were softer than FCR monoglyceride oleogels.

Figure 4-4: Hardness (N) of the 100% EIEPO, 50% EIEPO, and 20% EIEPO samples after 90 min isothermal crystallization and after storage for 48 h at 22 °C and 5 °C. Different letters indicate differences within a sample across all time points and crystallization conditions. n/a indicates that the samples were too soft to measure.

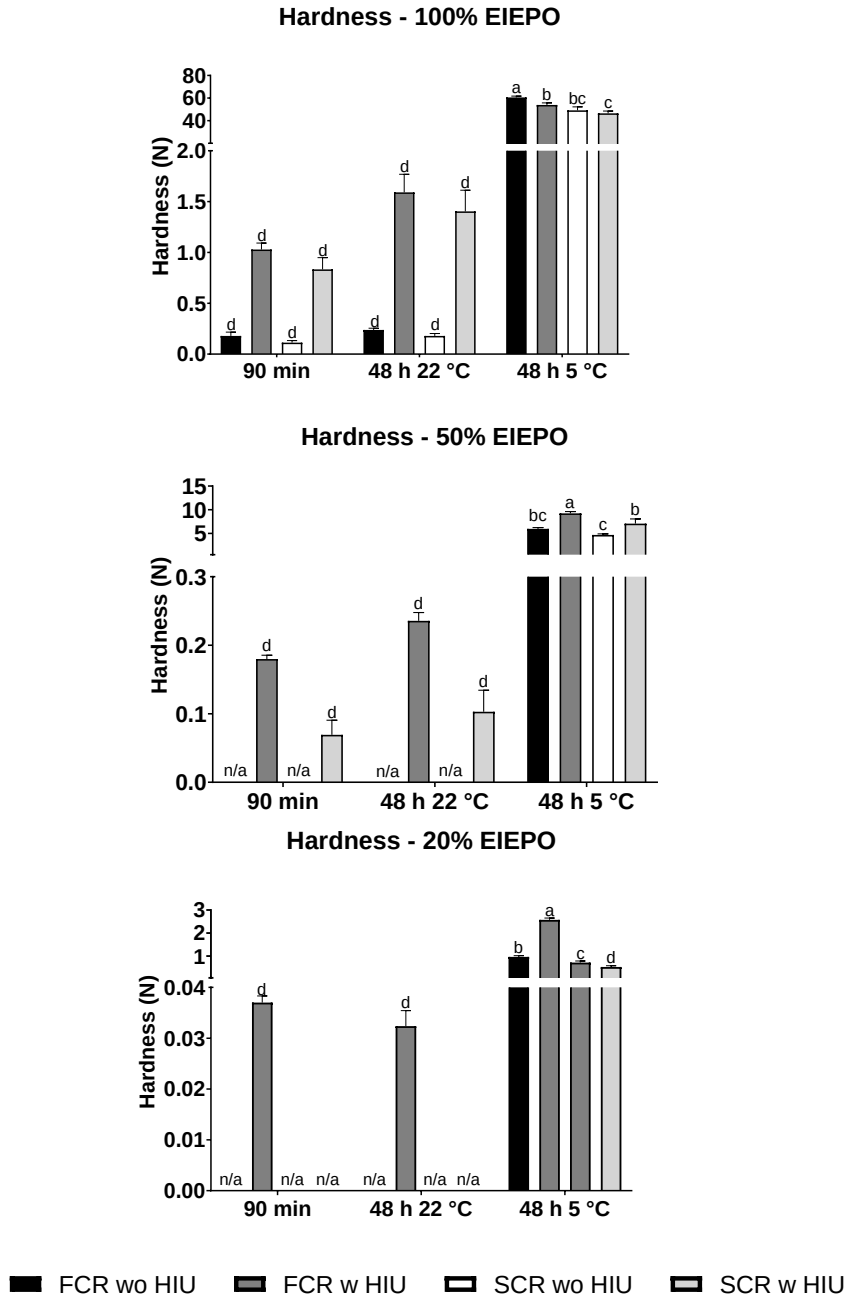

Rheological parameters

The elastic modulus (G′) results are summarized in Figure 4-5 and the viscous modulus (G″), and phase shift angle (δ) results are summarized in Figure 4-6. G′ increased when samples were stored at 5 °C for all crystallization conditions and dilutions. For the 100% sample, there were no significant differences in G′ between crystallization conditions after 90 min as well as after storage at 22 °C, however, there were significant differences when samples were stored at 5 °C which is the same trend that was observed for the hardness data. For the samples stored at 5 °C, the FCR samples had higher G′ than the SCR samples which is the same trend as the hardness data though the SFC data showed no differences between the crystallization conditions at 5 °C. For the 50% sample, there were few differences at 90 min or after 48 h at 22 °C, which matches the trends we saw in the hardness data as the samples were very soft, and no significant differences were observed between crystallization conditions. However, when the 50% samples were stored at 5 °C the non-sonicated samples had higher G′ values than their sonicated counterparts which is an opposite trend to the hardness data and instead aligns with the SFC data.

Figure 4-5: G′ (Pa) for the 100% EIEPO, 50% EIEPO, and 20% EIEPO samples after 90 min isothermal crystallization and after storage for 48 h at 22 °C and 5 °C. Different letters indicate differences within a sample across all time points and crystallization conditions.

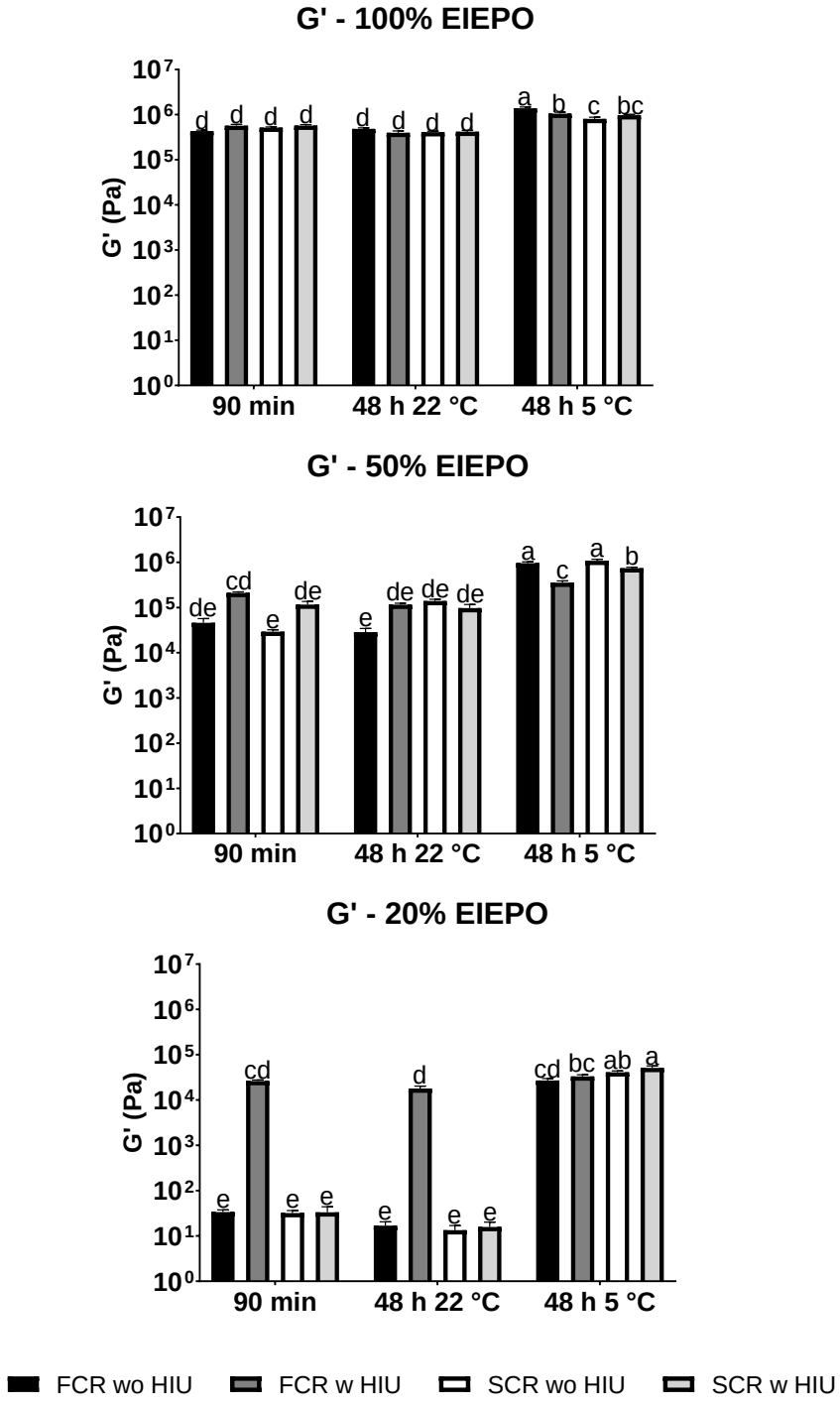

Typically, fats with higher SFC tend to have higher G′ though we found this was not always the case as G′ is influenced by not only SFC but also the structure of the crystal network (Acevedo *et al*., 2017). For the 20% sample, the FCR sonicated sample had the highest G′ at 90 min and after 48 h at 22 °C when compared with the other crystallization conditions. Interestingly, the 20% FCR sonicated sample was also the hardest at all time points. When samples were stored at 5 °C, crystallizing samples with an SCR produced more-elastic fats compared to counterparts crystallized using an FCR. Overall, G′ decreased with dilution which is the same trend observed for the hardness and SFC data. G′ was correlated with SFC (r_s=0.836, $p<0.001$) and hardness (r_s=0.693, $p<0.001$); however, in some cases, softer samples resulted in unexpectedly high G′. One explanation for this difference is that G′ is a small deformation technique whereas hardness is a large deformation and destructive technique.

G″ (Figure 4-6) follows similar trends to G′ though there are fewer differences. For the 100% sample, there were no differences in G″ after 90 min or 48 h at 22 °C, however, when samples were stored at 5 °C the FCR non-sonicated sample was the most viscous. Similar results were found for the 50% sample as there were no differences after 90 min or 48 h at 22 °C but when samples were stored at 5 °C the FCR sonicated sample had the lowest G″ and there was no difference between the other conditions. For the 20% sample, the FCR sonicated sample had the highest G″ after 90 min and 48 h at 22 °C, though, when samples were stored at 5 °C the SCR sonicated sample was the most viscous. In general, δ increased as dilution increased demonstrating that the samples become more viscous-like when diluted which is expected.

Figure 4-6: G″ (Pa), and δ (º) for the 100% EIEPO, 50% EIEPO, and 20% EIEPO samples after 90 min isothermal crystallization and after storage for 48 h at 22 °C and 5 °C. Different letters indicate differences within a sample across all time points and crystallization conditions.

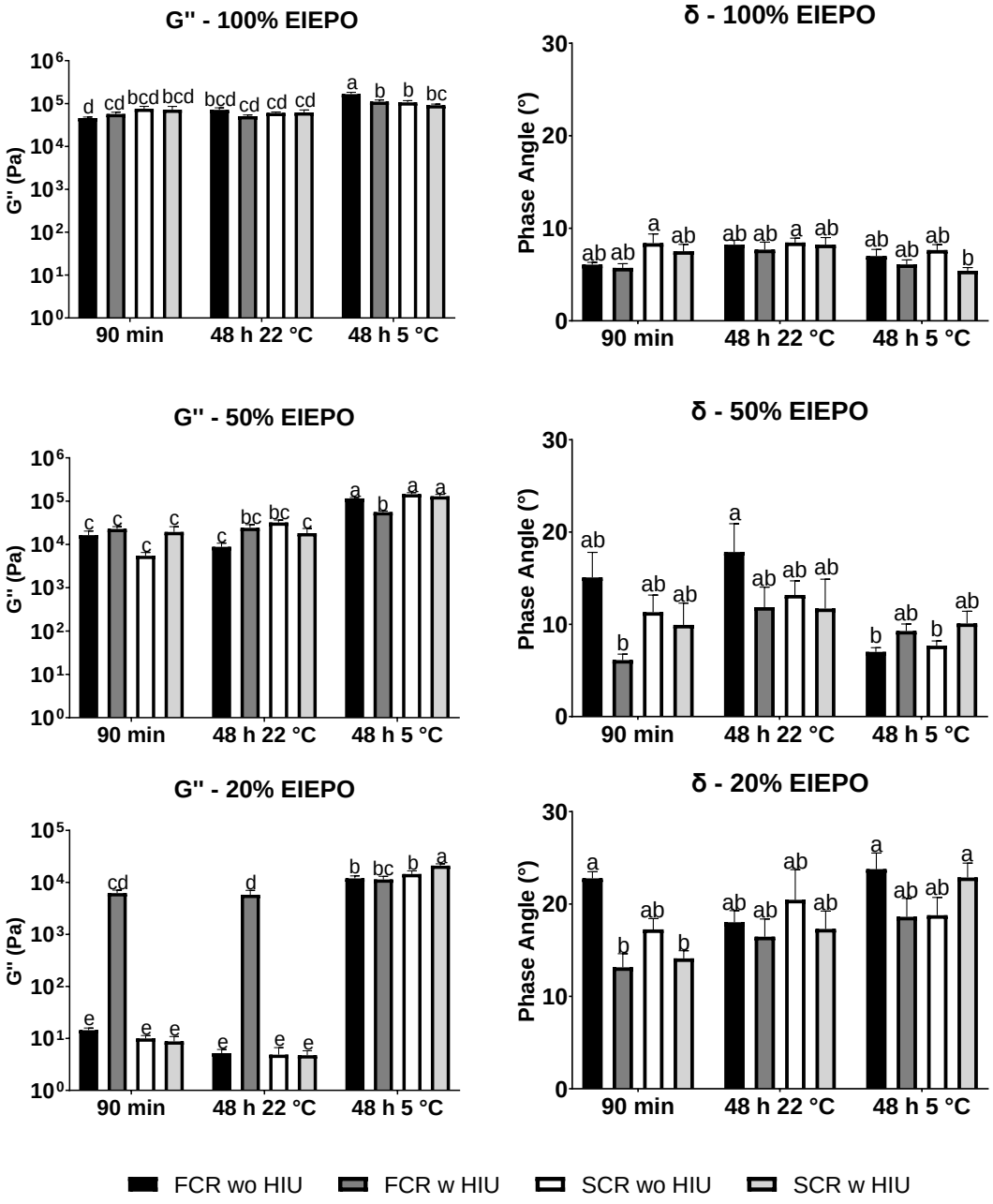

Melting Behavior

The melting profiles are shown in Figure 4-7 and peak temperatures and enthalpy values are summarized in Table 4-4. There were no differences in peak temperatures over time for all dilutions and crystallization conditions. In general, peak temperatures decreased as the dilution increased. For the non-sonicated samples, there were no differences in peak temperature due to the cooling rate. There was a similar trend with the sonicated samples, where there were no differences in peak temperature between the FCR and SCR conditions except for the 50% sample when stored at 5 °C and the 20% after 90 min and storage at 5 °C. There was a significant shift to lower peak temperatures for all sonicated samples except for the 50% SCR samples. The shift in temperature could be due to HIU promoting the co-crystallization of low melting TAGs (da Silva *et al.* 2020c; Lee *et al.*, 2018; Lee *et al*., 2020; Marsh and Martini 2022) which is further validated by there being no difference in polymorphic form between the sonicated and non-sonicated samples.

Figure 4-7: Melting profiles of the 100% EIEPO, 50% EIEPO, and 20% EIEPO samples after 90 min isothermal crystallization and after storage for 48 h at 22 °C and 5 °C.

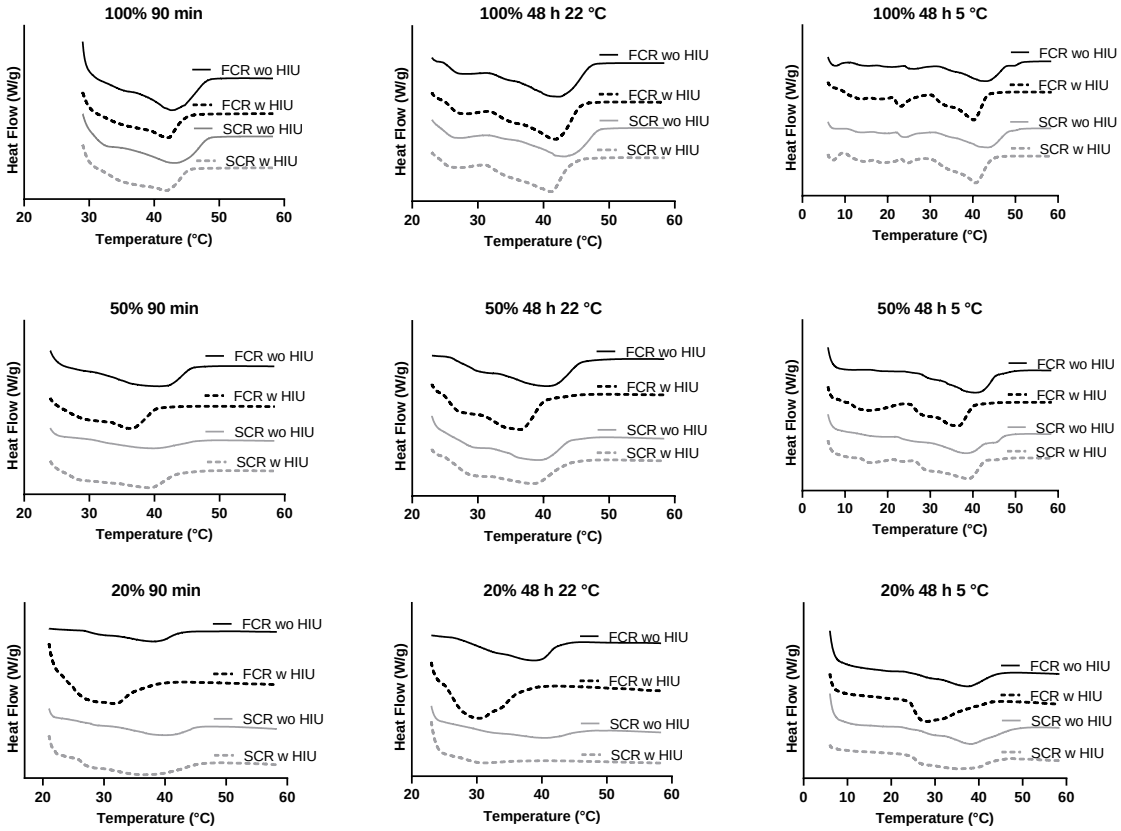

Enthalpy values tended to decrease as the dilution factor increased, which was expected due to the decrease in the total amount of crystalline material as reflected by the SFC data. In the case of the 100% samples, enthalpy increased after storage especially for samples stored at 5 °C which can be explained by the high SFC observed at this time. However, for the 100% samples, there were no significant differences in enthalpy between the crystallization conditions at any time point. For the 50% samples, after 90 min the SCR non-sonicated sample had the lowest enthalpy which could be explained by the low SFC observed for this sample. After storage, there were no significant differences in enthalpy between the crystallization conditions. For the 20% sample after 90 min, the FCR sonicated sample had the highest enthalpy, which was maintained when samples were stored at 22 °C. However, when samples were stored at 5 °C, there were no significant differences between crystallization conditions. Overall, enthalpy was correlated with SFC (r_s=0.783, $p<0.001$) suggesting that in general, higher enthalpy was associated with higher SFC.

Table 4-4: Mean peak temperatures (°C) and melting enthalpy (J/g) with standard errors for the 100% EIEPO, 50% EIEPO, and 20% EIEPO samples after 90 min isothermal crystallization and after storage for 48 h at 22 °C and 5 °C. Different letters indicate differences within a sample across all time points and crystallization conditions.

Peak Temperature (°C)

100% EIEPO				
	FCR wo HIU	FCR w HIU	SCR wo HIU	SCR w HIU
90 min	43.2 ± 0.2^{a}	41.8 ± 0.3^{bcd}	43.7 ± 0.3^{a}	41.6 ± 0.2^{cd}
48 h 22 °C	42.9 ± 0.2^{ab}	41.4 ± 0.2^{d}	43.5 ± 0.2^{a}	41.7 ± 0.3^{cd}
48 h 5 °C	42.8 ± 0.3^{abc}	41.2 ± 0.3^{d}	43.0 ± 0.3^{a}	41.2 ± 0.2^{d}
50% EIEPO				
	FCR wo HIU	FCR w HIU	SCR wo HIU	SCR w HIU
90 min	40.3 ± 0.3^{a}	36.6 ± 0.3^{de}	38.9 ± 0.3^{abc}	37.8 ± 0.7^{cde}
48 h 22 °C	39.7 ± 0.2^{ab}	36.6 ± 0.4^{de}	39.2 ± 0.1^{abc}	37.9 ± 0.4^{bcd}
48 h 5 °C	39.5 ± 0.3^{abc}	36.5 ± 0.2^{e}	39.1 ± 0.3^{abc}	38.2 ± 0.4^{bcd}
20% EIEIPO				
	FCR wo HIU	FCR w HIU	SCR wo HIU	SCR w HIU
90 min	38.0 ± 0.2^{abc}	31.5 ± 0.3^{ef}	41.0 ± 0.8^{a}	36.8 ± 1.5^{bcd}
48 h 22 °C	38.3 ± 0.2^{abc}	30.7 ± 0.4^{ef}	39.8 ± 0.4^{ab}	33.2 ± 1.3^{de}
48 h 5 °C	37.8 ± 0.2^{abc}	28.5 ± 0.2^{ef}	39.9 ± 0.7^{ab}	36.0 ± 0.9^{cd}

Enthalpy (J/g)

100% EIEIPO				
	FCR wo HIU	FCR w HIU	SCR wo HIU	SCR w HIU
90 min	17.5 ± 0.7^{cd}	16.3 ± 0.4^{d}	18.3 ± 1.1^{cd}	17.3 ± 0.4^{cd}
48 h 22 °C	21.2 ± 0.6^{bc}	22.3 ± 0.7^{b}	22.5 ± 0.7^{b}	20.3 ± 0.5^{bcd}
48 h 5 °C	28.5 ± 0.4^{a}	27.4 ± 1.8^{a}	29.1 ± 0.8^{a}	26.9 ± 0.9^{a}
50% EIEPO				
	FCR wo HIU	FCR w HIU	SCR wo HIU	SCR w HIU
90 min	9.4 ± 0.8^{ab}	9.2 ± 0.3^{ab}	6.2 ± 0.8^{c}	8.9 ± 0.2^{abc}
48 h 22 °C	7.8 ± 1.1^{bc}	10.0 ± 0.5^{ab}	9.0 ± 0.7^{abc}	10.0 ± 0.4^{ab}
48 h 5 °C	10.1 ± 0.3^{ab}	10.9 ± 0.2^{a}	10.5 ± 0.6^{ab}	10.3 ± 0.5^{ab}
20% EIEPO				
	FCR wo HIU	FCR w HIU	SCR wo HIU	SCR w HIU
90 min	2.3 ± 0.2^{cde}	3.2 ± 0.2^{abc}	1.3 ± 0.3^{ef}	2.4 ± 0.1^{bcd}
48 h 22 °C	1.5 ± 0.2^{def}	3.3 ± 0.1^{ab}	0.6 ± 0.1^{f}	1.1 ± 0.3^{f}
48 h 5 °C	2.8 ± 0.2^{abc}	3.7 ± 0.2^{a}	2.8 ± 0.2^{abc}	2.6 ± 0.2^{bc}

Oil Binding Capacity

The OBC data using the centrifuge and filter paper methods are summarized in Figure 4-8. OBC_c and OBC_p were positively correlated (r_s=0.818, p=0.003). Examining OBC_c measurements, there was no difference in OBC_c between crystallization conditions for the 100% and 50% stored at 5 °C. However, there were differences after 90 min and when samples were stored at 22 °C with the non-sonicated samples having lower OBC_c. The same trend is seen in the 20% FCR samples where the non-sonicated sample had lower OBC_c at all time points, however, when samples were crystallized using a SCR there were no significant differences between non-sonicated and sonicated samples. The lower OBC_c for non-sonicated samples could be due to these samples typically being softer, having higher peak temperatures, and having lower SFC. It is unlikely that the lower OBC is due to the crystal size since no correlation was found between OBC_c nor OBC_p and crystal size (r_s=-0.254, p=0.134) and (r_s=0.055, p=0.881); respectively. In terms of the relationship between OBC and polymorphism, all samples contained β′ crystals except for the 20% SCR samples which had β crystals. The presence of β crystals did not result in higher OBC_c as the 20% SCR samples with β crystals had the same or lower OBC as the FCR samples containing β′ crystals. Instead of increasing OBC_c, the presence of β crystals may have resulted in lower OBC_c. Unlike the other dilutions that contained β′ crystals, the OBC_c of the 20% SCR sonicated sample was not significantly higher than the nonsonicated sample.

Figure 4-8: Oil binding capacity values using a centrifuge method (OBC_c, %) and filter paper method (OBC_p, %) for the 100% EIEPO, 50% EIEPO, and 20% EIEPO samples after 90 min isothermal crystallization and after storage for 48 h at 22 °C and 5 °C. Different letter indicate differences within a sample across all time points and crystallization conditions.

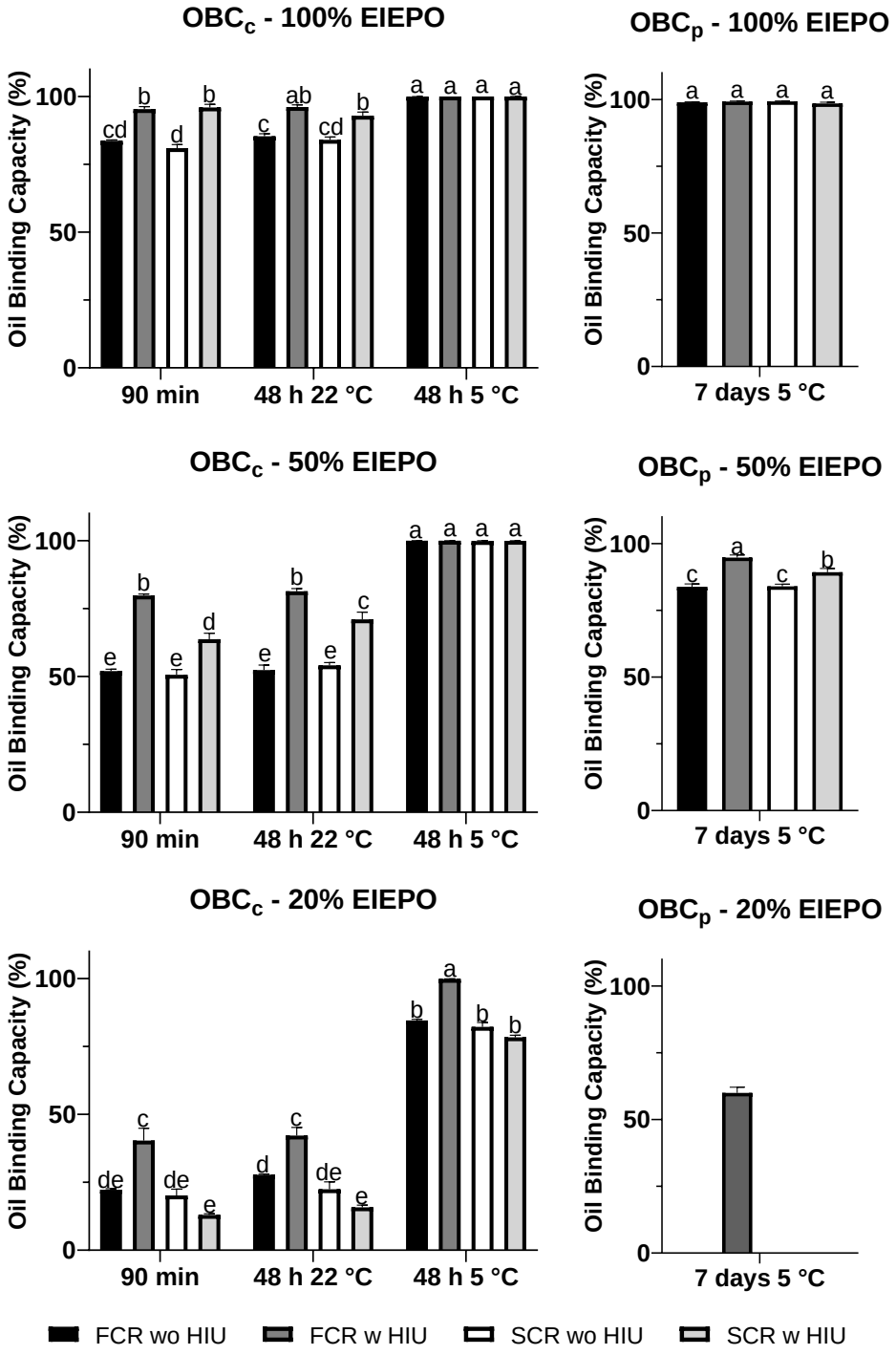

Interestingly, for the 50% and 20% sonicated samples, the use of a FCR resulted in higher OBC_c compared to the SCR at all time points except the 50% sample stored at 5 °C as there was very little oil loss and no difference between crystallization conditions. In general, the samples stored at 5 °C had higher OBC_c than samples immediately after crystallization and samples stored at 22 °C. The increase in OBC_c for samples stored at 5 °C could be attributed to the high SFC and hardness rather than the crystal size as the SFC and hardness significantly increased when stored at 5 °C while the crystal diameter remained the same as immediately after crystallization. Additionally, as the dilution factor increased, OBC_c tended to decrease due to the dilution of SFAs that helped to retain the liquid oil.

In terms of OBC_p, the 20% samples were too soft to mold and OBC_p could not be measured except for the 20% FCR sonicated sample which was hard enough to mold and measure. Results show that there were no differences between crystallization conditions for the 100% sample, however, there were differences for the 50% sample with the non-sonicated samples having lower ($p<0.05$) OBC_p. The differences for the 50% sample may be attributed to the sample's hardness and SFC as non-sonicated samples typically had lower hardness and SFC values than sonicated counterparts. Overall, OBC_p decreased as dilution increased.

Correlation Analysis

After measuring the physical properties, Spearman correlation analysis was performed to understand which physical properties were correlated with OBC (Figure B-4). Results show that OBC measured using a centrifuge, OBC_c, was positively correlated with SFC ($r_s=0.940$, $p<0.001$), hardness ($r_s=0.951$, $p<0.001$), G′ ($r_s=0.868$, $p<0.001$), G″

(r_s=0.872, p<0.001), peak temperature (r_s=0.376, p=0.024), enthalpy (r_s=0.799, p<0.001), and crystal number (r_s=0.447, p=0.006), and negatively correlated with δ (r_s=-0.650, p<0.001). Additionally, OBC measured using a filter paper method OBC_p was positively correlated with SFC (r_s=0.976, p<0.001), hardness (r_s=0.927, p<0.001), and enthalpy (r=0.764, p=0.009) and negatively correlated with δ (r=-0.627, p=0.044). Overall, both measurements were significantly correlated with SFC, hardness, δ, and enthalpy, suggesting that these physical properties are likely the most influential in increasing OBC, excluding any interaction effects.

Statistical Modeling

A LASSO regression model was developed to aid in predicting OBC_c with form [3]:

$$OBC_c = 5.2 * \log(\log(\text{Hardness} + 1)) + 27.34 * \log(\log(SFC + 1) - 0.28 * \text{Peak Temperature} + 5.9 * \log(\text{Enthalpy}) + 0.28 * \log(\text{Crystal Number}) \quad [3]$$

Note that the log and double-log transformations included in the model were used to ensure that each variable shares an approximate linear relationship with the response variable. Similar transformations were applied as necessary to other candidate explanatory variables prior to the LASSO variable selection procedure. The variables included in the final model are those that survived the LASSO variable selection penalty, which discourages large model coefficients, and forces many to zero, after standardizing the explanatory variables. The consequence of the penalty is that the LASSO tends to select only one variable from a group of highly related variables. This explains why G′, G″, and δ were removed from the model despite having significant pairwise correlations with OBC_c. It is possible that a different sample size may result in a different set of selected variables. Nevertheless, the

model results suggest that hardness, SFC, peak temperature, and crystal number are relatively more important than all other considered variables.

To justify the selection of the LASSO model the accuracy was tested using 10-fold cross- validation. In 10-fold cross-validation, the data are randomly separated into 10 groups, with nine groups being used for model training and one for testing. The process is repeated until all groups have been used exactly once for model testing. Accuracy was summarized using the root mean square error (RMSE), which is a measure of the difference between predicted and actual values. The LASSO model was compared to a null model, which used the average OBC_c to predict the test data, and the full model that included all variables. Overall, the RMSE values were 9.41, 30.67, and 9.14 for the LASSO, null, and full models; respectively. The results show that the LASSO model outperforms the null model reducing the error by 69.3% and performs similarly to the full model, indicating that OBC_c can be effectively predicted using only hardness, SFC, peak temperature, enthalpy, and crystal number.

DISCUSSION

Results from this study found that both measurements of OBC were most impacted by SFC, hardness, δ, and enthalpy as they were significantly correlated. Additionally, the model suggests that hardness, SFC, peak temperature, enthalpy, and crystal number are the most efficient set of variables to use in a linear model of OBC_c. Although OBC_c was correlated with the number of crystals, neither OBC_c nor OBC_p were correlated with crystal diameter (r_s=-0.254, p=0.134 and r_s=0.055, p=0.881; respectively). Additionally, the LASSO model found that OBC_c could be predicted well without using crystal diameter as an explanatory variable. The range of mean crystal diameters is shown in Figure B-1 and

no discernable trends were observed. These results imply increasing SFC, hardness, and enthalpy will have the most significant impact on increasing OBC and can be used to aid in the formulation of fats with this desirable property.

When compared with previous research some commonalities and differences were observed. For example, Green and Rousseau (2015) evaluated diffusion coefficients of mixtures of hydrogenated canola oil (HCO) with either canola oil (CO) or light mineral oil (LMO) through fluorescence recovery after photobleaching (FRAP). The authors found that the compositional differences of the fat matrix (canola oil versus light mineral oil in this case) impacted diffusivity which corroborates previous findings by Marsh and Martini (2022). The authors examined the influence of cooling rate, HIU, and dilution factor in an interesterified soybean oil sample in a similar manner to the current study. Marsh and Martini (2022) found that G″ was correlated with both measurements of OBC and in the present study G″ was only correlated with OBCc. Additionally, δ in the previous study was correlated with OBC_c only, and in the current study, both measurements of OBC were correlated with δ. In both studies, OBC_c and OBC_p were positively correlated with SFC, hardness, and enthalpy suggesting that these physical properties have a significant impact on OBC in both fats tested.

Interestingly, neither the previously studied EIESOY sample nor the EIEPO sample were correlated with crystal size. In contrast, work by Acevedo et al. (2012) examined the structure of fully hydrogenated soybean oil and soybean oil blends with and without added unsaturated monoglyceride crystallized statically or under laminar shear (rates of 30 and 240 s-1). The authors evaluated several physical properties including OBC through a filter paper method and found that OBC was negatively correlated with nano- and meso-crystal

size indicating smaller crystal size increased OBC. Afterwards, Acevedo et al. (2017) evaluated similar blends of fully hydrogenated soybean oil and soybean oil with and without the addition of seven different emulsifiers. OBC was measured using a filter paper method which was also used to calculate the diffusion coefficient (D_{eff}) based on the macroscopic scale. Additionally, diffusion coefficients (D_{mol}) were measured using NMR to understand the molecular mobility of oil within the fat matrix. Acevedo et al. (2017) found that oil diffusivity on the molecular level (D_{mol}) was inversely related to meso-crystal dimension indicating that smaller crystals resulted in greater oil movement on the microscopic level. The combination of Acevedo's works showcases that the impact of crystal size is not fully understood.

Kanagaratnam et al. (2013) investigated the deforming temperature's impact on the OBC of palm-based shortening. Three deforming temperatures were used – 25 °C, 40 °C, and 70 °C, and OBC was measured using a stability analyzer that applies a centrifugal force and has a built-in near infrared detector. Kanagaratnam et al. (2013) found that increasing the deforming temperature treatment led to significantly decreased OBC which was attributed to an increase in crystal size. However, as the deforming temperature increased both the hardness and SFC decreased so it is unclear if the observed decrease in OBC was due to an increase in crystal size or if it was due to a decrease in hardness and SFC. Later, da Silva *et al.* (2020c) examined the impact of HIU on a palm-kernel-based fat's physical properties including oil migration which was measured using both a centrifuge and paper method. The authors found that the application of HIU significantly decreased the size of the crystals, did not change the SFC values, and increased the OBC. Therefore, they attributed the increase in OBC to the decrease in crystal size. However, the authors also

found that HIU significantly increased the hardness of the samples which may have also led to the observed increase in OBC. An increase in hardness resulting in increased OBC was also observed in the current study as hardness was significantly correlated with both measurements of OBC.

Moser et al. (2019) examined the use of natural waxes at different levels as stabilizers in peanut butter. OBC of the peanut butters was evaluated using an accelerated centrifugation method as well as a long-term oil release method where tubes of peanut butter were left for up to 6 months and then inverted. Moser et al. (2019) found that increasing the amount of stabilizer resulted in harder peanut butters and increased OBC which matches the findings of Si et al. (2016). Si et al. (2016) measured the oil migration of soybean oleogels prepared using different oleogelators via a scanner imaging technique to track the movement of oil that had been stained. The authors found that firmer samples tended to have less oil movement despite having similar SFC. These studies align with the results of the present study as higher hardness was associated with increased OBC as well.

In terms of the impact of SFC on OBC, the present study found that SFC was significantly correlated with both measurements of OBC and was also an important variable used in predicting OBC_c according to the LASSO model. These results differ from previous research by da Silva et al. (2020a) who evaluated the OBC of an interesterified soybean-based fat using a centrifuge method. The authors found no correlation between SFC and OBC, though a relationship was established when evaluating the ratio of crystal size and SFC. da Silva et al. (2020a) suggested that it was the combination of small crystals and high SFC that led to increased OBC. The impact of SFC on OBC was also studied by Green and Rousseau (2015) in the same mixtures of hydrogenated canola oil (HCO) as

described above. Results from the study showed that at higher SFC (10-15%), diffusion decreased with increasing SFC; however, when the SFC of the samples was 1-9%, the diffusion was indistinguishable. Additionally, a second transition was observed when SFC ~ 40% and 55% for the HCO/LMO and HCO/CO mixtures; respectively where diffusion plateaued. Green and Rousseau's results suggest that the relationship between SFC and diffusion is not linear, which was also found in the current work as an exponential curve between OBC and SFC was observed (Figure A-1).

Although a significant relationship between enthalpy and OBC was established in the current work, the earlier research from da Silva et al. (2020a) as discussed above found no correlations between oil loss and enthalpy. The current study evaluates three dilutions of a palm-based fat resulting in ranges of enthalpy between 0.6 J/g to 29.1 J/g whereas, da Silva et al.'s (2020a) work evaluated a much narrower range of enthalpy between 6.46 J/g to 11.67 J/g. The differing results could be due to Silva et al.'s samples having similar SFC and enthalpy whereas the present study diluted samples to obtain a wider spread of SFC and enthalpy values.

CONCLUSIONS

In conclusion, from this study we found that OBC can be improved by modifying the physical properties of palm-based fats through different processing conditions such as HIU, cooling rate, and dilution factor. The use of HIU generated more and smaller crystals, a shift to lower peak temperatures, and harder and more elastic fats for some samples tested. Also, HIU resulted in higher OBC_c and OBC_p in general. Differences in cooling rates resulted in a wider range of crystal size, number, and morphology. Samples crystallized with SCR were softer and tended to have lower OBC_c compared to FCR counterparts. The

dilution of SFAs resulted in a wide range of textures. In general, as SFAs decreased, crystal number, SFC, hardness, enthalpy, G′, G″, OBC_c, and OBC_p decreased and δ increased. These differences in physical properties resulted in different OBC_c and OBC_p values. OBC_c was positively correlated with SFC, hardness, G′, G″, peak temperature, enthalpy, and the number of crystals and negatively correlated with δ. Additionally, the model found that SFC, hardness, peak temperature, enthalpy, and the number of crystals were the most influential in predicting OBC_c. OBC_p was positively correlated with SFC, hardness, and enthalpy, and negatively correlated with δ. These results can be used to help in the formulation of palm-based fats with higher OBC by increasing SFC, hardness, and enthalpy.

ACKNOWLEDGMENTS

This project was supported by Agriculture and Food Research Initiative (AFRI) grant no. 2020-67017-31193 from the USDA National Institute of Food and Agriculture. This project was also supported by the Utah Agricultural Experiment Station, Utah State University, and approved as paper number 9734. EIEPO samples were kindly donated by Archer-Daniels-Midland (ADM, Decatur, IL, USA). We would like to thank Dr. Robert Ward for measuring the fatty acid composition.

REFERENCES

Acevedo NC, Block JM, Marangoni AG. Critical laminar shear-temperature effects on the nano- and mesoscale structure of a model fat and its relationship to oil binding and rheological properties. Faraday Discuss 2012;158:171–194. https://doi.org/10.1039/C2FD20008B

Acevedo NC, MacMillan B, Newling B, Marangoni AG. Shear effects on the diffusive movement of oil in triacylglycerol networks. RSC Adv. 2017;7:1634–1642. https://doi.org/10.1039/C6RA24829B

Altimiras P, Pyle L, Bouchon P. Structure–fat migration relationships during storage of cocoa butter model bars: Bloom development and possible mechanisms. J Food Eng. 2007;80:600–610. https://doi.org/10.1016/j.jfoodeng.2006.06.022

AOCS. American oil chemists' society (5th ed.) 2009. Official Methods and Recommended Practices of the American Oil Chemists' Society.

Blake AI, Co ED, Marangoni AG. Structure and Physical Properties of Plant Wax Crystal Networks and Their Relationship to Oil Binding Capacity. J Am Oil Chem Soc. 2014;91:885–903. https://doi.org/10.1007/s11746-014-2435-0

Chen F, Zhang H, Sun X, *et al*. Effects of Ultrasonic Parameters on the Crystallization Behavior of Palm Oil. J Am Oil Chem Soc. 2013;90:941–949. https://doi.org/10.1007/s11746-013-2243-y

Da Pieve S, Calligaris S, Co E, *et al*. Shear Nanostructuring of Monoglyceride Organogels. Food Biophysics 2010;5:211–217. https://doi.org/10.1007/s11483-010-9162-3

da Silva TLT, Cooper Z, Lee J, *et al*. Tailoring Crystalline Structure Using High-Intensity Ultrasound to Reduce Oil Migration in a Low Saturated Fat. J Am Oil Chem Soc. 2020a;97:141–155. https://doi.org/10.1002/aocs.12321

da Silva TLT, Danthine S, Martini S. Effect of processing conditions as high-intensity ultrasound, agitation, and cooling temperature on the physical properties of a low saturated fat. J Food Sci 2020b;85:3380–3390. https://doi.org/10.1111/1750-3841.15436

da Silva TLT, Danthine S, Martini S. Influence of sonication, temperature, and agitation, on the physical properties of a palm-based fat crystallized in a continuous system. Ultrasonics Sonochemistry 2021;74:105550. https://doi.org/10.1016/j.ultsonch.2021.105550

da Silva TLT, Marsh M, Gibon V, Martini S. Sonocrystallization as a tool to reduce oil migration by changing physical properties of a palm kernel fat. J Food Sci 2020c;85:964–971. https://doi.org/10.1111/1750-3841.15099

De Graef V, Goderis B, Van Puyvelde P, *et al*. Development of a rheological method to characterize palm oil crystallizing under shear. Euro J Lipid Sci and Tech 2008;110:521–529. https://doi.org/10.1002/ejlt.200700315

Dibildox-Alvarado E, Rodrigues JN, Gioielli LA, *et al.* Effects of Crystalline Microstructure on Oil Migration in a Semisolid Fat Matrix. Crystal Growth & Design 2004;4:731–736. https://doi.org/10.1021/cg049933n

Giacomozzi AS, Palla CA, Carrín ME, Martini S. Physical Properties of Monoglycerides Oleogels Modified by Concentration, Cooling Rate, and High-Intensity Ultrasound. J Food Sci. 2019;84:2549–2561. https://doi.org/10.1111/1750-3841.14762

Green NL, Rousseau D. Oil diffusivity through fat crystal networks. Soft Matter 2015;11:5523–5530. https://doi.org/10.1039/C5SM01355K

Herrera ML, Hartel RW Effect of processing conditions on crystallization kinetics of a milk fat model system. J Am Oil Chem Soc. 2002;77:1177–1188. https://doi.org/10.1007/s11746-000-0184-4

Kadamne JV, Martini S. Sonocrystallization of Interesterified Soybean Oil With and Without Agitation. J Am Oil Chem Soc. 2018;95:571–582. https://doi.org/10.1002/aocs.12075

Kanagaratnam S, Enamul Hoque M, Mat Sahri M, Spowage A. Investigating the effect of deforming temperature on the oil-binding capacity of palm oil based shortening. J Food Eng. 2013;118:90–99. https://doi.org/10.1016/j.jfoodeng.2013.03.021

Lee J, Claro da Silva R, Gibon V, Martini S. Sonocrystallization of Interesterified Soybean Oil: Effect of Saturation Level and Supercooling. J Food Sci 2018;83:902–910. https://doi.org/10.1111/1750-3841.14084

Lee J, Marsh M, Martini S. Effect of storage time on physical properties of sonocrystallized all-purpose shortening. J Food Sci 2020;85:3391–3399. https://doi.org/10.1111/1750-3841.15435

Maleky F, Acevedo NC, Marangoni AG. Cooling rate and dilution affect the nanostructure and microstructure differently in model fats. Euro J Lipid Sci and Tech 2012;114:748–759. https://doi.org/10.1002/ejlt.201100314

Marangoni AG Fat Crystal Networks. 2004. CRC Press

Marsh MA, S. Relationship between oil binding capacity and physical properties of interesterified soybean oil. J Am Oil Chem Soc. 2022;99:313–330. https://doi.org/10.1002/aocs.12578

Martini S, Suzuki AH, Hartel RW. Effect of High Intensity Ultrasound on Crystallization Behavior of Anhydrous Milk Fat. J Am Oil Chem Soc 2008;85:621–628. https://doi.org/10.1007/s11746-008-1247-5

Peyronel F, Campos R, Marangoni AG. Prevention of oil migration in palm mid fraction and palm olein using a stabilizer rich in behenic acid. Food Res Int. 2016;88:52–60. https://doi.org/10.1016/j.foodres.2016.04.001

Sato K. Polymorphism of lipid crystals. In: Sato K, editor. Crystallization of lipids: fundamentals and applications in food, cosmetics, and pharmaceuticals. West Sussex: Wiley; 2018. p. 17–60.

Shih W-H, Shih WY, Kim S-I, *et al.* Scaling behavior of the elastic properties of colloidal gels. Phys Rev A 1990;42:4772–4779. https://doi.org/10.1103/PhysRevA.42.4772

Si H, Cheong L-Z, Huang J, *et al*. Physical Properties of Soybean Oleogels and Oil Migration Evaluation in Model Praline System. J Am Oil Chem Soc 2016;93:1075–1084. https://doi.org/10.1007/s11746-016-2846-1

Smith KW, Cain FW, Talbot G. Effect of nut oil migration on polymorphic transformation in a model system. Food Chem. 2007;102:656–663. https://doi.org/10.1016/j.foodchem.2006.05.045

Tibshirani R. Regression Shrinkage and Selection via the Lasso. J Royal Stat Soc. Series B (Methodological) 1996;58:267–288

Wang H, Shi X, Paluri S, Maleky F. Effects of processing and added ingredients on oil diffusion through cocoa butter using magnetic resonance imaging. RSC Adv 2016;6:88498–88507. https://doi.org/10.1039/C6RA11196C

Winkler-Moser JK, Anderson J, Byars JA, et al. Evaluation of Beeswax, Candelilla Wax, Rice Bran Wax, and Sunflower Wax as Alternative Stabilizers for Peanut Butter. J Am Oil Chem Soc 2019;96:1235–1248. https://doi.org/10.1002/aocs.12276

Ye Y, Martini S. Application of High-Intensity Ultrasound to Palm Oil in a Continuous System. J Agric Food Chem 2015;63:319–327. https://doi.org/10.1021/jf505041s

Ye Y, Wagh A, Martini S. Using High Intensity Ultrasound as a Tool To Change the Functional Properties of Interesterified Soybean Oil. J Agric Food Chem 2011;59:10712–10722. https://doi.org/10.1021/jf202495b

CHAPTER V. ENHANCING OIL BINDING CAPACITY IN A PALM-KERNEL-BASED FAT: IMPACT OF PROCESSING CONDITIONS AND PHYSICAL PROPERTIES

ABSTRACT

The ability of a fat crystal network to entrap liquid oil is known as oil binding capacity (OBC) and is an imperative property in semi-solid fats for use in confectionary, bakery, and snack products. In this study, fully hydrogenated palm-kernel based (FHPKO) lipid matrices were crystallized under different processing conditions to generate samples with a wide range of physical properties and OBC. Three dilutions were created by combining FHPKO with soybean oil (SBO) – 75% FHPKO (containing 25% SBO), 50% FHPKO (50% SBO), and 20% FHPKO (80% SBO) and were crystallized at 33 °C, 30 °C, and 22 °C; respectively. All the samples were crystallized using fast (FCR; 4.6 °C/min) and slow (SCR; 0.1 °C/min) cooling rates, as well as with (w) and without (wo) high-intensity ultrasound (HIU; 20kHz). These processing conditions resulted in four different sets of samples - FCR wo HIU, FCR w HIU, SCR wo HIU, SCR w HIU. Immediately after processing, the sample's hardness, solid fat content (SFC), viscoelasticity (G′, G′′, δ), microstructure, melting behavior (Tpeak, enthalpy), and OBC were analyzed. Samples were then stored at 22 °C and 5 °C for 48 h and the aforementioned properties were measured again as well as starting another OBC measurement. Due to the samples phase behavior, the former OBC was measured by a centrifuge method (labeled OBC_c) and the latter measurement was done by a filter paper method (labeled OBC_p). Results show that both OBC_c and OBC_p were positively correlated with the sample's SFC, storage moduli (G′), hardness, enthalpy, and the number of crystals. While no correlation between OBC_p

and the sample's peak melting temperature and microstructure was recorded, a negative association between the sample's peak melting temperature, phase angle (δ), and crystal diameter was documented for OBC_c. These results suggest oil binding capacity of palm-kernel based crystallized fats can be increased by formulating harder fats that are elastic, contain more crystals, and have higher SFC and enthalpy. Additionally, the FCR with HIU processing conditions was the most effective in increasing the OBC.

INTRODUCTION

Palm-kernel fat (PKO) is commonly used in the confectionary, bakery, and snack industry due to its distinctive fatty acid composition resulting in several advantageous properties. PKO primarily consists of medium chain fatty acids, mainly lauric and myristic acid (da Silva *et al*., 2017a; Lonchampt and Hartel, 2004). The high level of saturated fatty acids results in PKO having a high oxidative stability, rapid solidification, and having a similar texture to cocoa butter while costing less (Talbot, 2009; List, 2016; Watanabe *et al*., 2023; Shukla, 2005). Additionally, PKO can provide excellent gloss to confectionary products and the melting profile of PKO is steep and sharply melts resulting in a pleasant cooling sensation on the tongue. (Watanabe *et al*., 2023; Shukla, 2005; List, 2016).

Although the use of PKO in confectionary applications offers a wide range of advantages, there are some disadvantages namely due to the movement of oil from PKO-based filling to the outer chocolate coating. Fats that have high amounts of lauric acid such as PKO have a significant softening effect due to the incompatibility of PKO and cocoa butter yielding a greater drive for oil to transfer at the filling-coating interface (Tabolt, 2009; Beckett, 2009). The degree to which oil transfer will occur is impacted by the fat matrices' ability to retain liquid oil known as oil binding capacity (OBC). OBC is an

important property in several confectionary products including pralines, truffles, peanut butter cups, and enrobed bars and is often the factor limiting shelf-life (Subramaniam, 2000; Clercq *et al*., 2014). When the fats used in these applications have low OBC, oil movement outside of the fat matrix may result in unwanted physical and chemical changes resulting in fat bloom development, hardening of the filling, and softening of the coating (Tabolt, 2009; Smith *et al*., 2007). In fact, fat bloom is a primary defect in chocolates leading to up to $70 billion in industrial annual losses (Briones and Aguilera, 2005; da Silva *et al*., 2017b). The OBC of fats is impacted by several factors including the processing conditions used during the crystallization process, the composition of the fat, and storage temperature (Clercq *et al*., 2014; da Silva *et al*., 2017b).

Due to OBC largely impacting the shelf-life and profitability of confectionary products several processing conditions used to increase the OBC of fats have been evaluated including modifying the cooling rate and the use of high-intensity ultrasound (HIU). Giacomozzi *et al*. (2019) studied the impact of cooling rate (0.1 and 10 °C/min) on OBC in monoglyceride and sunflower oil-based oleogels. In the study, the use of different cooling rates resulted in differences in oil loss with samples crystallized under faster cooling rates having less oil loss than samples crystallized using slower rates. HIU has also been examined as a novel processing tool to increase the OBC of fats. Da Silva *et al*. (2020a) measured the oil loss of an interesterified soybean oil with and without the application of HIU. The authors found that HIU significantly decreased oil loss as measured with a filter paper and a centrifuge method. Later, da Silva *et al*. (2020b) studied the use of HIU to decrease oil loss in a PKO-based fat. In the study oil loss was measured using a filter paper and centrifuge method. The application of HIU significantly decreased

oil loss with a 52% measured reduction for the filter paper method and a 97.4% reduction for the centrifuge method.

Another factor that largely impacts the OBC is the composition of the fat including the type and concentration of TAGs present. Bouzidi *et al*. (2013) examined the OBC in weight per weight mixtures of 85% canola oil and 15% pure TAGs (SSS, PSP, LSL, MSM, LPL, PSS, PPS, LLS, MMS, and PPL). In the study, OBC was evaluated using a filter paper-based method. Results from the study found mixtures with asymmetrical TAGs had significantly higher OBC than symmetrical TAGs owing to the asymmetrical TAGs having higher nucleation rates. Recently, Watanabe *et al*. (2023) evaluated the impact of adding a 1,3-dioleoyl-2-stearoyl-triacylglycerol (OSO) fat to blends of cocoa butter (CB) and fully hydrogenated palm kernel stearin on the degree of fat bloom. It was concluded that the presence of OSO-fat inhibited fat bloom formation over 15 weeks for samples that had a 1:1 ratio of OSO-fat and CB.

Storage temperature is also believed to greatly impact the degree of oil migration. Depypere *et al*., (2009) studied the extent of oil migration that occurred in filled chocolates stored at 18 °C, 4 °C, and -20 °C and found that lower temperature storage significantly delayed oil migration and fat bloom development. Similarly, Ali *et al*., (2001) compared the bloom formation in filled chocolates stored at 18 °C and 30 °C and found that the samples stored at higher temperatures had pronounced fat bloom. Da Silva *et al*. (2017b) examined the fat bloom formation of dark chocolates that underwent six temperature cycles with each cycling corresponding to 33 °C for 24 h to 20 °C for 24 h compared to chocolate samples stored for 100 days at 20 °C. The authors found that temperature cycling resulted in significant visual fat bloom development whereas samples stored for 100 days at 20 °C

showed no fat bloom.

Differences in OBC due to composition, storage, and processing is largely a result of these conditions modifying the physical properties of fats including changes in hardness, SFC, polymorphism, and crystal size (da Silva *et al*., 2017a; da Silva *et al*. 2017b; da Silva *et al*., 2020a; da Silva *et al*., 2020b; Tietz and Hartel, 2000; Watanabe *et al*., 2023; Dibildox-Alvarado *et al*., 2004). The aim of this study is to understand how these factors impact the physical properties and consequently how the physical properties impact the OBC for a PKO-based fat. Thus, the composition of the samples was modified via dilution with SBO, the samples were stored at two temperatures – 22 °C and 5 °C, and four processing conditions were used. For each condition, physical properties – SFC, hardness, crystal size, polymorphism, viscoelasticity, and melting behavior were measured as well as the OBC. A similar approach was previously used to evaluate a soy-based fat and a palm-based fat (Marsh and Martini, 2022; Marsh *et al.*, 2024). However, due to the composition impacting the OBC of fats, it is imperative that a common confectionary fat (PKO) also be examined to aid in the development of fat-based foods that are more resistant to unwanted oil migration.

MATERIALS AND METHODS

Materials

In this study, three dilutions of FHPKO were used – 75% FHPKO diluted 25% weight by weight (w/w) with soybean oil (SBO), 50% FHPKO diluted 50% w/w with SBO, and a 20% FHPKO sample diluted 80% w/w with SBO. The FHPKO was kindly donated by AAK (Richmond, CA, USA) and the SBO was purchased at a local grocery store (Great

Value Brand, Bentonville, AR, USA)

Fatty Acid Composition

The fatty acid analysis of the dilutions was performed with a gas chromatogram (GC; Shimadzu 2010, Columbia, MD, USA) equipped with a flame ionization detector (Shimadzu, Columbia, MD, USA). The composition was determined through the generation of fatty acid methyl esters (FAME) via trans-esterification of the fatty acids. Samples were first melted at 60 °C for 15 min and a 40 µL aliquot of the melted sample was placed in a culture tube with 6.3 mL of MeOH and 0.7 mL of 10N KOH in water. The culture tubes were placed in a 55 °C water bath for 90 min with auto shaking and subsequently cooled on ice prior to adding 0.58 mL of 24 N H_2SO_4. Once the H_2SO_4 had been added, the tubes were again placed in 55 °C water bath for 90 min with auto shaking. Afterwards, 2 mL of hexane was added, the samples were centrifuged, and the hexane layer on the top was pipetted into a 2 mL GC vial. One microliter from the GC vial was injected into a 30m length x 0.25mm I.D. x 0.2um film thickness HP88 column (Agilent Technologies, Santa Clara, CA, USA). The split ratio was 50:1, and the carrier gas was hydrogen with a linear velocity of 41 cm/sec. The initial temperature of the oven was set to 125 °C and ramped to 145 °C at a rate of 26.2 °C/min. Once the oven had held the samples at 145 °C for 7.9 min, the temperature increased at a rate of 6.5 °C/min until it reached 220 °C and the samples were held at 220 °C for 8 min. The injector and detector were both held at 250 °C. Peaks were identified through comparison of retention times with FAME standards (GLC 463, NuChek Prep, Elysian, MN, USA). The samples were measured in duplicate and reported as normalized area percentage.

Melting Point

To determine the melting point of the dilutions a differential scanning calorimeter (DSC; Q20, TA Instruments, New Castle, DE, USA) calibrated with an indium standard was used. Between 10-15 mg of the sample was placed in a DSC hermetic aluminum pan and sealed before being placed in a DSC oven set to 22 °C with an empty pan as the reference. The sample underwent the following conditions – heat to 60 °C at rate of 5 °C/min, hold at 60 °C for 30 min, cool to -20 °C at a rate of 5 °C/min, and heat to 60 °C at a rate of 5 °C/min. The purpose of this procedure was to erase the existing crystal memory, then induce crystallization, and finally measure the melting behavior. The melting point was determined as the highest melting peak from the resulting thermograph and the measurement was performed in duplicate.

Crystallization and Processing Conditions

Prior to crystallization, 100 g of the molten sample was weighed in a beaker and placed in a 60 °C oven for 30 min. The purpose of this was to erase the crystal memory to ensure differences in the properties were due to the processing conditions that the sample underwent. The samples were crystallized in a double-wall crystallization cell attached to an external water bath. There was a thermocouple inside of the crystallization cell to track the temperature and calculate the cooling rate as well as a magnetic stir bar set to 200 rpm that was used to facilitate heat transfer. After being in the oven for 30 min, the sample was quickly transferred to the crystallization cell and a timer was started, the moment the sample was added to the cell is considered time zero. The dilutions were crystallized at 33 °C, 30 °C, and 22 °C for the 75% FHPKO, 50% FHPKO, and 20% FHPKO samples; respectively (Table 5-1).

Table 5-1: Crystallization temperatures for each of the samples, total time duration of the crystallization process, times at which agitation was stopped, and times that HIU was applied. Time zero is the time when samples were poured into the crystallization cell.

Crystallization Conditions

Sample	Crystallization temp (°C)	Total Duration (min)	Agitation stopped (min)	HIU applied (min)
75% FCR	33	90	8	12
75% SCR	33	360	225	255
50% FCR	30	90	10	12
50% SCR	30	390	250	265
20% FCR	22	90	8	10
20% SCR	22	470	315	330

Each dilution was crystallized under four processing conditions – fast cooling without HIU (FCR wo HIU), fast cooling with HIU (FCR w HIU), slow cooling without HIU (SCR wo HIU), and slow cooling with HIU (SCR w HIU). To achieve the fast and slow cooling rates, two water baths were used – a programmable water bath set to 60° which decreased the temperature 0.1 °C/min until the crystallization temperature was reached (Ecoline Staredition RE310, Lauda Brinkmann, Delran, NJ, USA) and a water bath set to the crystallization temperature which had a measured cooling rate of 4.6 °C/min (MX 7L R-20, VWR International, Radnor, PA, USA). The samples were crystallized at the crystallization temperature for 90 min, thus the SCR samples took between 270 to 380 min to reach temperature and then crystallized isothermally for 90 min. Previous work has found that HIU is most effective when applied to static samples at the onset of crystallization (Ye *et al*., 2011; Kadamne and Martini, 2018). Therefore, HIU was applied after the agitation from the magnetic stir bar was stopped and when the first crystals became visible to the naked eye. HIU (Q500 system, Qsonica, Newtown, CT, USA) was applied using a 3.2 mm titanium tip, 10 s pulse duration, 20 kHz frequency, and 40% amplitude

resulting in an average power of 44 Watts.

Crystal Size, Morphology, and Visual Appearance

The morphology of the crystals was determined by a polarized light microscope (PLM; Olympus BX41 microscope, Olympus, Tokyo, Japan) connected to a camera (Infinity 2, Lumenera Scientific, Ottawa, ON, Canada) under a 10x objective lens. One drop of the sample was placed on glass slide, covered with a glass cover slip, and observed under the microscope. The morphology of the crystals was observed immediately after crystallization as well as after storage for 48 h at 22 °C and 5 °C. Image-Pro Premier E 9.2 (Media Cybernetics, USA) was used to measure the size of the crystals were a minimum diameter of 5 μm was used as the threshold for the crystals. This measurement was performed in sextuplet for the 75% dilutions after 48 h of storage except for the FCR w HIU condition due to variance in crystal diameter as many small crystals were generated after storage. The measurement was performed in triplicate for all other conditions. In addition to imaging the microstructure of the samples, the visual appearance was observed immediately after crystallization.

Polymorphism

To determine the polymorphic form of the PKO crystals, an x-ray diffractor (XRD; MiniFlex600, Rigaku, Tokyo, Japan) was used. The samples were crystallized as described above (Section 2.4) and underwent the XRD measurement immediately after crystallization and after storage for 48 h. To obtain better resolution, samples with a SFC less than 18% were filtered under vacuum to concentrate the crystals prior to being placed on the XRD slide. The samples were measured 3 to 30 ° at a rate of 1.0 ° per min using 40 kV of voltage and a 15 mA current and a Cu Kα radiation source. The polymorphic form

of the crystals was determined from peaks shown on the intensity and position graph (°2θ).

Solid Fat Content

A time-domain nuclear magnetic resonance equipment (TD-NMR, 120 Minispec NMR analyzer, Bruker, Rheinstetten, Germany) was used to determine the SFC of the samples. After crystallization, six NMR tubes were filled with ~ 2 mL of sample and measured in the NMR. Afterwards, three of the tubes were placed at 22 °C and three were placed at 5 °C for 48 h. After storage, the SFC of the samples was measured again.

Hardness

A texture analyzer (TMS-Pro; Food Technology Corp., Sterling, VA, USA**)** was used to determine the hardness of the samples. After crystallization, three 10 mL beakers were filled with the sample, the hardness was measured after crystallization, and stored for 48 h. After storage, the hardness of the samples was measured again through a two-cycle penetration test using a 6-mm cylindrical probe and a 50 N or 500 N load cell depending on the sample's hardness**.** To initiate the measurement, the probe was lowered until it contacted the surface of the sample with a force of 0.01 N and then penetrated 15 mm into the sample at a cross-head speed of 1 mm/s. The probe then returned to the zero position at the surface of the sample, paused for 10 s to allow the sample to equalize, and penetrated 15 mm into the sample at a speed of 1 mm/s again before returning to the zero position. The maximum force of the first peak in the resulting force-time curve was determined as the hardness of the sample.

Viscoelasticity

Viscoelastic properties of the samples - storage modulus (G′) and loss modulus (G″) were measured and phase shift angles (δ) were calculated with a rheometer (AR-G2, TA

Instruments, New Castle, DE, USA) equipped with an 8 mm parallel plate geometry. An oscillatory test with a strain sweep procedure from 0.001% to 10% at a frequency of 1 Hz was used. The rheometer's stage was set to the crystallization or storage temperature and approximately 1 g of sample added. The size of the gap was between 500 to 2000 μm depending on the hardness of the sample. G′, G″, and δ were determined from the middle of the linear viscoelastic region corresponding to a strain of 0.01%. Measurements were performed in triplicate and the samples were evaluated immediately after crystallization as well as after storage for 48 h.

Melting Behavior

The melting behavior of the samples was measured immediately after crystallization as well as after 48 h at 22 °C and 5 °C using a DSC (Q20, TA Instruments, New Castle, DE, USA). Between 5-20 mg of the sample was weighed in a hermetic aluminum pan, sealed, and placed in a DSC oven with an empty pan as the reference. The temperature of the oven was set to either the crystallization or storage temperature and the samples were left for 1 min. After 1 min, the temperature increased 5 °C/min until it reached 60 °C. The resulting thermograph was analyzed, and the peak temperature and enthalpy were calculated. These measurements were performed in duplicate.

Oil Binding Capacity

Two methods were used to quantify the OBC of the samples – a centrifuge method and a filter paper method. Both methods were chosen due to limitations with a singular method. The centrifuge method is faster, it can be used to calculate the OBC of the samples immediately after crystallization, and it can be used for soft samples. However, the centrifugal forces that expediate the movement of liquid oil are not the typical conditions

that the samples would experience in food applications. The filter paper method takes a longer time and cannot be used with samples that are too soft as they stick to the paper. The approach of using both methods lends itself well to experimental rigidity.

Centrifuge Method

The centrifuge method has been previously used to quantify the OBC of fats (Marsh *et al*., 2024; Marsh and Martini 2022; Giacomozzi *et al*., 2019; da Pieve *et al*., 2010). For this measurement, four microcentrifuge tubes were weighed, filled with 1 g of sample, and reweighed. The microcentrifuge tubes were then placed in a centrifuge and spun for 15 min at 10,000 rpm (9600 rcf). After centrifugation, the tubes were opened and inverted for 3 min to remove the liquid oil. Afterwards, the tubes were weighed, and the following equation [1] was used to calculate OBC_c:

$$OBC_c = \left[1 - \left(\frac{w_b - w_a}{w_s}\right)\right] * 100 \quad [1]$$

where w_b is the sample and tube weight prior to centrifuging, w_a is the sample and tube weight after centrifuging and dispelling the liquid oil, and w_s is the sample weight. To control the temperature of the samples during centrifugation, three centrifuges were used. One centrifuge (accuSpin micro 17 centrifuge, Fisher Scientific, USA) was used for the samples immediately after crystallization and was kept in an incubator set to the crystallization temperature. A second centrifuge (Sorvall micro 17 centrifuge, Thermo Scientific, Germany) was kept on a counter at room temperature and used for the samples stored at 22 °C. The third centrifuge (Avanti 30 364104, Beckman Instruments, Palo Alto, CA, USA) was left in walk-in cooler and was set to 5 °C prior to the measurement.

Filter Paper Method

The filter paper method was adapted from previous studies (Marsh *et al*., 2024; Marsh and Martini, 2022; Altimiras *et al*., 2007; Peyronel *et al*., 2016). After crystallization, four circular molds (22 mm diameter x 3 mm height) were filled with the sample, covered with parafilm, and stored at 22 °C and 5 °C for 48 h. After 48 h, the samples were removed from the molds, weighed, and placed on a pre-weighed filter paper (Whatman #1, 125mm diameter). The filter papers and samples were subsequently stored at 22 °C and 5 °C and an empty filter paper was kept with these samples to account for environmental changes. Every day for seven days, the sample was removed from the filter paper, the filter paper was weighed, and the diameter of the oil stain was measured. The final weight of the filter paper was used to quantify the OBC_p using the following equation:

$$OBC_p = \left[1 - \left(\frac{wp_{(t)} - wp_{(0)}}{ws_{(0)}}\right)\right] * 100 \quad [2]$$

where $wp_{(t)}$ is the weight of the filter paper at specific times (day 1-7), $wp_{(0)}$ is the weight of the filter paper on day 0, and $ws_{(0)}$ is the weight of the sample on day zero. The reported values are the OBC_p on the last day.

Statistical Analysis

Crystallization experiments were conducted in triplicate. The reported values are the mean and standard errors of the three crystallization experimental replicates. Two-Way ANOVA tests were performed to compare processing and storage conditions and post-hoc tests were utilized to determine significant differences (α=0.05). Spearman correlation analysis was performed to understand the relationship between the physical properties and OBC. Spearman correlation was chosen over Pearson correlation due to the nonlinear relationship between OBC and the physical properties (Figure C-1). Statistical analyses

were performed in GraphPad Prism (v9, San Deigo, CA, USA).

RESULTS AND DISCUSSION

Fatty Acid Composition

Fatty acid composition of the dilutions is shown in Table 5-2 and Table C-1 contains the composition of the SBO and FHPKO used to prepare the dilutions. Overall, as the amount of SBO increases, there was a decrease in short and medium chain fatty acids such as caprylic, capric, lauric, and myristic acid and an increase in unsaturated fatty acids including oleic, linoleic, and linolenic acid. The percentage of saturated fatty acids (SFA) in the 75% PKO, 50% PKO, and 20% PKO samples was 78.40 ± 2.54%, 54.88 ± 0.02%, and 29.27 ± 0.01%; respectively.

Table 5-2: Mean fatty acid composition (% w/w) and standard errors for the 75% FHPKO, 50% FHPKO, and 20% FHPKO samples.

Fatty Acid	75% FHPKO	50% FHPKO	20% FHPKO
C8:0	2.43 ± 0.11	1.52 ± 0.01	0.62 ± 0.01
C10:0	2.33 ± 0.08	1.47 ± 0.01	0.10 ± 0.01
C12:0	33.97 ± 1.09	21.46 ± 0.03	8.15 ± 0.01
C14:0	11.72 ± 0.35	7.44 ± 0.01	2.81 ± 0.01
C16:0	10.27 ± 0.33	10.05 ± 0.01	10.09 ± 0.01
C16:1n7	0.02 ± 0.01	0.04 ± 0.01	0.06 ± 0.01
C18:0	17.19 ± 0.55	12.35 ± 0.01	6.78 ± 0.01
C18:1	6.85 ± 0.04	12.12 ± 0.01	18.66 ± 0.01
C18:2n6	14.97 ± 0.56	28.17 ± 0.01	44.77 ± 0.01
C18:3n3	1.80 ± 0.07	3.43 ± 0.01	5.46 ± 0.01
C20:0	0.29 ± 0.01	0.31 ± 0.01	0.33 ± 0.01
C20:1n9	0.05 ± 0.01	0.11 ± 0.01	0.17 ± 0.01
C20:2n6	0.00 ± 0.00	0.02 ± 0.01	0.03 ± 0.01
C20:3n6	0.01 ± 0.01	0.02 ± 0.01	0.03 ± 0.01
C22:0	0.12 ± 0.01	0.19 ± 0.01	0.28 ± 0.01
C24:0	0.8 ± 0.01	0.09 ± 0.01	0.11 ± 0.01
Others	1.14 ± 0.04	1.22 ± 0.01	1.55 ± 0.01
SFA	78.40 ± 2.54	54.88 ± 0.02	29.27 ± 0.01

Melting Point

The melting point for the dilutions was 41.61 ± 0.06 °C, 39.55 ± 0.14 °C, and 35.11 ± 0.11 °C, for the 75% FHPKO, 50% FHPKO, and 20% FHPKO samples; respectively. The decrease in melting point was expected based on the change in fatty acid composition as the amount of SBO increased (Table 5-2).

Crystal Size and Morphology, Visual Appearance, and Polymorphism

The use of the three dilutions and different processing conditions generated a wide range of crystal sizes, crystal morphologies, and visual appearances (Figure 5-1). In all dilutions, the crystal's diameter immediately after crystallization was the largest for the SCR non-sonicated samples and the smallest for the FCR sonicated samples (Table 5-3). This trend was maintained for the 50% and 20% FHPKO dilutions after storage for 48 h but was not seen in the 75% FHPKO dilution. During storage, the 75% FHPKO dilution generated many small crystals around the larger crystals formed after 90 min (Figure C-2 and Table 5-3). The formation of the small crystals resulted in no differences in crystal diameter and number between the processing conditions after storage for the 75% FHPKO samples. Da Silva *et al*. (2020b) observed similar formation of many small crystals around large crystals in a palm kernel-based fat. The small crystals were likely a result of the crystallization of TAGs with melting points below the crystallization temperature of 33 °C being able to crystallize when stored at 22 °C and 5 °C. For the 50% FHPKO dilution, the crystal diameter decreased after storage for the non-sonicated samples and did not change for the sonicated samples. In this instance, the application of HIU may have resulted in the co-crystallization of the lower melting point TAGs for the 50% samples when a FCR was used resulting in less of these TAGs crystallizing during storage.

Table 5-3: Mean crystal size diameter and standard errors for the 75% FHPKO, 50% FHPKO, and 20% FHPKO samples. Different letters indicate significant differences within a sample.

Crystal Diameter (μm)				
75% FHPKO				
	FCR wo HIU	FCR w HIU	SCR wo HIU	SCR w HIU
90 min	83.5 ± 20.1^{b}	16.6 ± 2.5^{c}	135.2 ± 4.0^{a}	81.7 ± 6.3^{b}
48 h 22 °C	13.3 ± 0.6^{c}	12.7 ± 2.5^{c}	10.7 ± 0.4^{c}	14.2 ± 0.8^{c}
48 h 5 °C	19.9 ± 6.5^{c}	9.5 ± 0.1^{c}	10.9 ± 0.1^{c}	14.7 ± 1.7^{c}
50% FHPKO				
	FCR wo HIU	FCR w HIU	SCR wo HIU	SCR w HIU
90 min	47.9 ± 1.2^{b}	10.2 ± 0.1^{d}	101.6 ± 2.1^{a}	28.5 ± 2.4^{c}
48 h 22 °C	29.8 ± 3.1^{c}	11.7 ± 1.7^{d}	32.7 ± 3.6^{c}	26.6 ± 1.5^{c}
48 h 5 °C	29.6 ± 4.5^{c}	10.4 ± 0.7^{d}	31.4 ± 3.3^{c}	23.1 ± 1.2^{cd}
20% FHPKO				
	FCR wo HIU	FCR w HIU	SCR wo HIU	SCR w HIU
90 min	18.7 ± 2.3^{b}	9.7 ± 0.5^{c}	36.1 ± 3.0^{a}	18.0 ± 2.2^{bc}
48 h 22 °C	20.1 ± 1.9^{b}	8.9 ± 0.3^{c}	31.7 ± 1.2^{a}	17.3 ± 1.6^{bc}
48 h 5 °C	19.4 ± 1.1^{b}	9.0 ± 0.3^{c}	30.3 ± 2.0^{a}	14.9 ± 1.6^{bc}
Number of Crystals				
75% FHPKO				
	FCR wo HIU	FCR w HIU	SCR wo HIU	SCR w HIU
90 min	57 ± 25^{bc}	607 ± 83^{a}	17 ± 1^{c}	42 ± 10^{bc}
48 h 22 °C	834 ± 102^{a}	580 ± 21^{ab}	798 ± 9^{a}	883 ± 43^{a}
48 h 5 °C	800 ± 280^{a}	766 ± 68^{a}	757 ± 71^{a}	888 ± 162^{a}
50% FHPKO				
	FCR wo HIU	FCR w HIU	SCR wo HIU	SCR w HIU
90 min	106 ± 5^{cd}	545 ± 80^{a}	24 ± 1^{d}	208 ± 30^{cd}
48 h 22 °C	209 ± 34^{cd}	629 ± 57^{a}	238 ± 35^{cd}	247 ± 13^{c}
48 h 5 °C	229 ± 56^{cd}	509 ± 42^{ab}	271 ± 47^{c}	304 ± 42^{bc}
20% FHPKO				
	FCR wo HIU	FCR w HIU	SCR wo HIU	SCR w HIU
90 min	287 ± 66^{abc}	388 ± 36^{a}	119 ± 12^{c}	291 ± 22^{abc}
48 h 22 °C	237 ± 9^{abc}	244 ± 42^{abc}	144 ± 9^{c}	397 ± 47^{a}
48 h 5 °C	238 ± 41^{abc}	346 ± 12^{ab}	164 ± 20^{bc}	428 ± 78^{a}

For the 20% FHPKO dilution, the crystal diameter did not change due to storage maintaining a similar diameter as the samples immediately after crystallization.

The morphology of the FCR non-sonicated samples tended to be an ill-defined spherulite whereas the SCR non-sonicated samples formed large, defined, spherulite shaped crystals. The FCR sonicated samples contained many small, organized crystals which was less evident for the sonicated samples crystallized using a SCR. HIU substantially impacted the visual appearance of the samples resulting in a more solid-like, homogeneous appearance which was especially drastic for the 20% FHPKO sample. In addition, the visual appearance of the FCR non-sonicated samples was more homogenous when compared to the SCR non-sonicated samples that contained large crystals. Similar visual observations were found by da Silva *et al*. (2020b) and Lee *et al*. (2021) when studying the impact of sonication on PKO-based fats and structured lipids; respectively. In these studies, HIU treatment resulted in the samples appearing more homogenous and visually harder than the non-sonicated counterparts. The polymorphic form of the samples was confirmed using XRD. All samples formed a β′ polymorphic form with peaks at 3.82 ± 0.01 Å and 4.22 ± 0.01 Å (Figure C-3).

Figure 5-1: Visual appearance and crystal microstructure after 90 min crystallization.

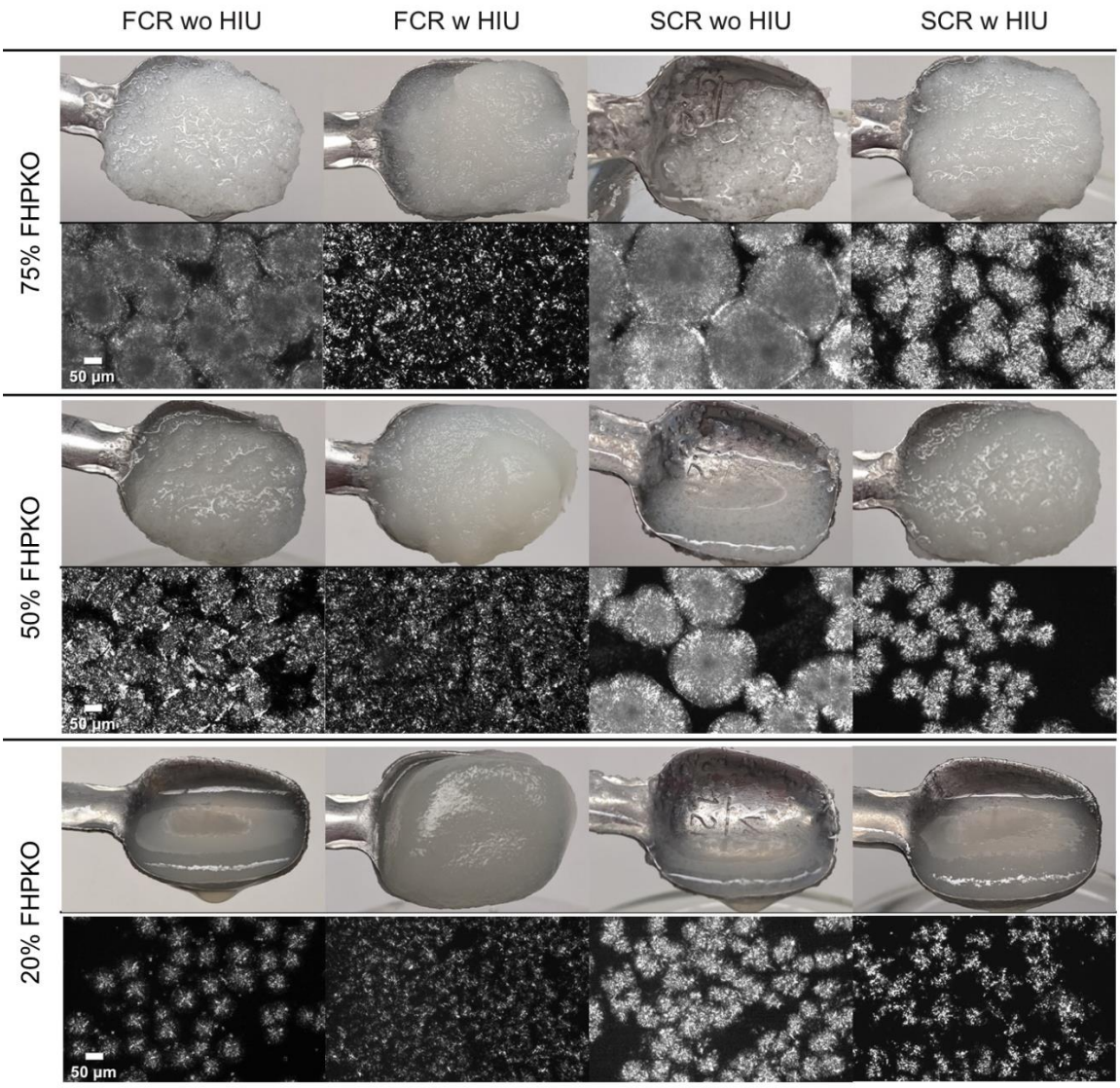

Solid Fat Content

SFC of the samples was measured immediately after crystallization as well as after storage (Figure 5-2). For the 75% FHPKO dilution crystallized using a FCR, sonication did not increase SFC; however, when samples were crystallized using a SCR, the sonicated samples had higher SFC ($p<0.05$). Previously, da Silva *et al*. (2020b) evaluated the impact of HIU in a PKO-based fat with similar SFA content of 73% and cooled using a FCR. In this study, HIU was found to significantly increase the hardness and decrease the crystal size without changing the SFC. Additionally, Giacomozzi *et al*. (2019) studied the combination of fast and slow cooling rates and the application and absence of HIU in monoglyceride oleogels. Results showed that HIU was more effective in increasing SFC for samples cooled using SCR than FCR which was attributed to HIU being more efficient in samples with slow crystallization kinetics (Giacomozzi *et al*., 2019; Kadamne *et al*., 2017)

The same trend was observed for the 50% FHPKO dilution after 90 min where sonication resulted in higher SFC for the samples crystallized with a SCR but not for the FCR samples. After the 50% FHPKO samples had been stored for 48 h there were no differences in SFC between the processing conditions. Similarly, Yubin and Martini (2015) observed sonicated palm oil had significantly higher SFC than non-sonicated palm oil after the 60 min initial crystallization. However, after storage at 25 and 5 °C, there were no significant differences between sonicated and non-sonicated samples.

The 20% FHPKO dilution had the opposite trend immediately after crystallization and storage at 22 °C with sonication resulting in higher SFC for samples crystallized using FCR conditions, and no differences in SFC for SCR samples were seen. The 20% FHPKO

SCR non-sonicated stored at 5 °C was statistically significantly higher than the other processing conditions; however, the SCR non-sonicated sample was only 1.22% higher than the SCR sonicated sample which had the lowest SFC at 5 °C. Generally, the SFC of the samples increased after storage except for the 20% dilution stored at 22 °C which contained similar SFC as the samples after 90 min. In this case, the crystallization and storage temperature were the same (22 °C) resulting in fewer changes in SFC due to storage.

Figure 5-2: Mean solid fat content and standard errors. Different letters indicate differences within a sample.

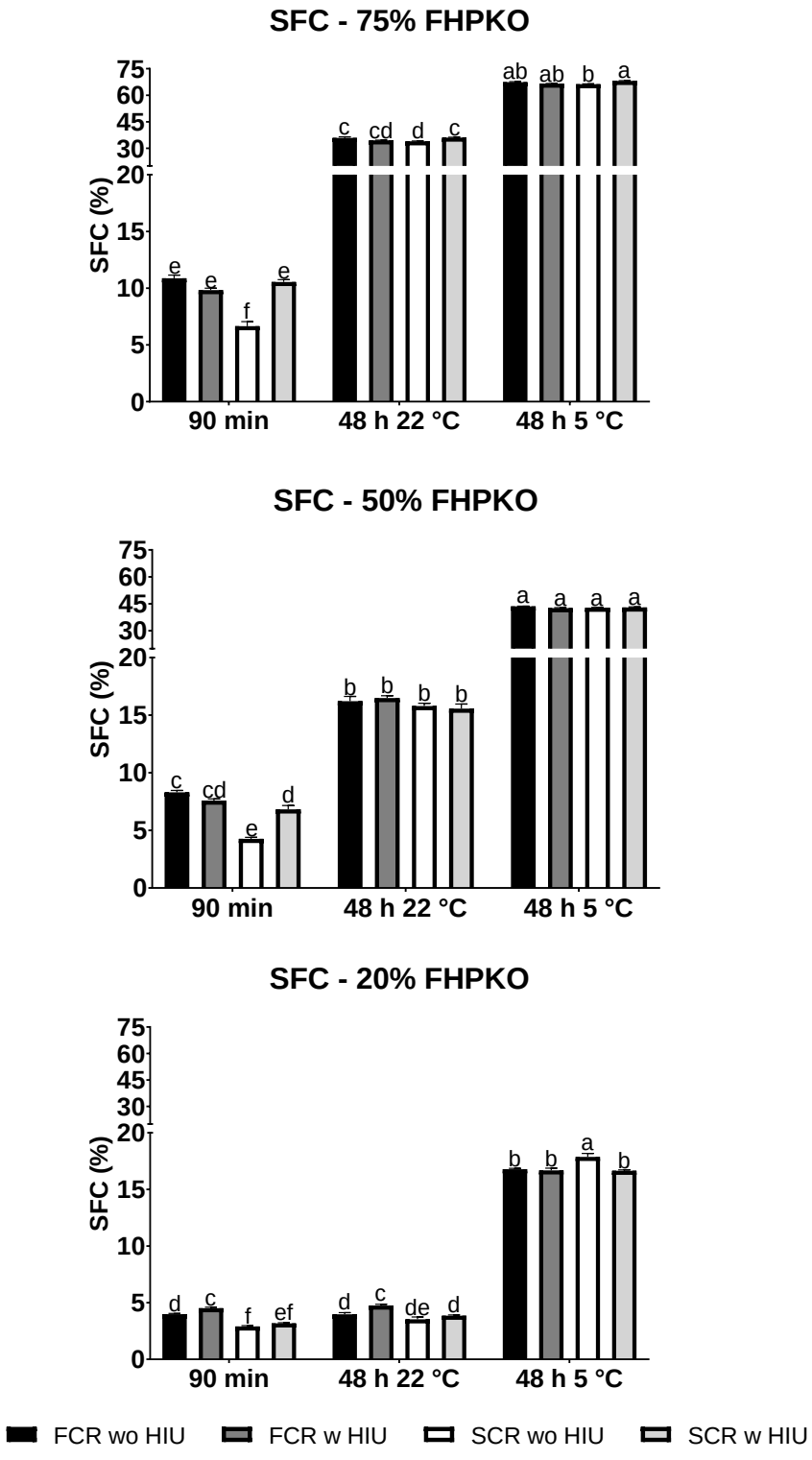

Hardness

In terms of hardness, there were no differences between processing conditions for the 75% FHPKO dilution stored at 5 °C; however, there were differences at 22 °C (Figure 5-3). For the 75% FHPKO samples at 22 °C, the SCR non-sonicated was harder than the SCR sonicated sample and there was no significant difference in hardness between the non-sonicated and sonicated samples crystallized using a FCR. Interestingly, the 75% SCR non-sonicated sample at 90 min was too soft to accurately measure; nevertheless, after storage at 22 °C, this sample was the hardest. The increase in hardness for the SCR non-sonicated sample could be due to the generation of many small crystals that occurred during storage as small crystal have been associated with high hardness in previous works (Lee *et al*., 2020; Gregersen *et al*., 2016; Kanagaratnam *et al*., 2013; Bouzidi *et al*., 2010).

A similar trend was observed for the 50% FHPKO and 20% FHPKO dilutions after 48 h at 5 °C as the FCR sonicated samples were the hardest and tended to have the smallest crystals compared to the other processing conditions. Previous studies have observed an increase in hardness for sonicated samples which has been attributed to the many small crystals formed after the HIU treatment (Suzuki *et al*., 2011; Kerr *et al.* 2011; Ye *et al*., 2011). The increase in hardness after sonication has also been observed despite the SFC remaining the same, further highlighting the impact of crystal size on hardness (da Silva *et al*., 2020a; 2020b; Marsh and Martini, 2022). Interestingly at 5 °C, the 50% FHPKO and 20% FHPKO sonicated samples were significantly harder than the non-sonicated samples when a FCR was used; however, when samples were crystallized with a SCR there was no difference in hardness.

Figure 5-3: Hardness after 90 min and 48 h storage reported as mean values with standard errors. Different letters indicate differences within a sample. Samples that were too soft to measure are indicated as n/a.

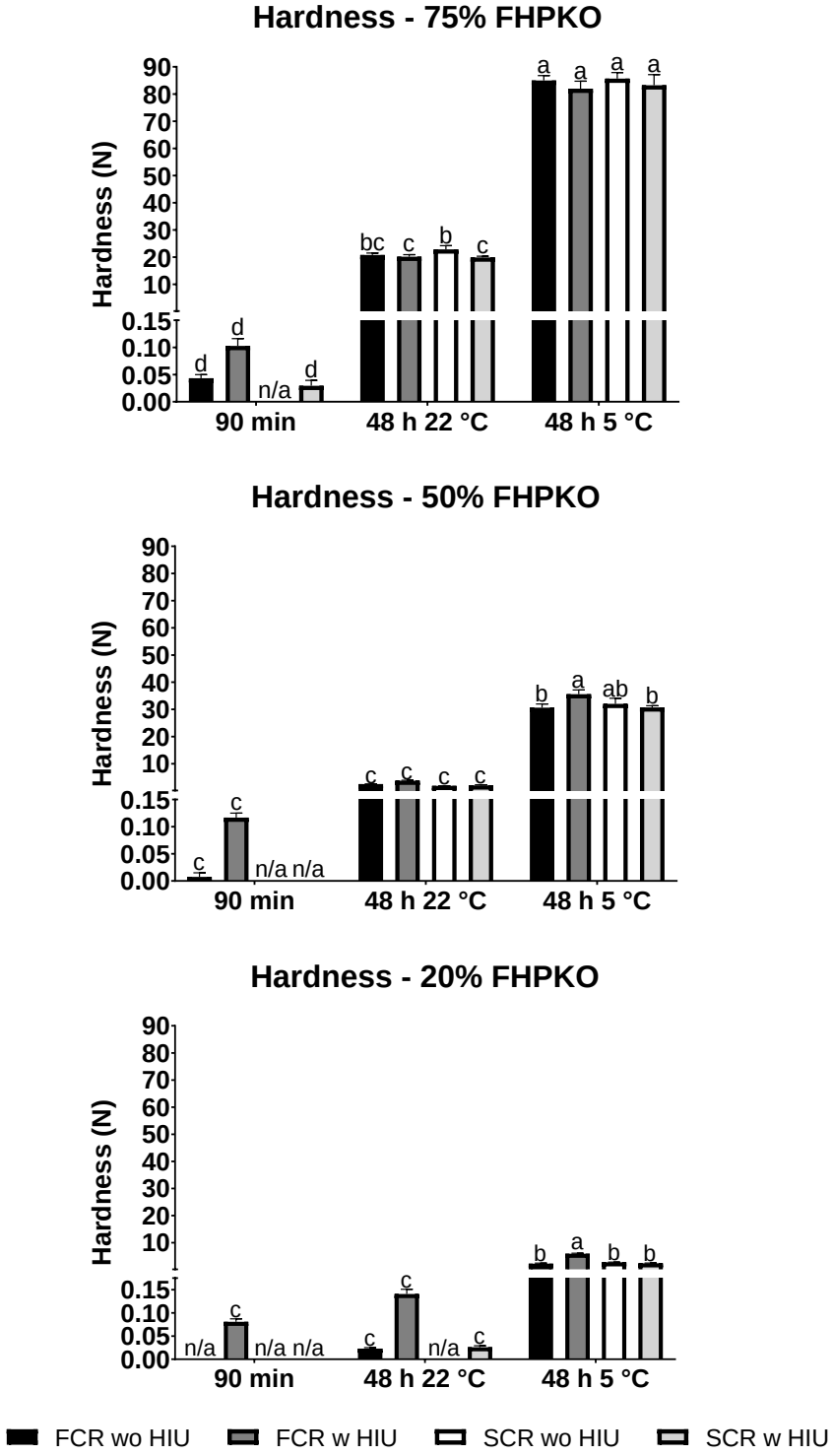

These results align with the previous study in a palm-based fat as FCR sonicated samples for the 50% and 20% dilutions stored at 5 °C were significantly harder than the non-sonicated samples which was not observed when a SCR was used (Marsh et al. 2024). Overall, samples stored at 5 °C were harder than the samples stored at 22 °C which was expected due to the increased SFC and was not attributed to crystal size as the crystal diameter was the same between the two storage temperatures.

Viscoelasticity

The storage modulus (G´) immediately after crystallization was not significantly different between the processing conditions for any dilution ($p<0.05$; Figure 5-4). Additionally, there were no differences between the processing conditions after storage for 48 h at 22 °C; except for the 50% FHPKO FCR non-sonicated sample which had higher G´ than the SCR non-sonicated sample. For the 75% FHPKO samples stored at 5 °C the use of HIU resulted in higher storage modulus when samples were cooled using a FCR; however, when a SCR was used there were no differences between sonicated and non-sonicated samples. In the case of the 50% dilution stored at 5 °C, the FCR sonicated sample had the highest G´ while the SCR non-sonicated sample had the lowest. There was a significant difference in G´ between the cooling rates for the 20% FHPKO sample stored at 5 °C where the FCR samples had higher storage moduli than the samples crystallized using a SCR.

Figure 5-4: Mean storage modulus (G′) and standard errors. Different letters indicate differences within a sample.

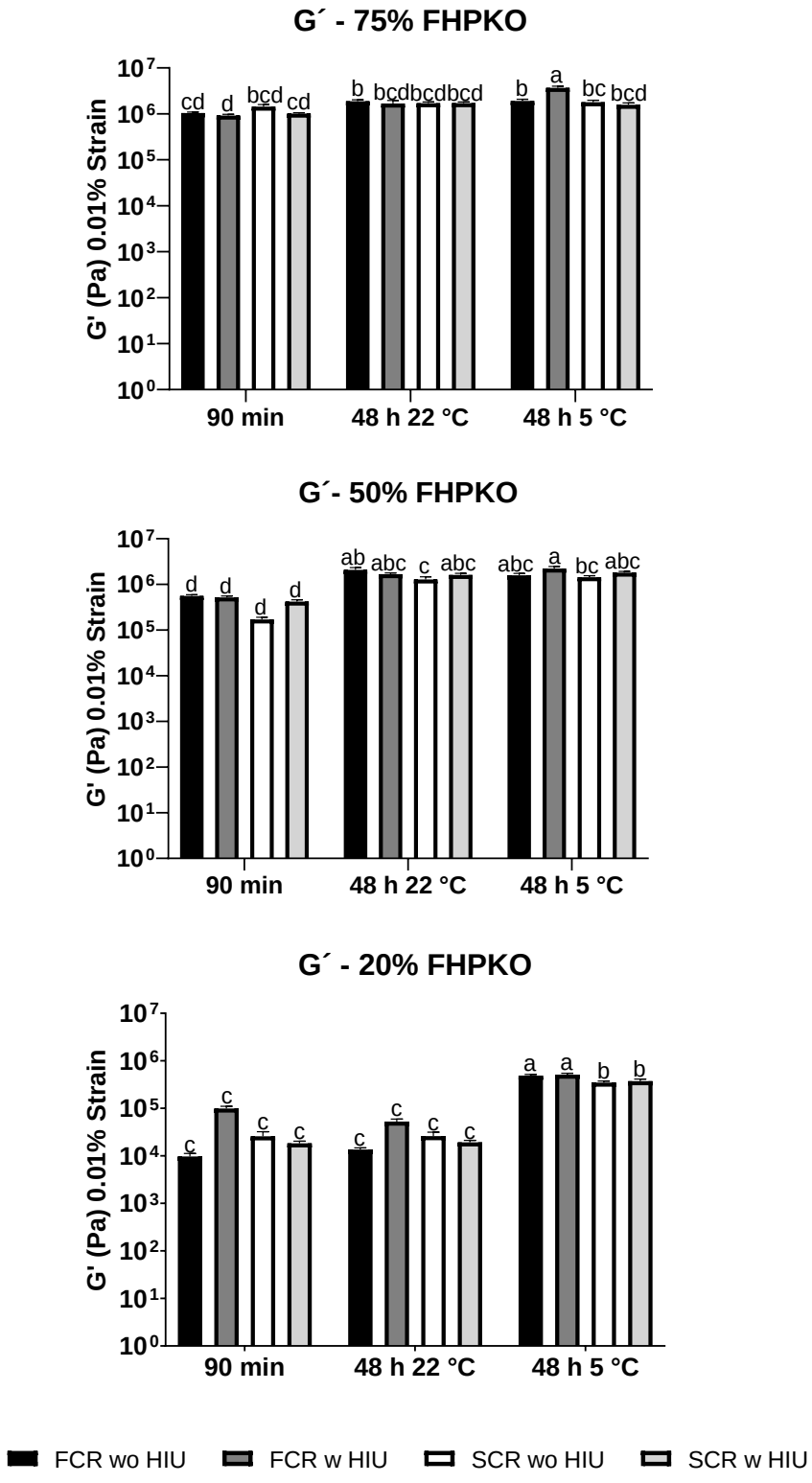

There were no differences in the loss modulus (G´´) between the processing conditions at a given time point except for the 75% FHPKO and 20% FHPKO samples stored at 5 °C where sonication resulted in a significantly higher G´´ when a FCR was used (Figure 5-5). Generally, G´´ tended to increase after storage and was lower in the 20% FHPKO sample when compared with the other dilutions.

The phase shift angles (δ) were not significantly different between the processing conditions for the 75% FHPKO and 50% FHPKO samples at each time point. However, there were differences between the samples immediately after crystallization and storage at 5 °C; with the samples stored at 5 °C tending to have lower δ than immediately after crystallization. The phase shift angle (δ) is related to the ratio of G´´ and G´ and conveys the elastic and viscous nature of a material. During the rheological measurement, sinusoidal strain was applied to the samples and the corresponding stress was measured; however different materials respond to sinusoidal strain differently. A purely elastic material will respond to the strain immediately resulting in no lag between stress and strain and a δ of 0° whereas a purely viscous material will have a lagged response to the stress and a δ of 90° (Zhong and Daubert, 2013; Tang & Marangoni, 2006). The measured decrease in δ after storage at 5 °C indicates the elastic behavior of the fats. For the 20% FHPKO sample the sonicated samples had significantly lower δ than the non-sonicated samples after 90 min; indicating the elastic nature of the sonicated samples. This trend was maintained for the FCR sonicated sample after storage at 22 °C while the SCR sonicated sample was not significantly different from its non-sonicated counterpart. After storage at 5 °C there was no difference in δ between the processing conditions.

Figure 5-5: Mean loss modulus (G″) and phase shift angles (δ) with standard errors. Different letters indicate differences within a sample.

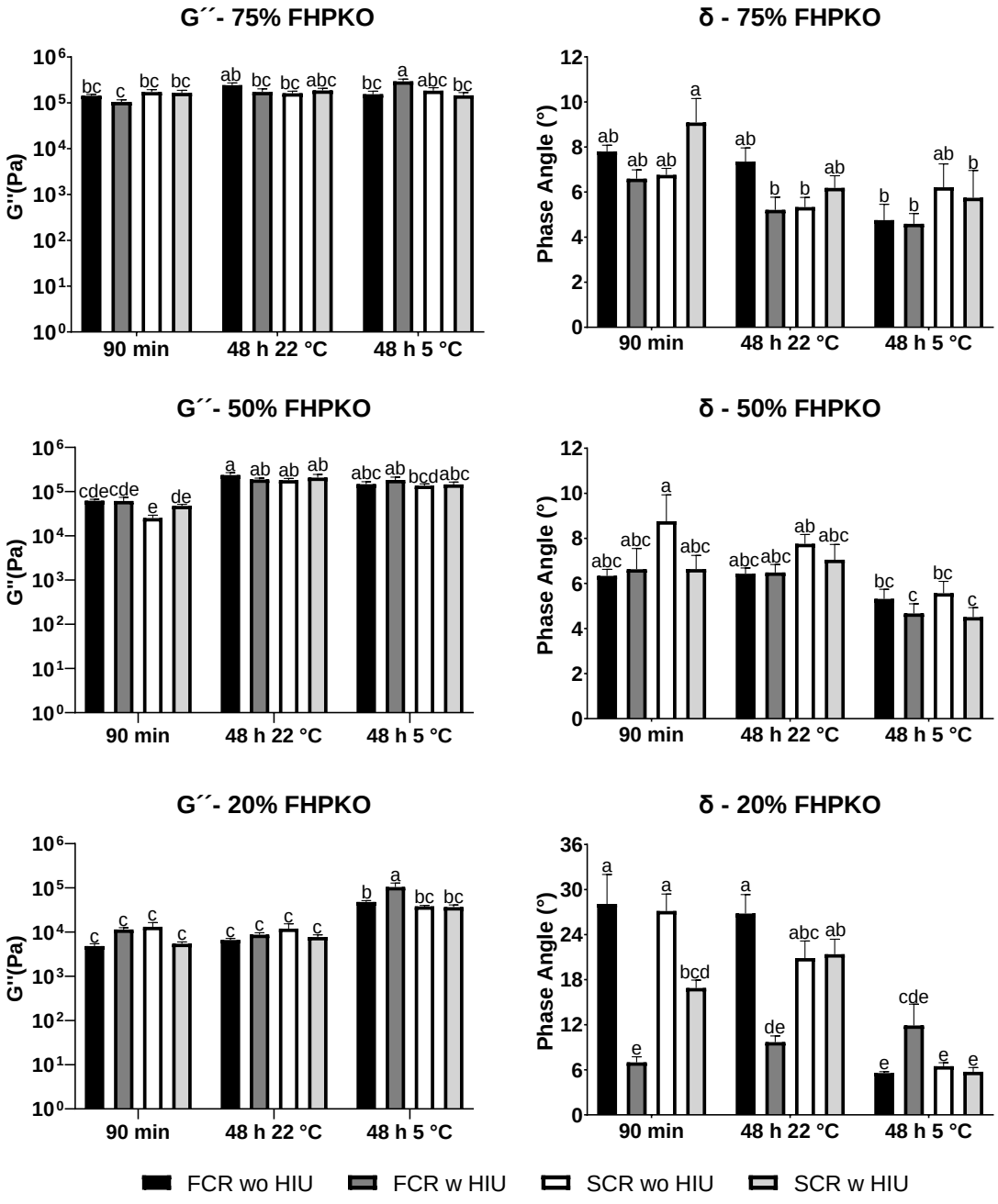

Melting Behavior

Peak temperature and enthalpy values are summarized in Table 5-4 and the DSC profiles are shown in Figure 5-6. In terms of peak temperatures, samples crystallized using a SCR had higher peak temperatures than those crystallized using a FCR after 90 min. Additionally, HIU resulted in a shift to lower peak temperatures after 90 min for the 75% FHPKO and 50% FHPKO samples crystallized using a FCR while HIU shifted the peak temperature of the 20% FHPKO samples crystallized using a SCR. Due to all the samples containing β′ crystals this shift in peak temperature was not a result of differences in polymorphism; instead, the shift is believed to be a result of HIU promoting the co-crystallization of low melting point TAGs (da Silva *et al.*, 2020b; Lee *et al.*, 2018; Lee *et al*. 2020; Marsh and Martini, 2022). Overall, peak temperatures decreased after storage and were lowest for the samples stored at 5 °C which is expected due to lower temperatures allow for the crystallization of low melting point TAGs.

Collectively, enthalpy values increased after storage especially when samples were stored at 5 °C. The one exception was that there was no difference in enthalpy between the 20% FHPKO samples after 90 min and storage at 22 °C because there was no difference in temperature between crystallization and storage. The same trend was observed for the SFC data where decreasing the temperature led to higher SFC. For the 75% FHPKO and 50% FHPKO samples the use of different processing conditions did not generate different enthalpies at any time. There were however differences for the 20% FHPKO sample with the SCR non-sonicated condition generally resulting in lower enthalpy than the other processing conditions.

Figure 5-6: Melting profiles of all samples and processing conditions.

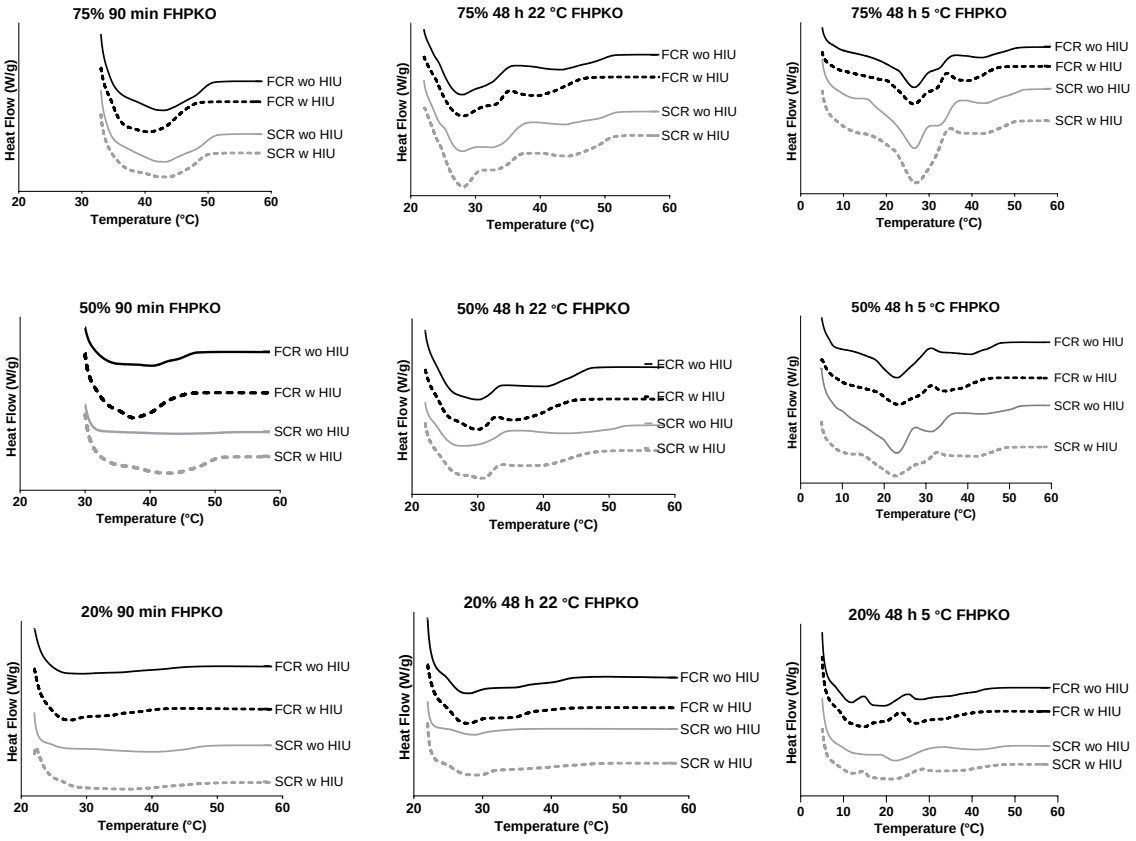

Table 5-4: Mean peak temperatures and enthalpies with standard errors. Different letters indicate differences within a sample.

Peak Temperature (°C)				
75% FHPKO				
	FCR wo HIU	FCR w HIU	SCR wo HIU	SCR w HIU
90 min	42.5 ± 0.4^{b}	41.0 ± 0.2^{c}	43.5 ± 0.2^{a}	43.6 ± 0.2^{a}
48 h 22 °C	28.3 ± 0.1^{d}	28.0 ± 0.1^{d}	27.6 ± 0.2^{def}	28.0 ± 0.2^{de}
48 h 5 °C	26.7 ± 0.1^{fg}	27.1 ± 0.1^{efg}	26.4 ± 0.2^{g}	27.0 ± 0.1^{efg}
50% FHPKO				
	FCR wo HIU	FCR w HIU	SCR wo HIU	SCR w HIU
90 min	40.5 ± 0.3^{b}	37.3 ± 0.1^{c}	43.6 ± 0.3^{a}	42.3 ± 0.2^{a}
48 h 22 °C	30.2 ± 0.3^{d}	30.0 ± 0.1^{de}	28.8 ± 0.4^{e}	31.3 ± 0.1^{d}
48 h 5 °C	23.6 ± 0.2^{f}	23.0 ± 0.5^{f}	23.0 ± 0.1^{f}	23.3 ± 0.2^{f}
20% FHPKO				
	FCR wo HIU	FCR w HIU	SCR wo HIU	SCR w HIU
90 min	29.3 ± 0.3^{c}	27.7 ± 0.2^{c}	40.5 ± 0.2^{a}	33.4 ± 1.7^{b}
48 h 22 °C	28.2 ± 0.1^{c}	27.9 ± 0.1^{c}	29.3 ± 0.4^{c}	29.6 ± 0.3^{c}
48 h 5 °C	20.0 ± 0.5^{e}	15.2 ± 0.8^{f}	23.3 ± 0.3^{d}	19.9 ± 0.6^{e}
Enthalpy (J/g)				
75% FHPKO				
	FCR wo HIU	FCR w HIU	SCR wo HIU	SCR w HIU
90 min	16.3 ± 1.8^{c}	18.0 ± 0.7^{c}	16.9 ± 1.4^{c}	20.5 ± 0.7^{c}
48 h 22 °C	58.7 ± 1.3^{b}	59.2 ± 0.3^{b}	55.8 ± 1.5^{b}	59.5 ± 1.2^{b}
48 h 5 °C	93.6 ± 2.2^{a}	96.7 ± 1.5^{a}	95.8 ± 1.0^{a}	91.4 ± 1.3^{a}
50% FHPKO				
	FCR wo HIU	FCR w HIU	SCR wo HIU	SCR w HIU
90 min	12.7 ± 0.7^{c}	12.8 ± 0.3^{c}	6.1 ± 2.4^{c}	11.6 ± 1.8^{c}
48 h 22 °C	28.7 ± 0.7^{b}	28.9 ± 0.2^{b}	26.5 ± 1.0^{b}	29.3 ± 0.5^{b}
48 h 5 °C	55.8 ± 2.5^{a}	58.1 ± 0.6^{a}	55.6 ± 2.0^{a}	57.6 ± 1.9^{a}
20% FHPKO				
	FCR wo HIU	FCR w HIU	SCR wo HIU	SCR w HIU
90 min	6.4 ± 0.4^{cd}	6.6 ± 0.1^{cd}	4.5 ± 1.0^{de}	5.8 ± 0.5^{cd}
48 h 22 °C	7.5 ± 0.3^{cd}	7.6 ± 0.2^{c}	1.9 ± 0.2^{e}	7.0 ± 0.2^{cd}
48 h 5 °C	17.3 ± 0.9^{a}	18.0 ± 1.0^{a}	13.4 ± 0.7^{b}	19.7 ± 0.9^{a}

Oil Binding Capacity

Results from both methods used to measure OBC are summarized in Figure 5-7. Samples crystallized using a FCR had significantly higher OBC measured using the centrifuge method (OBC_c) when compared to their SCR counterparts for all dilutions after 90 min and the 50% FHPKO and 20% FHPKO dilutions after 48 h at 22 °C. The increased OBC_c for the FCR samples was most likely driven by the crystal diameter as larger crystals resulted in lower OBC_c and smaller crystals resulted in higher OBC_c. After storage for 48 h at 5 °C there were no differences in OBC_c between the processing conditions as all the samples had nearly 100% OBC_c. In all cases, the hardness, enthalpy, and SFC were significantly higher for the samples stored at 5 °C when compared to the samples immediately after crystallization and after storage at 22 °C. Additionally, the crystal size was the same for the samples stored at 22 °C and 5 °C; therefore, the high OBC_c for samples stored at 5 °C is not believed to be a result of small crystals alone and instead other physical properties – SFC, hardness, enthalpy were responsible for increasing OBC_c. These results are further supported by the correlation analysis which showed that OBC_c was positively correlated with SFC (r_s=0.912, $p<0.001$), hardness (r_s=0.833, $p<0.001$), enthalpy (r_s=0.842, $p<0.001$), G´ (r_s=0.674, $p<0.001$) and G´´ (r_s=0.510, $p=0.001$), crystal number (r_s=0.655, $p<0.001$), and negatively correlated with crystal diameter (r_s=-0.470, $p=0.004$), Tpeak (r_s=-0.782, $p<0.001$), and δ (r_s=-0.801, $p<0.001$).

Interestingly, the OBC_c after 48 h at 5 °C was nearly 100% for all the dilutions despite the 20% FHPKO sample containing far less content of SFA (46.13% less than the 75% FHPKO dilution), being softer (76 N softer than the 75% FHPKO dilution) having lower SFC (48.39% lower than the 75% FHPKO dilution) and lower enthalpy (71.7 J/g

lower than the 75% FHPKO dilution) while containing a similar if not larger crystal diameter. These results further show the nonlinear relationship between the physical properties and OBC (Figure C-1). As the OBC cannot increase further than 100%, it is likely that once a certain threshold of the physical properties driving OBC_c has been met, the OBC_c will be 100% regardless of how much the SFC, hardness, or enthalpy increase at least when the OBC is measured using the centrifuge method. In this study, the OBC_c was consistently above 99% when SFC was 36% or higher, hardness was 22.8 N or higher, and the enthalpy was above 59 J/g.

Figure 5-7: Mean OBC and standard errors for the centrifuge (OBC_c) and filter paper (OBC_p) methods. Different letters indicate differences within a sample.

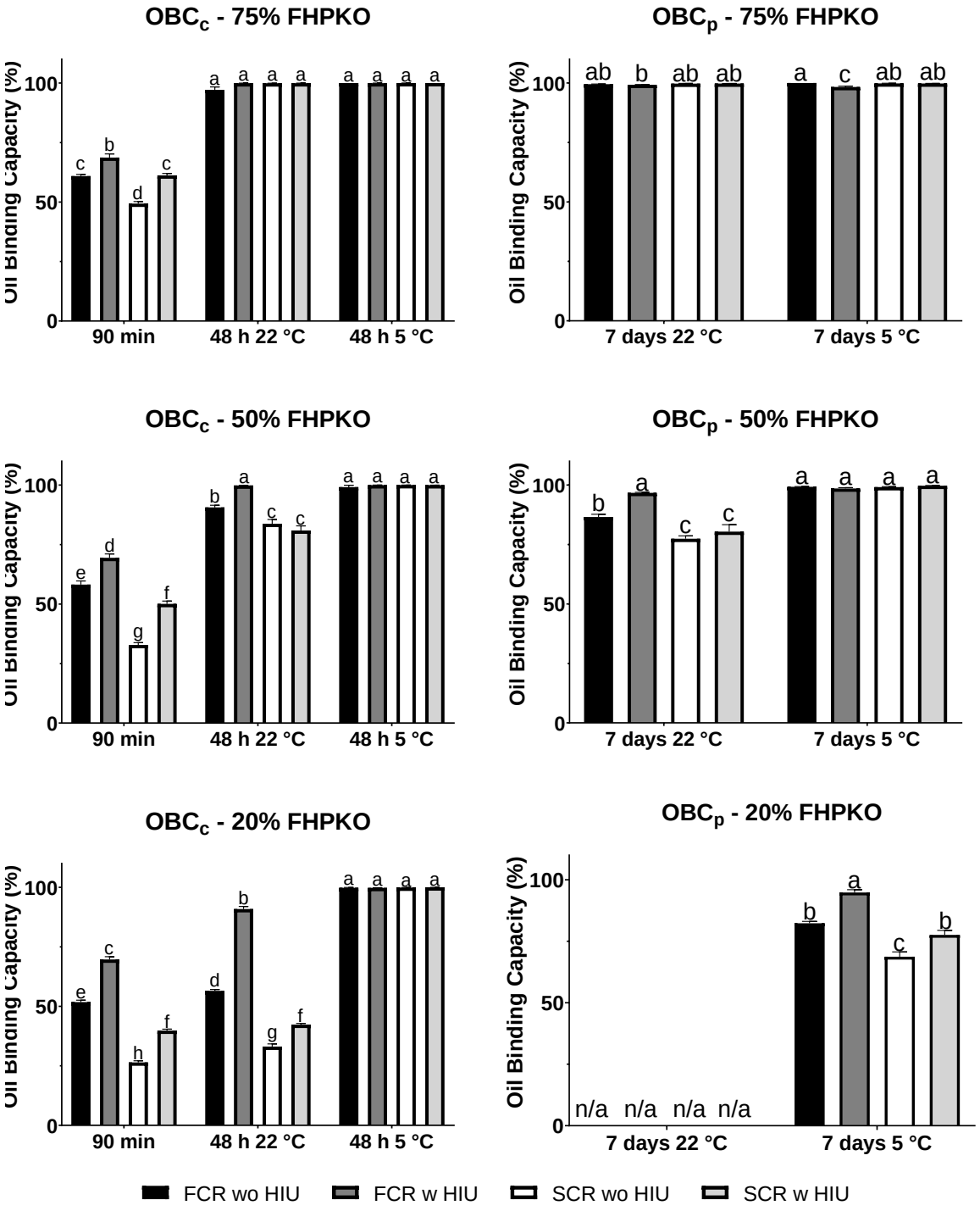

However, when OBC was measured for a longer period using the filter paper method (OBC_p), the OBC_p of the 20% FHPKO samples stored at 5 °C tended to be lower than the other dilutions except for the FCR sonicated sample which maintained an OBC_p of nearly 100%. In this case, the 20% FHPKO FCR sonicated sample at 5 °C was harder than the other processing conditions ($p<0.05$). Indicating that for a sample with low amounts of SFAs, hardness could be driving the high OBC_p. This is supported by the correlation analysis as hardness and OBC_p are significantly positively correlated ($r_s=0.804$, $p=0.003$) even if the high SFA samples (75% dilution) are removed from the analysis. Similarly, the 50% FHPKO FCR sonicated sample at 22 °C had the highest OBC_p and hardness when compared to the other processing conditions at the same temperature. Interestingly, the 50% FHPKO samples cooled using a SCR had significantly lower OBC_p than the FCR samples at 22 °C though this trend was not seen for the samples stored at 5 °C. For the 75% FHPKO samples, there were no significant differences between the processing conditions for the samples stored at 22 °C. However, there was a statistically significant difference at 5 °C with the FCR non-sonicated samples having a higher OBC_p than the FCR sonicated samples. Although this difference was statistically significant; it is important to note that the 75% FHPKO samples at 5 °C all had very high OBC_p with the FCR non-sonicated sample having 100% OBC_p and the FCR sonicated sample having 98% OBC_p. The correlation analysis revealed that OBC_p was significantly correlated with SFC ($r_s=0.777$, $p<0.001$), G´ ($r_s=0.526$, $p=0.017$), hardness ($r_s=0.812$, $p<0.001$), enthalpy ($r_s=0.812$, $p<0.001$), and the number of crystals ($r_s=0.728$, $p<0.001$).

The combination of the two methods used to determine OBC indicate hard and elastic fats, with high SFC and enthalpy, and many crystals tend to have higher OBC.

Additionally, the relationship between OBC and the physical properties of fats is likely nonlinear. When compared to other studies there are some commonalities and differences with these results. Wang *et al*. (2016) investigated the impact of shear on oil diffusion in cocoa butter using magnetic resonance imaging. The authors noted a decrease in oil diffusion for sheared samples which was attributed to the microstructure of the sheared samples containing small crystal fragments. In contrast, Acevedo *et al*. (2017) measured diffusion coefficients on the macroscopic level (D_{eff}) using a filter paper method and microscopic level (D_{mol}) measured via nuclear magnetic resonance in fully hydrogenated soybean oil and soybean oil blends with and without emulsifiers. The authors noted that D_{mol} was inversely related to meso-crystal dimension indicating that greater diffusion occurred when smaller crystals were present on the microscopic level. However, earlier work from Acevedo *et al*. (2012) measured the OBC of fully hydrogenated soybean oil and soybean oil blends crystallized statically or under shear using a filter paper method. OBC was found to be negatively correlated with nano- and meso-crystal size indicating smaller crystals increased OBC on the macroscopic level. Similarly, da Silva *et al*. (2020b) measured oil migration in a palm-kernel-based fat with and without the application of HIU. The authors found that HIU significantly decreased crystal size while maintaining similar SFC and resulted in higher OBC as measured through a filter paper and centrifuge method. The increase in OBC was attributed to a decrease in crystal size. In addition, Chai *et al*. (2018) studied the diffusion coefficients (D_{eff}) of mixtures of fully hydrogenated palm kernel (FHPKO) and soybean oil (FHSO) diluted with triolein at 5 different levels – 100%, 80%, 60%, 40%, and 20%. The diffusion of oil in these fats was measured using fluorescence recovery after photobleaching (FRAP). Chai *et al*. observed an increase in

D_{eff} with larger crystals indicating greater oil movement when large crystals were present.

Previously, the impact of processing conditions and physical properties on the OBC of soybean and palm-based fats were evaluated in a similar fashion to the current study (Marsh and Martini 2022; Marsh *et al*. 2024). Both studies found no correlation between OBC and crystal diameter though in the palm-based fat, OBC_c was significantly correlated with the number of crystals and the LASSO model indicated that it could be used to predict OBC_c (Marsh *et al*. 2024). In contrast, the current study of FHPKO fat did establish a significant negative correlation between OBC_c and crystal diameter but not OBC_p and crystal diameter as well as a positive correlation between both measures of OBC and the number of crystals. Unlike the previous studies, storage did result in the formation of many small crystals for the 75% and 50% FHPKO samples. Notably, storage also resulted in an increase in SFC and hardness which were found to be significantly correlated with OBC in all three studies. Therefore, the correlation between crystal diameter and OBC_c and both measures of OBC and crystal number in the current work is hypothesized to be due to the generation of small crystals after storage for the 75% and 50% FHPKO samples that was not observed previously. Additionally, previous works have shown that composition impacts OBC; therefore, the differences between the previous two studies and the current work could also be explained by compositional differences of the fats (Wang and Maleky, 2018; Tran *et al*. 2015; Chai *et al*., 2020; Jahaniaval *et al*., 2002).

In addition to crystal size, SFC was also significantly correlated with OBC in the current study which aligns with previous results. In the study described above, Chai *et al*. (2018) noted a significant decrease in D_{eff} as SFC increased and demonstrated that the relationship between D_{eff} and SFC was not linear indicating higher SFC resulted in less oil

movement. Chai *et al*. concluded that oil diffusivity was impacted by a combination of many factors which aligns with the results of the present study as several properties were significantly correlated with both measurements of OBC – SFC, hardness, G´, enthalpy, and crystal size. Later, Chai *et al*. 2020 investigated the micro-viscosity of oil in mixtures of palm kernel stearin (PKS)/soybean oil (SO) and fully hydrogenated rapeseed oil (FHRSO)/SO via molecular motors. In addition to measuring the micro-viscosity, which relates to the liquid oil entrapped within the crystal network, the authors also evaluated the SFC of the fat blends. The results showed an increase in micro-viscosity with increasing SFC suggesting that increasing SFC results in less movement of oil within the crystal network. Similarly, Green and Rousseau (2015) measured diffusion coefficients in mixtures of hydrogenated canola with FRAP and found that as SFC increased, diffusion of oil throughout the fat matrix decreased. The authors also noticed the nonlinear relationship between diffusion and SFC as when SFC reach sufficiently high levels, the diffusion plateaued. The same relationship between OBC and SFC was observed in the current study (Figure C-1).

CONCLUSION

In this study the impact of processing conditions (cooling rate and HIU), composition, and storage temperature on the physical properties and OBCs of a FHPKO fat were evaluated. In terms of processing conditions, the FCR sonicated condition typically resulted in the highest OBC most likely due to HIU generating harder, more elastic materials, with many small crystals. The FCR non-sonicated samples tended to have the next highest OBC, and the SCR non-sonicated samples tended to have the least. By diluting the FHPKO fat with SBO, the fatty acid composition of the samples was

significantly modified. Samples with greater amounts of unsaturated fatty acids tended to be softer, have lower enthalpy and SFC values, and were less able to entrap liquid oil as indicated by the OBC measurements. Storage temperature impacted the physical properties with samples stored at 5 °C having higher SFC, hardness, enthalpy, and lower peak temperatures. In general, samples stored at lower temperatures had higher OBC and were more resistant to unwanted oil movement.

Overall, the combination of these factors generated samples with significantly different physical properties and OBCs. The correlation analysis indicated that increasing SFC, hardness, enthalpy, and G´ was associated with higher OBC for both the centrifuge and filter paper methods. OBC also tended to be highest when samples were processed with HIU and using a FCR, when high SFAs were present, and when samples were stored at lower temperatures.

ACKNOWLEDGMENTS

This project was supported by Agriculture and Food Research Initiative (AFRI) grant no. 2020-67017-31193 from the USDA National Institute of Food and Agriculture as well as the Utah Agricultural Experiment Station, Utah State University. FHPKO samples were kindly donated by AAK (Richmond, CA, USA). We would like to thank Dr. Robert Ward for performing the fatty acid measurements.

REFERENCES

Acevedo NC, Block JM, Marangoni AG. Critical laminar shear-temperature effects on the nano- and mesoscale structure of a model fat and its relationship to oil binding and rheological properties. Faraday Discuss 2012;158:171–194. DOI: 10.1039/C2FD20008B

Acevedo NC, MacMillan B, Newling B, Marangoni AG. Shear effects on the diffusive movement of oil in triacylglycerol networks. RSC Adv 2017;7:1634–1642. DOI: 10.1039/C6RA24829B

Ali A, Selamat J, Che Man YB, Suria AM. Effect of storage temperature on texture, polymorphic structure, bloom formation and sensory attributes of filled dark chocolate. Food Chem 2001;72:491–497. DOI: 10.1016/S0308-8146(00)00271-5

Altimiras P, Pyle L, Bouchon P. Structure–fat migration relationships during storage of cocoa butter model bars: Bloom development and possible mechanisms. J Food Eng 2007;80:600–610. DOI: 10.1016/j.jfoodeng.2006.06.022

Beckett ST. Industrial chocolate manufacture and use, 4th ed. Wiley-Blackwell, Chichester 2009.

Bouzidi L, Omonov TS, Garti N, Narine SS. Relationships between molecular structure and kinetic and thermodynamic controls in lipid systems. Part I: propensity for oil loss of saturated triacylglycerols. Food Funct. 2013;4:130–143. DOI: 10.1039/C2FO30164D

Bouzidi L, Boodhoo MV, Kutek T, et al. The binary phase behavior of 1,3-dilauroyl-2-stearoyl-sn-glycerol and 1,2-dilauroyl-3-stearoyl-sn-glycerol. Chem Phys Lipids. 2010;163:607–629. DOI: 10.1016/j.chemphyslip.2010.05.002

Briones V, Aguilera JM. Image analysis of changes in surface color of chocolate. Food Res Int 2005;38:87–94. DOI: 10.1016/j.foodres.2004.09.002

Chai X, Meng Z, Cao P, et al. Comparative Analysis of Small-Molecule Diffusivity in Different Fat Crystal Network. J Agric Food Chem 2018;66:1015–1022. DOI: 10.1021/acs.jafc.7b04677

Chai X, Meng Z, Liu Y. Comparation of micro-viscosity of liquid oil in different colloidal fat crystal networks using molecular rotors. Food Chem 2020;317:126382. DOI: 10.1016/j.foodchem.2020.126382

Clercq ND, Depypere F, Delbaere C, et al. Influence of cocoa butter diacylglycerols on migration induced fat bloom in filled chocolates. Eur J Lipid Sci Technol 2014;116:1388–1399. DOI: 10.1002/ejlt.201300476

da Pieve S, Calligaris S, Co E, et al. Shear Nanostructuring of Monoglyceride Organogels. Food Biophys 2010;5:211–217. DOI: 10.1007/s11483-010-9162-3

da Silva TLT, Cooper Z, Lee J, et al. Tailoring Crystalline Structure Using High-Intensity Ultrasound to Reduce Oil Migration in a Low Saturated Fat. J Am Oil Chem Soc 2020a;97:141–155. DOI: 10.1002/aocs.12321

da Silva TLT, Grimaldi R, Calligaris GA, et al. Crystallinity properties and crystallization behavior of chocolate fat blends. J Food Sci Technol 2017;54:1979–1989. DOI: 10.1007/s13197-017-2634-4

da Silva TLT, Marsh M, Gibon V, Martini S. Sonocrystallization as a tool to reduce oil migration by changing physical properties of a palm kernel fat. J Food Sci 2020b;85:964–971. DOI: 10.1111/1750-3841.15099

Depypere F. Triacylglycerol migration and bloom in filled chocolates: Effects of low-temperature storage.

Dibildox-Alvarado E, Rodrigues JN, Gioielli LA, et al. Effects of Crystalline Microstructure on Oil Migration in a Semisolid Fat Matrix. Cryst Growth Des 2004;4:731–736. DOI: 10.1021/cg049933n

Giacomozzi AS, Palla CA, Carrín ME, Martini S. Physical Properties of Monoglycerides Oleogels Modified by Concentration, Cooling Rate, and High-Intensity Ultrasound. J Food Sci 2019;84:2549–2561. DOI: 10.1111/1750-3841.14762

Green NL, Rousseau D. Oil diffusivity through fat crystal networks. Soft Matter 2015;11:5523–5530. DOI: 10.1039/C5SM01355K

Gregersen SB, Andersen MD, Hammershøj M, Wiking L. Impact of triacylglycerol composition on shear-induced textural changes in highly saturated fats. Food Chem. 2017;215:438–446 DOI: 10.1016/j.foodchem.2016.08.008

Jahaniaval F, Kakuda Y, Abraham V. Oil-binding capacity of plastic fats: Effects of intermediate melting point TAG. J Am Oil Chem Soc 2002;79:389–394. DOI: 10.1007/s11746-002-0494-6

Kadamne JV, Ifeduba EA, Akoh CC, Martini S. Sonocrystallization of Interesterified Fats with 20 and 30% of Stearic Acid at the sn-2 Position and Their Physical Blends. J Am Oil Chem Soc 2017;94:1045–1062. DOI: 10.1007/s11746-017-3014-y

Kadamne JV, Martini S. Sonocrystallization of Interesterified Soybean Oil With and Without Agitation. J Am Oil Chem Soc 2018;95:571–582. DOI: 10.1002/aocs.12075

Kanagaratnam S, Hoque ME, Sahri MM, Spowage A. Investigating the effect of deforming temperature on the oil-binding capacity of palm oil based shortening. J Food Eng. 2013;118:90–99 DOI: 10.1016/j.jfoodeng.2013.03.021

Kerr RM, Tombokan X, Ghosh S, Martini S. Crystallization Behavior of Anhydrous Milk Fat−Sunflower Oil Wax Blends. J Agric Food Chem. 2011;59:2689–2695. DOI: 10.1021/jf1046046

Lee J, Claro da Silva R, Gibon V, Martini S. Sonocrystallization of Interesterified Soybean Oil: Effect of Saturation Level and Supercooling. J Food Sci 2018;83:902–910. DOI: 10.1111/1750-3841.14084

Lee J, Marsh M, Martini S. Effect of storage time on physical properties of sonocrystallized all-purpose shortening. J Food Sci 2020;85:3391–3399. DOI: 10.1111/1750-1.

Lee J, Willett SA, Akoh CC, Martini S. Impact of high-intensity ultrasound on physical properties and degree of oxidation of lipase modified menhaden oil with caprylic

acid and/or stearic acid. J Am Oil Chem Soc 2021;99:141–151. DOI: 10.1002/aocs.125603841.15435

List GR. Oilseed Composition and Modification for Health and Nutrition. In: Functional Dietary Lipids. Elsevier 2016;pp 23–46.

Lonchampt P, Hartel RW. Fat bloom in chocolate and compound coatings. Eur J Lipid Sci Technol 2004;106:241–274. DOI: 10.1002/ejlt.200400938

Marsh MA, Martini S. Relationship between oil binding capacity and physical properties of interesterified soybean oil. J Am Oil Chem Soc 2022;99:313–330. DOI: 10.1002/aocs.12578.

Marsh MA, Bean B, Maleky F, Martini S. Unveiling the physical properties predictive of oil binding capacity in an interesterified palm-based fat. J Am Oil Chem Soc 2022;99:313–330. DOI: 10.1002/aocs.12578

Peyronel F, Campos R, Marangoni AG. Prevention of oil migration in palm mid fraction and palm olein using a stabilizer rich in behenic acid. Food Res Int 2016;88:52–60. DOI: 10.1016/j.foodres.2016.04.001

Shukla V. Cocoa Butter, Cocoa Butter Equivalents, and Cocoa Butter Substitutes. In: Handbook of functional lipids 2005;pp 279–307.

Silva TLT da, Grimaldi R, Gonçalves LAG. Temperature, time and fat composition effect on fat bloom formation in dark chocolate. Food Structure 2017;14:68–75. DOI: 10.1016/j.foostr.2017.06.006

Smith KW, Cain FW, Talbot G. Effect of nut oil migration on polymorphic transformation in a model system. Food Chem 2007;102:656–663. DOI: 10.1016/j.foodchem.2006.05.045

Subramaniam PJ. Chapter 10 Confectionery products. In: The Shelf Life and Stability of Foods 2020.

Suzuki A, Lee J, Padilla S, Martini S. Altering Functional Properties of Fats Using Power Ultrasound. J Food Sci. 2010;75:E208–E214. DOI: 10.1111/j.1750-3841.2010.01572.x

Talbot G. Science and technology of enrobed and filled chocolate, confectionery and bakery products. Woodhead Publishing 2009.

Tang D, Marangoni AG. Microstructure and fractal analysis of fat crystal networks. J Am Oil Chem Soc 2006;83:377–388. DOI: 10.1007/s11746-006-1216-9

Tietz RA, Hartel RW. Effects of minor lipids on crystallization of milk fat-cocoa butter blends and bloom formation in chocolate. J Am Oil Chem Soc 2000;77:763–771. DOI: 10.1007/s11746-000-0122-5

Tran PD, Van de Walle D, Hinneh M, et al. Controlling the stability of chocolates through the incorporation of soft and hard StOSt-rich fats. Eur J Lipid Sci Technol 2015;117:1700–1713. DOI: 10.1002/ejlt.201400584

Wang H, Maleky F. Effects of cocoa butter triacylglycerides and minor compounds on oil migration. Food Res Int 2018;106:213–224. DOI: 10.1016/j.foodres.2017.12.057

Watanabe S, Yoshikawa S, Sato K. Physical Properties and Fat Bloom Stability of Compound Chocolates Made with Ternary Fat Blends of Cocoa Butter, 1,3-Dioleoyl-2-stearoyl-triacylglycerol-Fat, and Lauric-Based Cocoa Butter Substitute. J Oleo Sci 2023;72:1073–1082. DOI: 10.5650/jos.ess23159

Ye Y, Martini S.Application of High-Intensity Ultrasound to Palm Oil in a Continuous System. J Agric Food Chem 2015;63:319–327 DOI: 10.1021/jf505041s

Ye Y, Wagh A, Martini S. Using High Intensity Ultrasound as a Tool To Change the Functional Properties of Interesterified Soybean Oil. J Agric Food Chem 2011;59:10712–10722. DOI: 10.1021/jf202495b

Zhong Q, Daubert CR. Chapter 15 - Food Rheology. In: Kutz M (ed) Handbook of Farm, Dairy and Food Machinery Engineering (Second Edition). San Diego: Academic Press; 2013. pp 403–426.

CHAPTER VI. SUMMARY, CONCLUSION, AND FUTURE WORK

In this work the impact of processing conditions, storage conditions, and composition on the physical properties and OBC of fats was evaluated. The first experiment aimed to understand how a the OBC in a stearic-rich fat could be improved by determining the most influential physical properties driving OBC. In the second study, the OBC and physical properties of a palmitic-rich fat that underwent similar sample preparation and processing was evaluated. The data from the palmitic-rich fat was used to develop a LASSO Regression model to predict the OBC_c based on the physical properties. In the third study, the OBC and physical properties of a palm-kernel-based fat high in medium chain fatty acids, namely lauric acid, that is commonly used in the confectionery industry was examined.

The physical properties and OBC of a stearic-rich, soybean-based fat could be altered through processing conditions – HIU and cooling rates, dilution of SFAs, and storage (Chapter III). Notably, the application of HIU resulted in the generation of more and smaller crystals for all SFAs levels and tended to result in higher hardness, shifted peak temperatures, and increased OBC. Adjusting the cooling rate led to differences in crystal microstructure and peak melting temperatures while increasing the level of SFAs increased hardness, SFC, G´, and enthalpy which were significantly correlated to both measures of OBC. Interestingly, no correlation between OBC and crystal diameter nor crystal number were established suggesting that enhancing OBC was independent of crystal size in this context (Chapter III).

In a palmitic-rich palm-based fat OBC was found to be improved via the modification of the physical properties through processing conditions (HIU and cooling

rate), manipulation of SFA level, and storage conditions (Chapter IV). In terms of processing conditions, the application of HIU tended to generate more and smaller crystals, shift peak temperatures, and result in harder and more elastic fats similar to the findings obtained for a stearic-based fat. As a result of HIU modifying the physical properties, the OBC tended to be improved. Different cooling rates resulted in a wide range of crystal sizes, numbers, and morphologies. The impact of cooling rate on crystal size was more pronounced in the palmitic-based fat (Chapter IV) than the stearic-based fat (Chapter III). In general, SCR was found to result in larger crystals, softer materials, and lower OBC than FCR counterparts and dilution of SFAs decreased the SFC, hardness, enthalpy, G′, G″, OBCc, and OBCp while increasing δ. Strong correlations between both measurements of OBC and SFC, hardness, and enthalpy were established. In addition, the LASSO Regression model found SFC, hardness, peak temperature, enthalpy, and the number of crystals were pivotal predictors of OBC_c.

The processing, storage, and dilution in a lauric-rich palm-kernel-based fat resulted in a range of physical properties and OBCs. In a similar manner to the stearic-based (Chapter III) and palmitic-based fats (Chapter IV), dilution of the SFAs resulted in softer fats with lower enthalpy and SFC values, and reduced OBC. Furthermore, the FCR sonicated samples tended to demonstrate the highest OBC likely due to HIU's impact on the physical properties (hardness, elasticity, crystal size). Storing samples at lower temperatures increased the SFC, hardness, and enthalpy while lowering the peak temperature and resulted in the generation of many small crystals for the high SFA sample which was not observed previously in the stearic-rich and palmitic-rich fats (Chapter III and Chapter IV). In concurrence with the previous fats, the OBC of the palm-kernel-based

sample was also significantly correlated with SFC, hardness, and enthalpy.

The overarching conclusion drawn from this study is that the manipulation of processing conditions, composition, and storage temperature significantly impacts the physical properties and OBC of fats. In this work, OBC ranged from 11.4 to 100% and 53.8 to 100%; for the OBC_c and OBC_p measurements; respectively. Distinct trends are evident on the impact of these factors on the physical properties of the various fats used in these studies. It was shown that the processing conditions – HIU and cooling rate significantly impacted the crystal size, count, and morphology. HIU application resulted in smaller crystals and higher hardness while different cooling rates generated various crystal structures. The application and absence of HIU produced crystals spanning from 6.6 to 143.0 μm. The composition of the fats, particularly the SFA content, played a crucial role in determining the hardness, SFC, enthalpy, and elasticity of the fats with higher levels of SFAs leading to harder more elastic textures, greater enthalpy and SFC, and increased OBC values. Hardness ranged from 0.02 to 89.45 N, SFC varied from 1.4 to 68.5%, and enthalpy extended from 0.26 to 99.43 J/g. Overall, lower storage temperature resulted in higher hardness, SFC, and enthalpy and enhanced OBC. The correlation analysis highlights the relationship between specific physical properties and OBC. Correlation analysis for all of the fat matrixes described in this study was evaluated and it was found that both measures of OBC were positively correlated with SFC (r_s=0.938, $p<0.001$) (r_s=0.783, $p<0.001$), hardness (r_s=0.911, $p<0.001$) (r_s=0.815, $p<0.001$), G´ (r_s=0.764, $p<0.001$) (r_s=0.608, $p<0.001$), G´´ (r_s=0.761, $p<0.001$) (r_s=0.520, $p<0.001$), enthalpy (r_s=0.798, $p<0.001$) (r_s=0.798, $p<0.001$), and the number of crystals (r_s=0.451, $p<0.001$) (r_s=0.430, $p=0.004$) for the OBC_c and OBC_p methods; respectively. Surprisingly, the work presented in this

dissertation did not establish strong relationships between crystal size and OBC.

Overall, these studies emphasize the importance of understanding the interplay between processing conditions, saturation level, and storage conditions on generating various physical properties of fats to aid in the formulation of fats with ideal OBC. The results from this study suggest that formulating harder more elastic fats with higher SFC, and enthalpy is related to increased OBC of fats when evaluated using a filter paper and centrifuge method that model the capillary and sedimentation forces occurring during oil migration events. The physical property driving the OBC the most is likely the hardness followed closely by the SFC as these physical properties had the strongest correlations with both measures of OBC. In addition, these results suggest that OBC is not driven by a single physical property but rather a combination of physical properties and the relationship between OBC and the physical properties is non-linear. Interestingly, similar results were found across the three sources of fat suggesting that the type of fatty acid (stearic, palmitic, lauric) did not greatly impact the relationship between the physical properties and OBC.

To expand on these results, the diffusion of TAGs from the fat network described in this dissertation to cocoa butter will be measured using magnetic resonance imaging with Farnaz Maleky's research group at the Ohio State University. The combination of the physical characterization, capillary forces, and sedimentation events measured in this work with the diffusion events measured by Maleky will determine the impact of the physical properties of fats on three recognized mechanisms of oil migration. Additionally, the impact of these fats in model confectionery systems is being considered. Future work by Lidgard and Martini aims to expand on the results of this dissertation. Lidgard and Martini aim to evaluate the impact of the OBC on fat bloom development, physical properties, and

consumer preference of chocolates in contact with the fats described in this work over a six-month period. In addition, as the fats used for confectionery fillings are often blended with other ingredients, future work by Lidgard and Martini will examine blends of the fats described in this research with peanut flour, sugar, and peanut flour with sugar when in contact with chocolate.

APPENDICES

APPENDIX A: SUPPLEMENTARY TABLES AND FIGURES FROM CHAPTER III

Table A-1: Mean Tpeak and Enthalpy of each peak for the 100% and 50% samples stored at 5 °C. P1 indicates the first peak, P2 indicates the second, and P3 indicates the third peak in the melting profile. Different letters indicate differences over all time points and conditions within each concentration.

Peak Temperature (°C)

100% EIESOY

	FCR wo HIU	FCR w HIU	SCR wo HIU	SCR w HIU
48 h 5 °C – P1	15.8 ± 1.0^{a}	14.3 ± 0.9^{a}	13.0 ± 0.2^{a}	14.3 ± 0.3^{a}
48 h 5 °C – P2	25.9 ± 0.2^{ab}	24.9 ± 0.2^{b}	25.3 ± 0.1^{ab}	26.6 ± 0.7^{a}
48 h 5 °C – P3	53.0 ± 0.2^{a}	49.9 ± 0.2^{b}	52.6 ± 0.2^{a}	49.3 ± 0.2^{b}

50% EIESOY

	FCR wo HIU	FCR w HIU	SCR wo HIU	SCR w HIU
48 h 5 °C – P1	8.8 ± 0.2^{b}	9.8 ± 0.1^{a}	9.3 ± 0.1^{a}	9.4 ± 0.2^{a}
48 h 5 °C – P2	25.1 ± 0.5^{ab}	26.0 ± 0.2^{a}	23.8 ± 0.3^{b}	24.7 ± 0.4^{ab}
48 h 5 °C – P3	47.2 ± 0.3^{bc}	45.1 ± 0.2^{c}	48.0 ± 0.1^{b}	51.0 ± 1.1^{a}

Enthalpy (J/g)

100% EIESOY

	FCR wo HIU	FCR w HIU	SCR wo HIU	SCR w HIU
48 h 5 °C – P1	4.1 ± 0.9^{c}	8.6 ± 1.5^{b}	7.4 ± 0.8^{bc}	14.2 ± 1.0^{a}
48 h 5 °C –P2	9.0 ± 0.9^{a}	6.0 ± 0.9^{ab}	5.9 ± 1.1^{ab}	3.0 ± 0.4^{b}
48 h 5 °C –P3	12.7 ± 1.0^{a}	13.6 ± 0.4^{a}	12.2 ± 0.3^{a}	13.8 ± 0.3^{a}

50% EIESOY

	FCR wo HIU	FCR w HIU	SCR wo HIU	SCR w HIU
48 h 5 °C – P1	3.6 ± 0.4^{b}	4.9 ± 0.2^{a}	2.9 ± 0.4^{b}	4.0 ± 0.3^{ab}
48 h 5 °C –P2	0.5 ± 0.1^{ab}	0.1 ± 0.1^{b}	0.9 ± 0.3^{a}	0.9 ± 0.1^{a}
48 h 5 °C – P3	7.2 ± 0.4^{a}	7.3 ± 0.2^{a}	7.7 ± 0.3^{a}	7.5 ± 0.2^{a}

Figure A-1: Scatterplot matrix between the physical properties and both measurements of OBC for EIESOY

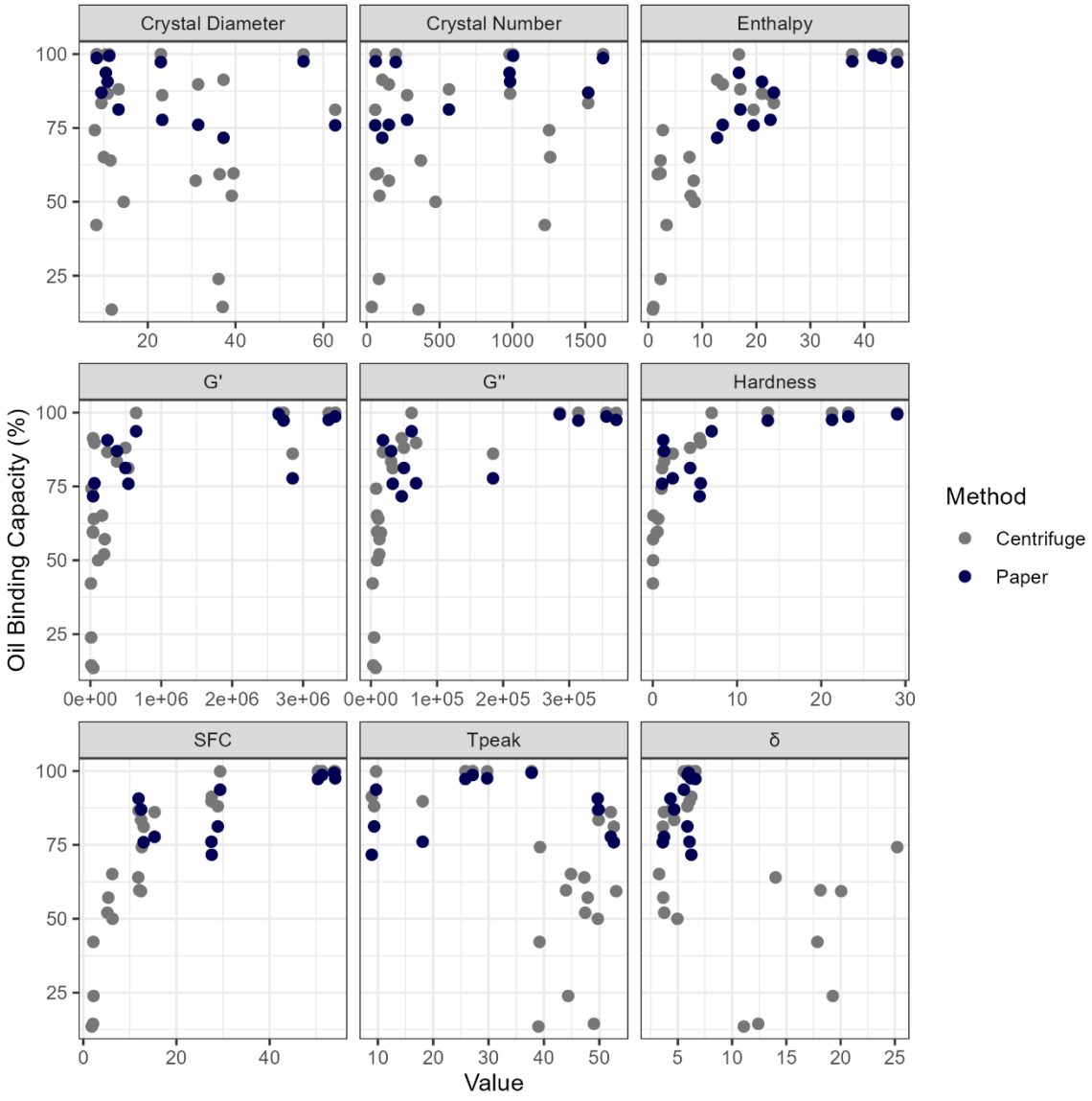

Figure A-2: Crystal microstructure after 48 h for all dilutions and processing conditions, scale bar denotes 50 μm.

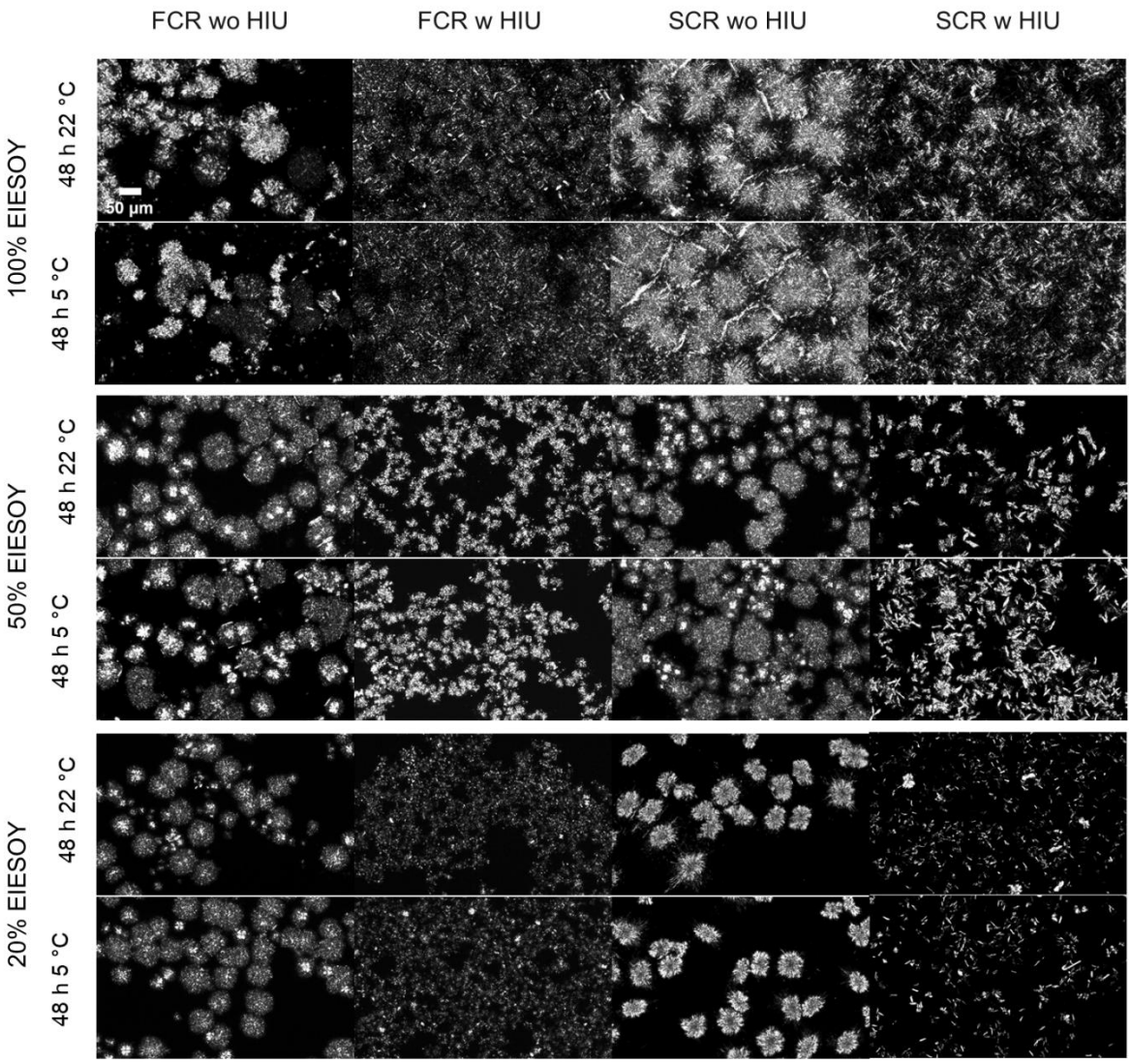

APPENDIX B: SUPPLEMENTARY FIGURES FROM CHAPTER IV

Figure B- 1: Scatterplot matrix between the physical properties and both measurements of OBC for EIEPO.

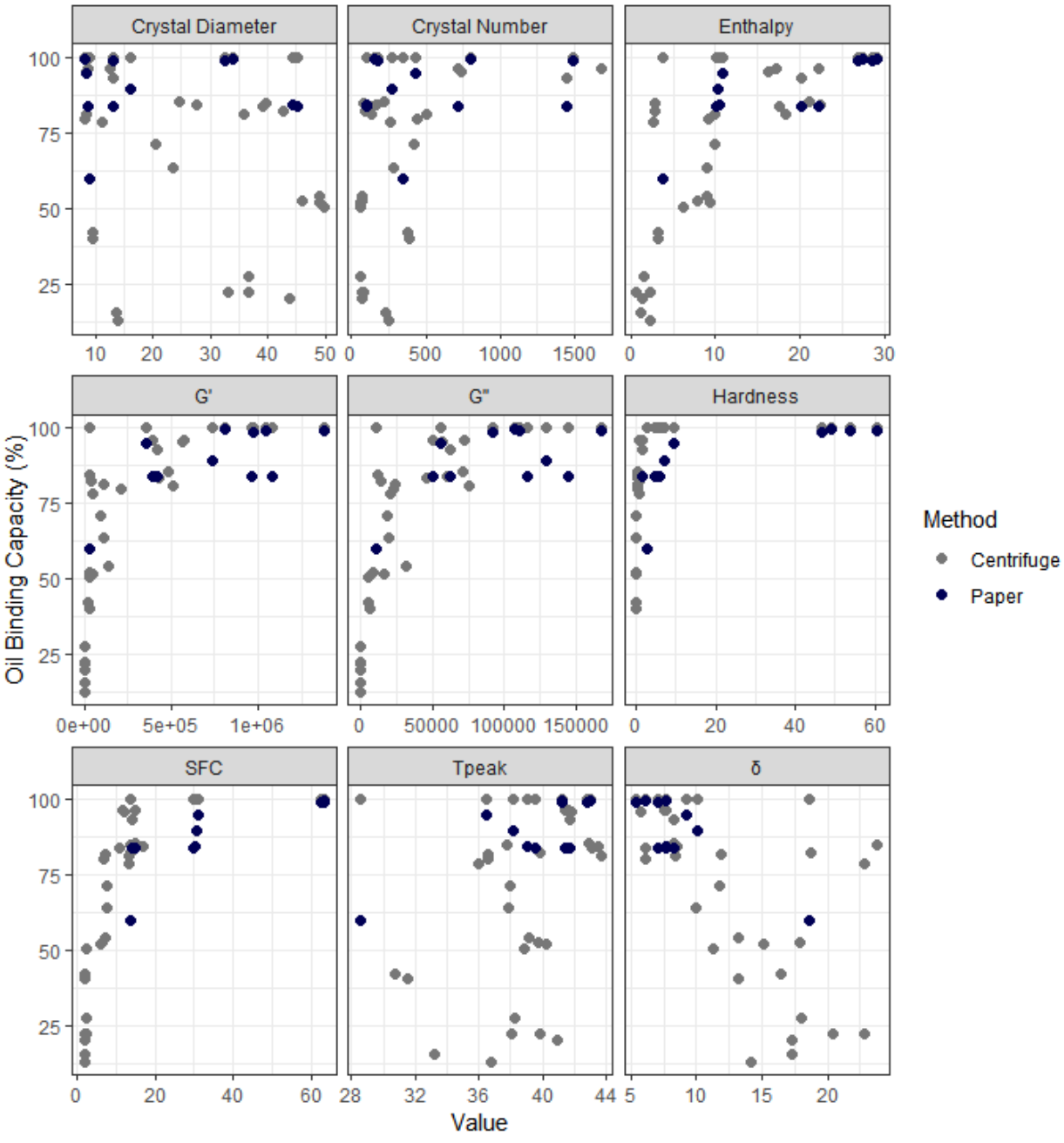

Figure B-2: X-ray diffraction patterns of all samples immediately after crystallization for β and β′ crystals. Lines indicate the average position of defining peaks in Angstroms with standard errors.

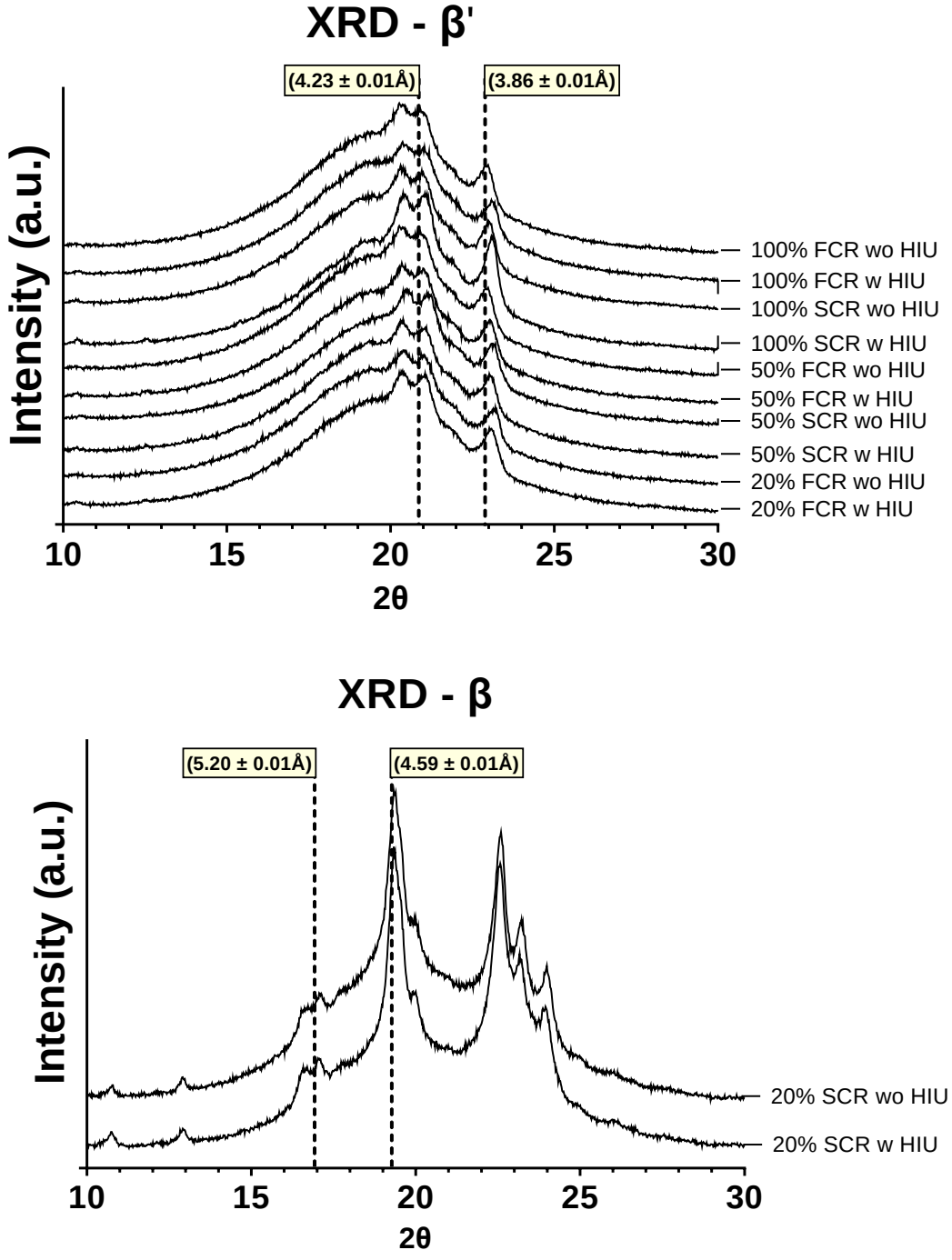

Figure B-3: Crystal microstructure after 48 h for the 100% EIEPO, 50% EIEPO, and 20% EIEPO samples. Scale bar denotes 50 μm.

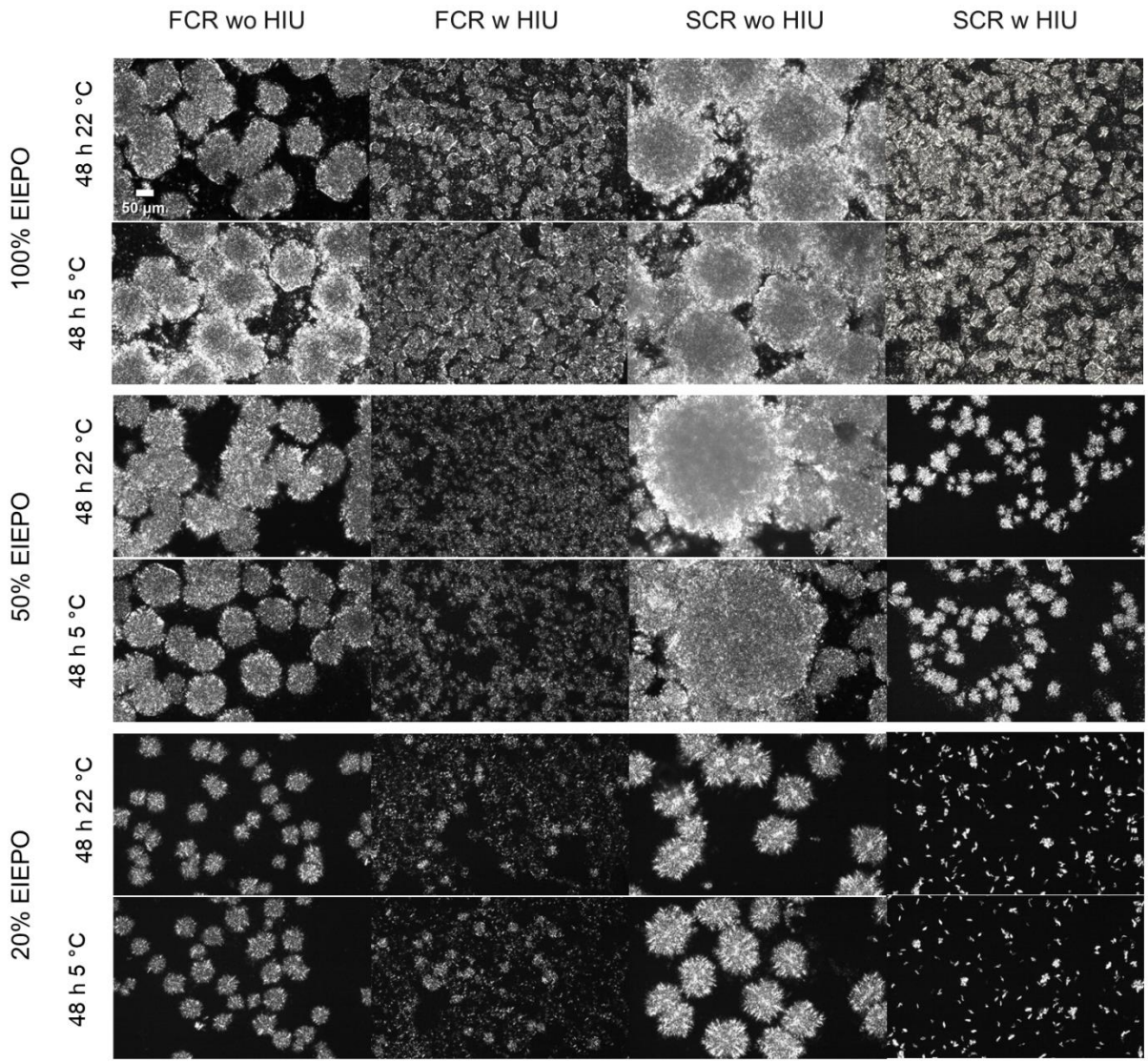

Figure B-4: Summary of the Spearman's r_s correlation coefficients and p-values for both measurements of OBC. The effects of the physical properties are combined over all time points and temperatures to understand the overall relationship between the physical properties and OBC.

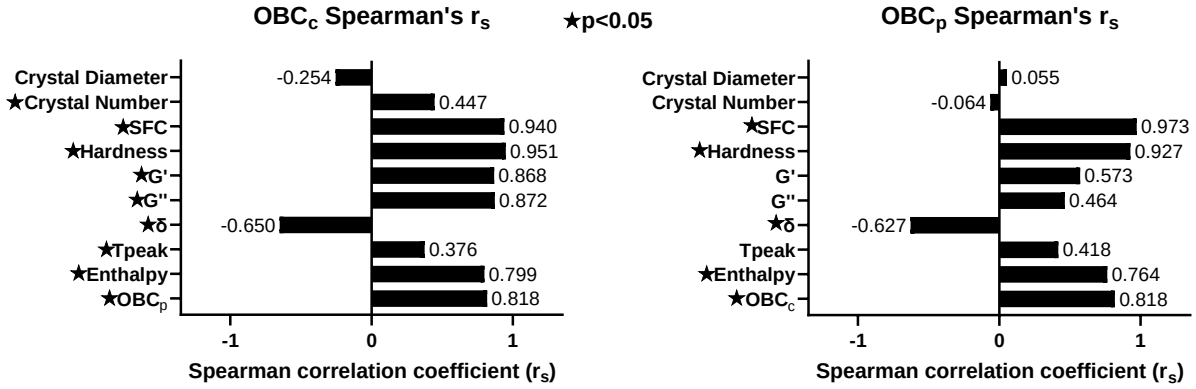

Summary of OBC_c p-values: crystal diameter (p=0.134), crystal number (p=0.006), SFC (p<0.001), hardness (p<0.001), G′(p<0.001), G″(p<0.001), δ (p<0.001), Tpeak (p=0.024), enthalpy (p<0.001), OBC_p (p=0.003)

Summary of OBC_p p-values: crystal diameter (p=0.881), crystal number (p=0.860), SFC (p<0.001), hardness (p<0.001), G′(p=0.071), G″(p=0.155), δ (p=0.044), Tpeak (p=0.203), enthalpy (p=0.009), OBC_p (p=0.003)

APPENDIX C: SUPPLEMENTARY TABLES AND FIGURES FROM CHAPTER V

Table C- 1: Mean fatty acid composition (% w/w) and standard errors for the FHPKO sample and SBO used to prepare the dilutions.

Fatty Acid	FHPKO	SBO
C8:0	3.56 ± 0.00	0.02 ± 0.00
C10:0	3.15 ± 0.01	0.02 ± 0.00
C12:0	41.80 ± 0.04	0.02 ± 0.00
C14:0	13.95 ± 0.02	0.07 ± 0.00
C16:0	8.42 ± 0.01	10.03 ± 0.00
C16:1n7	0.02 ± 0.00	0.14 ± 0.00
C18:0	17.17 ± 0.01	3.96 ± 0.00
C18:1	1.09 ± 0.00	21.09 ± 0.01
C18:2n6	0.25 ± 0.00	51.25 ± 0.01
C18:3n3	0.02 ± 0.00	6.36 ± 0.01
C20:0	0.21 ± 0.01	0.30 ± 0.00
C20:1n9	0.02 ± 0.00	0.27 ± 0.00
C20:2n6	0.02 ± 0.00	0.04 ± 0.00
C20:3n6	0.02 ± 0.00	0.02 ± 0.00
C22:0	0.03 ± 0.00	0.32 ± 0.01
C24:0	0.05 ± 0.00	0.12 ± 0.00
Others	10.25 ± 0.06	5.98 ± 0.03

Figure C-1: Scatterplot matrix between the physical properties and OBC measurements for FHPKO.

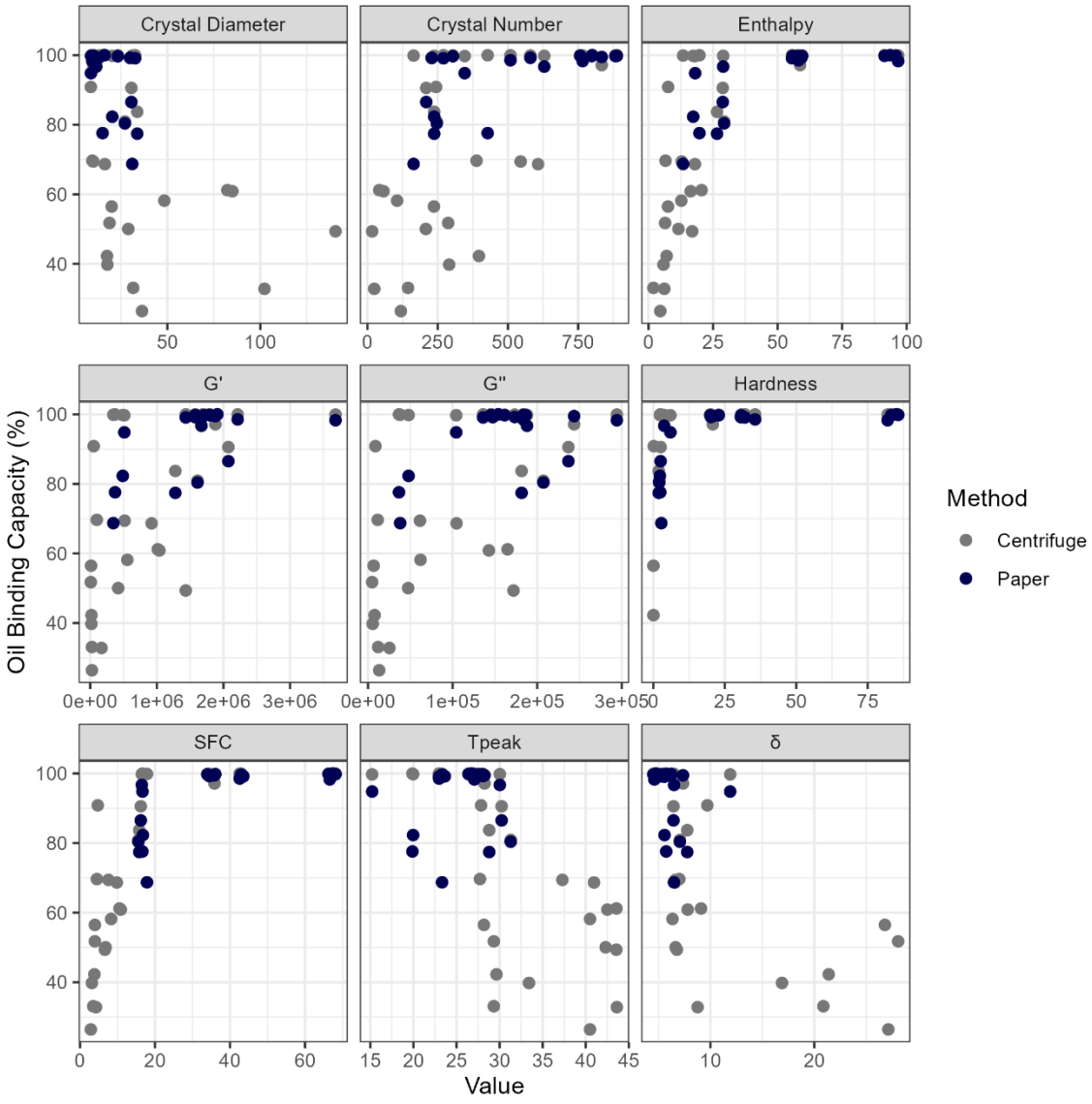

Figure C-2: Crystal microstructure after 48 h of storage. Larger crystals present at 90 min are highlighted around the many small crystals for the 75% FHPKO dilution.

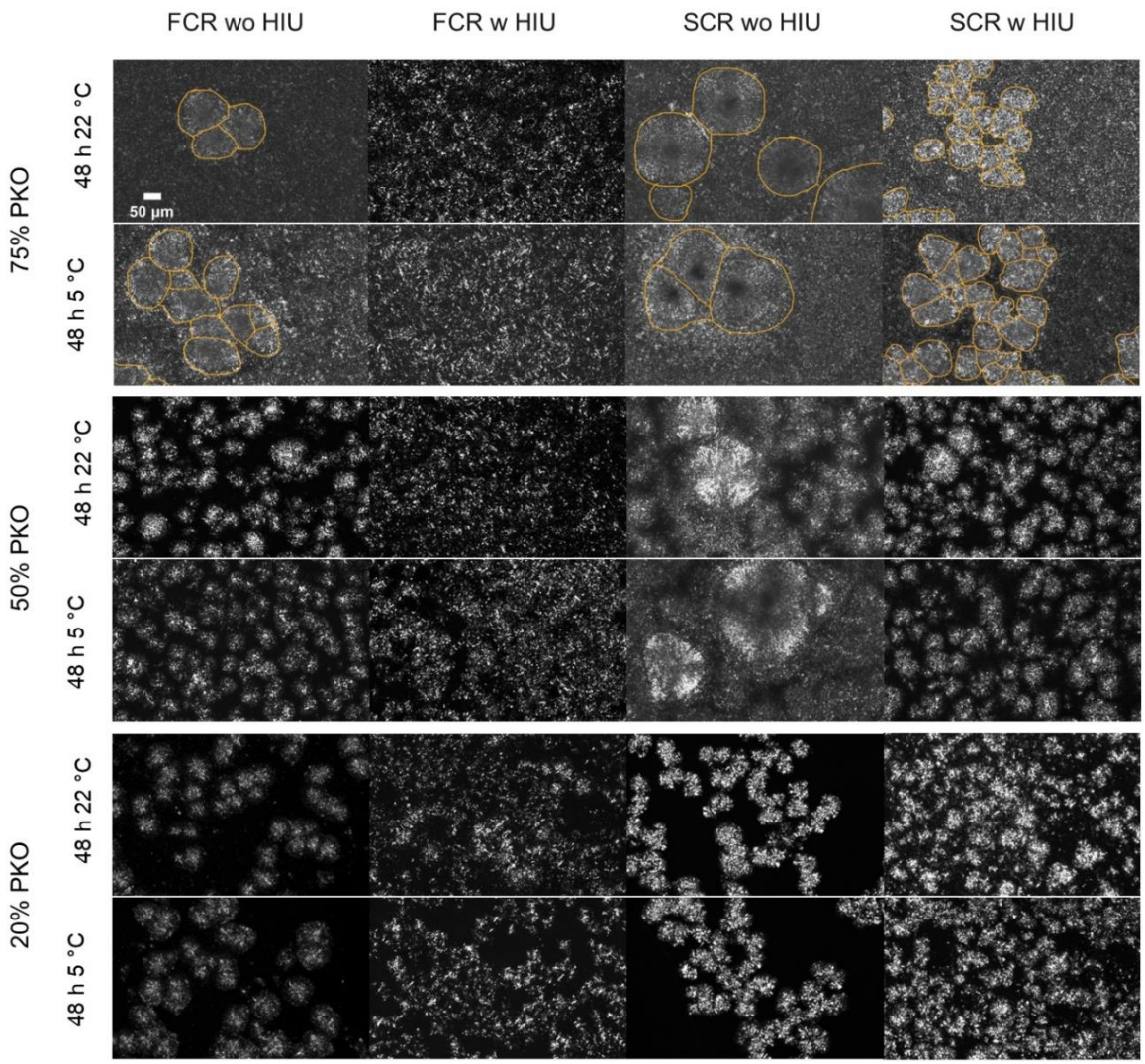

Figure C-3: X-ray diffraction patterns with the average position of defining peaks marked and labeled in Angstroms with standard errors.

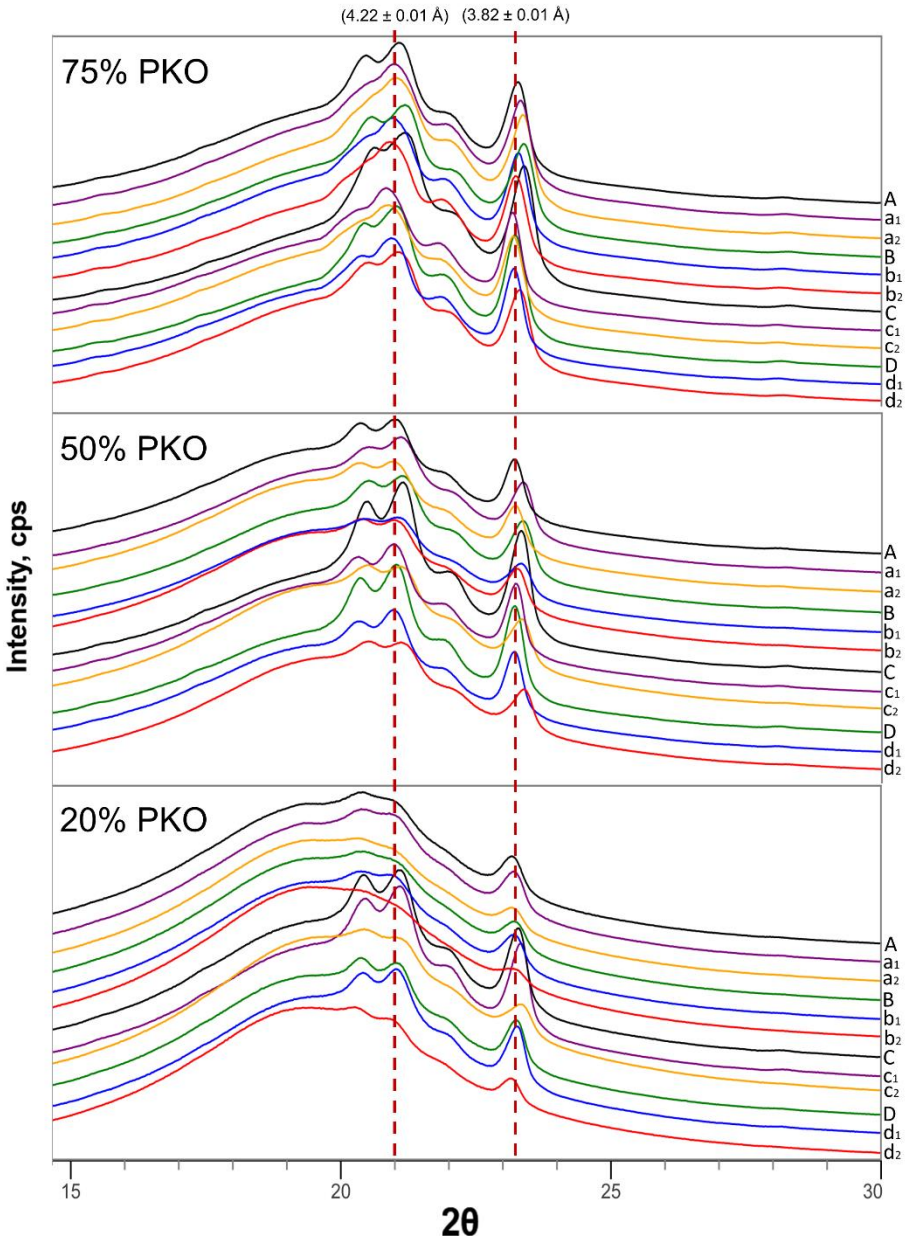

A=FCR wo HIU 90 min, a_1=FCR wo HIU 48 h 22 °C, a_2= FCR wo HIU 48 h 5 °C;
B=FCR w HIU 90 min, b_1=FCR w HIU 48 h 22 °C, b_2= FCR w HIU 48 h 5 °C;
C=SCR wo HIU 90 min, c_1=SCR wo HIU 48 h 22 °C, c_2= SCR wo HIU 48 h 5 °C;
D=SCR w HIU 90 min, d_1=SCR w HIU 48 h 22 °C, d_2= SCR w HIU 48 h 5 °C;

APPENDIX D. COPYRIGHT PERMISSIONS FOR PUBLISHED PAPERS

JOHN WILEY AND SONS LICENSE
TERMS AND CONDITIONS
Mar 07, 2024

This Agreement between Utah State University -- Melissa Marsh ("You") and John Wiley and Sons ("John Wiley and Sons") consists of your license details and the terms and conditions provided by John Wiley and Sons and Copyright Clearance Center.

License Number	5743691499595
License date	Mar 07, 2024
Licensed Content Publisher	John Wiley and Sons
Licensed Content Publication	JOURNAL OF THE AMERICAN OIL CHEMISTS' SOCIETY
Licensed Content Title	Relationship between oil binding capacity and physical properties of interesterified soybean oil
Licensed Content Author	Melissa Abigail Marsh, Silvana Martini
Licensed Content Date	Mar 2, 2022
Licensed Content Volume	99
Licensed Content Issue	4
Licensed Content Pages	18
Type of use	Dissertation/Thesis
Requestor type	Author of this Wiley article
Format	Print and electronic

Portion	Full article
Will you be translating?	No
Title of new work	RELATIONSHIP BETWEEN THE PHYSICAL PROPERTIES AND OIL BINDING CAPACITY OF FATS
Institution name	Utah State University
Expected presentation date	Apr 2024
Requestor Location	Utah State University 275 East 500 North Apt. #4 LOGAN, UT 84321 United States Attn: Utah State University
Publisher Tax ID	EU826007151
	0.00 USD
Total	

Terms and Conditions

TERMS AND CONDITIONS

This copyrighted material is owned by or exclusively licensed to John Wiley & Sons, Inc. or one of its group companies (each a "Wiley Company") or handled on behalf of a society with which a Wiley Company has exclusive publishing rights in relation to a particular work (collectively "WILEY"). By clicking "accept" in connection with completing this licensing transaction, you agree that the following terms and conditions apply to this transaction (along with the billing and payment terms and conditions established by the Copyright Clearance Center Inc., ("CCC's Billing and Payment terms and conditions"), at the time that you opened your RightsLink account (these are available at any time at http://myaccount.copyright.com).

JOHN WILEY AND SONS LICENSE
TERMS AND CONDITIONS
Mar 07, 2024

This Agreement between Utah State University -- Melissa Marsh ("You") and John Wiley and Sons ("John Wiley and Sons") consists of your license details and the terms and conditions provided by John Wiley and Sons and Copyright Clearance Center.

License Number	5743681335221
License date	Mar 07, 2024
Licensed Content Publisher	John Wiley and Sons
Licensed Content Publication	JOURNAL OF THE AMERICAN OIL CHEMISTS' SOCIETY
Licensed Content Title	Unveiling the physical properties predictive of oil binding capacity in an interesterified palm-based fat
Licensed Content Author	Silvana Martini, Farnaz Maleky, Brennan Bean, et al
Licensed Content Date	Mar 5, 2024
Licensed Content Volume	0
Licensed Content Issue	0
Licensed Content Pages	16
Type of use	Dissertation/Thesis
Requestor type	Author of this Wiley article
Format	Print and electronic
Portion	Full article
Will you be translating?	No

Title of new work	RELATIONSHIP BETWEEN THE PHYSICAL PROPERTIES AND OIL BINDING CAPACITY OF FATS
Institution name	Utah State University
Expected presentation date	Apr 2024
Requestor Location	Utah State University 275 East 500 North Apt. #4 LOGAN, UT 84321 United States Attn: Utah State University
Publisher Tax ID	EU826007151
	0.00 USD
Total	

Terms and Conditions

TERMS AND CONDITIONS

This copyrighted material is owned by or exclusively licensed to John Wiley & Sons, Inc. or one of its group companies (each a "Wiley Company") or handled on behalf of a society with which a Wiley Company has exclusive publishing rights in relation to a particular work (collectively "WILEY"). By clicking "accept" in connection with completing this licensing transaction, you agree that the following terms and conditions apply to this transaction (along with the billing and payment terms and conditions established by the Copyright Clearance Center Inc., ("CCC's Billing and Payment terms and conditions"), at the time that you opened your RightsLink account (these are available at any time at http://myaccount.copyright.com).

APPENDIX E: COPYRIGHT PERMISSION FOR FIGURES

ELSEVIER LICENSE
TERMS AND CONDITIONS
Mar 20, 2024

This Agreement between Utah State University -- Melissa Marsh ("You") and Elsevier ("Elsevier") consists of your license details and the terms and conditions provided by Elsevier and Copyright Clearance Center.

License Number	5753270425664
License date	Mar 20, 2024
Licensed Content Publisher	Elsevier
Licensed Content Publication	Chemical Engineering Science
Licensed Content Title	Crystallization behaviour of fats and lipids — a review
Licensed Content Author	Kiyotaka Sato
Licensed Content Date	Apr 1, 2001
Licensed Content Volume	56
Licensed Content Issue	7
Licensed Content Pages	11
Start Page	2255
End Page	2265
Type of Use	reuse in a thesis/dissertation

Portion	figures/tables/illustrations
Number of figures/tables/illustrations	1
Format	both print and electronic
Are you the author of this Elsevier article?	No
Will you be translating?	No
Title of new work	RELATIONSHIP BETWEEN THE PHYSICAL PROPERTIES AND OIL BINDING CAPACITY OF FATS
Institution name	Utah State University
Expected presentation date	Apr 2024
Portions	Figure 1
Requestor Location	Utah State University 275 East 500 North Apt. #4 LOGAN, UT 84321 United States Attn: Utah State University
Publisher Tax ID	98-0397604
Total	0.00 USD

TERMS AND CONDITIONS

The publisher for this copyrighted material is Elsevier. By clicking "accept" in connection with completing this licensing transaction, you agree that the following terms and conditions apply to this transaction (along with the Billing and Payment terms and conditions established by Copyright Clearance Center, Inc. ("CCC"), at the time that you opened your RightsLink account and that are available at any time at https://myaccount.copyright.com).

JOHN WILEY AND SONS LICENSE
TERMS AND CONDITIONS
Mar 07, 2024

This Agreement between Utah State University -- Melissa Marsh ("You") and John Wiley and Sons ("John Wiley and Sons") consists of your license details and the terms and conditions provided by John Wiley and Sons and Copyright Clearance Center.

License Number	5743700900895
License date	Mar 07, 2024
Licensed Content Publisher	John Wiley and Sons
Licensed Content Publication	European Journal of Lipid Science and Technology
Licensed Content Title	Lipase-catalyzed interesterification reactions for human milk fat substitutes production: A review
Licensed Content Author	Pierre Villeneuve, Marlène Pérignon, Mohamed M. Soumanou
Licensed Content Date	Feb 13, 2013
Licensed Content Volume	115
Licensed Content Issue	3
Licensed Content Pages	16
Type of use	Dissertation/Thesis
Requestor type	University/Academic
Format	Print and electronic
Portion	Figure/table
Number of figures/tables	1
Will you be translating?	No
Title of new work	RELATIONSHIP BETWEEN THE PHYSICAL PROPERTIES AND OIL BINDING CAPACITY OF FATS

Institution name	Utah State University
Expected presentation date	Apr 2024
Portions	Figure 1
Requestor Location	Utah State University 275 East 500 North Apt. #4 LOGAN, UT 84321 United States Attn: Utah State University
Publisher Tax ID	EU826007151
Total	0.00 USD

TERMS AND CONDITIONS

SPRINGER NATURE LICENSE

TERMS AND CONDITIONS

Mar 20, 2024

This Agreement between Utah State University -- Melissa Marsh ("You") and Springer Nature ("Springer Nature") consists of your license details and the terms and conditions provided by Springer Nature and Copyright Clearance Center.

License Number	5753280449672
License date	Mar 20, 2024
Licensed Content Publisher	Springer Nature
Licensed Content Publication	Food Analytical Methods
Licensed Content Title	Texture Profile Analysis: How Parameter Settings Affect the Instrumental Texture Characteristics of Fish Fillets Stored Under Refrigeration?
Licensed Content Author	Yago Alves de Aguiar Bernardo et al
Licensed Content Date	Aug 22, 2021
Type of Use	Thesis/Dissertation
Requestor type	academic/university or research institute
Format	print and electronic
Portion	figures/tables/illustrations
Number of figures/tables/illustrations	1

Will you be translating?	no
Circulation/distribution	50000 or greater
Author of this Springer Nature content	no
Title of new work	RELATIONSHIP BETWEEN THE PHYSICAL PROPERTIES AND OIL BINDING CAPACITY OF FATS
Institution name	Utah State University
Expected presentation date	Apr 2024
Portions	Figure 1
Requestor Location	Utah State University 275 East 500 North Apt. #4 LOGAN, UT 84321 United States Attn: Utah State University
Total	0.00 USD

Terms and Conditions

Springer Nature Customer Service Centre GmbH Terms and Conditions

The following terms and conditions ("Terms and Conditions") together with the terms specified in your [RightsLink] constitute the License ("License") between you as Licensee and Springer Nature Customer Service Centre GmbH as Licensor. By clicking 'accept' and completing the transaction for your use of the material ("Licensed Material"), you confirm your acceptance of and obligation to be bound by these Terms and Conditions.

49 Spadina Ave. Suite 200
Toronto ON M5V 2J1 Canada
www.biorender.com

Confirmation of Publication and Licensing Rights

June 9th, 2024
Science Suite Inc.

Subscription:	*Student Plan*
Agreement number:	*BH26X8SR3O*
Journal name:	*Relationship between the physical properties and oil binding capacity of fats*

To whom this may concern,

This document is to confirm that Melissa Marsh has been granted a license to use the BioRender content, including icons, templates and other original artwork, appearing in the attached completed graphic pursuant to BioRender's Academic License Terms. This license permits BioRender content to be sublicensed for use in journal publications.

All rights and ownership of BioRender content are reserved by BioRender. All completed graphics must be accompanied by the following citation: "Created with BioRender.com".

BioRender content included in the completed graphic is not licensed for any commercial uses beyond publication in a journal. For any commercial use of this figure, users may, if allowed, recreate it in BioRender under an Industry BioRender Plan.

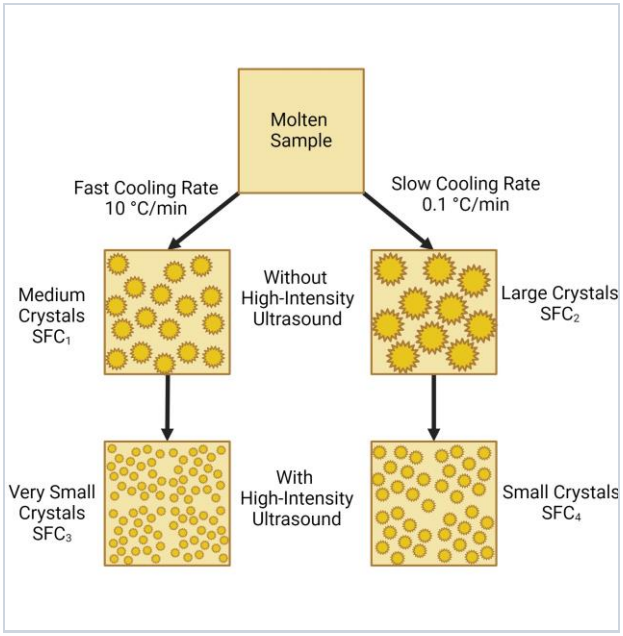

For any questions regarding this document, or other questions about publishing with BioRender refer to our BioRender Publication Guide, or contact BioRender Support at support@biorender.com.

49 Spadina Ave. Suite 200
Toronto ON M5V 2J1 Canada
www.biorender.com

Confirmation of Publication and Licensing Rights

May 13th, 2024
Science Suite Inc.

Subscription:	*Student Plan*
Agreement number:	*ZM26TCQHI2*
Journal name:	*Relationship between the physical properties and oil binding capacity of fats*

To whom this may concern,

This document is to confirm that Melissa Marsh has been granted a license to use the BioRender content, including icons, templates and other original artwork, appearing in the attached completed graphic pursuant to BioRender's Academic License Terms. This license permits BioRender content to be sublicensed for use in journal publications.

All rights and ownership of BioRender content are reserved by BioRender. All completed graphics must be accompanied by the following citation: "Created with BioRender.com".

BioRender content included in the completed graphic is not licensed for any commercial uses beyond publication in a journal. For any commercial use of this figure, users may, if allowed, recreate it in BioRender under an Industry BioRender Plan.

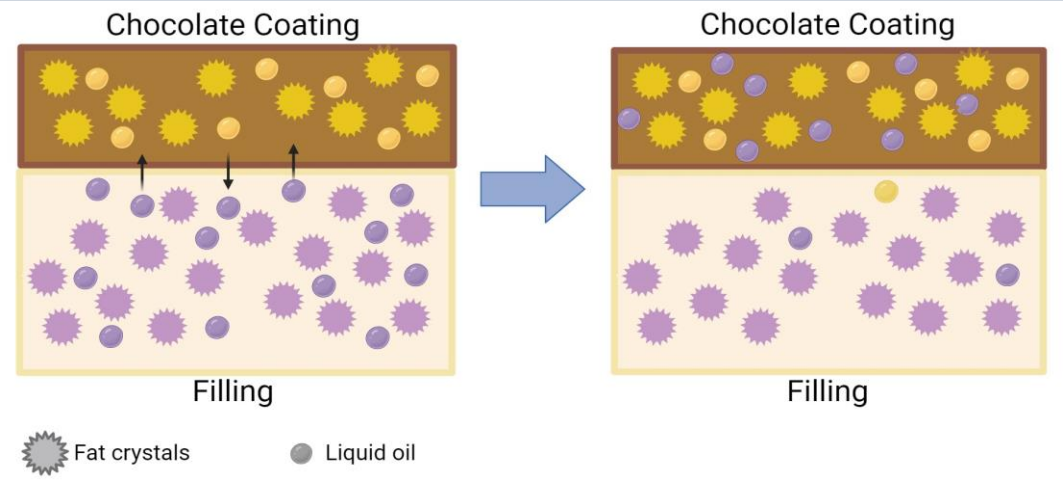

For any questions regarding this document, or other questions about publishing with BioRender refer to our BioRender Publication Guide, or contact BioRender Support at support@biorender.com.

49 Spadina Ave. Suite 200
Toronto ON M5V 2J1 Canada
www.biorender.com

Confirmation of Publication and Licensing Rights

May 13th, 2024
Science Suite Inc.

Subscription:	*Student Plan*
Agreement number:	*VK26TCQHEH*
Journal name:	*Relationship between the physical properties and oil binding capacity of fats*

To whom this may concern,

This document is to confirm that Melissa Marsh has been granted a license to use the BioRender content, including icons, templates and other original artwork, appearing in the attached completed graphic pursuant to BioRender's Academic License Terms. This license permits BioRender content to be sublicensed for use in journal publications.

All rights and ownership of BioRender content are reserved by BioRender. All completed graphics must be accompanied by the following citation: "Created with BioRender.com".

BioRender content included in the completed graphic is not licensed for any commercial uses beyond publication in a journal. For any commercial use of this figure, users may, if allowed, recreate it in BioRender under an Industry BioRender Plan.

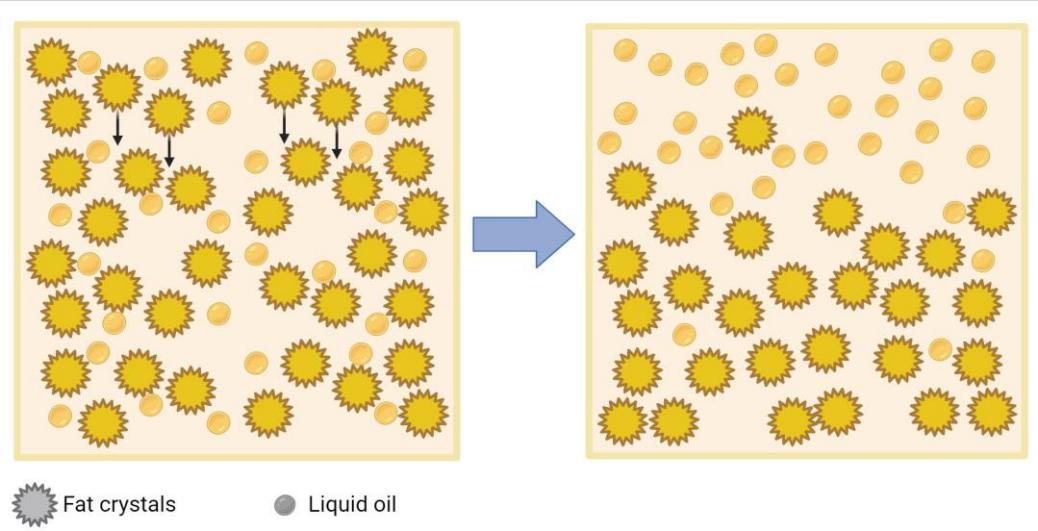

For any questions regarding this document, or other questions about publishing with BioRender refer to our BioRender Publication Guide, or contact BioRender Support at support@biorender.com.

49 Spadina Ave. Suite 200
Toronto ON M5V 2J1 Canada
www.biorender.com

Confirmation of Publication and Licensing Rights

May 13th, 2024
Science Suite Inc.

Subscription:	*Student Plan*
Agreement number:	*XK26TCQHJO*
Journal name:	*Relationship between the physical properties and oil binding capacity of fats*

To whom this may concern,

This document is to confirm that Melissa Marsh has been granted a license to use the BioRender content, including icons, templates and other original artwork, appearing in the attached completed graphic pursuant to BioRender's Academic License Terms. This license permits BioRender content to be sublicensed for use in journal publications.

All rights and ownership of BioRender content are reserved by BioRender. All completed graphics must be accompanied by the following citation: "Created with BioRender.com".

BioRender content included in the completed graphic is not licensed for any commercial uses beyond publication in a journal. For any commercial use of this figure, users may, if allowed, recreate it in BioRender under an Industry BioRender Plan.

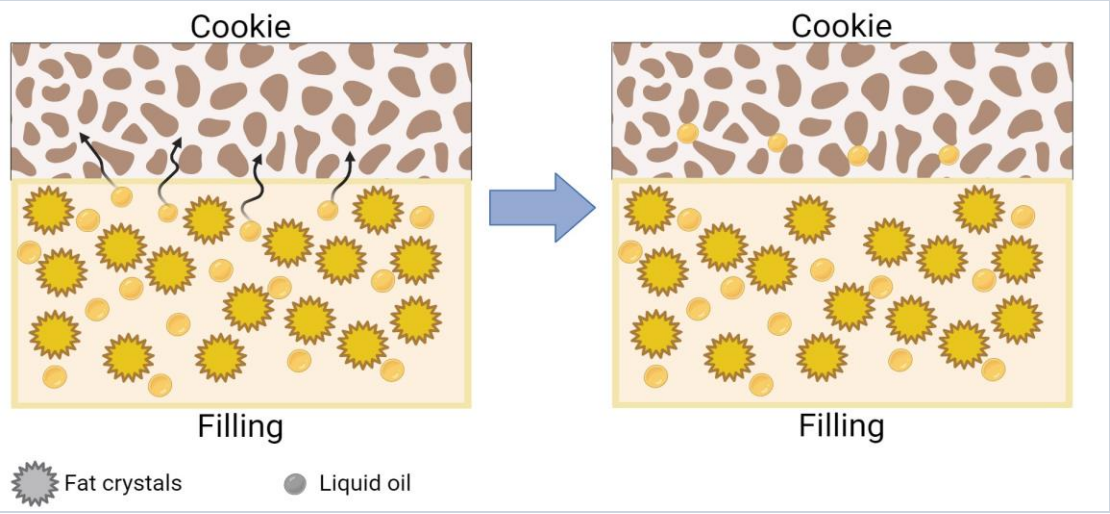

For any questions regarding this document, or other questions about publishing with BioRender refer to our BioRender Publication Guide, or contact BioRender Support at support@biorender.com.

49 Spadina Ave. Suite 200
Toronto ON M5V 2J1 Canada
www.biorender.com

Confirmation of Publication and Licensing Rights

March 20th, 2024
Science Suite Inc.

Subscription:	*Student Plan*
Agreement number:	*QA26LMUNFP*
Journal name:	*Relationship between the physical properties and oil binding capacity of fats*

To whom this may concern,

This document is to confirm that Melissa Marsh has been granted a license to use the BioRender content, including icons, templates and other original artwork, appearing in the attached completed graphic pursuant to BioRender's Academic License Terms. This license permits BioRender content to be sublicensed for use in journal publications.

All rights and ownership of BioRender content are reserved by BioRender. All completed graphics must be accompanied by the following citation: "Created with BioRender.com".

BioRender content included in the completed graphic is not licensed for any commercial uses beyond publication in a journal. For any commercial use of this figure, users may, if allowed, recreate it in BioRender under an Industry BioRender Plan.

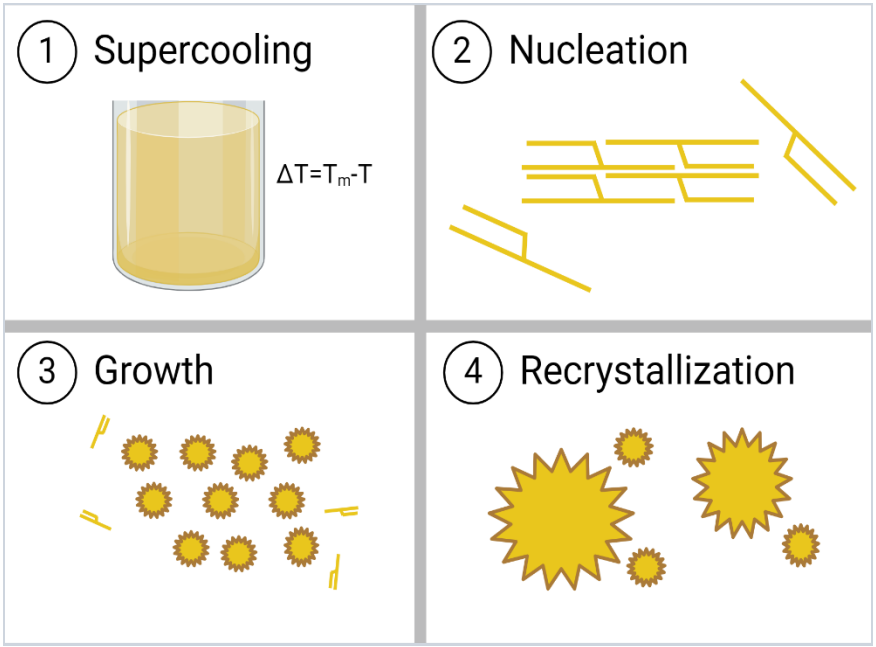

For any questions regarding this document, or other questions about publishing with BioRender refer to our BioRender Publication Guide, or contact BioRender Support at

support@biorender.com.

49 Spadina Ave. Suite 200
Toronto ON M5V 2J1 Canada
www.biorender.com

Confirmation of Publication and Licensing Rights

March 20th, 2024
Science Suite Inc.

Subscription:	*Student Plan*
Agreement number:	*RK26LMUNAM*
Journal name:	*Relationship between the physical properties and oil binding capacity of fats*

To whom this may concern,

This document is to confirm that Melissa Marsh has been granted a license to use the BioRender content, including icons, templates and other original artwork, appearing in the attached completed graphic pursuant to BioRender's Academic License Terms. This license permits BioRender content to be sublicensed for use in journal publications.

All rights and ownership of BioRender content are reserved by BioRender. All completed graphics must be accompanied by the following citation: "Created with BioRender.com".

BioRender content included in the completed graphic is not licensed for any commercial uses beyond publication in a journal. For any commercial use of this figure, users may, if allowed, recreate it in BioRender under an Industry BioRender Plan.

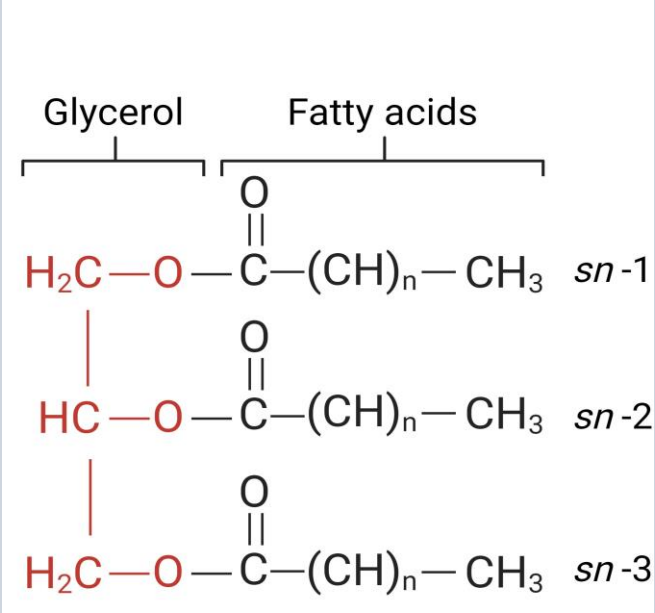

For any questions regarding this document, or other questions about publishing with BioRender

refer to our BioRender Publication Guide, or contact BioRender Support at support@biorender.com.

49 Spadina Ave. Suite 200
Toronto ON M5V 2J1 Canada
www.biorender.com

Confirmation of Publication and Licensing Rights

March 20th, 2024
Science Suite Inc.

Subscription:	*Student Plan*
Agreement number:	*TG26LMUND8*
Journal name:	*Relationship between the physical properties and oil binding capacity of fats*

To whom this may concern,

This document is to confirm that Melissa Marsh has been granted a license to use the BioRender content, including icons, templates and other original artwork, appearing in the attached completed graphic pursuant to BioRender's Academic License Terms. This license permits BioRender content to be sublicensed for use in journal publications.

All rights and ownership of BioRender content are reserved by BioRender. All completed graphics must be accompanied by the following citation: "Created with BioRender.com".

BioRender content included in the completed graphic is not licensed for any commercial uses beyond publication in a journal. For any commercial use of this figure, users may, if allowed, recreate it in BioRender under an Industry BioRender Plan.

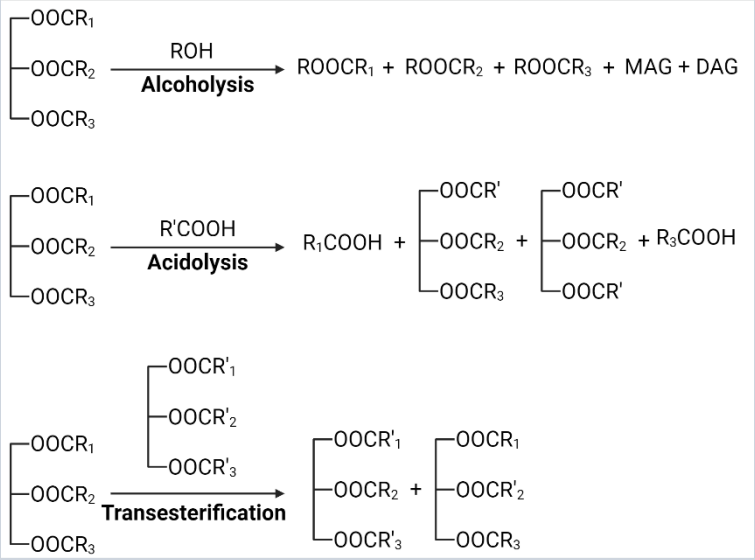

For any questions regarding this document, or other questions about publishing with BioRender refer to our BioRender Publication Guide, or contact BioRender Support at support@biorender.com.

49 Spadina Ave. Suite 200
Toronto ON M5V 2J1 Canada
www.biorender.com

Confirmation of Publication and Licensing Rights

March 20th, 2024
Science Suite Inc.

Subscription:	*Student Plan*
Agreement number:	*CL26LMUN8K*
Journal name:	*Relationship between the physical properties and oil binding capacity of fats*

To whom this may concern,

This document is to confirm that Melissa Marsh has been granted a license to use the BioRender content, including icons, templates and other original artwork, appearing in the attached completed graphic pursuant to BioRender's Academic License Terms. This license permits BioRender content to be sublicensed for use in journal publications.

All rights and ownership of BioRender content are reserved by BioRender. All completed graphics must be accompanied by the following citation: "Created with BioRender.com".

BioRender content included in the completed graphic is not licensed for any commercial uses beyond publication in a journal. For any commercial use of this figure, users may, if allowed, recreate it in BioRender under an Industry BioRender Plan.

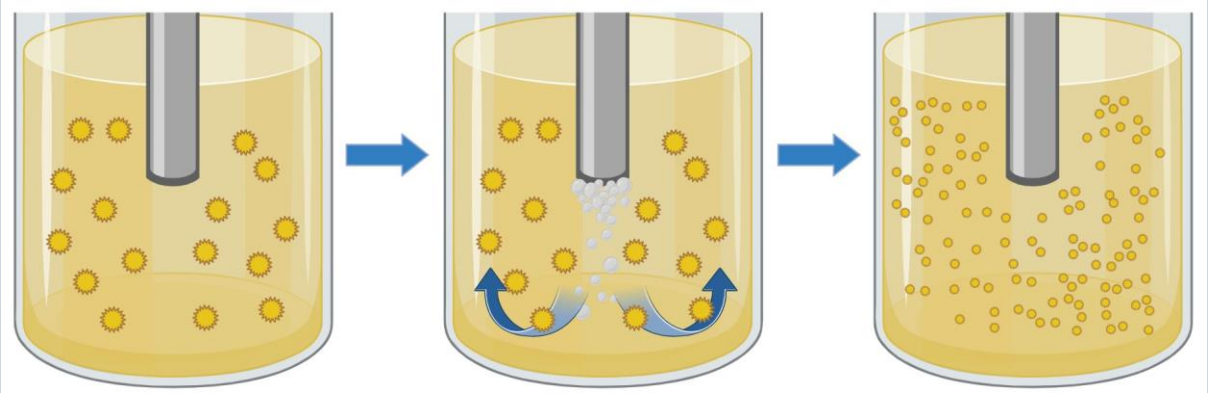

For any questions regarding this document, or other questions about publishing with BioRender refer to our BioRender Publication Guide, or contact BioRender Support at support@biorender.com.

Confirmation of Publication and Licensing Rights

March 20th, 2024
Science Suite Inc.

Subscription:	*Student Plan*
Agreement number:	*VW26LMUNI0*
Journal name:	*Relationship between the physical properties and oil binding capacity of fats*

To whom this may concern,

This document is to confirm that Melissa Marsh has been granted a license to use the BioRender content, including icons, templates and other original artwork, appearing in the attached completed graphic pursuant to BioRender's Academic License Terms. This license permits BioRender content to be sublicensed for use in journal publications.

All rights and ownership of BioRender content are reserved by BioRender. All completed graphics must be accompanied by the following citation: "Created with BioRender.com".

BioRender content included in the completed graphic is not licensed for any commercial uses beyond publication in a journal. For any commercial use of this figure, users may, if allowed, recreate it in BioRender under an Industry BioRender Plan.

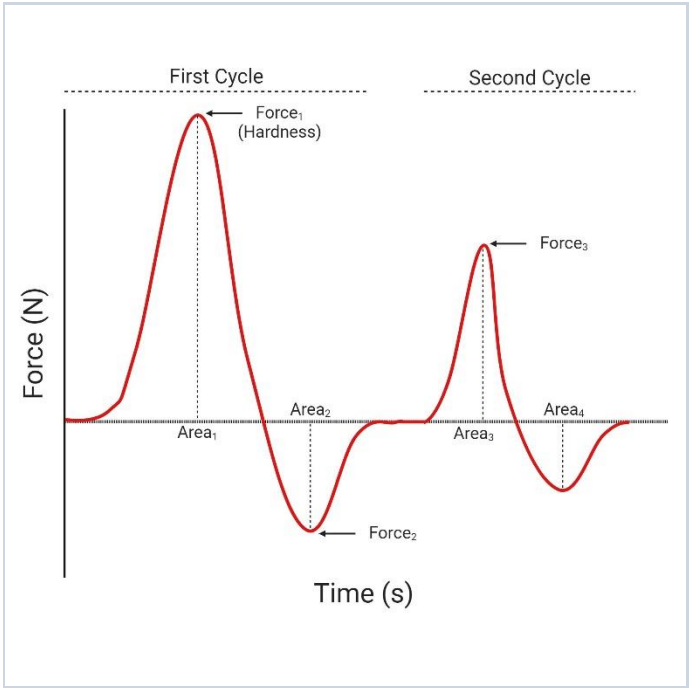

For any questions regarding this document, or other questions about publishing with BioRender refer to our BioRender Publication Guide, or contact BioRender Support at support@biorender.com.

APPENDIX E: CO-AUTHOR PERMISSION

Melissa Marsh <melissamarsh11@gmail.com> Thu, Mar 7, 2024 at 9:44 AM
To: Brennan Bean <Brennan.Bean@usu.edu>

Hello Dr. Bean,

I hope you and doing well. I am currently working on my dissertation, and I would like your permission to include our recent publication as one of the chapters -

Unveiling the Physical Properties Predictive of Oil Binding Capacity in an Interesterified Palm-Based Fat

Your response to this email will be included in the dissertation as proof. Please let me know if you have any questions or concerns.

Thank you,
Melissa

Brennan Bean <Brennan.Bean@usu.edu> Thu, Mar 7, 2024 at 11:28 AM
To: Melissa Marsh <melissamarsh11@gmail.com>

I would be delighted for you to use this paper in your dissertation. I give my full permission.

Brennan

Melissa Marsh <melissamarsh11@gmail.com> Thu, Mar 7, 2024 at 9:46 AM
To: "Maleky, Farnaz" <maleky.1@osu.edu>
Cc: Silvana Martini <silvana.martini@usu.edu>

Hello Dr. Maleky,

I hope you and doing well. I am currently working on my dissertation, and I would like your permission to include our recent publication as one of the chapters -

Unveiling the Physical Properties Predictive of Oil Binding Capacity in an Interesterified Palm-Based Fat

Your response to this email will be included in the dissertation as proof. Please let me know if you have any questions or concerns.

Thank you,
Melissa

Maleky, Farnaz <maleky.1@osu.edu> Thu, Mar 7, 2024 at 9:49 AM
To: Melissa Marsh <melissamarsh11@gmail.com>
Cc: Silvana Martini <silvana.martini@usu.edu>

Hi Mellisa

I am OK with Dr. Martini's decision.

Best.

Farnaz Maleky, Ph.D.

CURRICULUM VITAE

Melissa Marsh

EDUCATION

Doctorate in Food Science May 2024
Utah State University | GPA - 3.97/4.0 Logan, UT
Bachelors in Food Science, Minor in Chemistry May 2020
Utah State University | GPA - 4.0/4.0 Logan, UT

1. PROFESSIONAL EXPERIENCE

INTERNSHIP

Ingredient Chemistry Intern May 2023 – August 2023
Cargill Inc. Plymouth, MN

- Investigated ingredient ranges for vegan cheeses in terms material and sensorial characteristics.
- Processed and characterized 11 vegan pizza cheese and 13 vegan cream cheese prototypes.
- Surveyed 15 commercially available vegan cheese products in terms of texture, and flavor.

RESEARCH PROJECTS

Relationship between the physical properties and oil binding capacity of fats
Utah State University August 2020 – May 2024
Advisor – Silvana Martini Logan, UT
Research focus*:* determining factors that prevent unwanted oil movement in fats.

- Measured the macroscopic and microscopic properties of 324 fat samples.
- Proficient in operating laboratory equipment including x-ray diffractor, rheometer, texture analyzer, differential scanning calorimeter, pulsed nuclear magnetic resonance, polarized light microscope, and high-intensity ultrasound.

Research collaboration with outside company
Utah State University June 2020 – February 2023
Advisor – Silvana Martini Logan, UT

- Conducted research with a lab scale scraped-surface heat exchanger.

Crystallization behavior fats with and without the addition of cannabidiol
Utah State University June 2021 – May 2022
Advisor – Silvana Martini Logan, UT
Research focus*:* examining how CBD impacts the crystallization of fats.

- Trained 2 undergraduate students in 8 lab techniques to measure the properties of fats.

Gustatory perception of linoleic acid: detection thresholds
Utah State University September 2018 - April 2020
Advisor – Silvana Martini Logan, UT
Research focus*:* testing fat taste perception, hypothesized to be the 6th basic taste, in oil and water

- Led panel discussions and trainings for 12 panelists, testing absolute thresholds of linoleic acid in soybean oil and emulsions.
- Measured the oxidation of fats through peroxide value tests and rancimat test.

Calcium uptake in mitochondria and meat tenderness

Utah State University May 2019 - July 2019
Advisor – Sulaiman Matarneh Logan, UT
Research focus*:* evaluating the mitochondria's role on meat tenderness.
- Performed SDS-PAGE electrophoresis and western blot tests.
- Determined and standardized protein content using RCDC protein assay.
- Measured pH, calculated and created buffers.

Sonocrystallization as a tool to reduce oil migration by changing physical properties of a palm-kernel fat
Utah State University January 2019 - May 2019
Advisor – Silvana Martini Logan, UT
Research focus*:* evaluating high-intensity ultrasound as a tool to reduce unwanted oil movement.
- Quantified melting behavior, SFC, hardness, rheological properties, crystal microstructure, and oil binding capacity of fats with and without high-intensity ultrasound.

Effect of storage time on physical properties of sonocrystallized all-purpose shortening
Utah State University March 2018 - May 2018
Advisor – Silvana Martini Logan, UT
Research focus*:* examining the effect of long-term storage on sonicated fats.
- Crystallized 6 all-purpose shortening samples with and without high-intensity ultrasound and measured textural and rheological properties.

PUBLICATIONS

1. Marsh M, Bean B, Maleky F, Martini S (2024) "Unveiling the physical properties predictive of oil binding capacity in an interesterified palm-based fat" Journal of the American Oil Chemists' Society.
2. Cooney J, Hilton I, Marsh M, Jones A, Martini S (2022) "Crystallization behavior of milk fat, palm oil, palm kernel oil, and cocoa butter with and without the addition of cannabidiol" Journal of the American Oil Chemists' Society.
3. Marsh M, Martini S (2022) "Relationship between oil binding capacity and physical properties of interesterified soybean oil" Journal of the American Oil Chemists' Society.
4. da Silva T, Marsh M, Gibon V, Martini S (2020) "Sonocrystallization as a tool to reduce oil migration by changing physical properties of a palm kernel fat" Journal of Food Science.
5. Lee J, Marsh M, Martini S (2020) "Effect of storage time on physical properties of sonocrystallized all-purpose shortening" Journal of Food Science.

PRESENTATIONS

Oral Presentations

1. Marsh M, Anjum N, Maleky F, Martini S "Enhancing Oil Binding Capacity in Palm-Kernel-Based Fats: Impact of Processing Conditions and Physical Properties" Presented at the Presented at the American Oil Chemists' Society annual meeting in Montréal, Québec, CA in 2024
2. Marsh M, Maleky F, Martini S "Fat Bloom – Influence of tempering, storage, composition, and oil migration" Presented at the American Association of Candy Technologists annual meeting in Chicago, IL in 2022
3. Marsh M, Maleky F, Martini S "Relationship between oil binding capacity, oil loss, and the physical properties of an interesterified palm-based fat" Presented at the American Oil Chemists' Society annual meeting in Atlanta, GE in 2022
4. Marsh M, Maleky F, Martini S "Relationship between oil binding capacity and physical properties of interesterified soybean oil" Presented virtually at the American Oil

Chemists' Society annual meeting in 2021

Poster Presentations

1. Marsh M, Maleky F, Martini S "Unveiling the relationship between the oil binding capacity and physical properties in interesterified soybean and palm-based fats" Presented at the American Oil Chemists' Society annual meeting in Denver, CO in 2023 and the Food and Candy Expo in Salt Lake City, UT in 2023
2. Marsh M, Yang J, Feedelem I, Martini S "Sensory Perception of Linoleic Acid in Oil and Water" Presented virtually at the American Oil Chemists' Society annual meeting in 2020
3. Marsh M, da Silva T, Martini S "Application of High-Intensity Ultrasound to Reduce Oil Migration" Presented at the Food and Candy Expo in Salt Lake City, UT in 2019

PROFESSIONAL SOCIETIES

American Oil Chemists' Society (AOCS) — January 2019 - Present
Institute of Food Technologists (IFT) — February 2019 - Present
American Society of Baking (ASB) — October 2021 - Present

AWARDS

Departmental Ph.D. Candidate of the Year — October 2022
Nutrition, Dietetics, and Food Sciences Department, Utah State University

Departmental Graduate Student Teacher of the Year — October 2021
Nutrition, Dietetics, and Food Sciences Department, Utah State University

Thomas H. Smouse Memorial Fellowship Recipient — June 2021
American Oil Chemists' Society

- Highly competitive international award. Given to a scholastically outstanding graduate student conducting research in the field of interest to the American Oil Chemists' Society.

Valedictorian for the College of Agriculture and Applied Sciences — May 2020
Utah State University

A-Pin Award — December 2017, 2018, 2019
Utah State University

- Awarded to students who receive a 4.0 GPA while enrolled in at least 15 academic credits for two consecutive semesters.

Thomas M. Farley Chemistry Award — April 2018
Utah State University

- Awarded to the top 2% of students who excel in Principles of Chemistry courses across all campuses.

Valedictorian of High School Graduating Class — June 2016
Hunter High School

SCHOLARSHIPS/ASSISTANSHIPS

	School Year
Seely-Hinckley Scholarship	2023-2024
Ethelwyn B. Wilcox Human Nutrition Scholarship	2023-2024
W.C. Swanson Minority Scholarship	2022-2023
Dr. Niranjan R. & Mrs. Josephine N Gandhi Assistantship	2021-2022; 2022-2023
E.A. Miller Scholarship	2020-2021
Viola and George Larsen Trust Scholarship	2020-2021
Jed & MerLynn Pitcher Scholarship	2019-2020
Idaho Milk Processors Association Scholarship	2019-2020

Maurine and Anthon Ernstrom Scholarship	2018-2019; 2019-2020
Dr. Niranjan R. & Mrs. Josephine N Gandhi Scholarship	2018-2019; 2019-2020
Coy Fife Scholarship	2018-2019
Melvin Law Scholarship	2018-2019
USU Dean's Scholarship	2016-2017; 2017-2018; 2019-2020
Regents Scholarship	2016-2017; 2017-2018

2. TEACHING EXPERIENCE

COURSES

Chocolate Science Teaching Assistant August 2022 – December 2023
Utah State University Logan, UT
- Conducted weekly hands-on chocolate science labs for 40 students in a bean-to-bar facility.
- Demonstrated chocolate science concepts – tempering, enrobing, panning, roasting, winnowing, refining, and sorting.

Sensory Science Teaching Assistant January 2019 – May 2023
Utah State University Logan, UT
- Coordinated 25 consumer acceptance and difference tests held at USU using SIMS 2000 software.
- Taught sensory science principles – acceptance, difference, and descriptive test methods.

Assisted in Food Engineering and Food Chemistry Labs January 2019 – May 2023
Utah State University Logan, UT
- Food Engineering
  - Taught students how to use a rheometer to measure Newtonian and Non-Newtonian fluids.
- Food Chemistry
  - Taught students how to use polarized light microscopy for native and gelatinized starches.
  - Ran various fat's melting profiles on a differential scanning colorimeter so students could compare melting profiles and fatty acid composition.

STUDENTS MENTORED

Nabila Anjum April 2023 – December 2023
M.S. Food Science, Utah State University

Audrey Lidgard August 2022 – January 2023
M.S. Food Science, Utah State University

Joseph Cooney June 2021 - May 2022
B.S. Physics, Utah State University

Isaac Hilton June 2021 - May 2022
B.S. Civil Engineering, Utah State University

Annalisa Jones August 2020 - January 2021
M.S. Food Science, Utah State University

Weston Christensen May 2020 - August 2020
B.S. Food Science, Utah State University

Isaac Feyedelem August 2019 - January 2020
B.S. Food Science, Utah State University

Jung Mun Yang August 2019 - January 2020
B.S. Food Science, Utah State University

3. EXTRACURRICULAR

FOOD SCIENCE CLUB

Graduate Senator May 2023 – May 2024

- Oversaw a group of 2 students to coordinate 3 activities.

President May 2020 – May 2023

- Increased student involvement by 200% in 3 years.
- Managed 50 club activities delegating responsibilities to other council members.
- Collaborated with internal and external sources to generate over $5,000 in club funds.

Vice-President May 2019 – May 2020

- Assisted President with their responsibilities.

BeneFit Bars Consultant March 2021 - July 2021

- Discussed product goals and technical problems with business owner and provided suggestions for improvements.
- Created nutrient panels for products and evaluated health claims.
- Measured water activity and pH to help determine shelf-stability.
- Funds generated in the project were donated to the club.

PRODUCT DEVELOPMENT

American Egg Board Product Development Competition

Finalist	Macro Munchies: egg-based macro bites with peanut butter and cocoa nibs	2024

Ocean Spray Inc. Product Development Competition

1st Place	Cran-Pop: crunchy cranberry puffs with upcycled cranberry fiber ($3000)	2023
1st Place	Crocos: cranberry dessert tacos with upcycled cocoa shells ($5000)	2022
1st Place	Xalapa and Fresno Hot Sauce: cranberry hot sauce ($5000)	2021

Institute of Food Technologists Smart Snacks for Kids Product Development Competition

3rd Place	Saurus Snacks: mystery dinosaur cookie in a meringue shell ($500)	2022
1st Place	Moonola: instant granola with color changing milk ($3000)	2020

Dairy Management Inc. Product Development Competition

1st Place	Moba Boba: energy drink made from acid whey with boba ($8000)	2022
Finalist	Moodogs: cheese-based vegetarian corndog ($2000)	2020

Idaho Milk Processers Association

1st Place	Moogets: cheese-based vegetarian chicken nugget ($10000)	2019

American Society of Baking Product Development Competition

Entrant	Honey Hives: yeast-leavened cake with honey, almonds, figs, and dates	2023
Entrant	Smoochies: gluten-free chewy rice cookies with marshmallow center	2022
Entrant	Ruby Bites: high fiber chocolate brownies that upcycle cocoa shells	2021